Saturn Ring Observer - Final Report v2.0

Group 12

Delft University of Technology

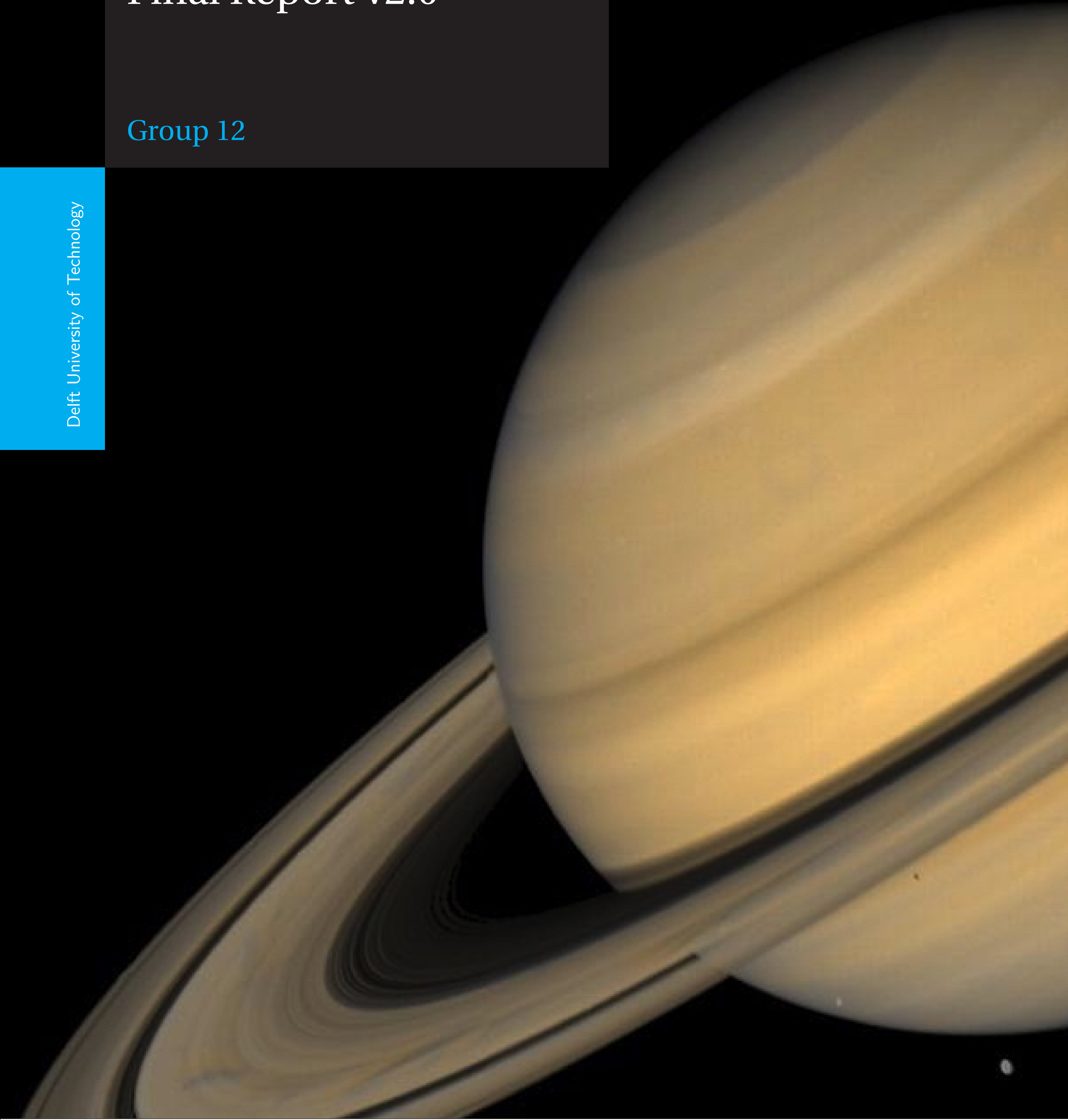

TU Delft Delft University of Technology

Challenge the future

Saturn Ring Observer

Final Report v2.0

by

Group 12

04-07-2017

in partial fulfilment of the requirements for the course of

Design Synthesis Exercise
AE3200

at Delft University of Technology,
Delft, the Netherlands

Project duration:	April, 2017 – July, 2017	
Supervisors:	Dr. ir. E. Mooij, ir. S. Woicke, dr. D. I. Gransden	
Group members:	O.A.M. Flannigan	4280741
	K. Johri	4363051
	R.V. Van der Leer	4371771
	C.A.B. van Lierop	4367707
	B.C.W.G. Meeuwissen	4366557
	A. Mekic	4303687
	A. Pappadimitriou	4340884
	E.G.F.B. Puts	4373456
	K. Sfikas	4361369
	S.A. Vis	4271718

Cover picture : https://nssdc.gsfc.nasa.gov/planetary/factsheet/saturnfact.html

Delft University of Technology

Preface

The Final Report is the outcome of work performed by a team of ten students for the Design Synthesis Exercise (DSE), in June 2017, within the context of Aerospace Engineering Bachelor's degree at Delft University of Technology. The purpose of this report is to present a final conceptual design a Saturn ring observing satellite, which can give insight into the physics behind Saturn's rings and lead to the understanding of how planetary discs are formed.

Readers who are especially interested in gaining a quick overview of the space system that has been designed can find this in the Executive Summary.

This report would not have been possible without the constant guidance and assistance of our mentors Erwin Mooij, Derek Gransden and Svenja Woicke. The group is also grateful for the valuable advice given by all the external contacts.

Group S12
Delft, July 2017

Summary

The purpose of this analysis is to present the design of the complete mission involving a dual spacecraft configuration that will analyse the rings of Saturn. The two spacecraft are an orbiter that will orbit at 142,000 km from the centre of Saturn, and a hovercraft that will hover at a distance of 2-3 km from Saturn its rings.

The designed spacecraft will satisfy various user requirements on science, performance and budget. Regarding primary science objectives, the spacecraft shall be able to characterise restitution coefficients between ring particle collisions, measure the ring particle velocity dispersion, study the development, dimensions, packing density and dissolution of self-gravity wakes and characterise the size distribution and spin states of the larger ring particles. Furthermore, information about the structures of propellers, perturbed ring edges and density waves shall be measured. Regarding performance, the dual orbiter shall perform ring measurements for a year, the hovercraft shall hover for a month in proximity between 2-3 km, the launch date shall be before 2026, multiple key locations will be observed with focus on the A- and B-ring. The designed spacecraft, including launch and operations, shall not exceed a budget of €1.5 billion

The market analysis analysed the opportunities for additional science goals that the mission could cover. Additional objectives are to investigate ring-moon interactions, spokes, physical interaction between the rings and atmosphere and material clumping.

The mission consists of two separate satellites that will perform the mission around Saturn. These satellites will be attached to two kick stages, which will transfer them to Saturn and insert them into a Saturn orbit. The first stage is a solar electric stage, that will perform the transfer to Saturn, until it no longer receives enough solar power to propel the spacecraft. The second stage is a high-thrust chemical stage used for Saturn orbit insertion and pump down of the orbit. After partial circularisation outside the F ring, the two satellites detach and transfer to their respective orbits.

For the final design, SAURON, the dual spacecraft, comprising of the orbiter, the hovercraft , and the SEP stage, will launch on 12 June 2024 from Cape Canaveral on a Falcon Heavy launcher. SAURON will depart Earth with a launch mass of 11,900 kg and an insertion velocity of 1.5 km/s. This will be the start of a 10.4 year interplanetary transfer to Saturn, using solar electric propulsion. An initial gravity assist from Venus followed by two Earth flybys will lower the ΔV requirement for transfer and maximise arrival mass. Several measurements will be performed during flybys to test the payload. On 19 November 2034, SAURON will reach Saturn and dive between the G and F ring for Saturn Orbit Insertion, requiring a propulsive ΔV of 310 m/s. This manoeuvre inserts SAURON into a 100 day orbit around Saturn with a periapsis at 155,069 km. After a periapsis raise manoeuvre of 150 m/s, SAURON is placed into an orbit encountering Titan, which is used as the first gravity assist for the 3.5 year pumpdown tour. This tour, also called a ΔV leveraging tour, uses gravity assist of the moons; Titan, Enceladus, Dione, and Rhea, to lower the required ΔV. A total of 350 m/s chemical propulsive ΔV shall provide the manoeuvres necessary to target the moons. At the end of the pump down tour, SAURON arrives in an elliptical orbit with periapsis at 142,000 km and apoapsis at Enceladus' orbit. During this orbit, SAURON will be staged into the orbiter and hovercraft. The orbiter and the hovercraft will then separately perform a propulsive ΔV of 1,215 m/s and 2,641 m/s, respectively, to circularise into a 142,000 km orbit.

The user requirements on science will be mainly satisfied using a wide angle camera and a narrow angle camera. Additional scientific measurements are performed using a dust analyser, magnetometer, plasma and energetic particle package, radio science experiment, ultraviolet and infrared imaging instruments. Cassini has given insights in the rings of Saturn and based on these measurements, models and theories have been developed. The SAURON mission will aim to validate these models and study the rings at higher resolutions than Cassini. At 0.05 m/pixel, the hovering spacecraft will be able to map individual particles in the rings and study their behaviour and composition.

The attitude orbit and control system design is based on the accuracy, stability and control requirements of the spacecraft. The narrow angle camera drives the requirements on accuracy, stability and control. Based on these requirements and the disturbance environment, sensors and actuators were selected to control the spacecraft attitude. Two gyroscopes, two star sensors, a wide angle camera, a narrow angle camera, four reactions wheels and twelve control thrusters are present on each spacecraft for attitude control, determination and navigation control. Additionally, the hovercraft contains a LIDAR and four hop thrusters. The LIDAR in combination with the camera instruments will detect the ring plane and potential collision hazards.

To calculate processing speeds, typical values from theory were taken. A sensitivity analysis on this allowed for assessing the worst case processing speeds. Based on the eclipses between the hovercraft and the orbiter the storage capacity was calculated. This value was then validated with the amount of data that a newer spacecraft such as New Horizons possesses. 78 MHz and a storage of 64 Gbits was determined to be required for the spacecraft. To satisfy these needs, the LEON3-FT processor on the OSCAR computer was selected. To connect all the various components

Table 1: Hovercraft and orbiter power characteristics.

	Hovercraft (300 W BOL) Mass [kg]	(170 W EOL) Costs [k€]	Orbiter (480 W BOL) Mass [kg]	(268 W EOL) Costs [k€]
RTG excluding Cu-244 fuel	43	80625	60	129000
Cu-244	2.1	320	3.5	525
Shielding	45		73	
Batteries	0	0	2.7	36
Power Processing Unit	1.5	135	2.4	216
Total	92	81000	142	13000

Table 2: Characteristics for the spacecraft thrusters.

Component	**Usage**	**Mass [kg]**	I_{sp} **[s]**	**Thrust [N]**
AMBR 623N Dual mode HP rocket engine	Main thruster on second stage.	5.40	333	623
Hi-pat 445 Dual mode HP liquid apogee thruster	Main thruster on orbiter and hovercraft.	5.44	329	445
Moog DST-11H	Hovering thruster on hovercraft and control thruster on second stage.	0.77	310	22
MR-103M 1N	Control thruster on orbiter and hovercraft.	0.16	221-206	0.99-0.28
NEXT ion thruster	Main thruster on first stage.	12.7	max 4190	max 0.236

together a military standard MIL-STD-1553 was selected. A model to estimate the requirements for the software were proposed but not implemented in this report. Correction methods that are needed to protect the data from corruption from the environment are incorporated as well.

The hovercraft carries a payload of 37 kg that consumes 54 W of power. It contains a wide angle camera and narrow angle camera for detailed imaging. A dust analyser and magnetometer are also included to determine particle flux and the magnetic field. The orbiter has the same instruments and contains additional instruments. These instruments are the infrared and ultraviolet spectrometers, the radio science transponder and the plasma & energetic particle package. The orbiter payload weighs 52 kg with a power consumption of 88 W.

The power system has two types of power generation: solar power for the transfer and radioisotope power for at Saturn.

The solar arrays power the ion thrusters. These are two 10 meter diameter arrays with a Begin-Of-Life (BOL) power of 37 kW. These weigh 250 kg in total. The arrays are round and mounted on a boom to enlarge the distance between the array and ion thrusters such that the plume does not intersect with the arrays to prevent degradation.

The RTGs power the hovercraft and orbiter. The hovercraft has two RTGs of 150 W and the orbiter two RTGs of 240 W each, see Table 1 for the mass, costs and power. The RTGs are fuelled with Curium-244. Due to the high radiation emission levels of Curium-244, shielding is required.

The orbiter has batteries to store energy when no communication link is possible, this energy can be used for higher data rates or payload power. The second stage is powered by the RTGs of the orbiter in the last part of the transfer, SOI and pumpdown phase.

The propulsion system is designed for high efficiency of I_{sp} and required burn times. Engines were selected based on high performance, resulting in relatively large thrusters on the two small satellites. To perform small manoeuvres, smaller thrusters were added since the burn time would become too small for the high performance thrusters to perform. The second stage required a large high thrust manoeuvre and multiple smaller manoeuvres. To do all of these, multiple high performance thrusters are used. All of them are used for the large manoeuvres and only one for the small manoeuvres. The first stage uses solar electric propulsion to perform low thrust gravity assists for the transfer to Saturn. The specifications on these thrusters can be seen in Table 2.

The tanks in the spacecraft are always configured in a point symmetrical way. This way whenever propellant is used, the shift in centre of gravity is limited and the thrusters will not require a large gimbal angle.

The fuel lines and valves in the propulsion subsystems are all designed to have redundancy when the primary lines fail. This also counts for the attitude control thrusters. If two of the four control thruster clusters fail, the spacecraft could still use them to rotate around all 3 axis.

The spacecraft will be launched using the Falcon Heavy launch vehicle. Its structure is of a cylindrical shape and is designed to withstand the most critical loads experienced during its lifetime, which refer to the launch loads. The required thickness of the structure for the two kick stages and for SAURON is 0.547 mm and is made of aluminium-lithium alloy 8,090, which results to the corresponding mass and cost for each section, found in Table 3. The layout of

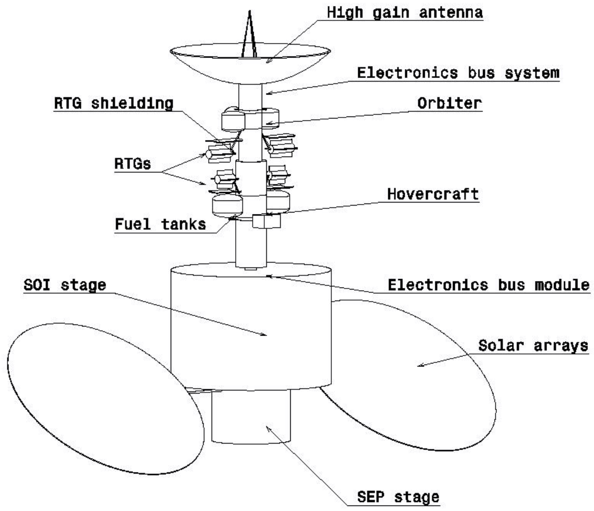

Figure 1: Spacecraft layout.

Table 3: Mass, Cost and Height for the structure of the two stages and SAURON.

	Height [m]	**Mass [kg]**	**Cost [€M]**
SEP stage	1.213	96	16.2
SOI stage	2.16	316	38.8
Hovercraft	2.45	77	13.8
Main orbiter	1.79	41	8.8

SAURON can be seen in figure Figure 1.

Each stage is divided into two modules, the propulsion module and the electronics module on top of it. Inside the cylinder the tanks of the propulsion system of each stage will be attached, except for the helium tanks which will be attached to the outer surface. Though, for SAURON the fuel tanks will also be attached on the outside. Inside the structure the thermal subsystem will be running from top to bottom to ensure all parts are functioning under their allowable temperature range. Regarding the main orbiter, the structure will be used to attach the payload and the antenna on top of the spacecraft.

The satellite must be able to handle the temperature extremes at Venus and Saturn. These are two different temperature extremes, where the temperatures at Venus are high and at Saturn low. The satellite needs to be able to keep the spacecraft's components within their operating ranges a both temperature extremes.

The thermal system includes 7 m of heat pipes throughout the orbiter and hovering spacecraft. Each pair of RTGs for the orbiter and hovering spacecraft will have an RTG radiator each with an area of 0.9 m^2. In addition, the orbiter, hovering spacecraft and each stage will have a separate radiator with an area of 0.3 m^2. This results in the mass, power and costs shown in Table 4.

The telecommunications subsystem was designed with high reliability and fast downlinks in mind. Considering the 10 AU distance from the orbiter to Earth, a high gain antenna with a diameter of 3.7 meters and an Ka band gain of 59 dBi is necessary to provide the necessary E_b/N_o ratio for a data rate of about 48 kbit/s. The relay link between both spacecraft can carry up to 284 Mbit/s at the closest range. Shortly before eclipse, maximum achievable data rate is 2.3 kbit/s. As the hovercraft is occupied with pointing thrusters and payload instruments, the antenna design on the

Table 4: Mass, power and cost of the thermal subsystem of SAURON.

Spacecraft Stage	**Mass [kg]**	**Power [W]**	**Cost [€M]**	**Comments/Remarks**
Orbiter	16	10	9	At hot case the power is 0 W.
Hovering Satellite	27	10	14	At hot case the power is 0 W.
First stage	43	0	23	-
Second stage	11	0	6	-
Total	98	20	52	-

hovercraft accommodates transceiving signals with rough pointing, as it uses medium and low gain antennas. These have large beamwidths, between 90 and 180 degrees, depending on the type. Redundancy measures were taken with respect to the transponders, amplifiers, cabling, and diplexers. In the case of component failure, there is always one redundant component that can take over to ensure high availability. The subsystem mass is estimated to be 80 kg for the orbiter and 40 kg for the hovercraft; the total cost would amount to approximately €120 million.

The spacecraft will be assembled and integrated at ESA. The required components and instruments will originate from European companies. After all the parts are manufactured and acquired, they are transported to the ESA facility for assembly and integration. Assembly will start in 2022 and completion of assembly and integration is planned for 2023. Special handling measures will be taken to deal with the Curium-244 RTGs. After integration, a period of testing will validate the system. The manufacturing, integration, assembly and testing is estimated to cost €120 million. After the spacecraft is launched, the spacecraft is monitored for its dynamic behaviour AOCS anomalies. When the early orbit phase is done, the payload is activated, checked and calibrated. The performance of the spacecraft will be tested to verify if data is correct. The operations and monitoring will be handled by the European Space Operations Centre (ESOC) using ESA its ground station network. Operations are estimated to cost €480 million for the full duration of the mission.

Table 5 presents the mass and cost budget breakdown of the SAURON mission. The total cost for the mission is estimated to be €1.46 billion for a one year operational time frame at Saturn. Approximately €750 million is required for the subsystems of the orbiter and hovering spacecraft. The total wet mass of the spacecraft is estimated to be approximately 11,206 kg. The solar-electric propulsion stage wet mass is approximately 1,467 kg. The Saturn orbit insertion stage is approximated to be 7,892 kg. The hovering spacecraft is estimated to be 1,125 kg and the main orbiter is estimated to be 723 kg. Distributions of the masses and cost on the subsystems is presented in Table 5.

The presented mission analysis of a dual spacecraft design that is able to investigate the composition and particle dynamics of Saturn's rings, shows compliance with the user requirements on science, performance, reliability and cost. The hovercraft will perform the science measurements at an altitude 2-3 km above the A- and B-ring and send it to the orbiter, which transmits the data back to Earth. The hovering measurements last for at least month and the orbiter measurements for at least a year. Mission success, which implies full completion of the primary science objectives, shall be larger than 95%. Besides the primary science objectives, additional scientific measurements will be taken on ring-moon interactions, spokes, material clumping and the physical interaction between the rings and atmosphere while not exceeding the mission cost of €1.5 billion, which includes production, operations and launch. To transition this mission analysis design into a preliminary design phase, further investigation into the subsystems is required. Recommendations include:

- Investigate the distance between RTGs and payload to estimate the hazardous effect on the payload.
- Investigate concentrated solar arrays to increase efficiency, thus decrease mass.
- Further investigate the optimised transfer trajectory to decrease the required ΔV, thus decrease mass.
- Add more nodes to the thermal analysis model to increase accuracy of the operational temperatures ranges.
- Analyse the tank mass for their optimisation.
- Investigate vibroacoustic environment, sinusoidal loads and random loads during launch to ensure the spacecraft structure survives launch.
- Investigate the control thruster sizing in relation to the centre of mass to acquire more accuracy of the AOCS design.
- Investigate better performing processors.
- Investigate the limitations of data processing calculations

Table 5: Mass & cost budget breakdown of the SAURON mission.

WBS element	**Actual values (kg)**	**Contingency (%)**	**Mass with contingency (kg)**	**Mass fractions of dry mass (%)**	**€M 2017**
WBS element	**Actual values (kg)**	**Contingency (%)**	**Mass with contingency (kg)**	**Mass fractions of dry mass (%)**	**€M 2017**
Main orbiter	720		795		
AOCS	25	22%	30	6.1%	10
Telecommunications	80	20%	96	19.4%	77
C&DH	14	21%	16	3.3%	80
Others (Cabling)	20	21%	24	4.9%	
Payload	54	0%	54	10.9%	105
Power supply	142	20%	170	34.3%	130
Propulsion (engines+tanks)	45	20%	54	10.9%	1
Structure (main)/bus	32	21%	39	7.8%	8
Thermal control	10	19%	12	2.4%	9
Bipropellants	255		255	32.1%	0
Monopropellants	44		44	5.6%	
Hovering spacecraft	1049		1117		
AOCS	45	20%	53	12.0%	16
Telecommunications	40	19%	48	10.7%	43
C&DH	14	18%	16	3.6%	80
Others (Cabling)	12	18%	14	3.2%	
Payload	39	0%	39	8.8%	83
Power supply	92	21%	111	25.1%	81
Propulsion (engines+tanks)	63	21%	76	17.1%	2
Structure (main)/bus	52	20%	62	14.0%	12
Thermal control	20	21%	24	5.5%	18
Bipropellants	633		633	142.6%	0
Monopropellants	40		40	9.0%	
SOI stage wet	7183		7324		69
Others (Cabling)	13	20%	16	2.0%	
Propulsion (engines+tanks)	394	22%	480	60.1%	
Structure	230	21%	278	34.8%	
Thermal control	21	20%	25	3.2%	
Bipropellants	6003		6003	750.8%	
Extra bipropellants	521		521	65.1%	
SEP stage wet	1403		1536		88
AOCS	1	0%	1	0.1%	
Power	247	20%	296	36.7%	
Propulsion (engines+tanks)	351	19%	418	51.8%	
Structure	70	21%	84	10.5%	
Thermal control	6	20%	7	0.9%	
Xenon gas	729		729	90.4%	
Total dry mass	2130	19%	2546		
Total wet mass	10355		10771		
Production					123
Operations					480
Total cost					1500

List of Symbols

Greek

α	Absorptivity	-
α	Angle of the outer radiation line with the RTG	rad
α	Roll-off factor	-
β	Angle of the inner radiation line with the RTG	rad
$\Delta\mathbf{x}$	Change in the spacecraft state at segment midpoint	–
Δi	Change in inclination	rad
Δt	Time of each segment	s
ΔV	Change in velocity	$\mathrm{m\,s^{-1}}$
δ	Outgoing relative velocity asymptote	rad
ϵ	Emissivity	–
η	Efficiency	-
Γ	Spectral efficiency	$\mathrm{bit\,s^{-1}\,Hz^{-1}}$
γ	Angel of the radiation line with the RTG	rad
λ	Magnetic latitude range	–
λ	Wavelength	m
μ	Standard gravitational parameter	$\mathrm{km^3\,s^{-2}}$
μ_i	Encoded throttles	–
Φ	Magnetic flux	Wb
Φ	Solar constant	$\mathrm{W\,m^{-2}}$
Φ	Keplerian transition matrix	–
ϕ	Angle of incidence	rad
ρ	Density of the material	$\mathrm{kg\,m^{-3}}$
σ	Stefan Boltzmann constant	$\mathrm{W\,m^{-2}\,K^{-4}}$
σ	Stress of the material	MPa
τ	Half life time of radioactive isotope	s
θ	Angle between the local vertical and the z-principle axis	rad
θ	Angle of incidence	rad
θ	Impact angle from target normal	rad
φ	Continuous Keplerian transition matrix	–

Roman

$\dot{m}$	Mass flow	$\mathrm{kg\,s^{-1}}$
$\bar{\mathbf{x}}$	Spacecraft state vector with backwards propagation	–
$\mathbf{u}$	Decision chromosome (vector)	–
$\mathbf{u}^*$	Feasible decision chromosome (vector)	–
$\mathbf{x}$	Spacecraft state vector with forwards propagation	–
A	Area	$\mathrm{m^2}$
a	Albedo	-
B	Bandwidth	Hz
B	Gebhart factor	-
b	Base	m
b	Vertical RTG boom length	m
BHN	Brinell hardness number of material	–
C	Conduction factor	$\mathrm{W\,K^{-1}}$
C	Conductive factor	-
c	Speed of sound in the material	$\mathrm{km\,s^{-1}}$
$C3$	Characteristic/Launch energy	$\mathrm{km^2\,s^{-2}}$
cm	Centre of mass	m
cp	Centre of pressure	m
D	Diameter	m
D	Dose	rad
D	Dose rate	$\mathrm{rem\,h^{-1}}$
D	Spacecrafts residual dipole moment	$\mathrm{Am^2}$
d	Distance	m
d	Height	m
DR	Data rate	$\mathrm{bit\,s^{-1}}$
E	Modulus of elasticity	GPa
F	Force	N
F	View factor	-
f	Frequency	Hz
G	Boresight antenna gain	dB
g	Vertical shield height from the RTG	m
H	Irradiance	$\mathrm{W\,m^{-2}}$
h	Hovering height	m

h	Tank height	m
I	Area moment of inertia of the structure	m^4
I	Impulse	
I	Mass moment of inertia	$kg\,m^2$
i	Inclination	rad
k	Damage parameter	–
k	Horizontal RTG boom length	m
k	Number sequence	-
k	Thermal conductivity	$W\,mK^{-1}$
L	Total height of the spacecraft	m
l	Length	m
l	Length of the RTG	m
M	Magnetic moment	Tm^3
M	Number of symbols	-
M	Total mass of the spacecraft	kg
m	Mass	kg
N_{Nyq}	Nyquist-Shannon criterion for sampling	–
N	Number of legs	–
n	Number of bits	–
n	Number of hops	–
n	Number of particles	mol
n	Number of segments	–
P	Component heat flux	W
P	Load acting on the structure	N
P	Power	W
p	Payload height	m
p	Pressure	Pa
Q	Heat flux	$W\,m^2$
q	Unit less reflectable surface	–
R_c	Encoded stream bit rate	bit s^{-1}
R	Distance between the spacecraft & body centre	m
R	Radiative factor	-
R	Universal gas constant	$J\,mol^{-1}\,K^{-1}$
r	Lower side of the shield between the outer radiation line and vertical RTG boom	m
r	Radius	m
S	Direct solar flux	$W\,m^{-2}$
S	Optimal scaling factor for manoeuvres	–
s	Upper side of the shield between the outer radiation line and vertical RTG boom	m
T	Temperature	K
T	Thrust	N
T	Torque	N m
t	Thickness	m
t	Time	s
t	Time	s
u	Lower side of the shield between the inner radiation line and vertical RTG boom	m
V	Particle velocity	$km\,s^{-1}$
V	Volume	m^3
V	Velocity	$m\,s^{-1}$
V_∞	Velocity at infinity	$m\,s^{-1}$
V_∞^+, V_∞^-	Incoming and outgoing relative velocity	$m\,s^{-1}$
w	Upper side of the shield between the inner radiation line and vertical RTG boom	m
x	Upper side of the shield between the radiation line and vertical RTG boom	m

Subscripts

0	At beginning
0	Launch
a	Albedo
bck	Backward propagated segments
C	Cold junction
cr	Critical
cyl	Cylinder
e	Electric
eq	Equivalent
f	Final/End
fwd	Forward propagated segments
g	Gravity gradient
HC	Hover Craft
i	Initial
i	Input
i	Node
ij	From node i to node j
lb	Lower bound
leg	Leg
m	Magnetic field

m	Manoeuvre
max	Maximum
min	Minimal
N	Nth leg
n	Number of hops per orbit
nat	Natural
p	Payload
$p-i$	Component as seen by the planet
s	Solar radiation pressure
$safe$	Planet safe
sp	Specific
T	Hot junction
T	Thrust
th	Thermal
ub	Upper bound
ult	Ultimate
x	x-direction
y	y-axis
y	y-direction
z	z-axis
z	z-direction

List of Abbreviations

AC Attitude Control.
ADCS Attitude Determination & Control System.
AOCS Attitude & Orbit Control System.

BER Bit Error Ratio.
BOL Begin Of Life.
BPSK Binary Phase Shift Keying.

C3 Characteristic Orbital Energy.
C&DH Command and Data Handling.
C&O Command and Operations.
CCSDS Consultative Committee for Space Data Systems.
COSPAR Committee on Space Research.
CRC Cyclic Redundancy Check.

DSE Design Synthesis Exercise.
DSN Deep Space Network.

ECSS European Cooperation for Space Standardization.
EJSM Europa Jupiter System Mission.
EOL End Of Life.
ESA European Space Agency.
ESAC European Space Astronomy Centre.
ESOC European Space Operations Centre.
ESTRACK European Space Tracking.
ETP Environmental Test Plan.
EVEES Earth Venus Earth Earth Saturn.

FBS Functional Breakdown Structure.
FDIR Fault Detection Isolation & Recovery.
FEC Forward Error Coding.
FFD Functional Flow Diagram.
FOV Field of View.

GALLOP Gravity-Assist Low-thrust Local Optimisation Program.

HC Hover Craft.
HGA High Gain Antenna.
HK Housekeeping.
HOI Hover Orbit Initiation.

IFOV Instantaneous Field of View.
INMS Ion and Neutral Mass Spectrometer.
IST Integrated System Test.
ITU International Telecommunication Union.

JUICE Jupiter Icy Moons Explorer.

KIPS Kilo Instructions Per Second.

LGA Low Gain Antenna.
LIDAR Light Detection and Ranging.
LOC Lines Of Code.
LOX Liquid Oxygen.
LP Loop.
LRO Lunar Reconnaissance Orbiter.
LROC Lunar Reconnaissance Orbiter Camera.

MAIT Manufacturing, Assembly, Integration & Test.
MALTO Mission Analysis Low-Thrust Optimiser.
MBH Monotonic Basin Hopping.
MEBM Main Engine Boost Mode.
MGA Medium Gain Antenna.
MIDAS Micro-Imaging Dust Analysis System.
MIL MIL-STD-1553.
MMH Monomethylhydrazine.
MOCET Mission Operations Cost Estimation Tool.
MON Mixed Oxides of Nitrogen.
MPPT Maximum Power Point Tracking.
MRO Mars Reconaissance Orbiter.

NAC Narrow Angle Camera.
NASA National Aeronautics and Space Administration.
NICM NASA Instrument Cost Model.
NTO Nitrogen Tetroxide.

OBT On-board Time.
OC Orbiter.
OCM Orbit Control Mode.

PDD Project Design & Development.
PPU Power Processing Unit.
PyGMO Parallel Global Multiobjective Optimiser.
PyKEP Parallel Keplerian toolbox.

QPSK Quadrature Phase Shift.

RAMS Reliability, Availability, Maintainability and Safety.
RST Radio Science Transponder.
RTG Radioisotope Thermoelectric Generator.
RW Reaction Wheel.
Rx Receiver.

SAM Sun Acquistion Mode.
SAURON Saturn AUtonomous Ring Observer Network.
SEE Standard Error of the Estimate.
SEL Single Event Latchup.
SEP Solar Electric Propulsion.
SEU Single Event Upset.
SHM Safe/Hold Mode.
SMAD Spacecraft Mission Analysis and Design.
SNOPT Sparse Nonlinear Optimiser.
SOI Saturn Orbit Insertion.
SQP Sequential Quadratic Programming.
SRO Saturn Ring Observer.
SSPA Solid State Power Amplifier.

TBD To Be Determined.
TCM Trajectory Correction Manoeuvres.
TLM Telemetry.
TOF Time Of Flight.
TSSM Titan Saturn System Mission.

TT&C Telemetry, Tracking and Command.
TTM Thrust Transition Mode.
TWTA Travelling Wave Tube Amplifier.
Tx Transmitter.

UDMH Unsymmetrical Dimethylhydrazine.
USO Ultra-stable Oscillator.
UTC Coordinated Universal Time.

VCB Verification Control Board.

WAC Wide Angle Camera.

Xpdr Transponder.

Contents

1 INTRODUCTION

The last voyage to Saturn, done by Cassini, focused its research on Saturn and its natural satellites. Only a limited amount of research was focused on the rings and no high resolution pictures of single ring particles exist. This leaves many questions about the exact ring dynamics and their origin. These rings might, for example, be representative for the formation of rocky planets around the sun. Thus, studying the Saturnian system in detail might shed new light on the formation and evolution of our immediate surroundings in the solar system.

Cassini's findings on the moons, Titan and Enceladus, showed the presence of complex molecules and maybe even prebiotic life, making the Saturnian system even more interesting for future research.

Currently, the JUNO mission is in orbit around Jupiter and will be followed by ESA's JUICE mission. This leaves the Saturn system unexplored after Cassini ends its Grand Finale in September 2017. The next step would be to send another mission to this system, which investigates unanswered science questions and search for answers to the big questions about Saturn's system.

The Saturn Autonomous Ring Observer Network (SAURON) mission will focus on the rings around Saturn, thus succeeding Cassini. The main goal will be to give insights on the formation and evolution of planetary ring systems. SAURON is a dual spacecraft concept, that will achieve this mission by performing scientific observations on the rings. SAURON can be seen in Figure 1.1.

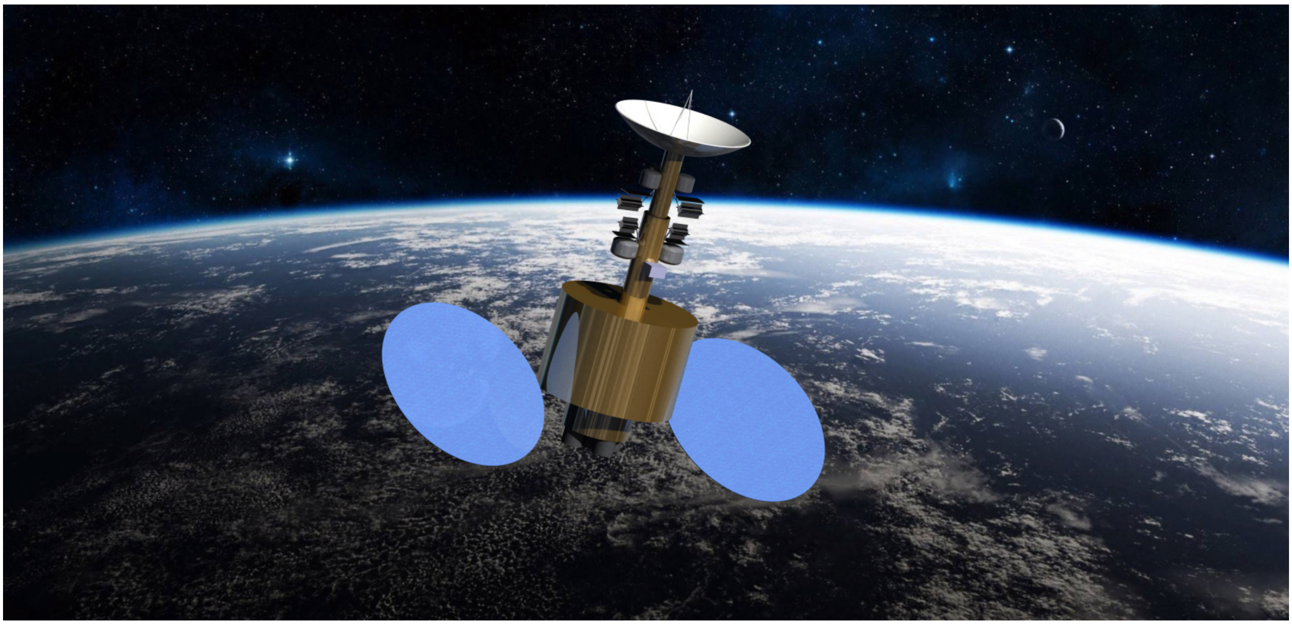

Figure 1.1: Schematic overview of the configuration

One spacecraft will stay in a high orbit around Saturn and map the rings, Saturn and the moons on a global level. The other spacecraft will move closer to Saturn and hover over the rings at a distance of 2-3 km to provide high resolution images of individual ring particles.

The scientific mission of SAURON has been subdivided in the following categories:

- Characterising the coefficients of restitution of the ring particles.
- Measuring velocity dispersion of the ring particles.

- Studying the characteristics of self-gravity wakes.
- Studying the detailed structure of propellers.
- Studying the perturbed ring edges.
- Characterising density waves.
- Determining the size distribution and spin states of ring particles with a diameter between 1-10 m.

The entire spacecraft segment will consist of four parts. The first two are the transfer stages: the solar electric transfer stage, and the chemical Saturn orbit and F ring orbit insertion stage. The hovercraft is then located on top of the orbit insertion stage, with the orbiter located on top of the hovercraft with an adapter.

The following report presents the work done on the detailed design for the SAURON mission. First, the Saturnian environment and science goals will be discussed in Chapter 2, which are followed by the requirements in Chapter 3. Next, the mission itself is analysed in Chapter 4 and its risks are assessed in Chapter 5. Afterwards, the top level system is presented in Chapter 6, followed by the subsystem designs and analysis in Chapter 7. The system performance is then described in Chapter 8. Having described the detailed design for the spacecraft, a planning for the next stages is included in Chapter 9 and the methods for verification and validation are described in Chapter 10. Lastly, conclusions and recommendations will be given in Chapter 11.

2

Saturn System and Science Goals

The following chapter presents the science case of the SAURON mission. First, the environment is described, followed by the science goals of the mission. Finally, the payload is selected and linked to the science objectives.

2.1. Saturn

Although the main scientific goals of the SAURON mission focus on the rings, a thorough investigation of Saturn itself remains important for the mission, since study of the planet will provide requirements to the design, but it might also provide additional science goals to the mission.

2.1.1. Orbit Properties and Related Phenomena

Assessing Saturn's motion around the Sun is of importance to the design of the spacecraft system. Trajectory planning, telecommunications, thermal control and several other subsystems depend on the orbit and the phenomena that are related to this motion.

2.1.1.1. Saturnian Seasons

Since Saturn's axis of rotation is tilted with respect to its orbital plane by 26.73° [1], the planet exhibits seasons. During the course of one Saturnian year, there will be two equinoxes and two solstices. During the equinoxes, the rings are positioned parallel to the orbital plane: observers from Earth see the rings edge-on. Approximately 7 years after an equinox, the maximum tilt is observed as Saturn reaches its solstice, during which one can distinguish its rings as they reflect sunlight back to Earth. Two solstices and one equinox are shown in Figure 2.1. From the image, one can see that a satellite orbiting at the edge of the A ring will have a longer communications eclipse time during equinox than at solstice. In the latter case, the orbit will form a 'corona' around the planet, rendering communications available nearly the entire orbit, as its orbital plane almost coincides with the ring plane.

This seasonal effect on communications windows requires the investigation of Saturn's position in orbit during mission operations at the planet. The last equinox took place on August 11, 2009 according to NASA [2]. Approximately 15 years later (half its orbital period), Saturn will reach another equinox in 2024. Since launch is scheduled for 2025, the spacecraft will arrive at Saturn in a solstice season. As the mission progresses, Saturn slowly moves back to equinox, reducing the orbiter's availability by approximately two hours every orbit. For more information, refer to Section 7.6.

2.1.2. Saturn's Radiation

The radiation emission level on Saturn is relatively low, because the Saturnian moons absorb some of the energy. Therefore, the radiation level from Saturn does not pose a major threat to the spacecraft. To protect the spacecraft's electronics from radiation, several techniques can be used. The Cassini-Huygens missions implemented the following techniques [3]:

- Shielding of materials
- Redundant use of hardware and software
- Avoiding materials that generate harmful byproducts
- Encapsulation
- Self-shielding spacecraft configurations

The estimated amount of open magnetic flux (Φ) at Saturn varies between 10 GWb and 50 GWb [4].

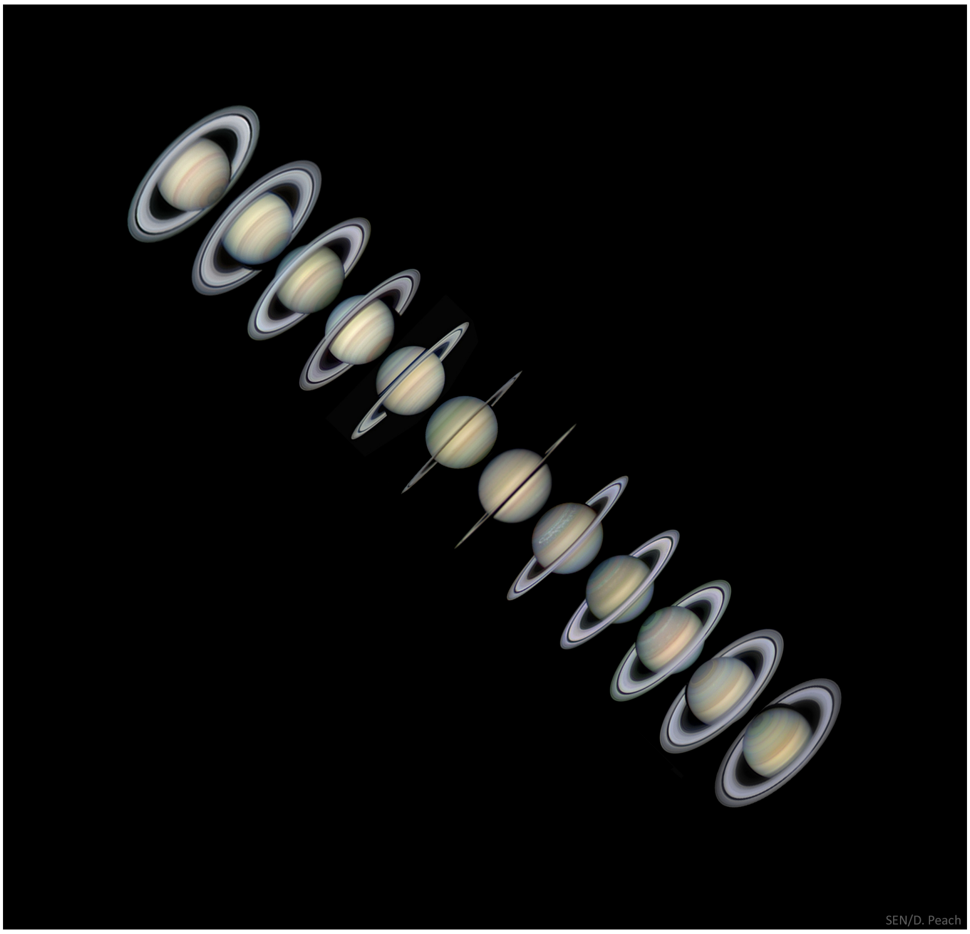

Figure 2.1: The different appearances of Saturn as it transits from one solstice to another [1]

2.1.3. SATURN'S MAGNETOSPHERE

Cassini's measurements have expanded the understanding of Saturn's magnetosphere, however, questions still remain about the magnetosphere that have yet to be answered. It is not known why the magnetosphere is lined up with the rotational axis of the planet. Furthermore, the spokes that occur in the rings may be caused by electrically charged particles trapped in the planet's magnetosphere [5]. The structure and strength of the magnetic fields can give insight on Saturn's structure, rotational rate and interaction with solar wind [2]. Since magnetic fields are best studied from within, being in close proximity to the rings would provide more information. Understanding the spokes phenomenon can contribute to the mission objective.

Observations by Cassini have given insight on the ionosphere of the rings The plasma flow velocity seems to be linked to the Keplerian velocity of the rings themselves. This plasma flow creates a current which closes along the magnetic field lines and through Saturn's ionosphere at latitudes between 36° and 48°, as well as producing Joule heating [6].

2.2. RING SYSTEM

The ring system forms the baseline for the scientific mission. Thus, it is important to know what questions are still left to answer after Cassini-Huygens. Knowledge of the dimensions and structure of the ring will give a clearer view on the areas of interest for the mission, especially the hovering spacecraft. This section will discuss both topics, starting with a general overview of the rings, after which the obtained knowledge of the rings will be investigated based on the Cassini, Voyager and Pioneer missions.

2.2.1. RING SUBDIVISION

Each of the main rings is named using alphabetical letters, based on their order of discovery. The main rings are comprised of the A ring, with the B ring lying closer to the planet, followed by the C ring, which lies even closer to the planet. In addition to these main rings, Saturn possesses a number of dusty rings. The D ring is located between Saturn and the C ring, while three other dusty rings are located outside of the A ring, which are in order of distance

[2] https://saturn.jpl.nasa.gov/science/magnetosphere/, consulted on 11/05/2017.

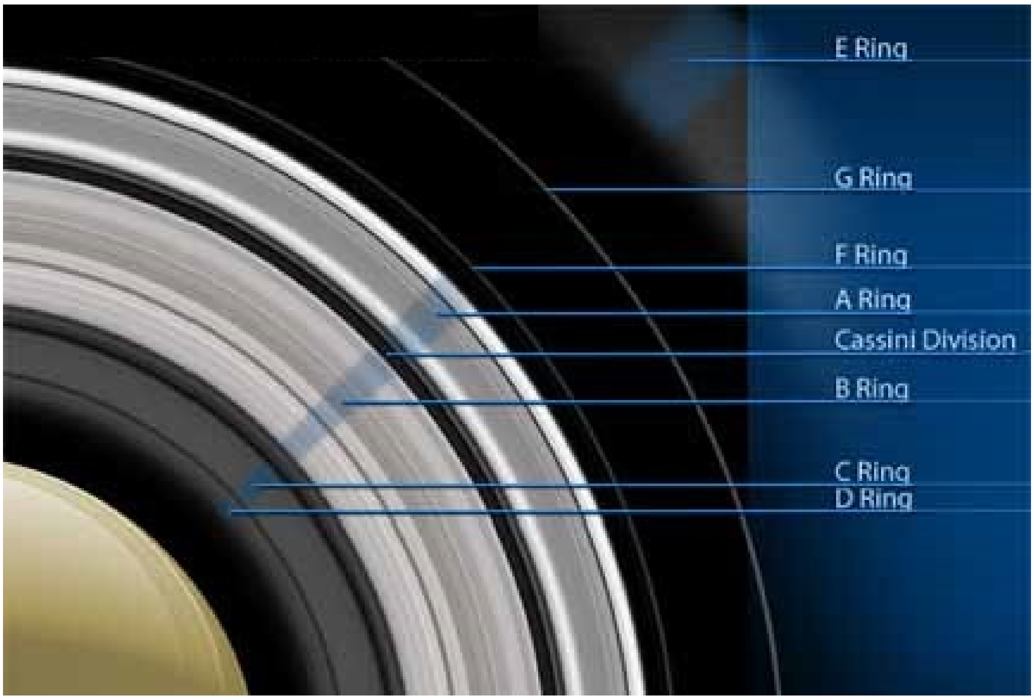

Figure 2.2: An overview of the rings of Saturn[3].

the F, G and E ring [7]. An overview of the ring system is seen in Figure 2.2[3]. The SAURON mission will focus its investigations on the A and B rings.

The rings are divided by regions of comparatively low particle densities, which are often created by moons or moonlets that clear their orbit of particles or by resonances of larger moons as described by Tiscareno [8].

Other key factors in the investigation of the formation of the rings are the composition and size distribution of the ring particles. The ring composition evolves over time, under influence of irradiation by photons and bombardments by magnetospheric and ionospheric particles or interplanetary meteoroids and possibly also by chemical reactions with the oxygen atmosphere that are locally produced by the rings. The bulk of the rings are made of water-ice, however, the rings seem red at visual wavelengths, which indicates that other materials can be found in the rings as well, according to Cuzzi [9].

2.2.2. A RING

The A ring forms the second ring of Saturn that can be observed from the Earth. It is located approximately between 122170-136775 km from the centre of Saturn. Similar to the B ring, the A ring is mostly composed of water-ice [10].

The Cassini mission found that the birth of a number of Saturnian moons could be revealed by investigation of the A ring[4]. The A ring includes about 150 different, discovered moonlets [11]. Through the SAURON mission, these moonlets can be further studied.

Inside the A ring, two small divisions are observed, the Encke and Keeler gaps. These two gaps are created by two of Saturn's smaller moons. The Encke gap is created by Pan, while the Keeler gap is cleared of particles by Daphnis, which have radii of 15 km and 4 km, respectively [12]. When the Cassini mission observed the small moon Daphnis, scientists found that Daphnis' orbit had an inclination of about 0.0036°, resulting in vertical excursions of about 9 km from the ring plane [13].

Waves haves also been observed at the edge of the Keeler gap, called spiral density waves; these can be seen in Figure 2.3. They occur only near Daphnis and have an amplitude of approximately 1.5 km from the ring plane [10].

At the outer edge of the A ring lies another large gap. This is caused by the gravitational pull of the moons Janus and Epimetheus. Any particles just outside the outer edge of the A ring will be pulled into the rings by the gravitational pull of these moons [10].

These phenomena are of interest for scientists that were contacted during the market analysis and are included in the science objectives for this reason[5].

Between the A and B rings, the Cassini Division is located. This gap is thought to exist due to the gravitational pull of the different moonlets that are in the A and B ring. The clearing of the ring particles in this gap is thought to be the work of the moon Mimas [14]. The gap appears to be nearly empty, but some small particles might be present in the

[3] http://www.skymarvels.com/infopages/saturninfo.htm, consulted on 10/05/2017.
[4] https://www.jpl.nasa.gov/news/news.php?release=2014-112, consulted on 11/05/2017.
[5] Spilker, L.J., private communication, May 11, 2017.

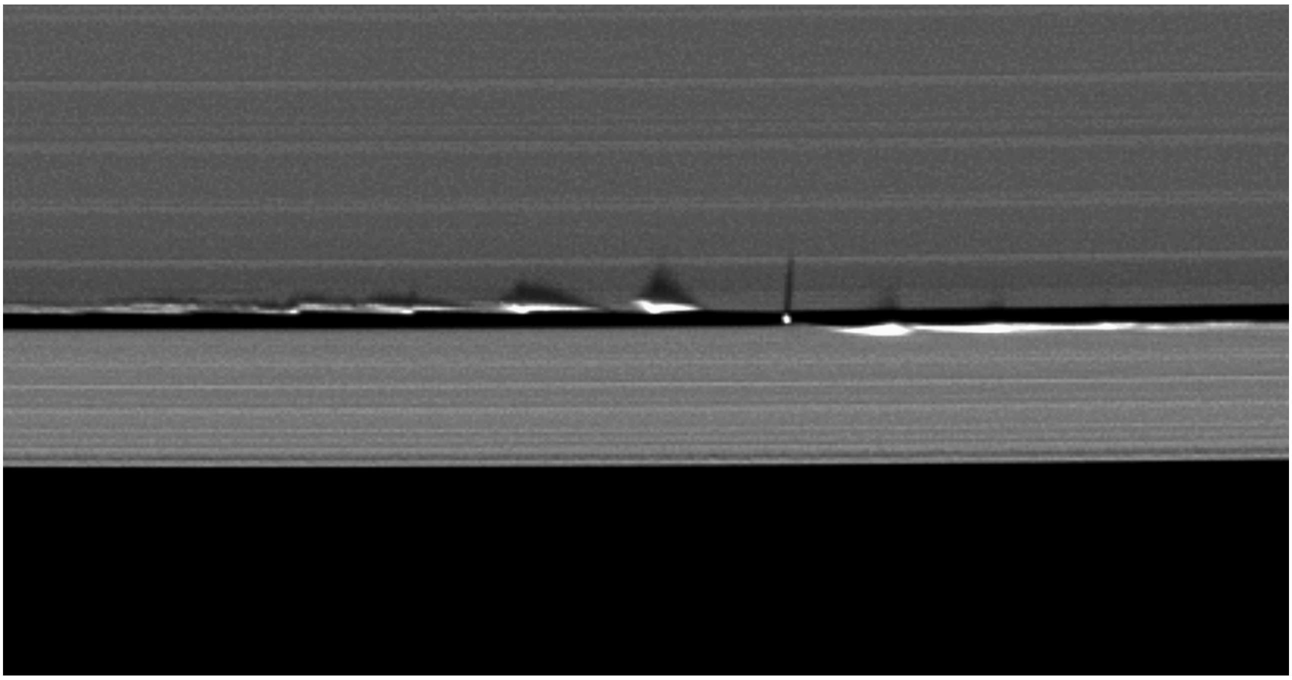

Figure 2.3: Daphnis together with the vertical structures at the edges of the Keeler gap. Picture taken by the Cassini spacecraft[4].

region. A close proximity observation of the Cassini Division allows for a study of the presence and composition of these particles.

2.2.3. B RING

The B ring is one of the brightest regions of the rings of Saturn, which would be a good location to see the dynamic relationship between the ring particles. It is mostly composed of water-ice particles of varying size. This region covers a distance of approximately 92000-117580 km from the centre of Saturn[6]. The ring particles deviate about 2.5 km vertically from the median ring plane at the outer edge[7].

Furthermore, small moonlets are present in the rings, which were already identified by the Cassini mission, but with a close proximity exploration new insights on their formation and interaction with the rings could be obtained.

Saturn's rings also contain phenomena known as spokes, which appear seasonally around the Saturnian equinox and vanish around midwinter. If the spacecraft observes the rings when the spokes are visible, they can be studied in more detail[8].

2.2.4. F RING

Although the F ring is not a primary target for the mission, it is necessary to investigate its structure since it lies next to the A ring, divided by the Roche division, as it could influence the trajectory of the hover orbit insertion.

The ring has an inclination of about 0.006° with respect to the equatorial plane, resulting in maximum vertical deviations of 15 km [15]. Together with a thickness of 10 km, it is clear that the trajectory for the hover orbit insertion has to maintain a considerable distance to prevent particle collisions.

2.3. NATURAL SATELLITES

Saturn currently has 53 confirmed moons and 9 provisional moons[9]. In Figure 2.4, the location of some of Saturn's moons are illustrated. The largest moon is Titan with a diameter of 5150 km. Cassini-Huygens revealed that Titan had many parallels to Earth - clouds, dunes, mountains, lakes, and rivers[9]. It was also estimated that there could be prebiotic life on Titan. Therefore, interest in observing the moons of Saturn has increased. In addition, it was estimated that there is potential for prebiotic life on Enceladus. For this reason, both moons have been specifically mentioned in the COSPAR Planetary Protection regulations, which is explained further in Section 2.4 [16].

There are 16 tidally locked moons orbiting Saturn. Some moons stay in the lagrangian points of Saturn. This phenomenon occurs 60° ahead or behind a larger moon in the same orbit. The moons Telesto and Calypso are on lagrangian points of Tethys, and the moons Helene and Polydeuces are on lagrangian points of Dione[9].

[6] https://caps.gsfc.nasa.gov/simpson/kingswood/rings/, consulted on 11/05/2017.
[7] https://photojournal.jpl.nasa.gov/catalog/PIA11668, consulted on 11/05/2017.
[8] http://www.space.com/25856-saturn-ring-spokes-photo.html, consulted on 11/05/2017.
[9] https://solarsystem.nasa.gov/docs/14_Moons%20of%20Saturn_Revision%202013_tagged_FC_order_FINAL.pdf, consulted on 12/05/2017.

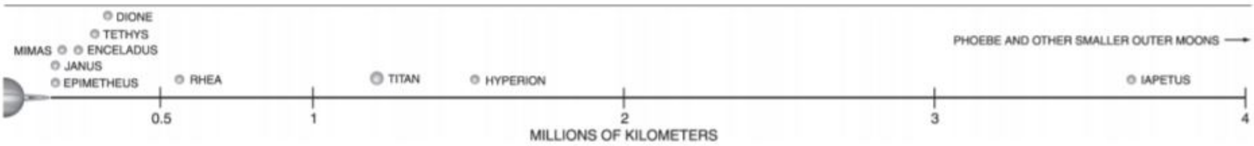

Figure 2.4: Some of Saturn's moons are shown at relative distances to the planet[9].

2.4. PLANETARY PROTECTION

To deal with any concerns from the scientific community and public, planetary protection regulations have been set up by the Committee on Space Research (COSPAR). The categories that are of importance to this specific mission are categories II and III. Category II missions include any targets that might give insights into the chemical evolution or formation of life. For this mission, Saturn and Titan are the main objects that fall into this category. Category III includes flyby and orbiter missions to targets where a contamination could significantly damage the future investigations into chemical evolution and the formation of life. Flybys of Enceladus would require this level of decontamination procedures.

2.5. MARKET ANALYSIS

Using a market analysis, the interests of the scientific community were investigated. Several experts have been consulted to find out what the SAURON mission could contribute to their area of expertise.

The first set of additional goals relate to the moons of Saturn. Contact with professor Bert Vermeersen has rendered more question regarding the ring moon interactions. The exchange of material and the magnetic field interactions might give new insights on the formation and evolution of planetary systems[10].

Secondly, the interaction between the rings and the Saturnian atmosphere was brought to the team's attention by professor Daphne Stam. In particular, the influence of the shadow of the rings and the loss of material from the innermost rings into the atmosphere might provide new insights on the composition and dynamics of Saturn's atmosphere, and the evolution of the rings[11].

Professor Imke de Pater was contacted to confirm the previously provided science goals and to obtain more knowledge on little studied phenomena in the rings. This led to the confirmation of the value of the main science requirements, as well as the introduction of spoke and material clumping[12].

Finally, email contact with Dr. Linda Spilker confirmed that the main science goals have not yet been covered in high resolution and close proximity by previous fly-bys or orbits of the Saturn system. This led to the inclusion of a high-resolution camera in the science requirements. Specifically, the exact dimensions of ring particles and their interactions remain unknown as of now and would contribute to the scientific yield[13].

2.6. MISSION SUCCESS AND OBJECTIVES

Both to analyse the science case and to generate requirements, mission success has to be defined. The scientific objectives have been grouped into two categories. The primary mission objective and the secondary mission objective. The primary mission objective is the main focus on the mission and the spacecraft will be designed around this. The secondary mission objectives only enhance the mission and will not be preformed at the cost of the primary mission objective and will not drive the selection of instruments.

2.6.1. DEFINITION OF MISSION SUCCESS

The mission success will be defined using a point system, thus ensuring that missing any measurements due to phenomena that cannot be influenced by the mission design. In the point system both conditions for full mission success and partial mission success are determined. Each of the objectives is given a score, which is based on their importance, the chance that the spacecraft will not be able to observe it and the difficulty of performing the measurements. The point system can be seen in Table 2.1. The objectives that are definitely required for mission success are named as essential. If any of the essential objectives are not accomplished the mission is considered to be a failure. These are objectives that the SRO mission will be able to perform much better than other missions, specifically due to the proximity to the rings. The high yield mission objectives provide the mission with data that sets this mission apart from other previous observations of the system, mainly by providing higher quality images. However, these would also be achievable by another The low yield main objectives include measurements that have already been studied before and for which detailed models already exist. The high yield additional objectives are defined in the same way as the

[10] Vermeersen, L.L.A., Delft University of Technology, private communication, May 1, 2017.
[11] Stam, D.M., Delft University of Technology, private communication, May 2, 2017.
[12] De Pater, I., University of California, Berkeley, private communication, April 30, 2017.
[13] Spilker, L.J., Jet Propulsion Laboratory, private communication, May 11, 2017.

high yield main mission. However, these additional objectives are not included in the project description and this not essential for the design. The low yield additional objectives are also not described in the project description and do also not provide a high scientific yield. They will only be performed when all of the above objectives are achieved or determined to be unachievable due to for example instrument failure.

Apart from that, each objective that is accomplished provides the mission with a certain amount of points based on their importance. In order to reach partial mission success at least 25 points should be achieved. This was based on the 15 points from the essential objectives along with half of the non-essential main objectives (total of 21 points). Complete mission success is only achieved when all of the main mission objectives have been accomplished.

The additional mission objectives are not yet included, since it is not certain that they will be included in the final mission design.

Table 2.1: Scoring system for mission success

Points	Objective value
5	Essential objective
4	High yield objective
3	Low yield objective
2	High yield secondary objective
1	low yield secondary objective

Table 2.2: Scoring system for mission success

Mission objective	Points
Coefficients of restitution	5
Velocity dispersion	5
Larger Particles	5
Gravity wakes	4
Propellers	4
Perturbed ring edges	4
Density waves	3
Spokes	3

2.6.2. PRIMARY MISSION OBJECTIVES

The primary mission objective is to investigate the composition and particle dynamics of Saturn's Rings. If any of these measurements are not performed and received at the ground station, it will reduce the mission success. The primary mission objective to investigate the composition and dynamics of the rings can be described by the list of measurements in this subsection.

- Make observations of kinematics processes at the level of individual particles.
  1. Characterising the coefficients of restitution of typical collisional interaction for collisions of particles of at least TBD individual collisions.
  2. Measuring the components of the rings particles' velocity dispersion based on TBD particles at TBD locations.
  3. Determining the spin states and size distribution of particles larger than 1m for at least TBD independent particles with an approximately equal distribution over the size range.
- Study the dynamics of the rings.
  1. Study the development, dimensions, packing density and dissolution of self-gravity wakes achieved if the packing density and dimensions are known for TBD wakes. Study the development and dissolution if they occur at the locations of interest.
  2. Determine the detailed structure of propellers for at least TBD propellers.
  3. Study the perturbed ring edges for at least TBD ring(let)s.
  4. Characterise density waves in the rings for at least the entire A and B rings.

2.6.3. SECONDARY MISSION OBJECTIVES

In addition to the primary mission objective, secondary mission enhancing science objectives have been identified. The secondary mission objectives cover some measurements that are not in the primary mission objectives, but could also be preformed during the mission. However, any secondary mission objectives will be discarded if it negatively effects the primary mission objective. The list in this subsection displays the various secondary objectives that could be preformed by this mission. Also, the exact conditions for achieving them is not yet determined, since those conditions have to be investigated further and might depend on the space system design and payload selection as well.

- Study the changes in the atmosphere due to the shadow of the rings.
- Determine whether ring particles are raining down into the atmosphere.
- Analyse the the magnetic field connections between the rings and the moons.
- Determine the rate of loss of material in the rings.
- Determine the change in location of the rings due to changes in moon mass and orbit.
- Characterise changes in the stability of the rings.
- Study the composition of the ring particles.

Additional scientists have been contacted regarding the mission and instrumentation and thus this list might still undergo changes. However, none of the main mission objectives will be removed.

2.7. INSTRUMENTATION

After the determination of the science objectives and measurements, instruments have to be matched to these measurements. For the current stage of design, only the options per objective will be listed and a final selection will be made after the concept that is worked out in the final design is selected. Based on the science objectives in this chapter the following instruments are proposed. In addition to these instruments, on board sensors used for orbit and attitude determination could also be used to gather scientific data.

- Altimeter
- Dust analyser
- INMS
- LIDAR sensor

- Magnetometer
- Radar/Radiometer
- Spectrometer
- Visual imaging instrument

2.8. SCIENCE OBJECTIVES

The Cassini-Huygens mission greatly increased the understanding of the Saturnian environment and the solar system dynamics in general, however, still many questions are left and new ones have arisen that cannot be covered by Cassini before the end of its Grand Finale. A detailed study of the Saturnian rings and surrounding system will provide answers to many of these questions, which are summarised in the science objectives for the SAURON mission. These top-level objectives can be found in Table 2.3, along with the subsection where they will be discussed in detail.

Table 2.3: Top-level science objectives for the SAURON mission.

Label	Science objective	Reference
AR	Investigate the physical interaction between the rings and the atmosphere	Subsection 2.8.1
DW	Characterise the density waves that are found in the rings	Subsection 2.8.2
IP	Determine the specific properties of individual ring particles	Subsection 2.8.3
MR	Characterise the interactions between Saturn's moons and rings	Subsection 2.8.4
RE	Study the perturbed ring edges	Subsection 2.8.5
PR	Study the propellers in the rings	Subsection 2.8.6
RD	Characterise the ring dynamics	Subsection 2.8.7
GW	Characterise the behaviour of self-gravity wakes	Subsection 2.8.8
SP	Observe the development of spokes	Subsection 2.8.9

2.8.1. ATMOSPHERE-RING INTERACTIONS

The investigations with regard to the atmosphere-ring interactions have been obtained through contact with Professor Daphne Stam. The region underneath the ring is assumed to be influenced by the rings. Material which falls down from the rings and the shadow that the ring casts on the atmosphere are considered.

The 'ring rain' was investigated during the SOI of the Cassini spacecraft and, during its Grand Finale, Cassini will study this phenomenon in greater detail, which allows for estimates of the ring age [17]. Electron densities have been found to be lower than expected in the upper atmosphere, which might originate from magnetic field connections between the rings and the atmosphere, since a glow in the upper atmosphere can be observed along the gaps in the rings. This suggestion implies the rain-down of water particles into the atmosphere, as explained by O'Donoghue [18].

2.8.2. DENSITY WAVES

The density waves form a prominent feature of the rings in the Saturn system and a more detailed study might give insights in the mass of the rings themselves [19]. Research does suggest that these density waves change over time. Thus, new observations following Cassini might shed new light on the dynamics of the rings and their evolution over time [20].

2.8.3. INDIVIDUAL RING PARTICLES

Ring particles are compactly packed in the rings, making it difficult to deduce characteristics of individual ring particles from Cassini measurements [21]. Ring particles have often been assumed to be spherical, fast-rotating particles, but this does not fit the clumping and thermal models that have been made [22]. In the SAURON mission, the hovering spacecraft will provide close-up images of these individual particles at higher resolutions, which will allow to judge the accuracy of the aforementioned models.

2.8.4. MOON-RING INTERACTION

The moons affect the rings as well. The rings are composed of 90%-95% ice, which is also observed in moons interior to and including Thetys. Current models cannot reproduce the distribution of rocks and ice in the moons [23]. Other interactions include the replenishment of E ring material by plumes on Enceladus, which includes ice, organic compounds and salts [24].

2.8.5. PERTURBED RING EDGES

Previous observations of the rings showed that the outer edge of Saturn's B ring is strongly perturbed by resonance with Mimas. The structure immediately interior to the ring edge has not yet been observed, but will give insight on the propagation of the perturbations [20]. Other rings also show perturbations of the edges due to Lindblad resonance with Saturn's moons, which can be studied through imaging [25].

2.8.6. Propellers

Propeller gaps form around small moonlets in the ring, which are not massive enough to clear their orbit from particles like the smaller moons [26]. The only observed propeller that show clear propeller gaps is Bleriot, which has been observed by Cassini's Narrow Angle Camera [27]. Research has shown that there are three propeller belts within 127,000-132,000 km from Saturn's centre. Together, these belts contain 7,000-8,000 propeller moonlets with radii larger than 0.15 km and form a main area of study for the mission [28].

2.8.7. Ring Dynamics

The ring dynamics include a number of phenomena in the rings. These include, coefficients of restitution between particles and their clumping, the particle velocity dispersion and their spin states. Cassini's UVIS occultation data indicated clumping of material in the F ring and outer B ring and is perturbed by the moons Prometheus and Mimas. Clumping is expected in the other perturbed ring regions, such as propellers and density waves [29]. The collisions between the particles are expected to lose a relatively high amount of kinetic energy, due to surface roughness and porosity, which lower the coefficient of restitution. This also lowers the velocity dispersion of the ring particles, which is linked to the collisions in the rings [30].

2.8.8. Self-Gravity Wakes

Self-gravity wakes have been observed in Saturn's rings through stellar occultation by Cassini's UVIS. The wakes were found to be highly flattened structures with height/width ratios between 0.15 and 0.37 in the A ring [31]. The B ring includes even more flattened wakes, with height/width ratios smaller than 0.1 [32].

2.8.9. Spokes

During Saturn's equinox in 2009, dusty clouds have been observed above the rings, called spokes. These spokes are suggested to originate from streams of recently disrupted material from a meteoroid impact, which were observed hours before the dust clouds occurred [33]. Theoretical models have been developed, but no consensus has been reached for the exact origin of these spokes. Possibly the particles hover over the ring plane by interacting with the plasma environment until they reach charge neutralisation, however, this would require a very low grain mass [34]. Another influence on the dust particles is presented by the electromagnetic field. Large ring particles are dominated by gravitational forces, while dust-sized particles are dominated by electromagnetic forces [35]. SAURON will look deeper into these interactions and search for possible meteoroid impacts which might impact the spoke formation.

2.9. SAURON Timeliness and Link to ESA Cosmic Visions

The Cassini mission will end its mission on September, 2017, without a follow-up mission as of yet. NASA's JUNO mission and ESA's JUICE mission both explore the Jovian system and will be the furthest orbiting spacecraft in the Solar system. The JUICE mission will aim to answer questions about the solar system by considering Jupiter as a miniature Solar system. The Saturnian system might similarly be considered as a miniature Solar system, albeit in a different stage. The more dense and extensive rings might give insights in the formation of the rocky planets in our system, as well as the formation of natural satellites.

Multiple mission concepts have already been proposed to investigate the Saturn system, mostly focusing on Titan and Enceladus for their potential for life. The Titan Saturn System Mission (TSSM) is currently still under study, while it was put on hold when the Europa Jupiter System Mission was given priority[14]. All of the missions put emphasis on the search for organical compounds and potential micro-organisms, which the orbiter of the SAURON mission can also perform. Thus, the SAURON mission falls in line with the relatively short-term goals of ESA's Cosmic Visions and will differentiate itself from other missions by giving a more detailed investigation into the ring systems and their origins.

2.10. Instrument selection

This subsection will discuss the selection and performance of the selected instruments.

2.10.1. Wide Angle Camera

A Wide Angle Camera (WAC) was selected based on the ring dynamics requirements. To map a larger area of the ring and to determine the locations of areas of interest, the WAC has an advantage over the Narrow angle camera in the form of a wider field of view.

[14] http://sci.esa.int/cosmic-vision/44249-nasa-and-esa-prioritize-outer-planet-missions/, consulted on 13/06/2017.

The WAC for the SAURON mission will be the same for both spacecraft and uses JunoCam as its heritage. It will be used to provide high-resolution images of the Saturnian system both for scientific purposes and for scientific outreach to the general public. The WAC will be a pushbroom imager, similar to JunoCam and MRO's Mars Color Imager [36]. Table 2.4 and Table 2.5 show the specifications for the WAC [37]. The WAC has a resolution of 3 km/pixel at 5000 km and will allow the orbiter to determine the areas of interest in the rings in high detail.

2.10.2. NARROW ANGLE CAMERA

A Narrow Angle Camera (NAC) was included in the design for a detailed study of individual particles and structures in the rings. The rate of ring particles raining down in the atmosphere might be obtained through observations by this instrument as well. The NAC relates mainly to the requirements on the characterisation of individual ring particles. Other objectives that will be met by the use of this instrument include ring edges, density waves, propellers and ring dynamics. The specifications of the NAC were based on the Lunar Reconnaissance Orbiter Camera (LROC), however, the instrument design itself will have to undergo a number of changes to make it fit for the Saturn environment [38].

The NAC system included two monochrome cameras. Specifications for the combined system can be found in Table 2.4 and Table 2.5.

2.10.3. DUST ANALYSER

The dust analyser that will be used for this mission, was based on Rosetta's MIDAS heritage [39]. The instrument was based on an atomic force microscope and will perform three-dimensional imaging of small particles. This will give insight on the particle composition. The dust analyser will be able to perform measurements of dust particles with a resolution of 4 nm and is able to determine the shape, volume and size of individual particles. Additionally, it will measure the temporal variation in particle flux.

For this purpose, the dust analyser will be able to create both global images of its entire scan field and images of individual particles. The individual particles are identified by the on-board computer system and are then re-scanned at a higher resolution.

A performance summary of the dust analysis system can be found in Table 2.4 and Table 2.5.

2.10.4. MAGNETOMETER

The magnetometer will be able to measure the magnetic field strengths around Saturn. Ring structures, such as spokes, are thought to be influenced by Saturn's magnetic field. Since, the magnetic field is best measured from the inside, the closer mission to the rings allows for better observations than Cassini could perform during its mission.

The selected magnetometer has been investigated by the Österreichische Akademie der Wissenschaften and has been specifically designed for space applications in radiation environments. The electronics can handle a radiation dose of up to 100 krad, sufficient for Jupiter missions [40]. Since the Saturn environment is less severe than the Jovian system, it is safe to assume that the magnetometer will also remain functional for this mission. Specification for the magnetometer can be found in Table 2.4 and Table 2.5.

2.10.5. RADIO SCIENCE INSTRUMENT

The radio science instrument is included to measure the Doppler effect of ring particles, moonlets and larger components in Saturn's rings. This will allow scientists to measure relative velocities of these particles relative to the spacecraft. The radio science will also be used to determine the atmospheric composition.

The radio science instrument will consist of a radio science transponder and an ultra-stable oscillator and will use parts of the telecommunications subsystem. The system will allow for characterisations of the gravity field of the rings and the moons, as well as a study of the atmosphere of Saturn and Titan. As a reference the JUICE radio science experiment has been used [41].

Table 2.4 shows the specifications of the radio science instrument.

2.10.6. IR SPECTROMETER

The IR spectrometer will be used for thermal mapping of the components of the Saturnian system. In addition, the IR spectrometer will be used to determine the composition of ring particles at a closer distance, focusing on rocky particles, which make up only a small amount of the rings. These rocky particles might indicate that meteorite bombardments contributed to the formation or replenishment of the rings.

The SAURON IR Spectrometer is based on the instrument designed for the Titan Saturn System Mission concept, which is in turn based on the Cassini CIRS and Mars TES on the Mars Global Surveyor [42] [43].

2.10.7. ULTRAVIOLET IMAGING INSTRUMENT

The ultraviolet imaging instrument will be used to perform measurements on the atmospheric composition and will be used for occultation measurements to observe ring particle distributions. The instrument will be used during the eclipse, where measurements at visual wavelengths will result in lower scientific yield. The UV Imaging Instrument will be based on LRO's LAMP legacy, which in turn is based on Rosetta's and New Horizon's ALICE [44] [45].

2.10.8. Plasma and Energetic Particle Package

The plasma and energetic particle package will be used to study the plasma and radiation in the Saturnian system. The influence of plasma and radiation on the degradation of ring particles will be investigated to determine the ring's stability. From this, the ring age and the replenishment of ring particles will be studied.

The plasma and energetic particle package was based on Juno's JEDI instrument [46]. Its measurements will characterise the radiation environment around the rings, which can consequently be linked to degradation of ring material.

2.11. Instrument configuration

The instruments are divided over both spacecraft, based on the requirements flowing from the science objectives. First, the main orbiter instrument layout is discussed, followed by the hovercraft.

2.11.1. Main Orbiter

Based upon the above science objectives, a selection has been made for the instrument suite. This selection assumes that budgets allow for a maximum scientific yield and therefor takes into account a level of redundancy in the instruments. Table 2.4 presents an overview of the payload selection for the main orbiter, including the name, mass, power and data rate of the subsystems. Additionally, the contribution to the science mission, the heritage instruments and the science objectives that are linked to the instrument are linked. Each of the instruments is shortly discussed and an explanation for their role in fulfilling the objectives is presented.

The main orbiter will use a wide angle camera for the global mapping of the rings, from which areas of interest for further investigations can be determined. It will be used for public outreach as well, similar to Junocam [47].

The main orbiter NAC is mainly used for the detailed study of larger ring structures. It will focus its measurements on the detailed dimensions of propellers, gravity wakes and larger ring particles, such as the moonlets. b The infrared spectrometer will be used to determine the temperatures of ring particles, Saturn and the moons. It will also help to track cloud features, which is linked to the scientific objective of characterising the atmosphere-ring interactions. On a global level, the composition of water in the rings can be measured from the main orbiter.

The ultraviolet spectrometer will also be used for these atmosphere measurements, while also focusing its investigations on relatively smaller ring particles and their effect on the rings.

A magnetometer will measure the interaction between the magnetic field of Saturn and the natural satellites with the rings at a relatively large distance.

The Plasma and Energetic Particle package complements the measurements from the magnetometer by measuring the energetic particle flux at a larger distance to the rings. This both helps determine the radiative environment of the Saturnian system, but might also show the absorption by ring materials, thus giving insights in the composition of these.

The Radio Science Instrument is included in the telecommunications subsystem. Through occultation it will measure the density waves in the rings. Additionally, it will use doppler shift to give insights in the gravitational field of the Saturnian system.

Finally, the dust analyser will be used to determine the composition of dust particles in the system. This can be linked to both spokes, which are pillars of dust, and to the composition of ring particles themselves.

2.11.2. Hovercraft

Table 2.5 shows the layout of the instruments on the hovercraft. Each of the instruments is based on the same heritage as the main orbiter, however, the scientific objectives that it fulfils differ. The wide angle camera will be used to create a higher detail in the mapping of the ring structures such as propellers and gravity wakes.

The NAC will be used to observe ring particles with a resolution of up to 3cm/pixel and measure their restitution after a collision. It will also provide a closer look at the perturbed ring edges and potential ring material raining down into Saturn's atmosphere.

An Infrared Spectrometer and Dust Analyser will together give insights in the composition of the ring particles. Again, the dust analyser will give insights in the composition and formation of spokes. The IR Spectrometer is also used to obtain the spin states of the particles.

Finally, a magnetometer is included to measure the magnetic field in close proximity to the phenomena in the rings to find out how these influence each other.

2.11.3. Payload Market Analysis and Cost Analysis

The payload selection was based on the market analysis for the scientific objectives and will be assumed appropriate for the demands from the scientific community. A more detailed market study for the instruments is difficult to perform, since for space missions, the instruments are designed specifically for the mission, while using the heritage of older missions. All instruments do have a large number of predecessors and will not take excessive levels of required development.

The cost estimate makes use of the NASA Instrument Cost Model (NICM) [48]. The total cost is found in Table 2.6.

Table 2.4: Instrument overview for the main orbiter

Model instrument	Mass [kg]	Power [W]	Downlink data rate [kbps]	Science contribution	Example heritage	Linked science objectives
Wide Angle Camera	5.0	6.0	10,000.0	Global mapping of the rings; Determining areas of interest; Public outreach	JunoCam	RD; RE
Narrow Angle Camera	13.2	9.3	30,000.0	Detailed imaging of propellers, gravity wakes and large ring particles	OSIRIS-NAC/ LROC	PR; GW; IP; RE
Infrared Spectrometer	9.3	17.6	10.0	Composition of non-water ice components of ring particles; State and crystallinity of water ice. Saturn: Tracking of cloud features; temperatures; Measuring the effect of larger particles	TSSM concept	IP; AR; RD
Ultraviolet Spectrometer	6.1	6.1	10.0	Ring-atmosphere interactions; Measuring the effect of smaller particles through stellar occultation	LAMP	AR; RD
Magnetometer	1.4	1.0	4.0	Interaction between rings and magnetic field;	Österreichische Akademie der Wissenschaften	SP; MR
Plasma and Energetic Particle Package	7.2	9.1	48.0	Study the plasma environment around the rings; Determine interactions between the rings and the environment	JEDI	SP; MR
Radio Science Instrument	0.0	0.0	100.0	Density waves; Determination of the gravitational field	JUICE/Cassini	DW; RD
Dust Analyser	8.0	7.4	0.1	Composition of spokes; Dust environment near the rings; Composition of ring particles	MIDAS/CDA	SP; IP
Total	50.2	56.50	40,172.1			

Each of the cost estimates is based on the type, mass, peak power and design life of the instruments and is used by NASA and all its subcontractors.

2.11.4. RAMS ANALYSIS

Each of the instruments were based on flight-proven designs from previous missions, all of which have operated for at least their nominal lifetime. This makes it reasonable to assume that each of the instruments has a sufficient reliability to meet the requirements. In addition, the instruments overlap each other for many of the scientific objectives, leading to a level of redundancy in the payload design.

Due to power requirements, the full payload suite is not operable at all times. A planning for the active instruments per orbit will have to be created during the development stage, based on the location and scientific objectives. All of the instruments have been flown before, with the exception of the magnetometer. In general, the payload would thus be readily available without much further development. Also, the concepts for the magnetometer and has been worked out extensively and thus it can be safely assumed that this instrument will be available for the spacecraft.

Like other parts of the spacecraft, the instruments will not be maintainable after launch. For this reason, a kinematic mounting system for sensitive equipment should be considered in the detailed design to account for deformations due to the change in environment.

In case of a delay in launch, instruments can be regularly in a laboratory environment to confirm that they remain

Table 2.5: Instrument overview of the hover spacecraft

Model instrument	Mass [kg]	Power [W]	Downlink data rate [kpbs]	Science contribution	Example heritage	Linked science objectives
Wide Angle Camera	5.0	6.0	10,000.0	Mapping of propellers, gravity wakes;	JunoCam	PR; GW
Narrow Angle Camera	13.2	9.3	30,000.0	Determining the dimensions and structure of ring particles at a resolution of 3cm/pixel; Characterising the coefficient of restitution	OSIRIS-NAC/ LROC	IP; RD
Infrared Spectrometer	9.3	17.6	10.0	Determining heat signature of the ring particles; Determining rough composition of particles; Characterising spin states of ring particles	TSSM concept	IP; RD
Magnetometer	1.4	1.0	4.0	Measuring the magnetic field originating from the rings;	Österreichische Akademie der Wissenschaften	RD
Dust Analyser	8.0	7.4	0.1	Studying composition of dust around the rings; Determining the composition of spokes	MIDAS/CDA	RD; SP
Total	36.9	41.30	40,014.10			

Table 2.6: Cost overview of the scientific payload

Main orbiter		**Hovercraft**	
Instrument	**Cost (M€)**	**Instrument**	**Cost (M€)**
Wide Angle Camera	15.5	Wide Angle Camera	15.5
Narrow Angle Camera	8.5	Narrow Angle Camera	8.5
Infrared Spectrometer	17.4	Infrared Spectrometer	17.4
Ultraviolet Spectrometer	8.3	Magnetometer	28.5
Magnetometer	28.5	Dust Analyser	12.7
Plasma and Energetic Particle Package	13.8		
Radio Science Instrument	In telecommunications		
Dust Analyser	12.7		
Total	104.7		82.6

functional and calibrated.

During flight, the instruments will also be calibrated with measurements from other spacecraft to validate their correct functioning and accuracy.

The production and operation of the scientific instruments will not impose any additional safety hazards to the mission and crew involved. No hazardous materials are used in the production process of the individual instruments.

2.11.5. Payload Technology Verification and Validation

Verification of the payload measurements can be performed through the use of environmental models. Different spectra are to be considered, the SATRAD model can be used for radiation [49].

Related to the main mission goals, models of the ring dynamics can be used to verify the payload performance, but it should be considered that the new measurements can prove the models wrong.

To validate the measurements performed by the scientific payload, data from previous missions can be used. The most obvious choices are Cassini and the Voyager missions, however, missions to Venus and Earth can provide a valuable option to calibrate and validate the instrument performance before the main mission begins.

3

Requirements Analysis

This chapter restates the customer requirements that were obtained at the start of the design process and groups them together. Further requirements have been identified from this set, which are tracked internally. The chapter presents the requirements in their original form. Where ever applicable, the numbers have been updated when a requirements was changed during the design process.

The requirement are revisited in the chapter on verification (Chapter 10), where it is checked whether the design meets the set system requirements in the compliance matrix.

Science

- **SRO-Sys-Sci-01**: Satellite measurements shall characterise the radial and tangential coefficients of restitution for typical collisions between ring particles.
- **SRO-Sys-Sci-02**: The measurements shall provide the three components of the ring particles' velocity dispersion.
- **SRO-Sys-Sci-03**: For self-gravity wakes and similar structures, the satellite shall study the:
  - **SRO-Sys-Sci-03A**: development;
  - **SRO-Sys-Sci-03B**: dimensions;
  - **SRO-Sys-Sci-03C**: packing density;
  - **SRO-Sys-Sci-03D**: eventual dissolution.
- **SRO-Sys-Sci-04**: With measurements, the detailed structure shall be studied of:
  - **SRO-Sys-Sci-04A**: propellers;
  - **SRO-Sys-Sci-04B**: perturbed ring edges;
  - **SRO-Sys-Sci-04C**: density waves.
- **SRO-Sys-Sci-05**: For ring particles having a diameter of 1 to 10 meters, the satellite shall measure the:
  - **SRO-Sys-Sci-05A**: size distribution;
  - **SRO-Sys-Sci-05B**: spin states.

Performance

- **SRO-Sys-Per-01**: The total measurement duration in proximity of the rings shall be 1 year.
- **SRO-Sys-Per-02**: Measurement regions shall be focused primarily on the A- and B-ring.
- **SRO-Sys-Per-03**: Ring particle properties shall be observed and quantified at six key locations.
- **SRO-Sys-Per-04**: One measurement location shall be 180 degrees apart from the other locations.
- **SRO-Sys-Per-05**: For the close-proximity observations, the maximum hover distance over the rings shall be no more than 3 km.
- **SRO-Sys-Per-06**: The duration of close-proximity hovering shall be one month.
- **SRO-Sys-Per-07**: Launch shall be no later than December 31, 2025.

SAFETY AND RELIABILITY

- **SRO-Sys-Saf-01**: Throughout the life cycle of the spacecraft, exposure to hazardous materials shall be avoided for all personnel.
- **SRO-Sys-Rel-01**: Excluding launch failure, the mission success shall be greater than 95%.

SUSTAINABILITY

- **SRO-Sys-Sus-01**: The mission design shall include a clear end-of-life (EOL) strategy.
- **SRO-Sys-Sus-02**: The use of radioisotope propulsion systems and thermal generators shall be avoided.

ENGINEERING BUDGETS

- **SRO-Sys-Bud-01**: Technical requirements shall come from research and negotiations with clients and potential users. At any time it should be demonstrated that chosen solutions fulfil the emission requirements and are in line with similar initiatives for missions to (the moons of) Jupiter and Saturn.

COST

- **SRO-Sys-Cos-01**: The total mission cost shall not exceed €1.5 billion, including launch and operations.

OTHER

- **SRO-Sys-Oth-01**: A market analysis shall determine additional science objectives and show their impact on the mission design.
- **SRO-Sys-Oth-02**: The design shall be presented as a 'begin-to-end' design, including launcher selection, interplanetary transfer, in-situ operations, and end-of-life strategy.
- **SRO-Sys-Oth-03**: The selected launcher shall be an existing one.

4

Mission Analysis

4.1. Functional Flow Diagram

In this section the Functional Flow Diagram (FFD) of the mission will be discussed. Using the functional flow the various functions of the spacecraft are ordered in a chronological order. Using the FFD, requirements on different functions can be derived. The top level functions can be found in Figure 4.1. The mission is divided into 8 different phases; the pre-launch, the launch, the transfer, orbit insertion, hover orbit insertion, the mission operations, sending and receiving data, and end of life.

The pre-launch phase consists of all the functions from the development and manufacturing of the spacecraft until launch. This includes the development and testing of the spacecraft, the transport and assembly of the different components, possible storage of the spacecraft and finally the preparation for launch. These functions can be found in detail in Figure 4.2.

The launch phase describes the functions of the launcher during lift-off and finally the functions the spacecraft performs before separation from the launcher. These functions include the lift-off, the control of the launcher and stage separations, achieving the right orbit, the activation of the spacecraft and finally the injection into transfer orbit. These functions are explained in Figure 4.3.

The transfer phase describes the functions that are performed by the transfer stage from the moment the spacecraft separates from the launcher to the moment the first stage decouples. These functions include the start up of the stage, performing the low thrust manoeuvres and gravity assists, performing in transfer functions, orbit corrections and finally the decoupling of the transfer stage. These functions can be found in detail in Figure 4.4.

Orbit insertion consists of two major phases. The first of these phases is Saturn orbit insertion (SOI), during which the spacecraft is captured by Saturn's gravity. This phase consists of preparing the spacecraft for SOI, starting the insertion burn and performing post-SOI operations. These functions are explained further in Figure 4.5. The second phase is the pumpdown phase. During this phase, the spacecraft receives multiple gravity assists from Saturn's moons to circularise and lower the orbit. The main functions in this phase are approaching a moon, preparing for gravity assist, entering the sphere of influence of that moon and leaving it again. After repeating this sequence, the spacecraft will split up and either execute hover orbit insertion or proximity orbit insertion. These functions can be seen in detail in Figure 4.6.

Hover orbit insertion (HOI) is initiated, on the hovercraft, after the two spacecraft decouple from the launcher. The hovercraft will perform a circularisation, reduce its orbit inclination, prepare for HOI and finally enter hovering orbit. These functions are further detailed in Figure 4.7.

After the two spacecraft are inserted into the right orbit they will perform their mission operations. This phase is split up in two parts. The first part is performed by the hovercraft and the second part is performed by the orbiter. The orbiter will hover using hops and in between hops it will enter operational mode and perform its measurements. These functions can be found in detail in Figure 4.8. The orbiter performs orbit corrections, enters its operational mode and performs measurements, like the hovercraft. These functions can be found in detail in Figure 4.8.

The data gathered during mission operation also need to be sent back to earth and commands must also be able to reach the spacecraft. The functions in 'send and receive data' cover the communication between the two spacecraft and earth. The spacecraft prepares data for T_x, initialises T_x subsystem, transmits the data, receives data and processes the received data. These functions can be found in detail in Figure 4.9.

After the spacecraft performs all of its mission operations and transmits all its data, the spacecraft will enter its end-of-life phase. First, it performs a system check to determine if it is possible to extend the mission. If it is not possible, the spacecraft will perform an end-of-life strategy. It can transfer into the Cassini division or a different division. It could stay in the rings or it can burn up in Saturn its atmosphere. During the end-of-life, it will conduct measurements and send back the data. These functions are further detailed in Figure 4.10.

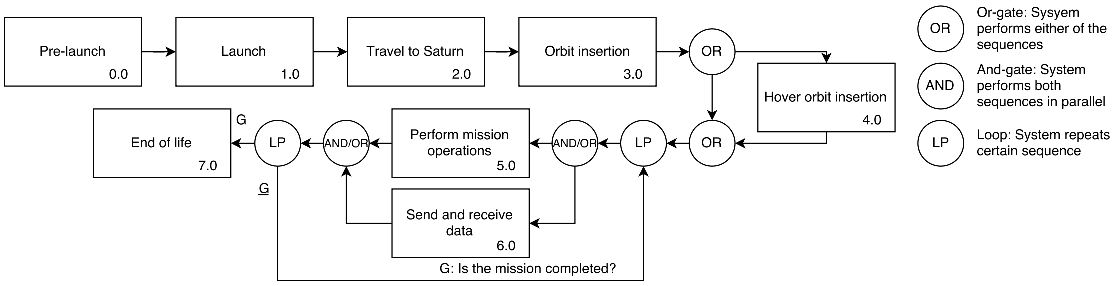

Figure 4.1: The top level functional flow diagram of SAURON.

4.2. Functional Breakdown Structure

In this section, the Functional Breakdown Structure (FBS) will be discussed. The FBS describes the hierarchical order of functions the system needs to perform during the mission. The diagram groups different functions of the system together, under different phases of the mission. It is divided into five main phases, pre-launch, transfers, hovercraft mission operations, orbiter mission operations and end-of-life.

The first phase of the mission is the pre-launch. It describes all the activities performed from the development of the spacecraft to the moment right before launch. This phase includes the development of the spacecraft, building and testing of the subsystems, the transportation and assembly of the spacecraft, the integration into the launcher, possible storage of the spacecraft and finally, the dress rehearsal for launch. More detailed functions in this phase are described in Figure 4.11.

The transfer phase describes the entire transfer from the ground to the insertion of the two spacecraft in their operational orbits. This phase starts with the launch and the manoeuvres preformed by the launcher. Afterwards, the transfer to Saturn is preformed by the electrical phase, followed by Saturn orbit insertion, pump-down phase and orbit circularisation. Finally, the insertion into hover orbit is described. More detailed functions are described in Figure 4.12.

The hovercraft mission operations describe the functions performed by the hovercraft while it is operational. The hovercraft mission operations are divided into three subphases, each detailed further in Figure 4.13. These subphases are the hovercraft measurement operations, the transfer of the data and the mission manoeuvres.

The orbiter mission operations are very similar to those of the hovercraft. The differences are the quantity of data it sends and receives, the type of measurements it performs and the manoeuvres it performs during its mission. Due to the similarity, some functions are not as detailed, but they refer to the functions in the hovercraft mission operations. This phase can be seen in Figure 4.14.

The end-of-life phase is divided into two parts. The first part concerns the hovercraft end-of-life and the other one the orbiter end-of-life. They both include a system check, consider a mission extension, but their options for the end-of-life strategy are different. This mission phase is described in more detail in Figure 4.14.

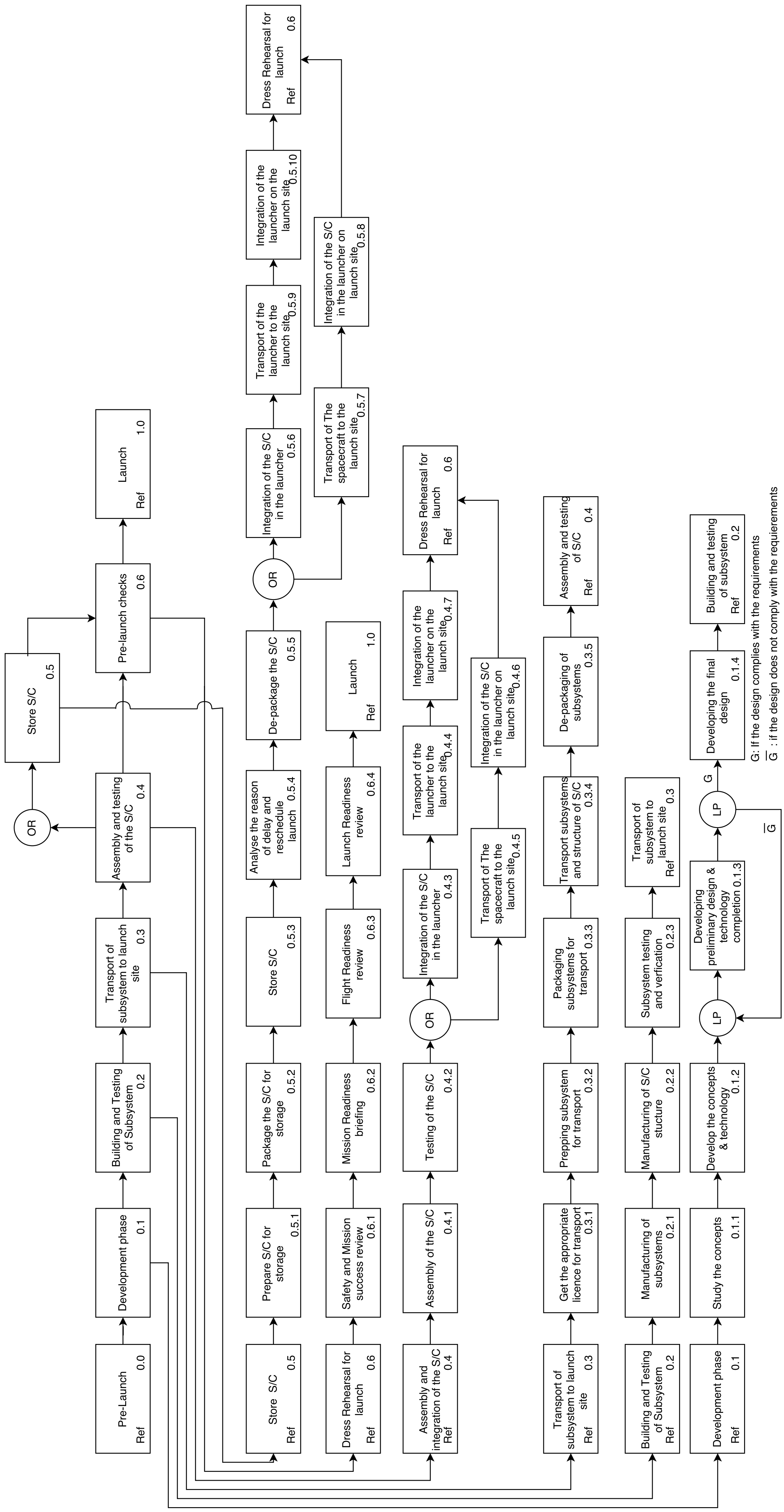

Figure 4.2: The functional flow diagram of the pre-launch phase for SAURON.

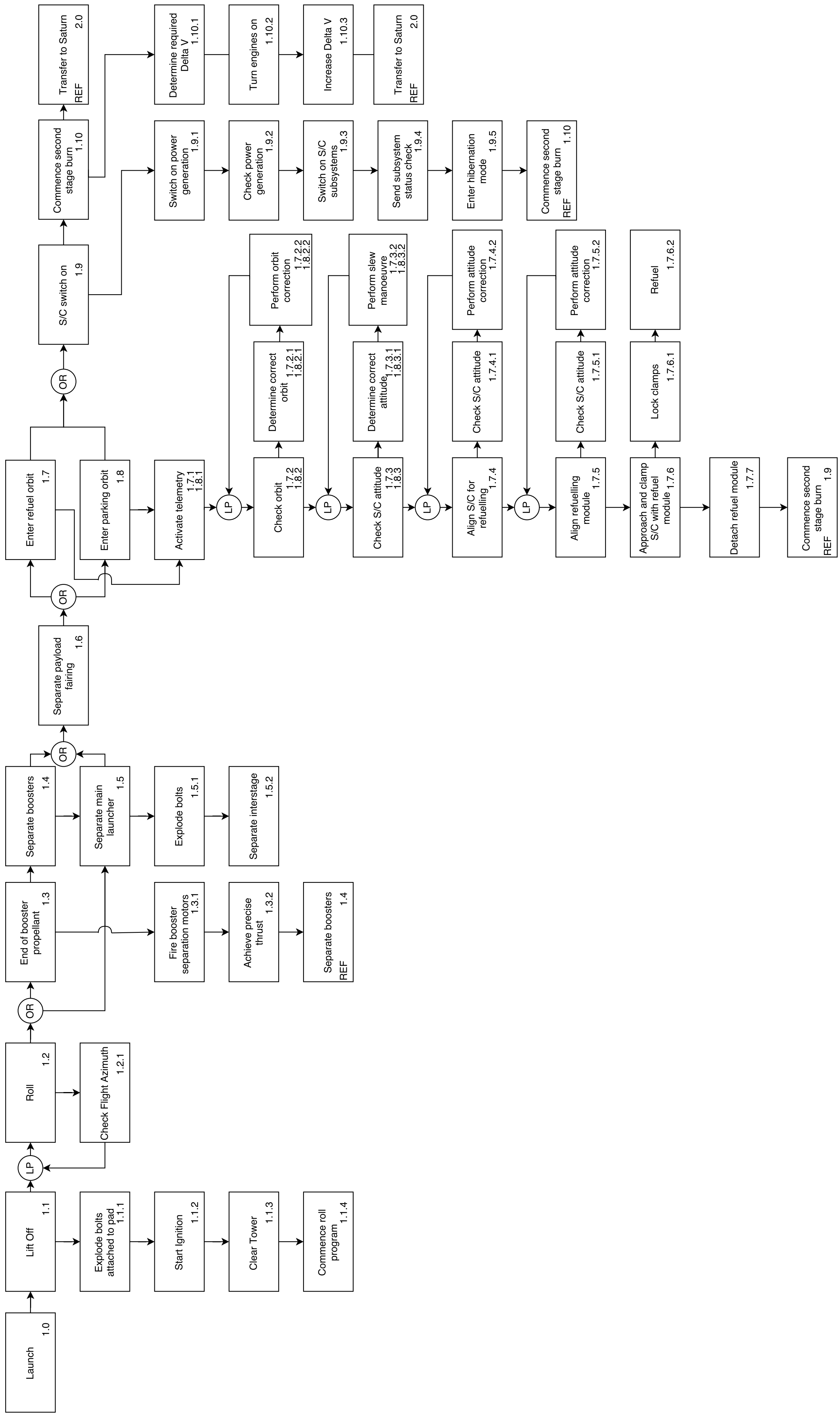

Figure 4.3: The functional flow diagram of the launch phase for SAURON.

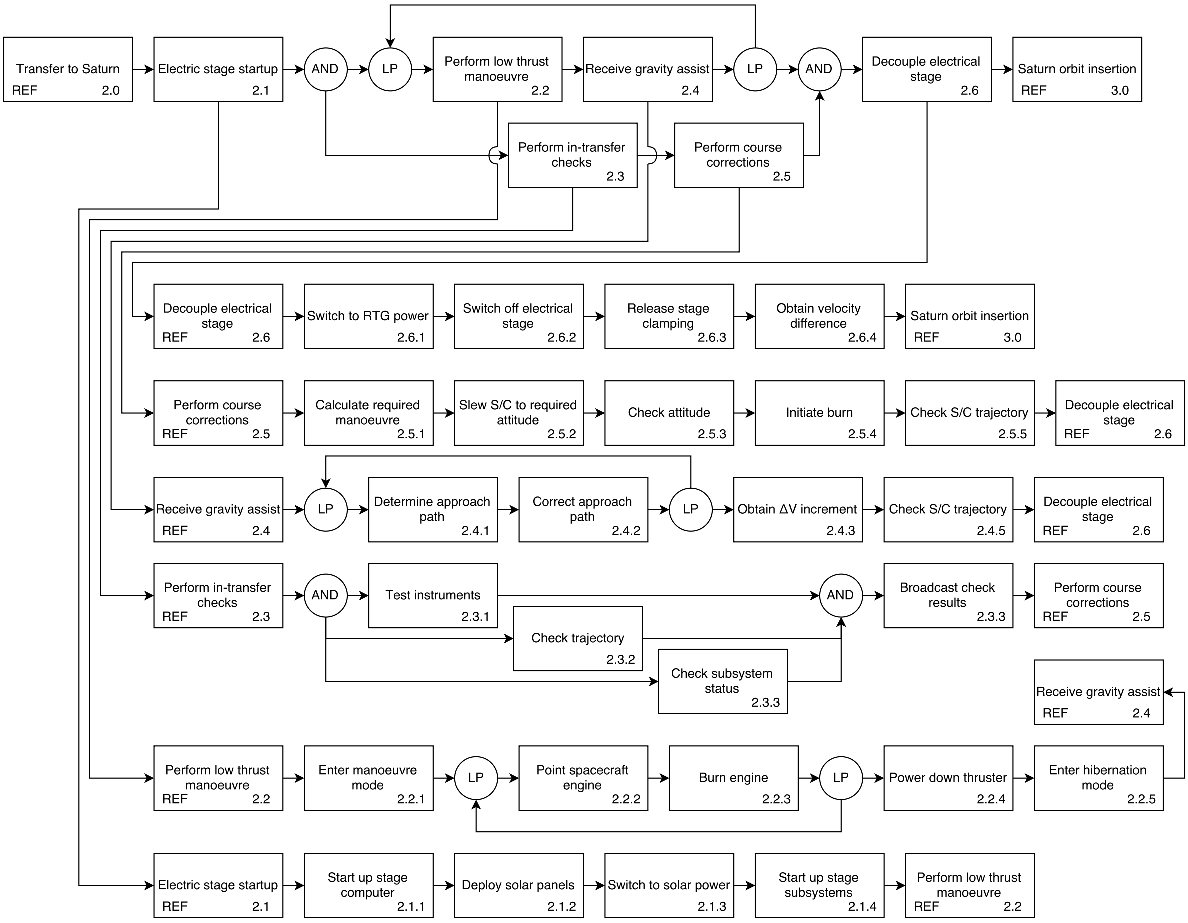

Figure 4.4: The functional flow diagram of the transfer phase for SAURON.

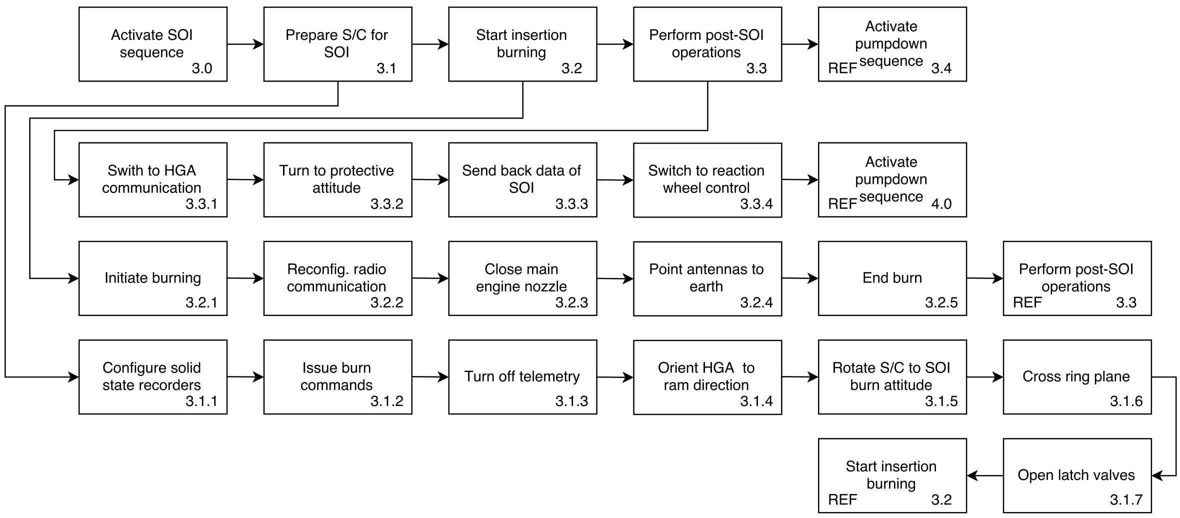

Figure 4.5: The functional flow diagram of the Saturn orbit insertion for SAURON.

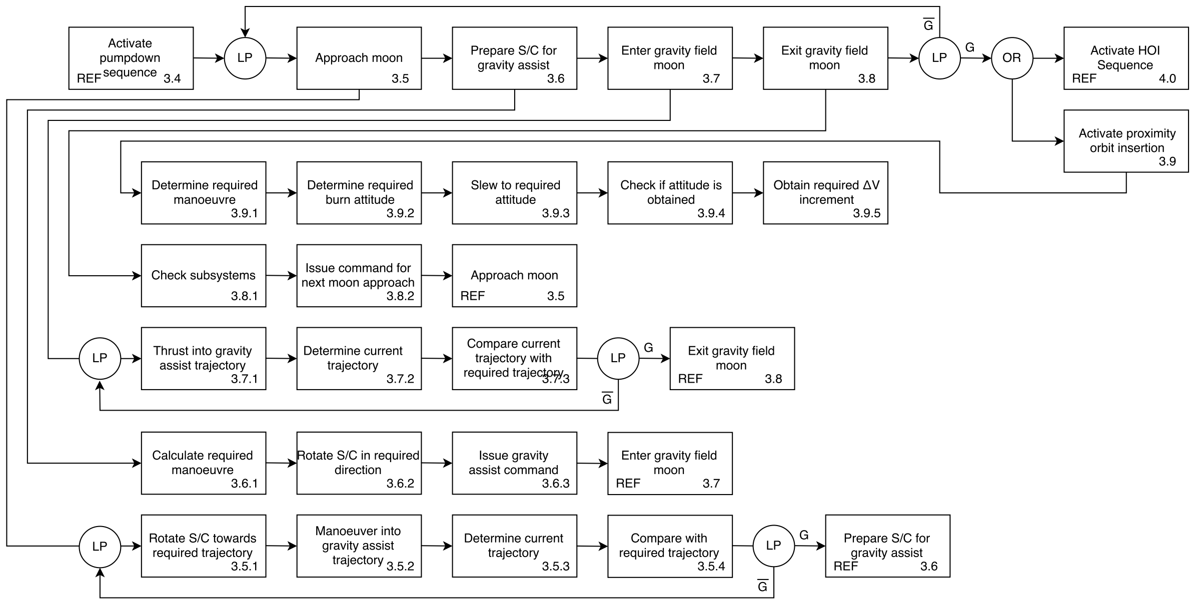

Figure 4.6: The functional flow diagram of the pumpdown phase for SAURON.

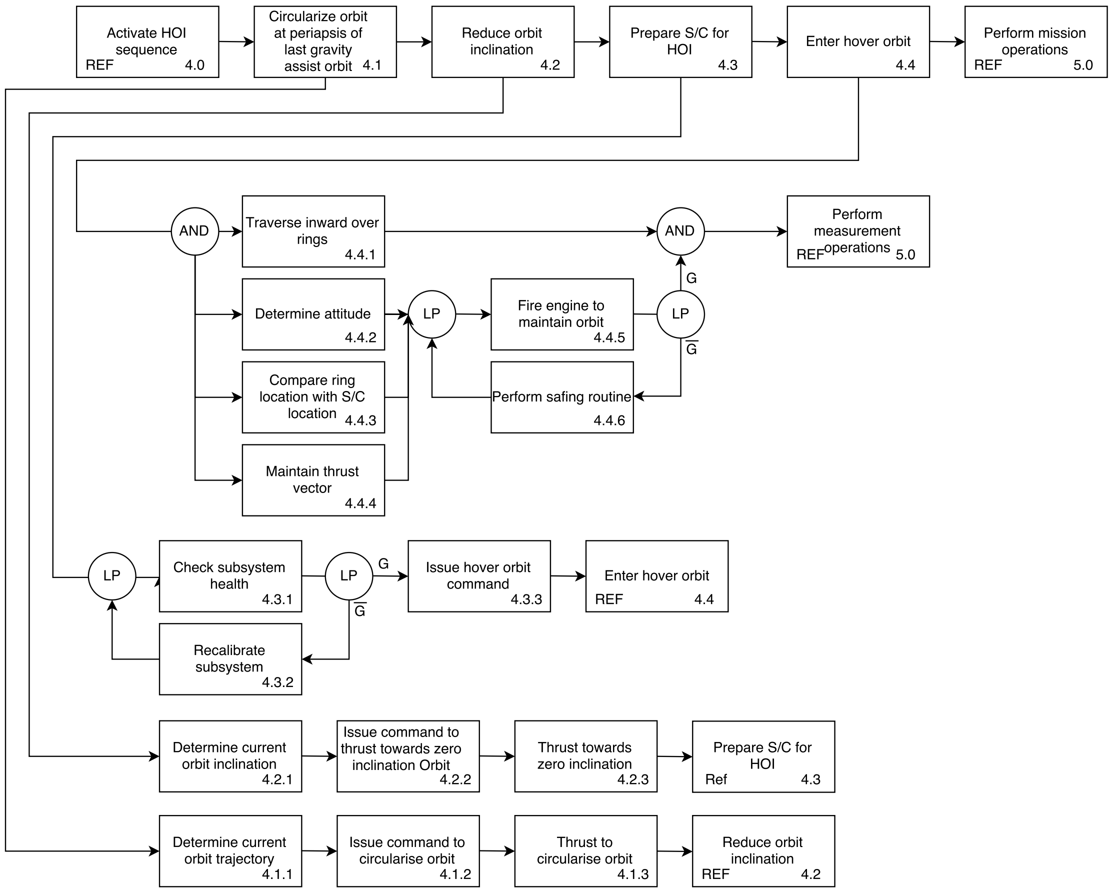

Figure 4.7: The functional flow diagram of the hover orbit insertion for SAURON.

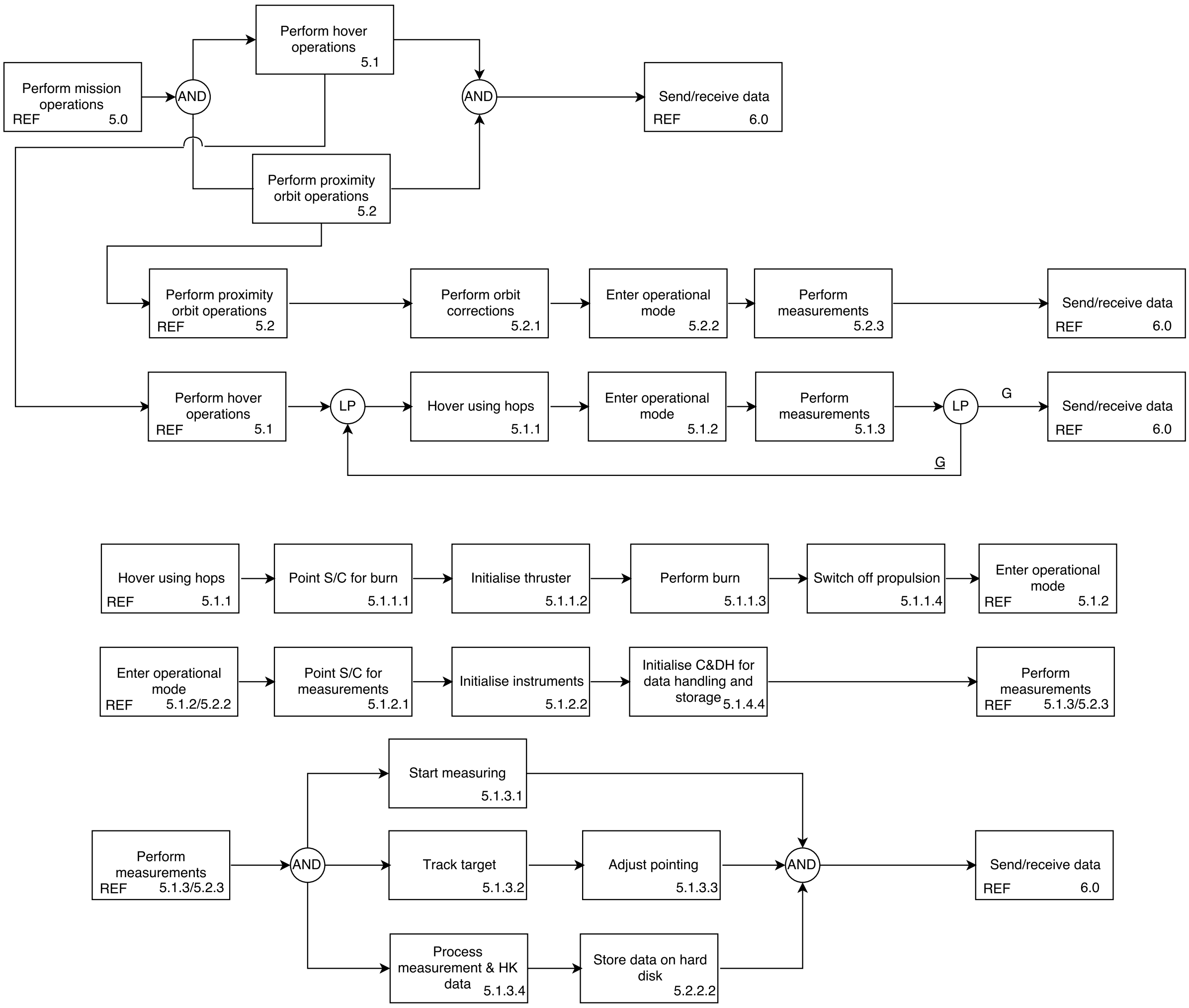

Figure 4.8: The functional flow diagram of the mission operations phase for SAURON.

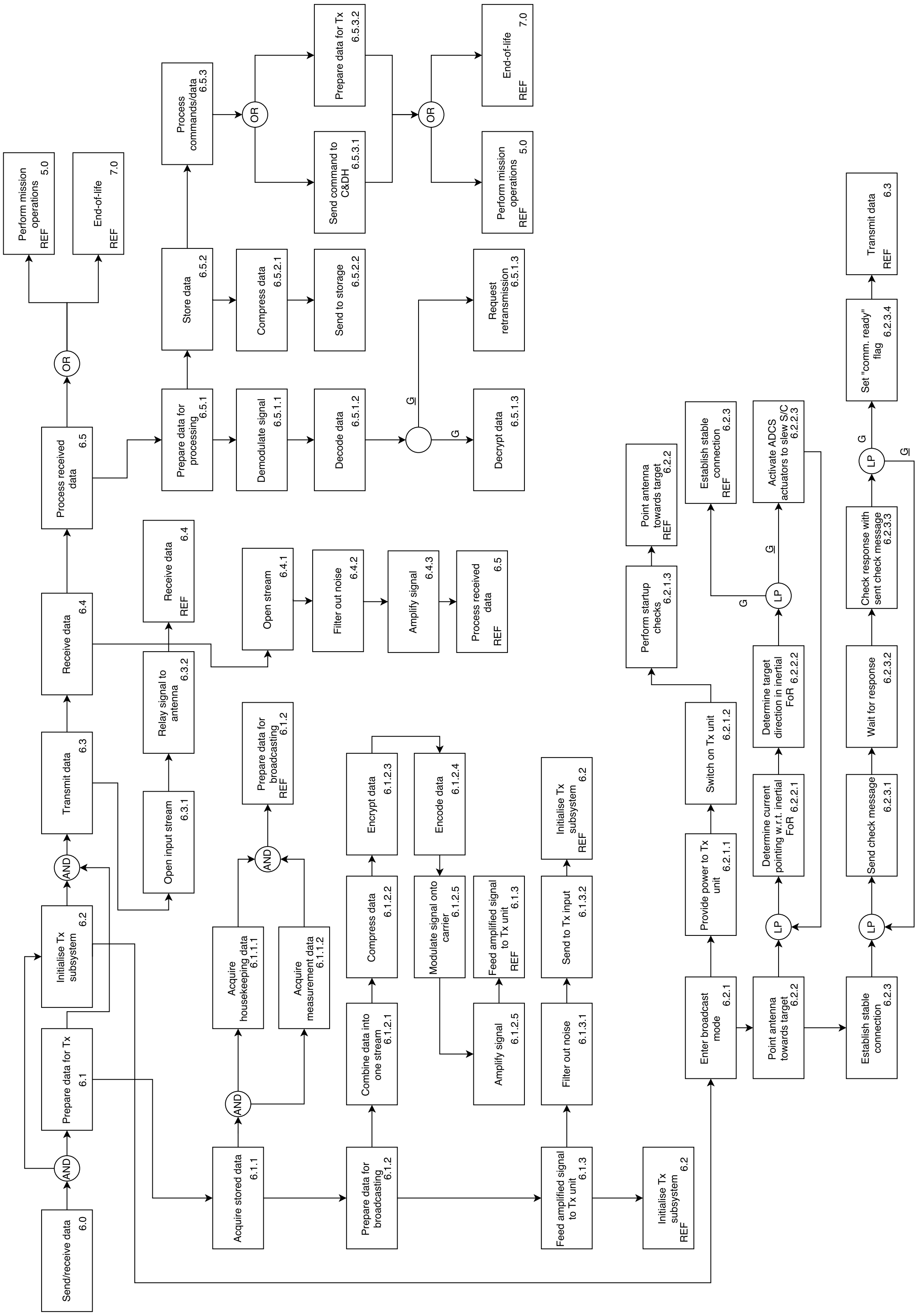

Figure 4.9: The functional flow diagram of the spacecraft data sending and receiving phase for SAURON.

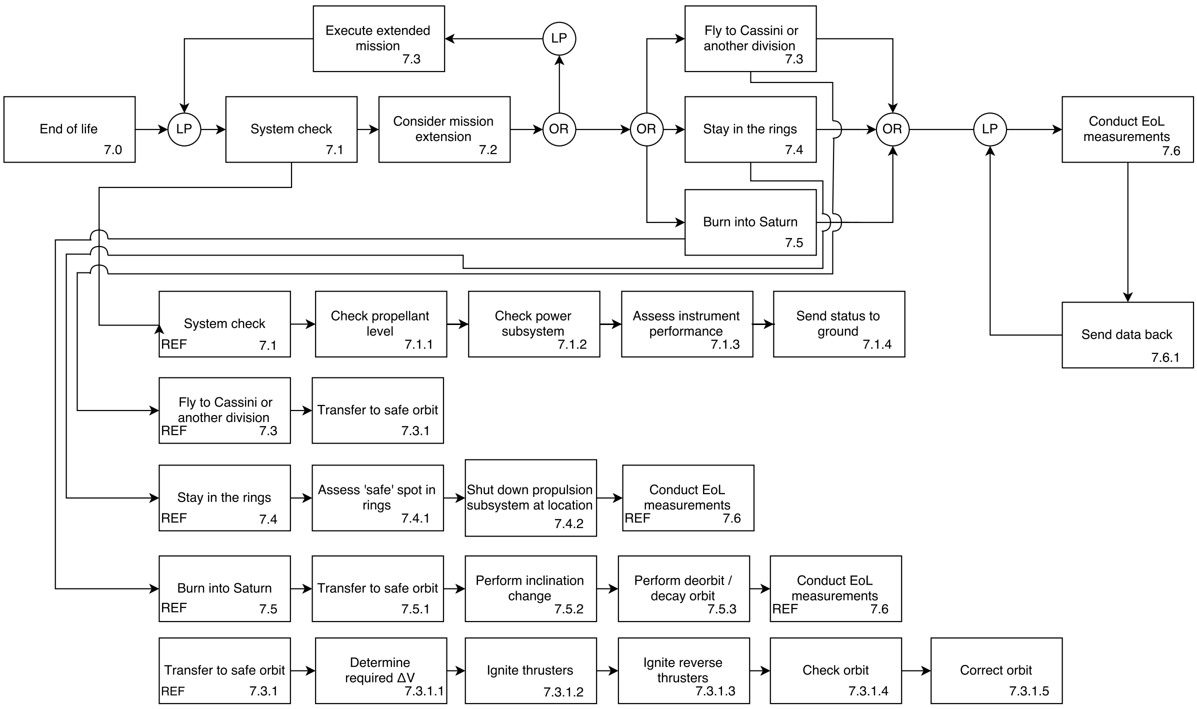

Figure 4.10: The functional flow diagram of the end-of-life phase for SAURON.

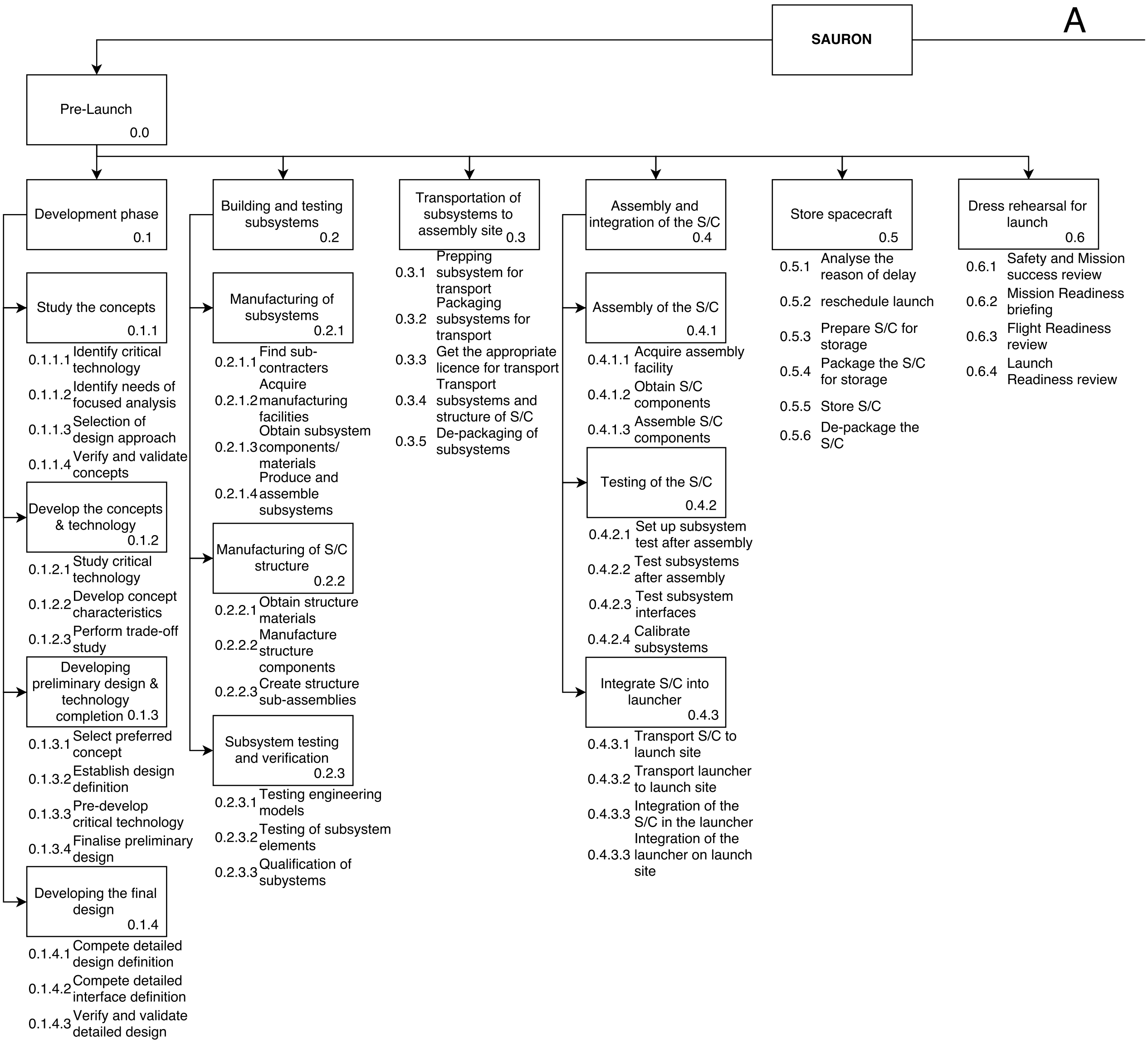

Figure 4.11: Functional breakdown structure of the pre-launch phase.

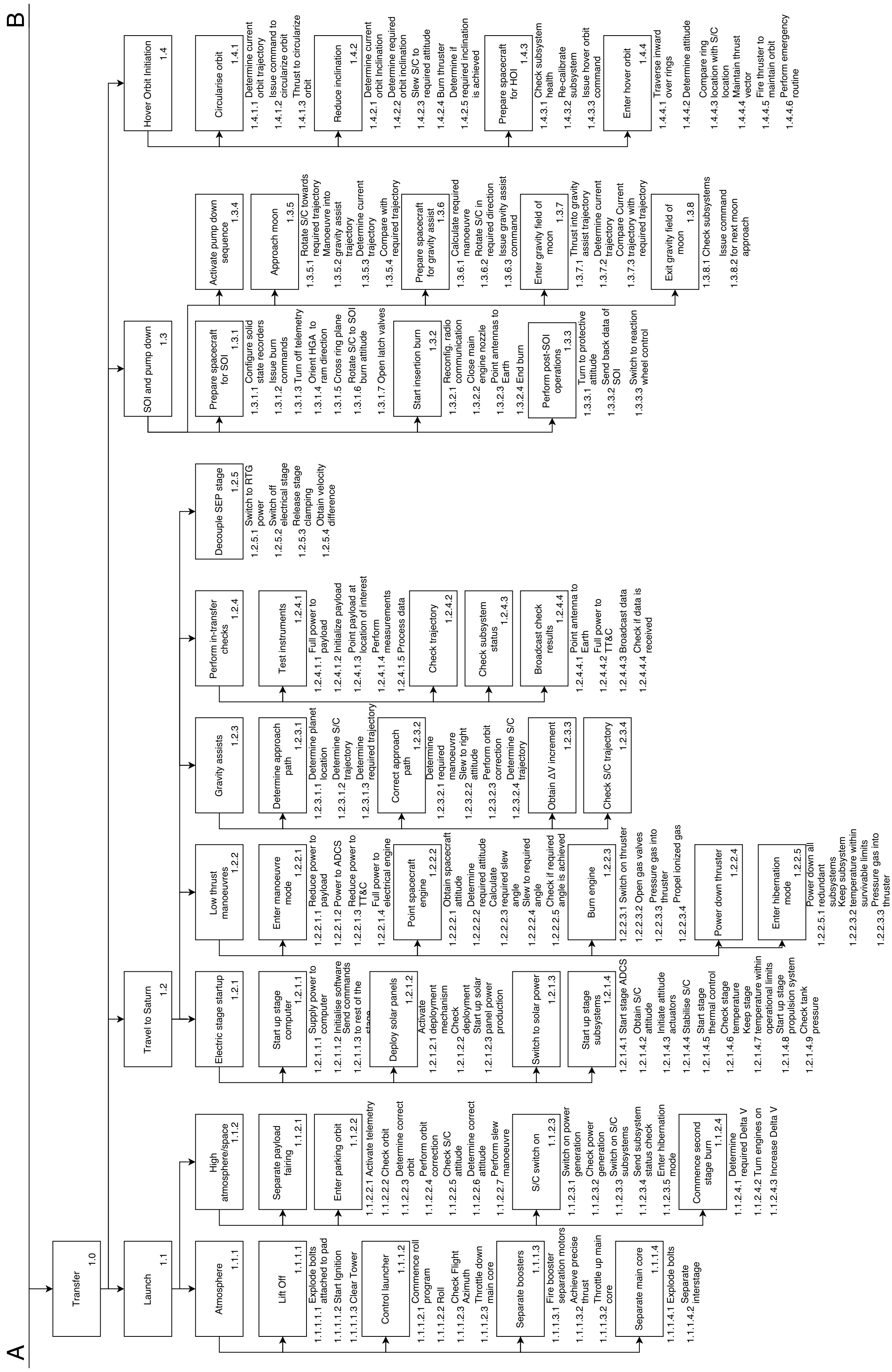

Figure 4.12: Functional breakdown structure of the transfer phase.

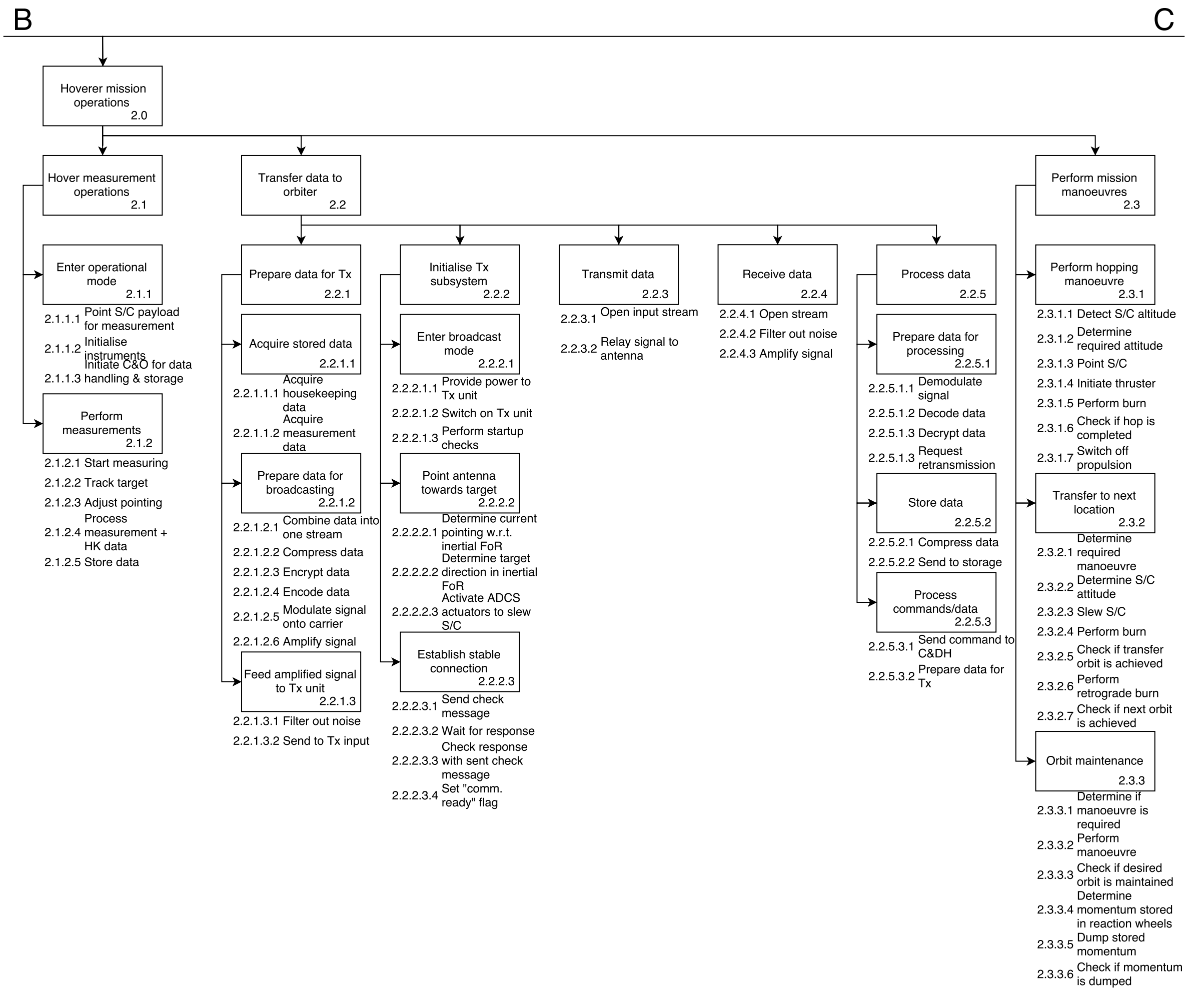

Figure 4.13: Functional breakdown structure of the hovercraft mission operations phase.

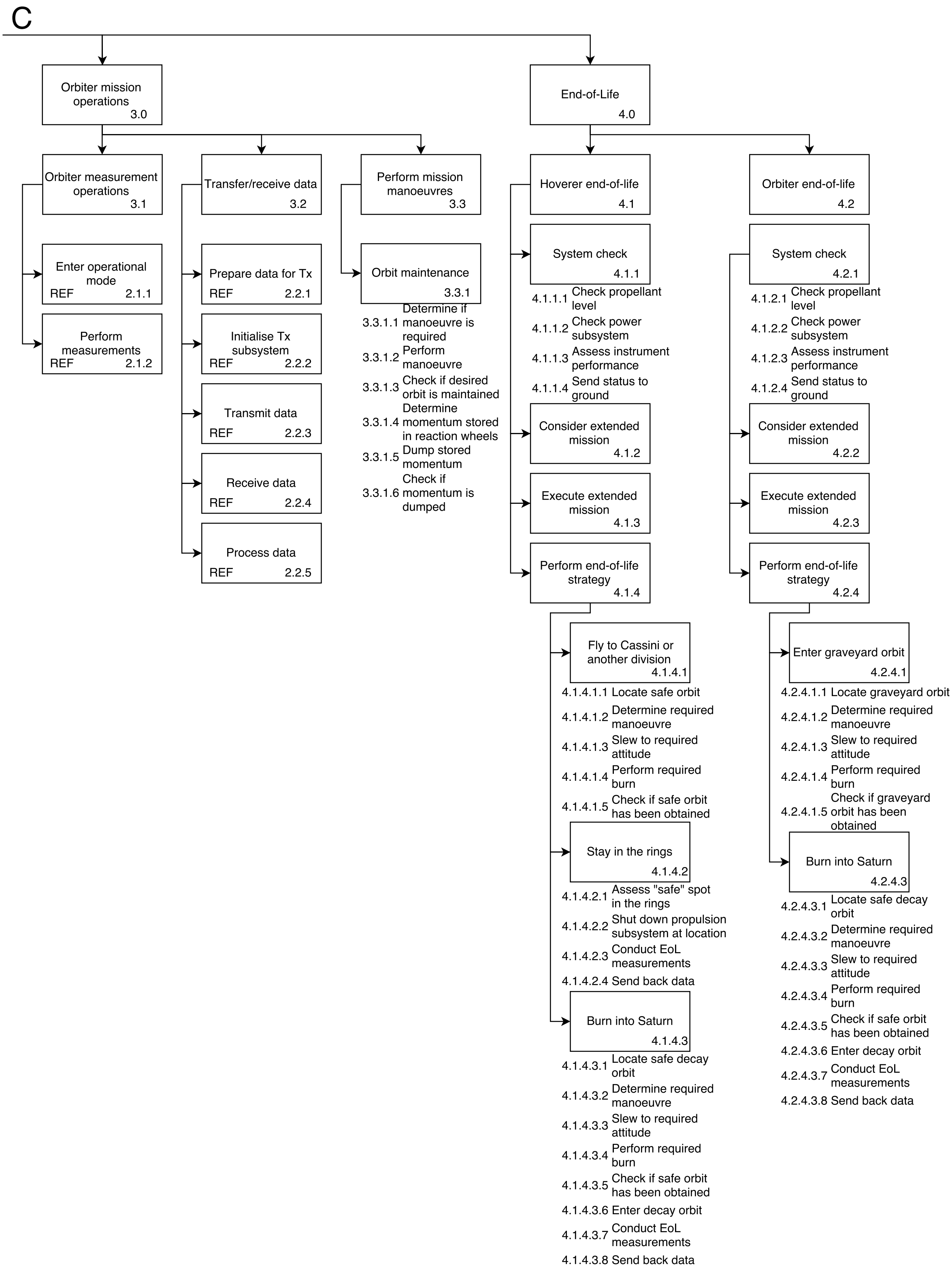

Figure 4.14: Functional breakdown structure of the orbiter mission operations and end-of-life phase.

4.3. MISSION OVERVIEW

In this chapter, the mission design of SAURON is discussed. Several alternative mission design options were considered, as discussed in Chapter 1. The mission was divided into different phases, which are presented in Subsection 4.3.2 through Subsection 4.3.5. For the trajectory optimisation, a model was developed using PyKEP and PyGMO [50]. Discussions of the theory and the algorithms implemented in the model are presented in Subsection 4.3.1. Table 4.3.6 presents the verification and validation process of this model.

For the final design, SAURON will be launched on 12 June, 2024 from Cape Canaveral on a Falcon Heavy launcher. SAURON will have a launch mass of 11,200 kg and an insertion velocity of 1.5 km/s. This will be the start of a 10.4 year interplanetary flight to Saturn, using solar electric propulsion. An initial gravity assist from Venus followed by two Earth flybys will lower the ΔV requirement for the transfer and maximise the arrival mass. Several measurements will be performed during flybys to test the payload. On 19 November 2034, SAURON will reach Saturn and dive between the G and F ring for Saturn Orbit Insertion, requiring a propulsive ΔV of 310 m/s. This manoeuvre will insert SAURON in a 100 day orbit around Saturn with a periapsis at 155,000 km. After a periapsis raise manoeuvre of 150 m/s, SAURON is placed into an orbit encountering Titan, which is used as the first gravity assist for the 3.5 year pumpdown tour. This tour, also called a ΔV leveraging tour, uses gravity assists of the moons Titan, Enceladus, Dione, and Rhea, to lower the required ΔV. A total of 350 m/s chemical propulsive ΔV shall provide the manoeuvres necessary to target the moons. At the end of the pumpdown tour, SAURON will arrive in an elliptical orbit with periapsis at 142,000 km and apoapsis at Enceladus' orbit. During this orbit, SAURON will be staged into the orbiter and hovercraft. The orbiter and hovercraft will then separately perform a propulsive ΔV of 1215 m/s and 2641 m/s, respectively, to circularise into a 142,000 km orbit.

The orbiter will remain in this orbit to aid the hovercraft as a communication relay with Earth. It will also perform secondary mission objectives. The hovercraft will perform an inclined Hohmann Transfer to travel to a circular orbit between the A and F ring at 139000 km. After final checks, the hovercraft will hop over the A ring and initiate the one month hovering phase. This will be the start of the primary mission. To complete all primary scientific objectives, the hovercraft must perform measurements at six locations above the rings. Figure 4.15 provides an illustration of these locations. Via inclined hopping Hohmann Transfers, the hovercraft will traverse inwards and translate to the subsequent locations. All measurements are sent to the orbiter, which will relay the data back to Earth.

4.3.1. MODEL DESCRIPTION

A conjunction of the Sparse Nonlinear Optimiser (SNOPT) [51] and Monotonic Basin Hopping (MBH) [52] algorithm was found to be a feasible interplanetary trajectory optimisation tool. Since the algorithm is non-deterministic, multiple runs were necessary to find an optimal trajectory. This section describes the process of SNOPT and MBH to solve the problem of multiple gravity assists in low-thrust trajectories.

4.3.1.1. MONOTONIC BASIN HOPPING AND SNOPT

The problem of a low-thrust multiple gravity assist trajectory has many local solutions within global solutions. These local solutions are usually clustered together into so called "funnels", where one is better than the rest. Within the solution space, multiple funnels are present. Monotonic Basin Hopping provides global coverage of the solution space as well as local optimisation. The actual solver of the local minima is performed by SNOPT.

The optimiser, SNOPT, is based on a Sequential Quadratic Programming (SQP) algorithm, and is well-suited for large-scale, nonlinear problems. It has to be noted that convergence to a feasible locally optimal trajectory depends

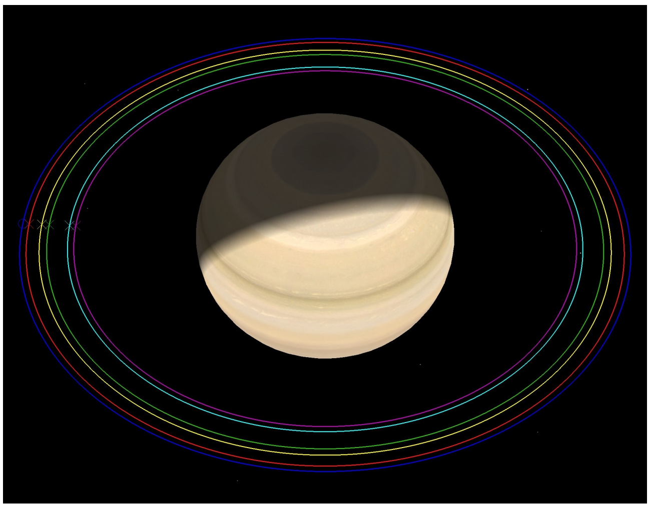

Figure 4.15: The orbits at which the spacecraft are in close proximity to the rings.

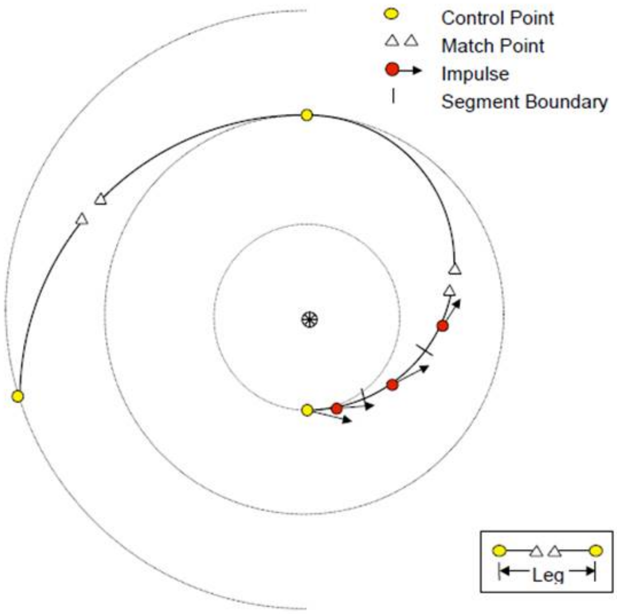

Figure 4.16: Sims-Flanagan model. Image credit: Sims and Flanagan.

critically on the initial guess for the independent variables. Thus, an initial guess that is sufficiently "close" to the optimal solution is required. This results in excessive computing time. Several user options determine the exit conditions for SNOPT, including the number of iterations and the optimality and feasibility tolerances.

The MBH optimisation procedure works as follows. First, an initial guess **u** is made, where **u** is the decision chromosome. In this case, **u** has the structure seen in Equation 4.1.

$$\mathbf{u} = [t_0, [t_{leg_1}, m_{f_1}, V_{xi_1}, V_{yi_1}, V_{zi_1}, V_{xf_1}, V_{yf_1}, V_{zf_1},], ..., [t_{leg_N}, ..., V_{zf_N},]] \tag{4.1}$$

The local non linear optimiser, SNOPT, is then applied to find a solution. If the found solution, **u*** is feasible, the MBH algorithm starts its local optimisation. A solution is found feasible if it does not violate any of the constraints set, see section Subsubsection 4.3.1.2. If feasible, a new random guess is made until a feasible solution is found. The local optimisation, called hopping, is performed in two steps. First, a perturbation is applied to **u***, resulting in **u**'. SNOPT is then applied to find the new solution. If the acquired solution is feasible and superior to **u***, it is adopted and a new hop is performed. When **u**' is found to be inferior to **u*** or unfeasible a counter is started. If this occurs N_{no-imp} in a row, MBH terminates the optimisation process and returns the best solution found. The threshold, N_{no-imp}, provides the maximum amount of hops/perturbation to be applied to **u*** if **u**' is inferior or unfeasible.

To see if the new solution is superior to the previous, the following strategy is applied from [50].

> "The number of constraints satisfied (equality and in-equality) are first compared. If both individuals are equally feasible (to a fixed tolerance), the norm of the constrained violations is evaluated and compared. If both individuals have no constraint violation, the one that is dominated by the least number of individuals is considered best and if also this fails, then the individuals are considered, simply, as different and the comparison fails, returning false."

MBH's capability to globally search the solution space and exploit the local minima, makes it a viable algorithm to use for trajectory optimisation.

It is possible for SNOPT to freeze during optimisation when applied with MBH. If this occurs the process is terminated and a new optimisation sequence is initiated.

4.3.1.2. SIMS-FLANAGAN

The Sims-Flanagan model was used to solve the problem [53]. This model is implemented in widely used tools such as MALTO and GALLOP. The purpose of the model is to maximise the final mass at the destination planet, in this case Saturn. The method approaches the problem by approximating low-thrust arcs as a series of impulsive manoeuvres. Figure Figure 4.16 visualises this method.

Figure Figure 4.16 illustrates one leg between 2 bodies. The leg is divided into equal time spaced segments. At each midpoint of a segment a thrust vector is applied. Through forwards and backwards propagation, the state of the spacecraft at the mismatch point is determined, defined by the thrust vectors. Imposing this mismatch to be zero gives rise to the first equality constraint, as seen in Subsubsection 4.3.2.2. The problem at hand becomes non-linear, for which a SQP method is used to solve, i.e., SNOPT. Equation 4.2 and Equation 4.3 were used for forward and backward propagation respectively.

$$\begin{aligned} \mathbf{x}_{i+1}^{m^-} &= \Phi_{\mathbf{x}_i}(\Delta t/2)\,\mathbf{x}_i \\ \mathbf{x}_{i+1}^{m^+} &= \mathbf{x}_{i+1}^{m^-} + \Delta\mathbf{x}_{i+1} \qquad \forall i = 0,...,n_{fwd}-1 \\ \mathbf{x}_{i+1} &= \Phi_{\mathbf{x}_{i+1}^{m^+}}(\Delta t/2)\,\mathbf{x}_{i+1}^{m^+} \end{aligned} \tag{4.2}$$

$$\begin{aligned} \bar{\mathbf{x}}_{i-1}^{m^+} &= \Phi_{\bar{\mathbf{x}}_i}(-\Delta t/2)\,\bar{\mathbf{x}}_i \\ \bar{\mathbf{x}}_{i-1}^{m^-} &= \bar{\mathbf{x}}_{i-1}^{m^+} - \Delta\bar{\mathbf{x}}_{i-1}, \qquad \forall i = N,...,N-n_{bck}+1 \\ \bar{\mathbf{x}}_{i-1} &= \Phi_{\bar{\mathbf{x}}_{i-1}^{m^-}}(-\Delta t/2)\,\bar{\mathbf{x}}_{i-1}^{m^-} \end{aligned} \tag{4.3}$$

Where $\mathbf{x} = (\mathbf{r}, \mathbf{v}, m)$ is the spacecraft state, $\Phi_{\mathbf{x}}(t)$ is the Keplerian transition matrix. $\Delta\mathbf{x}_i = \left(\mathbf{0}, \Delta\mathbf{V}_i, m_i^-[exp(-\Delta V_i/I_{sp}g_0)-1]\right)$ represents the change in the spacecraft state at the midpoint of each segment due to thrusting. n_{fwd} and n_{bck}, represent the number of forward and backward propagated segments. At each of the midpoint an inequality constraint holds, seen in Equation 4.4. This equation sets the maximum ΔV to be deployed in each segment. This is a function of the maximum thrust to be delivered as defined by the user. This in turn is dependent on the number and type of thrusters of the propulsion subsystem during transfer.

$$\Delta V_i \leq \frac{T_{max}\Delta t}{N} \tag{4.4}$$

Since the model assumptions include impulsive thrusting at the midpoints of each segment, the solution would not be dynamically feasible. This is because electric propulsion systems fire continuously, not impulsively. Therefore, an improvement to the model was made by J. Englander, 2014 [52]. In essence, throttles, denoted by μ_i, are introduced to encode the various thrust actions. The inequality constraint becomes Equation 4.5.

$$\Delta V_i = \frac{\mu_i T_{max}\Delta t}{N} \tag{4.5}$$

which results in the inequality constraint seen in Equation 4.6.

$$\mu_i \leq 1 \tag{4.6}$$

Equation 4.7 generalises the problem of a low thrust interplanetary trajectory. It states that a solution needs to be found, consisting of the maximum final mass and the ΔV requirements for which this mass is optimised. The problem is subjected to several equality and inequality constraints. The first equality constraint is the mismatch constraint in the time spaced middle of a leg. It states that the spacecraft state must be equal through both forwards and backwards propagation. The derivatives of all the constraints can be found, which enhances the efficiency of SNOPT.

$$\begin{aligned} \text{find:} \quad & \mathbf{y} = \left(m_f, \Delta\mathbf{V}_1, \cdots, \Delta\mathbf{V}_N\right) \\ \text{maximise:} \quad & m_f \\ \text{subject to:} \quad & \bar{\mathbf{x}}_{N-n_{bck}} = \bar{\mathbf{x}}_{n_{fwd}} \\ & \mathbf{x}_0 = (\mathbf{r}_s, \mathbf{v}_s, m_s) \\ & \mathbf{x}_N = \left(\mathbf{r}_f, \mathbf{v}_f, m_f\right) \\ & \mu_i \leq 1 \\ & \mathbf{lb} \leq \mathbf{y} \leq \mathbf{ub} \end{aligned} \tag{4.7}$$

The propagation scheme can also be simplified, when implementing the continuous thrusting scheme, see Equation 4.8 and Equation 4.9.

$$\mathbf{x}_{i+1} = \varphi(\Delta t, \mathbf{x}_i), \quad \forall i = 0,...,n_{fwd}-1 \tag{4.8}$$

$$\bar{\mathbf{x}}_{i-1} = \varphi(-\Delta t, \mathbf{x}_i), \quad \forall i = N,...,N-n_{bck}+1 \tag{4.9}$$

Here, $\varphi(-\Delta t, \mathbf{x}_i)$ is computed as the result of the full propagation of the spacecraft state subject to a constant thrust $T = \mu T_{max}$. For a multiple gravity assist trajectory, the previous discussed theory and equation is applied to each

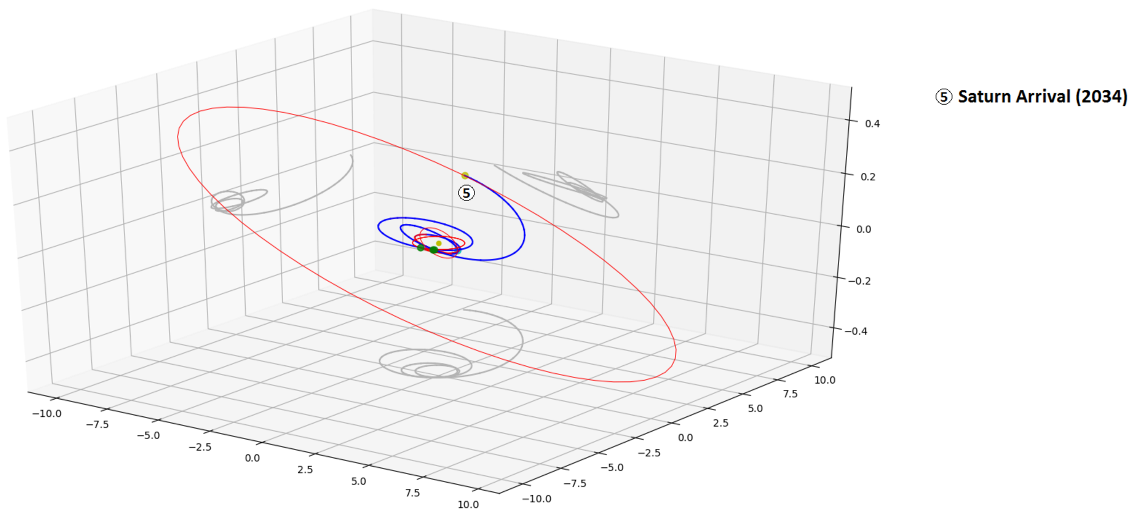

Figure 4.17: Visualisation of the EVEES transfer.

leg. In addition, one equality and inequality flyby constraint is set for each gravity assist planet. Equation 4.10 and Equation 4.11 denote these constraints.

$$v_\infty^+ = v_\infty^- \tag{4.10}$$

Equation 4.10 states, that the incoming and outgoing relative velocity, v_∞^+ and v_∞^- of the spacecraft, with respect to the flyby planet, is equal.

$$\frac{\mu_{planet}}{v_\infty^2}\left[\frac{1}{sin(\frac{\delta}{2})}-1\right] \geq r_{planet} + h_{safe} \tag{4.11}$$

Here, the left side of Equation 4.11 denotes the distance to periapse of the hyperbolic trajectory, with the gravitational constant of the flyby planet, μ_{planet}, the angle between the incoming and out going relative velocity asymptote, δ, and the magnitude of the relative velocity, v_∞. The right side of Equation 4.11 denotes the radius of the planet, r_{planet}, and the user-defined safety height above the surface of the flyby planet, h_{safe}.

4.3.2. TRAJECTORY

This section will present the optimisation results of a low thrust, multiple gravity assist, trajectory problem. A software package called PyKEP/PyGMO was used to provide the framework of the model. To initiate the optimisation, several constraints had to be set for the problem. These input parameters are visible in Table 4.1. Since gravity assists were implemented in the trajectory, certain parameters of interest at these planets needed to be computed. The result of these computations are presented in Table 4.3.

Note that at Venus and Earth, a flyby altitude of 500 m was found. Given the model uncertainties, a 500 m flyby is easily corrected for with little ΔV implementations. Therefore, this trajectory will still be considered.

4.3.2.1. RESULT

In Figure 4.17 and Figure 4.18, the arrival dates at each planet are given in the legend. In addition, the midpoints, nodes and mismatch points are indicated. Each leg is divided into ten equal time-space segments, which are bordered by the nodes. The inclination of the orbits are also visible. It has to be noted that the z-axis is differently scaled than the x- and y-axis, which results in the "seemingly" high inclinations.

4.3.2.2. INPUT AND OUTPUT

To solve the problem of a low thrust transfer, several constraints need to be set. The arrival and departure conditions, including the Time Of Flight (TOF) are vital arguments to the problem. An in depth discussion on the constraints can be found in Subsection 4.3.1. Furthermore, a constraint is set on the maximum launch energy, $C3$. From Table 4.2, it can be seen that the launch energy is very low, i.e., 2.25 km^2/s^2. This is the key driving characteristic which makes an electric propelled transfer superior to a chemical transfer.

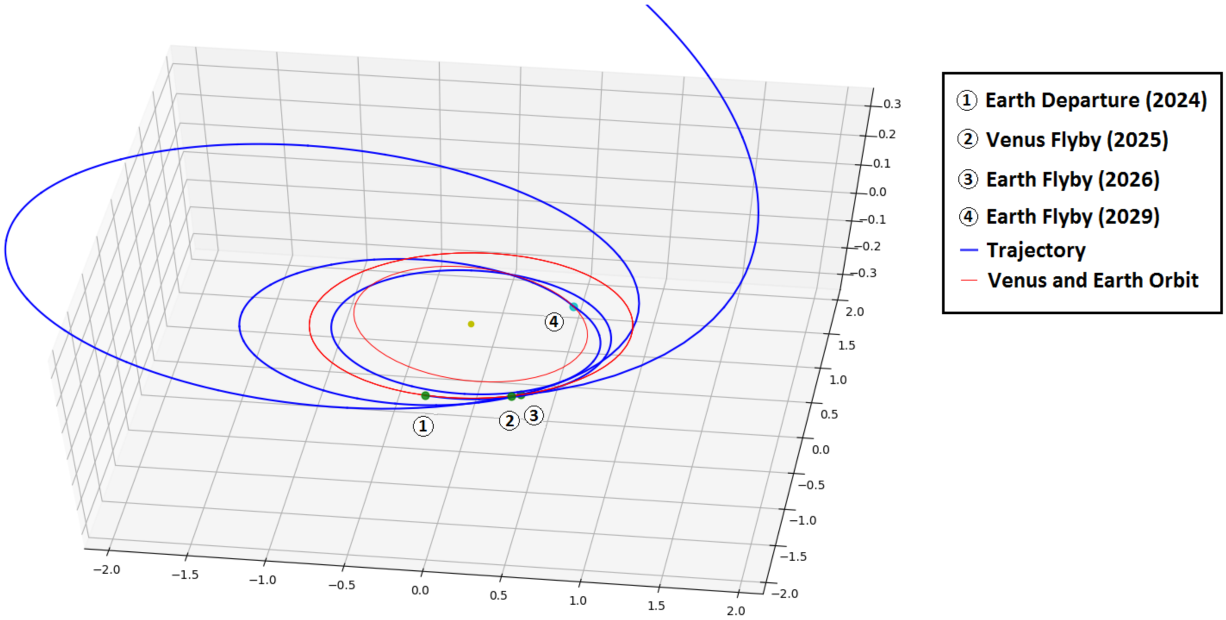

Figure 4.18: Close up of inner flyby system of the interplanetary transfer.

Table 4.1: Input parameters to PyKEP.

Parameters	Value
Sequence	Earth-Venus-Earth-Earth-Saturn
Number of Segments per leg	10
Launch Date	2024-2026
Launch Mass [kg]	12300
Maximum TOF per Leg [days]	400,500,900,2000
Maximum Departure V_{∞} [km/s]	1.5
Maximum Arrival V_{∞} [km/s]	7.0
Maximum thrust [N]	1.18
Specific Impulse [s]	4190
Minimum flyby altitude [km]	500
Maximum flyby V_{∞} [km/s]	12
High Fidelity	ON

Table 4.2: Important transfer characteristics from the output of the optimisation.

Parameter	Value
Launch date	12-JUN-2024
Propellant mass [kg]	729
Time of flight [yrs]	10.4
Launch C3 [km^2/s^2]	2.25

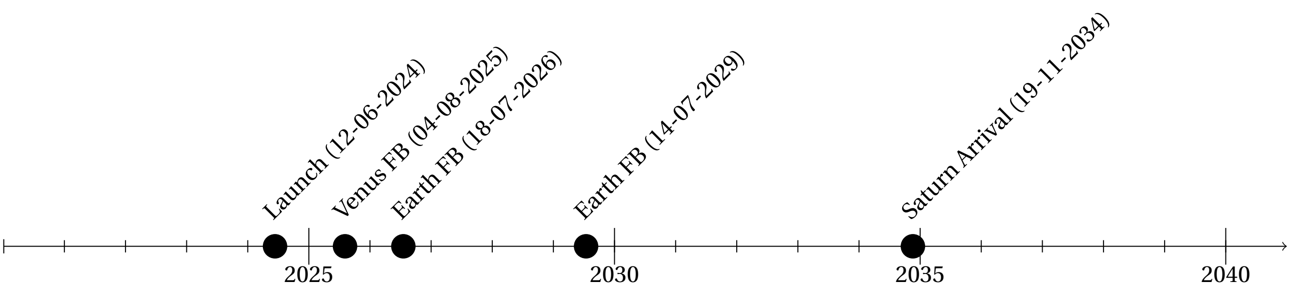

4.3.3. SATURN ORBIT INSERTION

To investigate the strategy for Saturn Orbit Insertion (SOI), the relation between ΔV and arrival C3 was established, as seen in Figure 4.19. The arrival conditions resulting from the trajectory optimisation state that SAURON would arrive at Saturn with an arrival $V_{\infty arr}$ of 5.7 km/s. Using Figure 4.19, the ΔV required to insert in a 100 day period was found to be 300 m/s. This orbit was chosen, because inserting into an orbit with a longer period would require more ΔV. In addition, a 100 day period would give sufficient time to prepare for the first Titan flyby. A periapsis raise manoeuvre of 150 m/s will change the inclination of SAURON, aligning with the equatorial plane of Saturn.

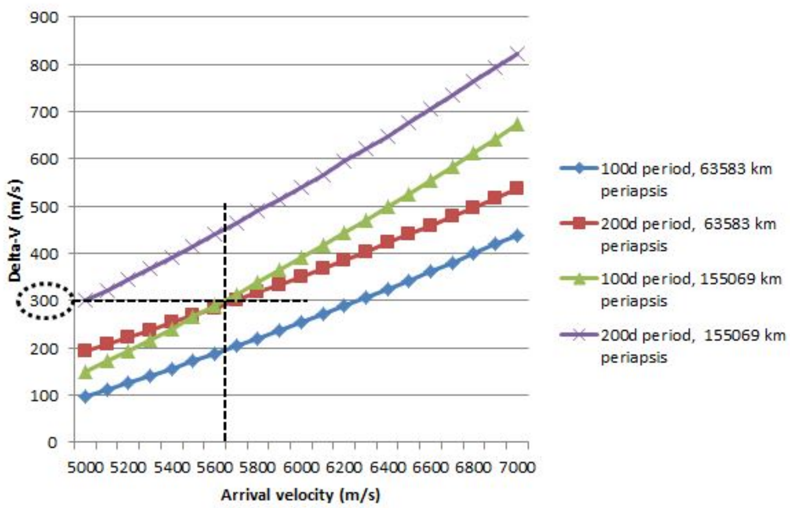

Figure 4.19: The relation between ΔV and arrival C3.

4.3.4. PUMPDOWN PHASE

A pumpdown phase is preferred over a direct insertion to the location for HOI, because it saves ΔV. A circular orbit at 142000 km from Saturn's centre, outside the F ring, requires a velocity of 16.3 km/s. Since the arrival velocities to Saturn are below 6-7 km/s, a propulsive ΔV of 10 km/s would be required. In addition, an inclination change would be needed, which results in a higher ΔV. This additional propulsive ΔV would require more propellant mass, thus reducing the propellant available for hovering.

When using an all chemical orbit insertion, the pumpdown tour will approximately take three and a half years. The tour uses multiple gravity assists in the order of Titan, Rhea, Dione and Enceladus, totalling to 50-70 flybys. The ΔV savings for this number of moons is worth the risk introduced by those flybys. Figure 4.20 and Figure 4.21 visualise the pumpdown tour. Note that this is taken from the mission concept of Nicholson et al. (2010) [54]. Nonetheless, it is presented to provide a clear visualisation of the process. Leverage propulsive manoeuvres will be used in between gravity assists, totalling approximately 350 m/s ΔV, for a chemical propulsion subsystem [54]. The final orbit would have its periapsis outside the F ring at a distance of 142000 km and its apoapsis near Enceladus' orbit, which is visible as orbit 8 in Figure 4.21.

After the pumpdown tour, the spacecraft circularises orbit 8 from Figure 4.21 outside the F ring, requiring a ΔV of 2.95 km/s. This orbit will be used to perform checks and tests. Afterwards, it will perform an inclined Hohmann transfer to a position between the A and F ring and circularise, requiring a ΔV of approximately 230 m/s.

4.3.5. HOVERING PHASE

During this phase, the hovercraft separates itself from the orbiter and starts its own transfer on top of the ring plane. The orbiter will then stay in between the A- and F-ring on the same plane as the ring plane. This was chosen to achieve as much communication time with the orbiter as possible. Afterwards, the hovercraft would make an inclined Hohmann transfer to get to the next orbit. This inclination differs based on the height that was needed to avoid collisions. This is not the situation for each transfer. The biggest hops will have to be applied at the edges of the rings.

Table 4.3: Flyby characteristics

Flyby planet	Altitude [km]	V_∞ [km/s]	Date
Venus	0.5	5.72	04-AUG-2025
Earth-1	1157	10.11	18-JUL-2026
Earth-2	0.5	10.65	14-JUL-2029

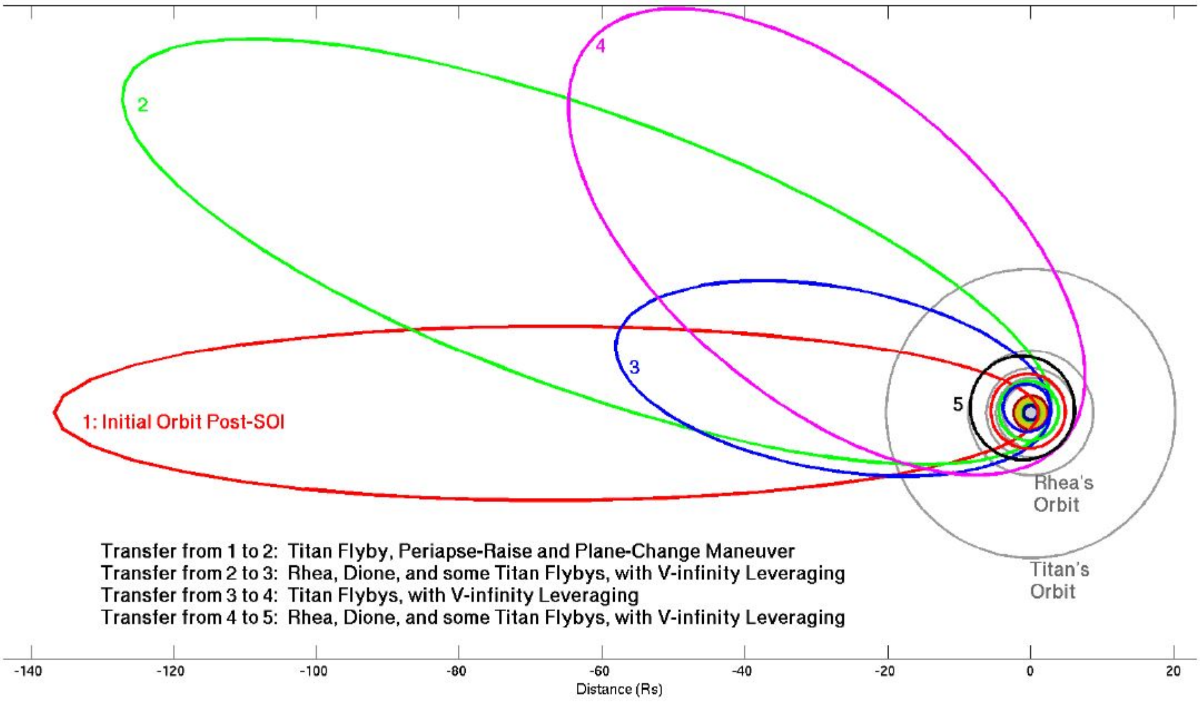

Figure 4.20: First part of the pumpdown phase, starting from SOI [4].

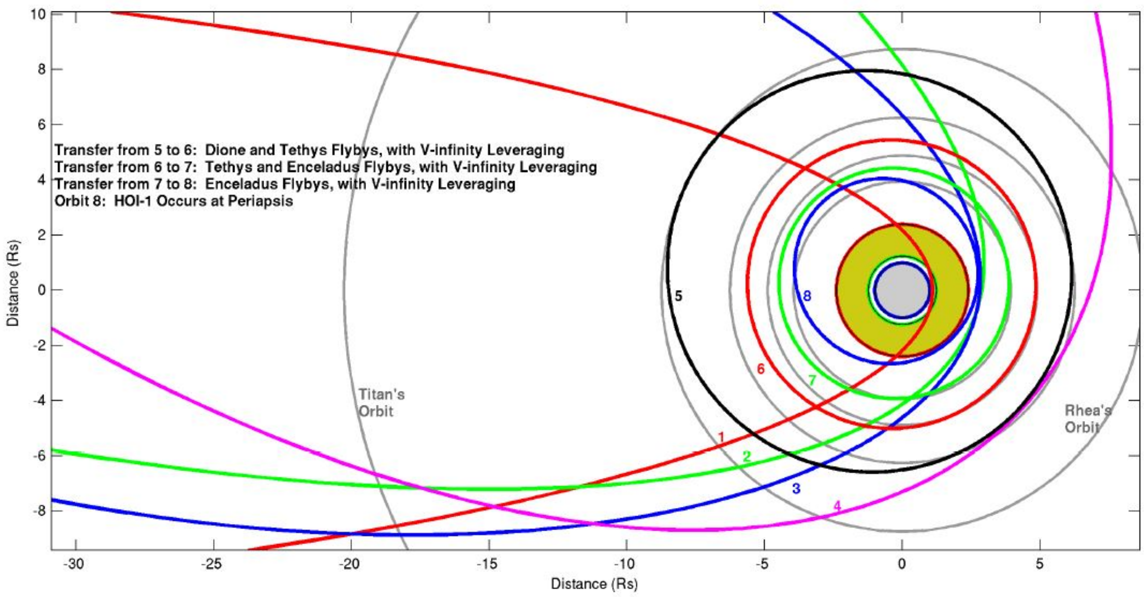

Figure 4.21: Second part of the pumpdown phase

Hovering measurements start after passing the Encke gap and ends at the inner edge of the B-ring. Before the Encke gap, the requirement cannot be met[1]. There were some points of interest chosen to orbit. These points were found in the Saturn ring observer mission concept from NASA [54]. From this, the orbits that would be analysed are at 133000, 129560, 119924 and 117000 km from the centre of Saturn. These orbits correspond with the outer edge of the A-ring, middle of the A-ring, in the Cassini Division and the outer edge of the B-ring. The spacecraft will not hop over the Cassini Division since it would have an inclined orbit of $9.55 \cdot 10^{-4}$ ^{o}. This orbit chosen as a 'safety' orbit in between the hovering phase, if there is a need to transfer more data, or if the hovercraft must park to get a new objective. The Cassini Division was chosen since dust particles are known to be there, thus it would be relatively safe to stay in orbit here[2].

[1] https://www.britannica.com/place/Saturn-planet/The-ring-system#ref514942, consulted on 20-05-2017.

[2] http://www.esa.int/Our_Activities/Space_Science/Cassini-Huygens/Solving_the_puzzles_of_Saturn_and_Titan/(print), consulted on 25/06/2017.

The requirements state that the spacecraft should be 2-3 km from the ring plane and have a hovering time of 1 month. The requirements can be seen in Chapter 3. To comply with the requirement of a month of hovering, the hovercraft would hover 17 times at 133000 and 117000 km from Saturn and 32 times at 129560 km. More orbits at the centre of the A-ring were chosen because at this location the interactions between the particles would be more noticeable. The amounts of orbits at the Cassini Division might vary to the situation that is presented when the hovercraft is there. The locations at which the spacecraft shall hover and orbit are visible in Figure 4.15.

4.3.5.1. HOPPING MANOEUVRE

Hopping is achieved by applying a short time force perpendicular to the ring plane, in which the spacecraft makes a cap parabola movement over the rings. Every time the spacecraft reaches the allowed minimum height, the thrusters would ignite. The spacecraft then gets an axial velocity pointing away from the ring plane, which becomes zero when it reaches the maximum height. Then it continues accelerating slowly toward the rings until the minimum height is reached again, which would begin a new cycle. The amount of hops that take place have a direct link to how much time the engine needs to ignite, which influences the ΔV that would be applied. The relation of the ΔV with the amount of hops is given in Equation 4.12 [55].

$$\Delta V_n = 2h_{min}\sqrt{\frac{\mu_{Saturn}}{r^3}}\tan\left(\frac{\pi}{n}\right) \quad \text{With n given the number of hops.} \tag{4.12}$$

The ΔV per hop per orbit is given in the following list.

- At 133000 km ΔV of 0.245 m/s per hop.
- At 117000 km ΔV of 0.254 m/s per hop.
- At 129560 km ΔV of 0.296 m/s per hop.

A total ΔV of 121.37 m/s was found for the hopping manoeuvre. For this ΔV, seven hops were chosen per orbit since more hops result in a lower ΔV. However, more hops will result in less time between the hops. With seven hops, the lowest orbit hop time would be 1.38 hours, which was found to be sufficient for manoeuvring and doing measurements.

4.3.5.2. TRANSFERRING BETWEEN ORBITS

To change orbits, an inclined Hohmann transfer orbit is applied. The inclination is determined by the height that the hovercraft has to climb and the difference in radius between the orbits. For every transfer, the height that must be avoided was chosen to be 15 km, except for going from 133000 to 129560 km which was 0 km. This gives a delta inclination range of 0 to 0.0017 rad. Knowing the inclinations and putting the corresponding inputs in Equation 4.13, the ΔV of this transfer orbit can be calculated[3].

$$\Delta V_i = \sqrt{V^2_{transfer,\,a} + V^2_{begin} + 2V_{begin}V_{transfer,\,a}\cos(S\Delta i)} + \sqrt{V^2_{transfer,\,b} + V^2_{final} + 2V_{final}V_{transfer,\,b}\cos(S\Delta i)} \tag{4.13}$$

In Equation 4.13, $V_{transfer,i}$ is the velocity of the spacecraft in the transfer orbit at the beginning and end. $V_{begin/final}$ is the orbital velocity of the spacecraft at the beginning and final orbit. The formulae for $V_{begin/final}$ can be found in [3]. The S in this formula is for optimal scaling for the manoeuvre, this would then give the minimum ΔV cost. The S factor can be calculated with Equation 4.14.

With this method, every orbit change can be calculated for these trajectories. This would be given in the following list.

- From 139000 to 133000 km with a inclination of 0.00083 rad a ΔV of 368.91 m/s is needed.
- From 133000 to 129560 km with a inclination of 0.0 a ΔV of 222.72 m/s is needed.
- From 129560 to 119924 km with a inclination of 0.00052 rad a ΔV of 673.98 m/s is needed.
- From 119924 to 117000 km with a inclination of 0.0017 rad a ΔV of 224.66 m/s is needed.

Thus, a ΔV of 1490 m/s was found for the summation of all the transfers.

$$S \approx \frac{1}{\Delta i}\tan^{-1}\left(\frac{\sin(\Delta i)}{\frac{V_{begin}V_{transfer,a}}{V_{final}V_{transfer,b}}\cos(\Delta i)}\right) \tag{4.14}$$

[3] http://www.braeunig.us/space/orbmech.htm, consulted on 25/06/2017.

Table 4.4: Input parameters used by MALTO.

Parameter	Range
Launch date	2017-2023
Launch mass	6300
Maximum Flight Time	9 yrs
Isp	4190
Maximum thrust	0.472
Maximum arrival V_∞	7 km/s
Maximum departure V_∞	Flyby
Maximum altitude	300 km

4.3.6. VERIFICATION AND VALIDATION

This section discusses the verification and validation of the model used. The model uses the framework provided by PyKEP to optimise a low-thrust multiple gravity assist trajectory. Validation was performed by comparing the model with data found from literature for which MALTO, a low thrust trajectory optimiser used by NASA, was used to optimise a trajectory. The same initial conditions applied to model and Table 4.5, show that the model was capable of finding trajectories in each year. The propellant mass required for such trajectories is in good comparison as those from MALTO. It was noted that adding a gravity assist planet, increased the computing time significantly, in the order of 3.

Table 4.5: Validation process of PyKEP, comparing to MALTO.

Sequence	**Launch date**		**Time of Flight [yrs]**		**Arrival V_∞ [km/s]**		**Propellant mass [kg]**	
2 Flyby results	**MALTO**	**PyKEP**	**MALTO**	**PyKEP**	**Malto**	**PyKEP**	**MALTO**	**PyKEP**
EEES	07-AUG-2017	03-NOV-2017	9.00	9.00	7.00	5.70	449	779
EEES	21-DEC-2018	21-DEC-2018	9.00	9.00	6.41	5.70	747	515
EEES	16-FEB-2019	05-APR-2019	8.50	8.90	6.87	5.80	721	603
EEES	29-AUG-2020	12-MAR-2020	9.00	9.00	6.82	5.80	416	527
EEES	17-JAN-2021	28-MAY-2021	8.50	9.00	7.00	5.75	748	849
EEES	27-JUL-2022	16-FEB-2022	9.00	8.80	7.00	6.00	510	489
EEES	24-SEP-2023	23-AUG-2023	9.00	9.50	6.64	7.00	752	655
4 Flyby results	**MALTO**	**PyKEP**	**MALTO**	**PyKEP**	**MALTO**	**PyKEP**	**MALTO**	**PyKEP**
EEVVES	25-AUG-2017	15-JUN-2017	9.00	8.50	7.00	6.30	427	1062
EEVVES	29-JAN-2018	23-FEB-2018	8.50	9.00	6.97	6.50	772	754
EEVVES	14-SEP-2019	06-JUN-2019	9.00	8.70	6.89	6.77	678	633
EEVVES	30-AUG-2020	28-FEB-2020	9.00	9.00	6.92	6.00	411	573
EEVVES	08-AUG-2022	07-SEP-2021	9.00	9.00	7.00	7.00	543	654
EEVVES	15-OCT-2023	14-JUL-2022	9.00	9.00	6.71	6.10	405	800

5
Risks

In this chapter, a risk management plan will be discussed for this mission. This would also include risk mitigation strategies and a risk map. In Section 5.1, the risk events will be identified with their corresponding causes, effects and mitigation strategies. This is followed by Section 5.2, where the highest ranking risks are established and risk maps, before and after mitigation strategies, are discussed.

5.1. Risk Identification and Assessment

The risk events that were identified are presented in the following lists. There were some variations in the type of risks, so they are clustered together in one list.

5.1.1. General

- **GR-1 Forward contamination.**
  - **Cause:** Contaminated parts of the spacecraft reach the moons of Saturn.
  - **Effect:** Planetary protection laws are violated by contaminating the environments of the celestial bodies orbiting Saturn.
  - **Mitigation:** Decontaminate the spacecraft, so the risk of contamination is as low as possible. A clear End-of-Life strategy to avoid Saturn's moons should also be applied.
- **GR-2 Heat produced by the power subsystem damages surrounding parts.**
  - **Cause:** Power subsystem is placed close to critical components.
  - **Effect:** Critical failure of the power subsystem or damage to other subsystems of the spacecraft.
  - **Mitigation:** Use of passive thermal control to cool surrounding parts. Position power subsystem at a safe distance from critical components.
- **GR-3 The Command & Data Handling subsystem is damaged.**
  - **Cause:** Multiple causes, such as short circuits, particle impact.
  - **Effect:** Subsystems can no longer be controlled.
  - **Mitigation:** Build redundancy in the Command & Data Handling subsystem.
- **GR-4 Freezing of the propellant during operations.**
  - **Cause:** Failure of the thermal subsystem.
  - **Effect:** Required ΔV cannot be obtained.
  - **Mitigation:** Test functionality of the thermal subsystem before launch. Using heat pipes to keep the fuel in operating temperature ranges.
- **GR-5 No separation of stages by the spacecraft.**
  - **Cause:** The presence of two or more stages required for the mission. Commands cannot be executed correctly due to errors in the hardware or software of the stages. Mechanical issues with the decoupling mechanism.
  - **Effect:** Could lead to mission failure if separation does not occur at all.

- **Mitigation:** To use of known separation techniques that are flight proven. A verification and validation procedures of these stages hardware and software would also be done.

- **GR-6 The main orbiter is damaged from impact with ring particles.**
  - **Cause:** Unexpected encounter with ring particles.
  - **Effect:** Loss of scientific measurements, could lead to failure of the mission.
  - **Mitigation:** Include sensors on the spacecraft which detect particles, upon which the AOCS system takes action to avoid the particles. Also, increasing shielding of the main orbiter.

- **GR-7 No separation of the dual satellite during orbit around Saturn.**
  - **Cause:** Commands cannot be executed correctly due to errors in the hardware or software of the separation system.
  - **Effect:** Could lead to not performing all required mission objectives and mission failure if separation does not occur at all.
  - **Mitigation:** Test and demonstrate the separation mechanism.

5.1.2. PRE-LAUNCH

- **PR-1 Spacecraft is damaged during transportation.**
  - **Cause:** The main reasons why this event could occur is mainly due to poor integration of the spacecraft to the transportation vehicle as well as improper checking that it has been integrated correctly.
  - **Effect:** This event could have severe consequences to the mission, because if parts need to be repaired this could lead to exceeding the cost budget of the mission, as well as delaying the launch. It could also result in complete mission failure in case the spacecraft has suffered severe damages.
  - **Mitigation:** To avoid this risk event, high quality personnel should be responsible for the integration process that would ensure integration is done properly and the spacecraft can be transported safely to the launch site.

5.1.3. LAUNCH

- **LR-1 Launcher explodes.**
  - **Cause:** Malfunction of the launcher during flight. This malfunction could concern the launcher's hardware or software. In addition, poor testing and quality checks of the launcher could lead to its failure during operation.
  - **Effect:** An apparent consequence of this risk event is the complete failure of the mission, since it leads to the complete destruction of the spacecraft.
  - **Mitigation:** Chose a trusted launcher that has already been proven in flight. Also include high quality checks and testing to be performed on the launcher, to ensure its operational success.

5.1.4. TRANSFER

- **TR-1 The spacecraft is unable to obtain the required power to initiate the transfer trajectory.**
  - **Cause:** Software and hardware errors, mechanical errors.
  - **Effect:** Spacecraft cannot rely on generating power from the solar panels. Failure in the deployment of the solar panels might cause mission failure.
  - **Mitigation:** Verification and validation procedures on the spacecraft's software and hardware, simulation and analysis of the mechanism and the deployment systems.

- **TR-2 Incorrect orbit insertion in Saturn.**
  - **Cause:** Incorrect model or propulsion or ADCS subsystem anomaly.
  - **Effect:** Extra propellant required to obtain correct orbit.
  - **Mitigation:** Verification and validation of these subsystem and add extra redundancy on these subsystem. This was done for propulsion subsystem where the main engine of the insertion stage has 4 fuel lines to have a extra redundant system.

- **TR-3 The solar panels cannot be deployed when the spacecraft switches on.**

- **Cause:** Mechanical or computing issues with the spacecraft.
- **Effect:** Spacecraft cannot generate and provide power to the subsystems.
- **Mitigation:** Test solar panel deployment and power generation performance in testing facilities, after spacecraft assembly, by simulating the deployment method.

5.1.5. HOVERING

- **HR-1 The propulsion unit of the spacecraft shuts down during hovering.**
  - **Cause:** The thrusters do not fire during hopping, due to failed ignition and propulsion leakage.
  - **Effect:** The consequences of this risk, is that the hovercraft loses attitude control and most likely crashes into the ring. This will result in mission failure as well as the possibility of contaminating the Saturn environment and/or moons.
  - **Mitigation:** Having redundant thrusters and a redundant piping of the propulsion system.
- **HR-2 The ADCS subsystem cannot determine the attitude of the spacecraft during hovering.**
  - **Cause:** The main cause would be that the sensors of the control subsystem are unable to determine the actual attitude of the spacecraft.
  - **Effect:** The propulsion subsystem will receive no or incorrect control inputs. As a result, the propulsion subsystem could let the spacecraft fall into the rings.
  - **Mitigation:** Having a redundant ADCS system could mean having more then one sensor, that could determine the attitude of the spacecraft.
- **HR-3 The hovercraft is damaged from impact with ring particles.**
  - **Cause:** Unexpected encounter with ring particles.
  - **Effect:** A ring particle could damage the spacecraft, meaning a loss of scientific measurements and partial failure of the mission.
  - **Mitigation:** Include sensors around the spacecraft which detect particles, upon which the AOCS system takes action to avoid the particles. Increasing the hover distance and increasing shielding of hovercraft could be done as well.

5.1.6. DATA ACQUISITION AND MEASUREMENTS

- **DR-1 Maximum memory capacity exceeded.**
  - **Cause:** Inefficient storage of memory could cause an early memory capacity reach. Software/coding errors could also be a cause to prematurely reaching the maximum memory capacity.
  - **Effect:** The inability to obtain more data. This could diminish the mission success.
  - **Mitigation:** Include additional data storage space for redundancy.

5.1.7. SENDING DATA

- **SR-1 Communication between the dual satellites cannot be established.**
  - **Cause:** Dual satellites cannot orient to each other, failure of the TT&C subsystem and/or damage of the antenna of the secondary satellite.
  - **Effect:** Transfer of data from the secondary satellite to the main one and subsequently to Earth cannot be achieved, loss of scientific measurements, no health status of the secondary satellite.
  - **Mitigation:** Include a secondary antenna for redundancy.

5.1.8. SUBSYSTEMS

These risk events relate to the subsystems of the spacecraft. They will cover the most important risks from each subsystem.

- **AOCS-RISK/AR-1 Failure of one or more reaction wheels.**
  - **Cause:** Degradation of the reaction wheels due to radiation over time. The spacecraft experiences cosmic radiation and there are some on-board RTGs that could accelerate the degradation process.
  - **Effect**: There are some losses in control torques over the axes. The reduction of the amount of control torque is dependent on which reaction wheel fails.

  - **Mitigation:** Have more than three reaction wheels and choose a configuration for them that does not have a big influence on the loss of control torques. For the configuration elaborate in Section 7.1. Having 4 reaction wheel, one on each axis and one on the xy-plane. The most damaging case would be that RW 2,3 & 4 fails simultaneously, which reduces the control torques by half and the control torque only applies on the x-axis. Having a failure on the RW 4 reduces the control torque of every axis to half. The other cases would just reduce one axis control torque by half. This configuration then mitigates the impacts of some of the reaction wheel failure.

- **DATA HANDLING-RISK/DHR-1 Errors in the spacecraft software.**
  - **Cause:** The code was coded incorrectly.
  - **Effect:** Some systems could not perform their function correctly or could have system failure.
  - **Mitigation:** Verifying and validating the whole system with tests.

- **DATA HANDLING-RISK/DHR-2 Bit flips could occur in the data gathered.**
  - **Cause:** The cosmic radiation that influences the processor.
  - **Effect:** This could cause the electronic components to age faster then predicted.
  - **Mitigation:** Applying memory scrubbing or reconfiguration modules on the data that is received.

- **PAYLOAD-RISK/PAR-1 The measurements gathered has errors in them.**
  - **Cause:** The instruments are not sufficiently calibrated.
  - **Effect:** The measurements that have been gathered are incorrect or useless.
  - **Mitigation:** A verification of the calibration can be performed with reference to other mission measurements.

- **PAYLOAD-RISK/PAR-2 A failure occurs in one of the instruments.**
  - **Cause:** A micro-meteoroid impacts the instruments or a short circuit occurs inside the instrument.
  - **Effect:** The amount of scientific yield that the mission could provide is reduced.
  - **Mitigation:** Adding redundancy into the science investigations.

- **PROPULSION-RISK/PROPR-1 There is a leak in the propulsion pipes or the pipes get blocked.**
  - **Cause:** The pressure inside the pipes reach a critical level.
  - **Effect:** Propellant is wasted and could contaminate the spacecraft.
  - **Mitigation:** Relief valves and filters are places at appropriate locations in the propulsion system.

- **THERMAL CONTROL-RISK/TCR-1 The surface temperatures of the satellite do not remain within the designed range.**
  - **Cause:** Failure of the thermal control system.
  - **Effect:** Large temperature differences would lead to induced thermal stresses on the structure. This can cause buckling and tension on the spacecraft surfaces.
  - **Mitigation:** The use of heat pipes and radiators to control the temperatures.

- **THERMAL CONTROL-RISK/TCR-2 A failure of the thermometers.**
  - **Cause:** Damaged thermometers.
  - **Effect:** The components will be cooled below their operating temperatures.
  - **Mitigation:** Verifying and validating the thermometers through testing before launch and have health checks od this subsystem over the course of the mission.

- **TELECOMMUNICATIONS-RISK/TER-1 There is no high data rate connection due to pointing failure of the HGA.**
  - **Cause:** The pointing acquisition or spacecraft slewing fails.
  - **Effect:** No data could be transmitted nor could commands be received.
  - **Mitigation:** The orbiter posseses a HGA, MGAs and LGAs. These could be used for lower data rate transmission.

- **TELECOMMUNICATIONS-RISK/TER-2 The transponder, amplifier, diplexer or other components fail.**
  - **Cause:** Disruption of the power provided to these subsystem.
  - **Effect:** Failure of one of the key components in the subsystem would render the specific signal pipeline inoperable.
  - **Mitigation:** The chosen design incorporates line interconnections.

5.2. RISK ANALYSIS

To analyse the mentioned risks, the likelihood and impact need to be determined for each event. A risk map was made to visualise the risk events and identify the highest ranking risks. Then, in the mitigated risk map, the mitigated risk events are included and are provided to show the effects, the mitigation strategies have on the risk events. In Figure 5.1 the risk map for the common risks are shown, which also shows the risk map after mitigation. For the report, only the most important risks will be presented.

The process to determine the likelihood and impact was done using a semi-qualitative assessment. In Table 5.1 and Table 5.2, the range of semi-qualitative likelihood, and qualitative range and description of the impact are defined, respectively.

Table 5.1: Description of the semi-qualitative probability scaling used during risk assessment.

ID	Qualitative Definition	Aiding Percentage
A	Very unlikely	Less than 1%
B	Remote	1% to 5%
C	Occasional	5% to 15%
D	Reasonably Probable	15% to 25%
E	Frequent	>25%

Table 5.2: Description of the impact scaling used during risk assessment

ID	Qualitative Definition	Description
I	Negligible	Inconvenience/Non-operational issues
II	Marginal	Degradation of secondary missions/Minor reduction of technical performance
III	Critical	Questionable mission success/Some reduction of technical performance
IV	Catastrophic	Mission failure

In Figure 5.1, the colours green, yellow and red denote low, medium and high risk, respectively. The likelihood and impact of some risks were determined based on past mission failures [56]. From the figure, it can be seen that after mitigation no risk event exists in the red zone of the risk map, meaning that all high ranking risks are mitigated. There are several risks that have a high impact and can be catastrophic, but due to their low likelihood they do not pose a big problem for the mission.

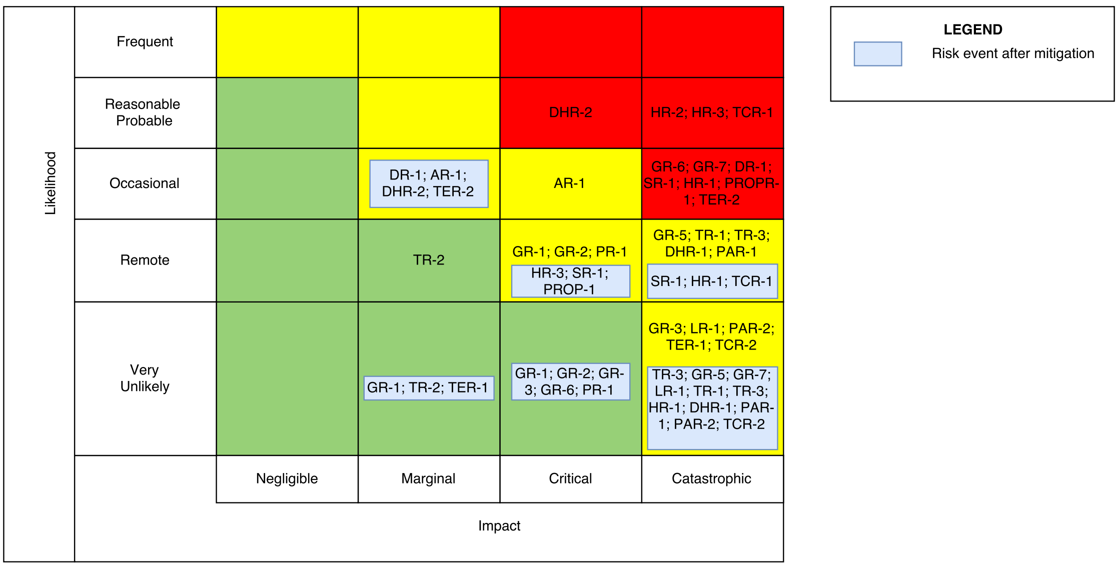

Figure 5.1: A risk map overview, with the risk events given in abbreviations. The risk events given in abbreviations after mitigation is also given.

6

SAURON - Top Level Description

This section will discuss the budget allocations for SAURON, the cost breakdown for SAURON and will illustrate the communication flow diagram. An illustration of SAURON at Saturn can be seen in Figure 6.1. This shows that the orbiter and hovercraft will not be connected and will require communications between the hovercraft and the orbiter to transmit data. That way, the orbiter will transmit data to Earth.

6.1. Budget Allocations

6.1.1. Mass Budget Allocation

The identified subsystems that require mass are instruments, propulsion, power, structures, TT&C, AOCS, C&DH, thermal control and 'others', which includes cabling. For the hovercraft and the orbiter all of them are applicable. For the SOI stage the propulsion, structures, thermal control and others are applicable and for the SEP stage propulsion, power, structures and thermal control are applicable. This can be seen in Table 6.1.

The contingencies are 18% [57], however due to changes in the actual mass because of design choices, some increased and others decreased. Still the minimum contingency is 12%. The contingency values for the structures part stand out. Only the primary structure is calculated, however there is much more. With the structure of the hovercraft and orbiter is set at 20% of the spacecraft dry mass [58], the contingencies increases. The fist stage will have a small increase, resulting in 23% because it carries all loads from the higher stages. The second stage is approximately 50% because it only carries fuel.

6.1.2. Power Budget Allocation

The power budget is discussed in Table 7.16.

6.2. Cost Breakdown

The cost breakdown has been created using the work breakdown structure for the post-DSE development and operations. The estimation methods can be found in the respective chapters. Table 6.1 shows the cost breakdown of the top-level.

6.3. Hardware diagram

Figure 6.2 and Figure 6.3 shows the hardware diagrams. These diagrams give a good overview of all the hardware included and its interdependencies, power lines and data lines.

6.4. Communication Flow Diagram

When a signal is sent towards a spacecraft near Saturn from Earth, it takes over an hour before it is received. Thus, it is paramount that the communication flow is well understood and that the spacecraft can function autonomously. For this purpose, the general communication flow is investigated and presented in a flow diagram.

6.4.1. Ground Segment

The ground segment will make use of ESA's ESTRACK network. A schematic overview of the communication flow is presented in Figure 6.4. For the purpose of clarity, the uplink and downlink flows have been separated, however, in reality these likely occur through the same antenna or array. One can see that the operator, through the command centre, uplinks their commands to the space system. The space system downlinks the telemetry and science data to the ESTRACK network, after which it will reach the operator who processes the data and stores it in the project database. From this database, data will be provided to scientists who can analyse it further.

Table 6.1: Mass and cost breakdown budget of the SAURON mission.

WBS element	**Actual values (kg)**	**Contingency (%)**	**Mass with contingency (kg)**	**Mass fractions of dry mass (%)**	**€M 2017**
Main orbiter	720		795		
AOCS	25	22%	30	6.1%	10
Telecommunications	80	20%	96	19.4%	77
C&DH	14	21%	16	3.3%	80
Others (Cabling)	20	21%	24	4.9%	
Payload	54	0%	54	10.9%	105
Power supply	142	20%	170	34.3%	130
Propulsion (engines+tanks)	45	20%	54	10.9%	1
Structure (main)/bus	32	21%	39	7.8%	8
Thermal control	10	19%	12	2.4%	9
Bipropellants	255		255	32.1%	0
Monopropellants	44		44	5.6%	
Hovering spacecraft	1049		1117		
AOCS	45	20%	53	12.0%	16
Telecommunications	40	19%	48	10.7%	43
C&DH	14	18%	16	3.6%	80
Others (Cabling)	12	18%	14	3.2%	
Payload	39	0%	39	8.8%	83
Power supply	92	21%	111	25.1%	81
Propulsion (engines+tanks)	63	21%	76	17.1%	2
Structure (main)/bus	52	20%	62	14.0%	12
Thermal control	20	21%	24	5.5%	18
Bipropellants	633		633	142.6%	0
Monopropellants	40		40	9.0%	
SOI stage wet	7183		7324		69
Others (Cabling)	13	20%	16	2.0%	
Propulsion (engines+tanks)	394	22%	480	60.1%	
Structure	230	21%	278	34.8%	
Thermal control	21	20%	25	3.2%	
Bipropellants	6003		6003	750.8%	
Extra bipropellants	521		521	65.1%	
SEP stage wet	1403		1536		88
AOCS	1	0%	1	0.1%	
Power	247	20%	296	36.7%	
Propulsion (engines+tanks)	351	19%	418	51.8%	
Structure	70	21%	84	10.5%	
Thermal control	6	20%	7	0.9%	
Xenon gas	729		729	90.4%	
Total dry mass	2130	19%	2546		
Total wet mass	10355		10771		
Production					123
Operations					480
Total cost					1500

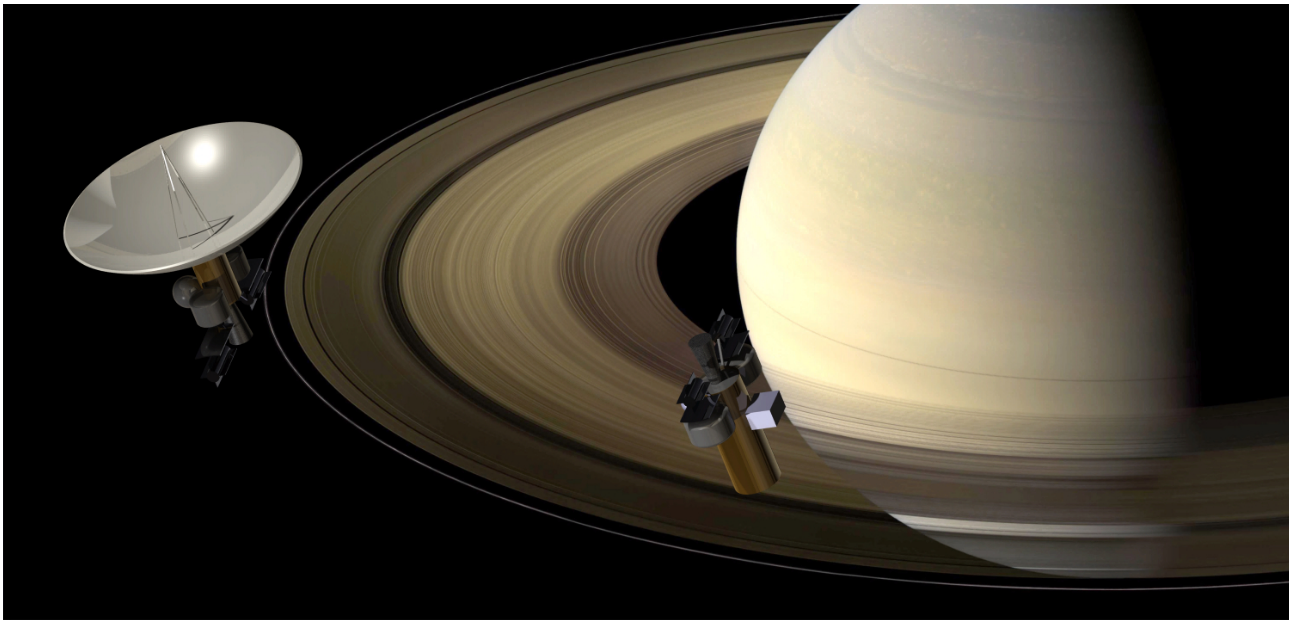

Figure 6.1: Representation of SAURON in the Saturnian environment.

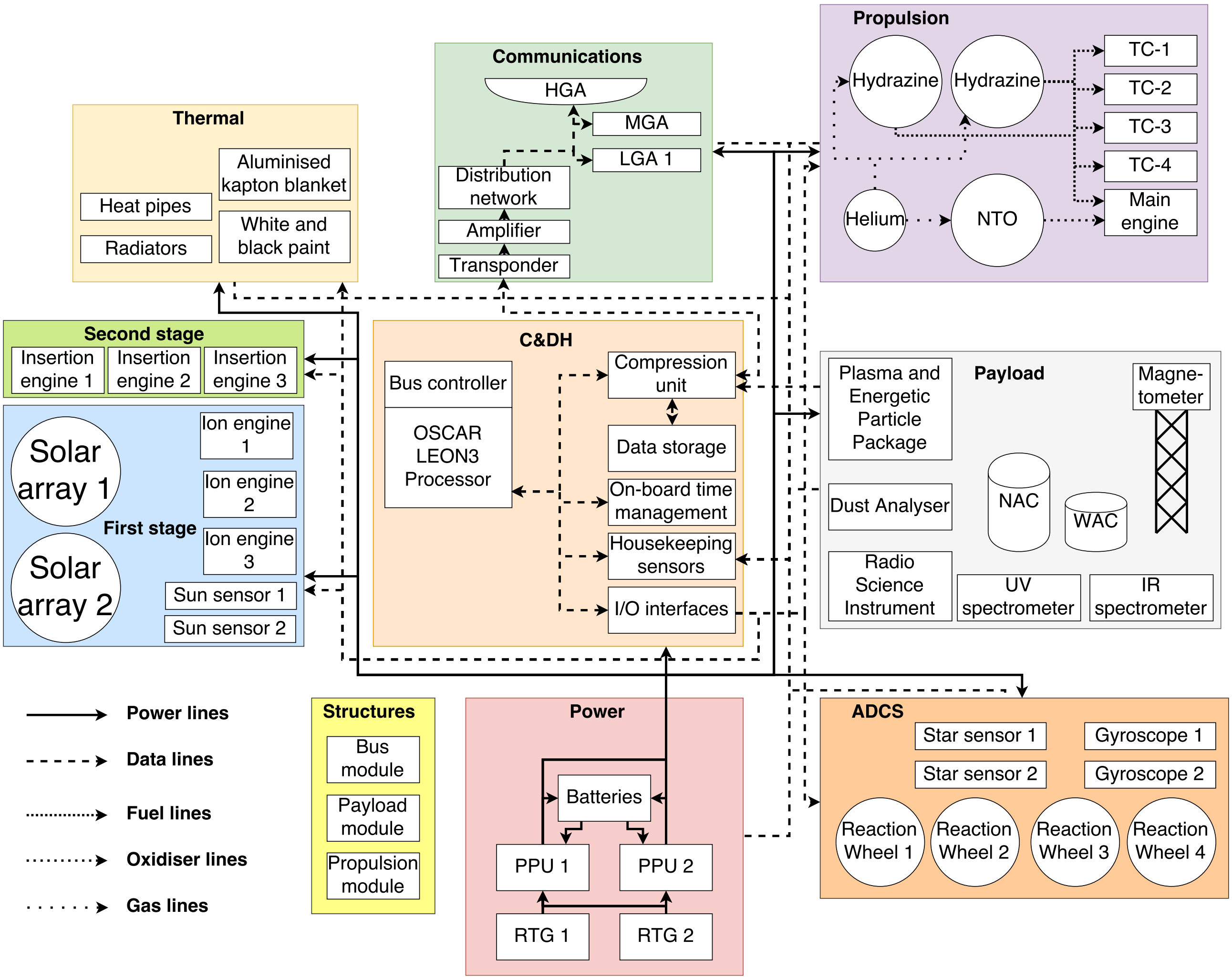

Figure 6.2: The hardware diagram of the orbiter.

6.4.2. Space Segment

The schematic overview of the space segment is found in Figure 6.5. Since it will have to function autonomously, it is important to know exactly which inputs are required and which subsystems influence each other. The space-

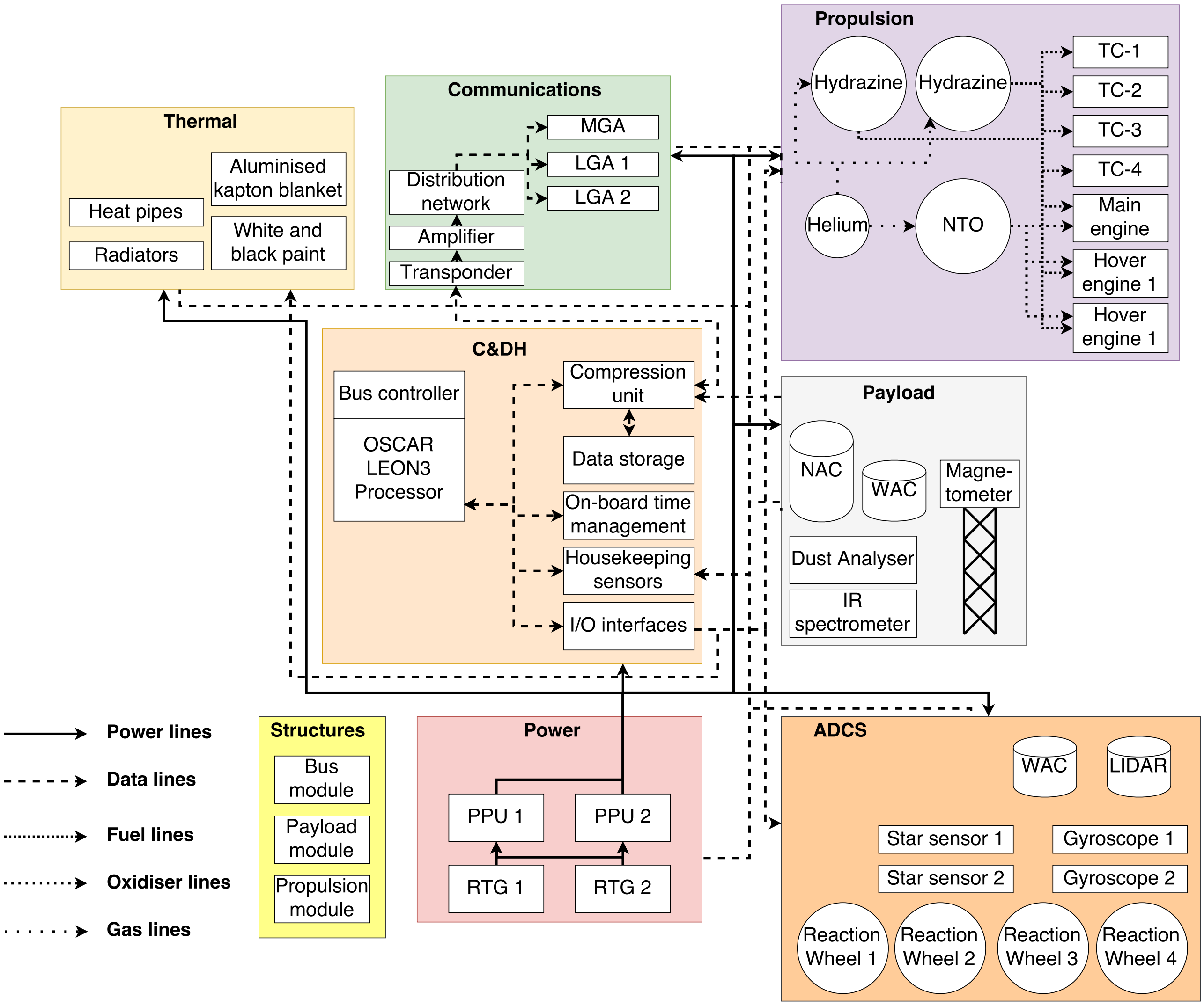

Figure 6.3: The hardware diagram of the hovercraft.

craft will use its antennas to receive commands from the ground stations and send telemetry and data back to Earth. The incoming and outgoing data is handled by the Command and Data Handling subsystem, which will in turn give commands and obtain data from the other subsystems. The Command and Data Handling subsystem should be able to operate autonomously when the attitude or orbit has to be altered. In the figure, the red full lines represent the command signals in the system, while the black dotted lines represent the data flowing between the subsystems. The black dashed lines above the antenna represent external data flows and show the link to the ground segment. The data flows are specified in the figure. On this data commands are based, this results in an action performed by the subsystem. Data is send back as feedback and an adjustment is made if the action is not performed accordingly. The data between the subsystems and the Command and Data Handling subsystem is not specified, because it is consists all of the specific subsystem operation status and subsystem operations.

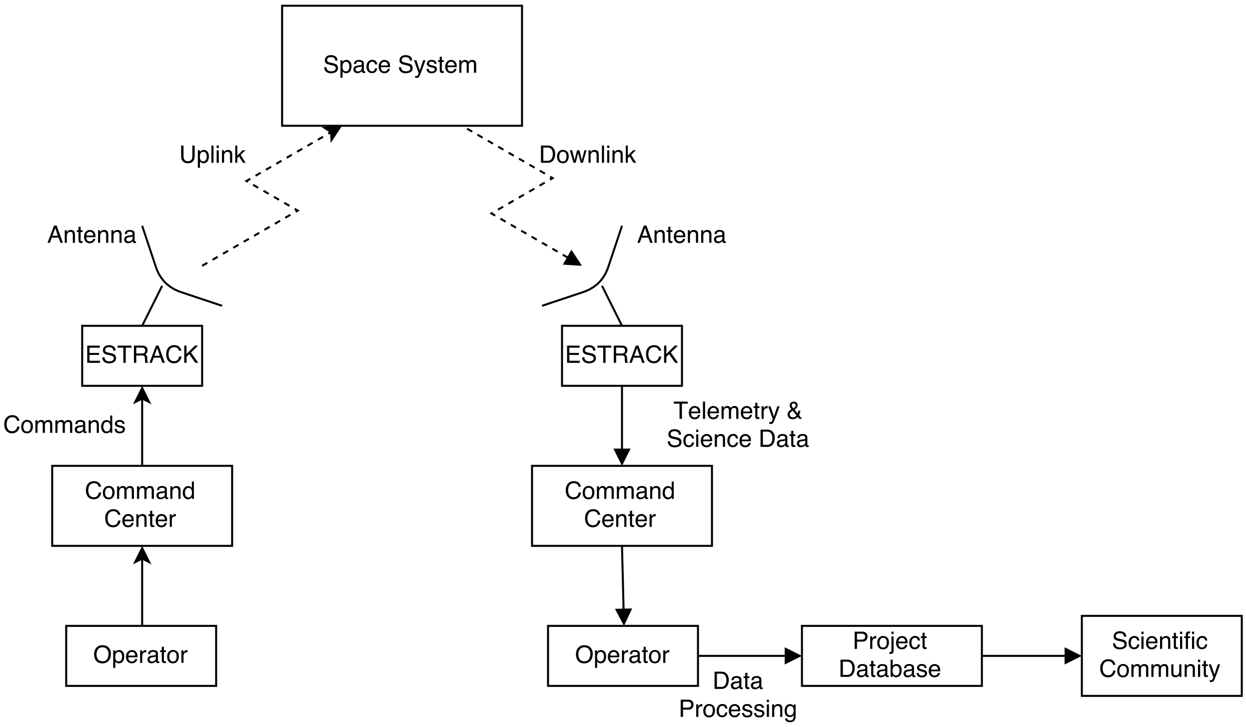

Figure 6.4: A schematic overview of the communication flow of the ground segment.

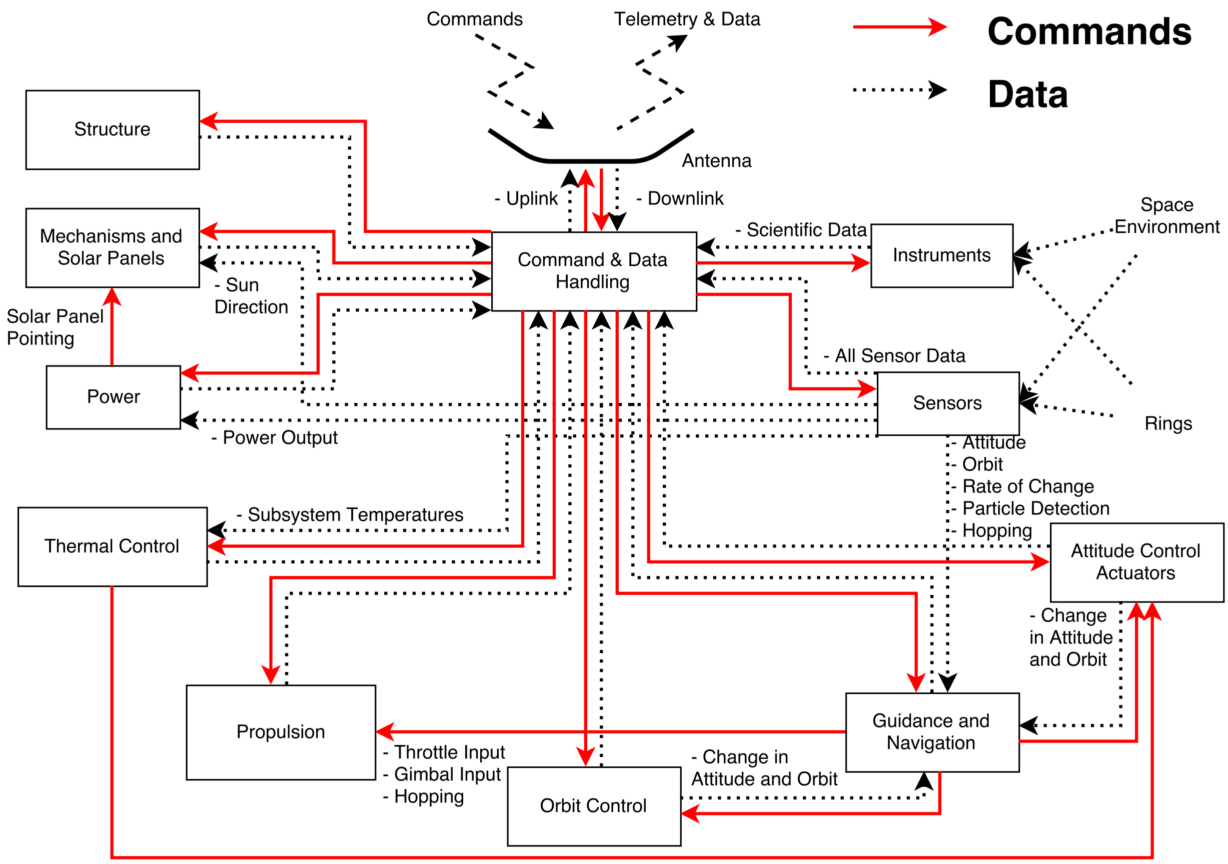

Figure 6.5: A schematic overview of the communication flow of the space segment.

7 SAURON - SUBSYSTEMS

7.1. AOCS

Section 7.1 describes the design process and the design choices for the the Attitude & Orbit Control System (AOCS) of the spacecraft. A layout and quick overview of the subsystem is presented first in Subsection 7.1.1, followed by an identification of the subsystem and mission interactions on the Attitude Determination & Control system (ADCS) in Subsection 7.1.2. It presents an overview of what influences the ADCS design. Following interaction identification, driving requirements are identified in Subsection 7.1.3. Next, the disturbance environment that the spacecraft will experience is quantified in Subsection 7.1.4. Based on the requirements and operating environment, the control strategy is selected and the hardware is selected and sized. This is described in Subsection 7.1.5. Then Subsection 7.1.6 describes the trajectory navigation & control. This section then ends with description of the power consumption, cost estimation, AOCS RAMS and Risk and Verification plan for AOCS.

7.1.1. AOCS LAYOUT & QUICK OVERVIEW

The AOCS subsystem consists of sensors and actuators that are used to maintain stability and track the location of the spacecraft. An overview of the sensors and actuators is given in the Table 7.1. These were chosen with the use of the requirements that were set for this subsystem in Subsection 7.1.3. In this table the location of the unit is also indicated, which is further specified in the respective instrument subsections.

Table 7.1: An overview of the units in the AOCS.

Sensors	**Gyroscopes**	**Star Sensor**	**Sun Sensor**	**LIDAR**	**WAC**
Amount	4 & 4	4 & 4	2	1	1
Location	HC & OC	HC & OC	1^{st} stage of S/C	HC	HC
Actuators	**Reaction Wheel**	**Control Thrusters**	**Hop Thruster**		
Amount	4 & 4	12 & 12	4		
Location	HC & OC	HC & OC	HC		

For every unit used in the AOCS design, a reference value was researched. Table 7.2 gives an indication of each unit with its mass and power consumption. Further explanation of these units is given in Subsection 7.1.5. An agreement was made to let the propulsion department design the attitude thrusters. Thus, in Section 7.4 an extensive description of the selected thrusters can be found. The cost of the whole subsystem is estimated to be around €26.6 million. This cost estimation method will also be further elaborated in Subsection 7.1.8.

Table 7.2: An overview of the mass and power consumption of different units.

Per Unit	**Mass [kg]**	**Power consumption [W]**
Gyroscopes	0.2	0.1
LIDAR	16	6
Reaction Wheels	3.6	7
Star sensor	5	5.6
Sun sensor	0.3	1
Wide angle camera	3.7	5.9

7.1.2. ADCS DESIGN INTERACTIONS

Figure 7.1 shows subsystem and mission interactions of the ADCS. Part of the inputs are subsystems that influence the ADCS design. Special thermal manoeuvres, as rotating the spacecraft, could be required for thermal control. The pointing accuracy will have to be satisfied for communication between the spacecraft and ground segment. The pointing of the solar array during the first stage of the spacecraft affects the ADCS as well. The 'mission' input drives the design of the ADCS as they are directly related to the mission objective. To investigate the composition and particle dynamics of Saturn's rings, requirements for the imaging instruments will have to be established. These driving requirements for knowledge, stability and control will be elaborated in Subsection 7.1.3. After the inputs are analysed and requirements are established, the ADCS is designed. Trades will be made regarding control strategy, sensors, actuators and the computational architecture. The design of the ADCS will influence several subsystems described as outputs in Figure 7.1. The ADCS sensors will draw an amount of power. The actuator selection has an influence on the propulsion and structure of the spacecraft. The selection and output in Figure 7.1 will be described in Subsection 7.1.5.

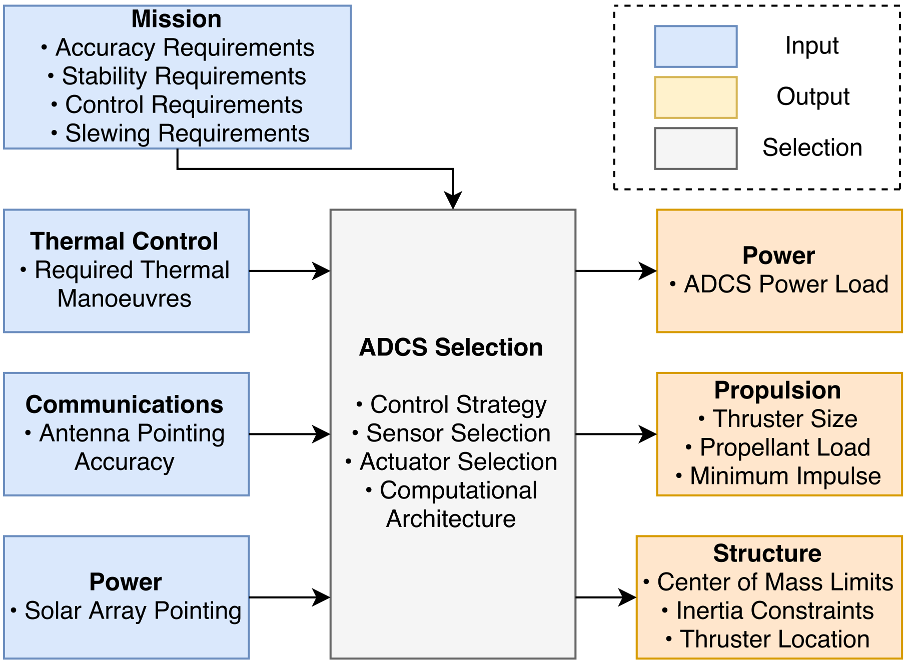

Figure 7.1: Subsystem and Mission Interactions of the ADCS system [58].

7.1.3. DESIGN DRIVING REQUIREMENTS

The three driving attitude control requirements are knowledge, control and stability. These requirements flow down from top-level system requirements on science. The hovercraft will have to be able to characterise the size distribution and spin states of ring particles with a diameter of 1-10 m. To accomplish this, the spatial resolution of the images will have to be at least 10 cm [54]. The hovercraft hovers at a distance of 2-3 km from the rings. Therefore the imaging requirements are designed for the longest distance of 3 km. At 3 km hover distance, 10 cm spatial resolution corresponds to 33 microradians. Taking a 1 megapixel image at a spatial resolution of 10 cm would result in a field of view of 100 m. According to Nicholson et al. [54], taking one frame of 1 megapixel per minute would satisfy all determined top-level system requirements on science.

Table 7.3 shows the requirements on imaging such that the images are of a quality that makes extraction of scientific information possible. Knowledge implies how well the orientation of the spacecraft known with respect to an absolute reference. Control, also known as pointing accuracy, implies how well the attitude can be controlled with respect to the required direction. Stability implies the rate of change of angular orientation. The requirement values in Table 7.3 should not be exceeded for the particular instrument. The ADCS will be designed for the NAC requirements as these requirements are stricter than the WAC requirements and antenna pointing accuracy requirements for the communication system. Additionally, the spacecraft shall be able to perform the required thermal manoeuvres and point its solar array during interplanetary transfer. These requirements have to be accounted for, but will not drive the design such as the knowledge, stability and control requirements.

7.1.4. DISTURBANCE FROM THE ENVIRONMENT

In the life span of the spacecraft, there are some environmental characteristics that could make the spacecraft unstable. The following sections describe disturbance torques that the spacecraft will encounter. In Table 7.4 the magnitude of the disturbance torques at which phase could be seen.

Table 7.3: Knowledge, Control and Stability Requirements on the Imaging Instruments [54].

	Narrow Angle Camera (NAC)	Wide Angle Camera (WAC)
Knowledge Requirement	0.0004 deg	0.0058 deg
Control Requirement	0.06 deg	0.5 deg
Stability Requirement	0.004 deg/sec	0.058 deg/sec

7.1.4.1. Solar Radiation Pressure

Solar radiation is something that every spacecraft encounters and has to be designed for to manage this disturbance. Solar radiation becomes a larger issue when the spacecraft has a solar array on it, which is the case for this mission. Also, an interplanetary transfer trajectory was chosen that would have a fly-by past Venus. This would mean that there is a section of the transfer in which the solar constant is considerably higher than during the rest of the trajectory. When determining the solar constant, Equation 7.1 was used, which is dependent on the distance to the centre of the Sun[1].

$$\Phi = \frac{r_{Sun}^2}{d^2} H_{Sun} \tag{7.1}$$

Taking the spacecraft dimensions from Section 7.5 for the centre of mass, the centre of pressure was assumed to be the midpoint of the solar array. The respectability factor and angle of incidence were left in their appropriate range. Using these inputs the solar radiation pressure torque was calculated using Equation 7.2 [58].

$$T_s = \frac{\phi}{c} A_s (1+q)(cp_s - cm)\cos\varphi \tag{7.2}$$

7.1.4.2. Magnetic Field

Saturn's magnetic field is the second largest in the Solar System, thus disturbances due to the magnetic field would occur. The disturbance torque is affected by the spacecraft residual dipole moment and the magnetic field strength of the body that it is orbiting. The residual dipole moment depends on the size of the spacecraft, which ranges anywhere from 0.1-20 Am^2. The strength of the magnetic field is determined by the magnetic moment of the orbiting body and the magnetic latitude range. Magnetic latitude range ranges from 1 at equator to 2 at poles. The magnetic strength is also dependent on the distance of the spacecraft to the body centre. To calculate the magnetic disturbance torque, Equation 7.3 is used [58]. For this design the spacecraft's size will be large, thus the highest spacecraft residual dipole moment was used to apply these calculations.

$$T_m = DB = D\left(\frac{M}{R^3}\lambda\right) \tag{7.3}$$

7.1.4.3. Gravity Gradient

The gravity gradient disturbance occurs when the centre of mass of the spacecraft is not aligned with the centre of gravity with respect to the local vertical. This occurs when the spacecraft body is subject to a non-uniform gravity field which can cause external torques about the body centre. The disturbance torque is dependent on the gravitational constant of the orbiting body and the distance to the centre of this body. A bigger difference between the moments of inertia will increase the disturbance torque. The disturbance torque is also influenced by the angle between the local vertical and the z-principal axis. This was chosen to have a range of 0 to π. The disturbance torque could be calculated with Equation 7.4 [58].

$$T_g = \frac{3\mu}{2R}\left|I_z - I_y\right| sin(2\theta) \tag{7.4}$$

Other disturbance torques that were considered are leakage within the propulsion system, fuel sloshing in the propulsion tanks and moving parts of the satellite structure. These were found to be difficult to quantify for this design stage, but should be further studied to get a more detailed design of the AOCS system.

When analysing these disturbance torques, they were calculated for every phase of this mission. This was then put in a list which gives a clear indication of when in the mission they occur. Next, this was used to calculate the total disturbance torques that the spacecraft could encounter and this was then used to design an ADCS system to counteract these torques. This must be done keeping in mind the requirements set for this subsystem. The following

[1] http://pvcdrom.pveducation.org/SUNLIGHT/SPACE.HTM, consulted on 19/06/2017.

Table 7.4 will illustrate the maximum disturbance torques that were found and at which phase they occurred. This table gives the maximum torque found over all the axes.

Table 7.4: Disturbance torque encountered by the spacecraft.

	Interplanetary transfer [Nm]	**Operations [Nm]**
Solar Radiation Pressure	0.93	0.0054
Magnetic Field	0.0011	0.00011
Gravity-Gradient	0.00041	0.040

7.1.5. ADCS DESIGN

7.1.5.1. CONTROL STRATEGY

Due to the high required accuracy of the instruments, 3-axis stabilisation is necessary [58]. Passive control technique and spin control technique were also looked into. These three control strategies have various methods on how to achieve a certain pointing accuracy, but after analysing their pointing accuracy ranges, doing zero momentum attitude control method was chosen [58]. This control method has a pointing accuracy for thrusters between $\pm$ 0.1° to $\pm$5°(per axis), control wheels between $\pm$0.0001° to $\pm$ 1°(per axis) and gyroscope between $\pm$0.001° to $\pm$1°[58]. Due to that the AC has to comply with a knowledge requirement and control requirement as stated in the Subsection 7.1.3, reaction wheels were chosen to achieve this goal. When the spacecraft would be travelling near Venus the solar radiation disturbance is one of the largest disturbance torques. As a result of this control thrusters are also used to stabilise the spacecraft. In Figure 7.2, a block diagram can be seen describing the ADCS functioning. This gives an idea of which inputs there are on this system and how the feedback loop of the sensor works on the given desired attitude input.

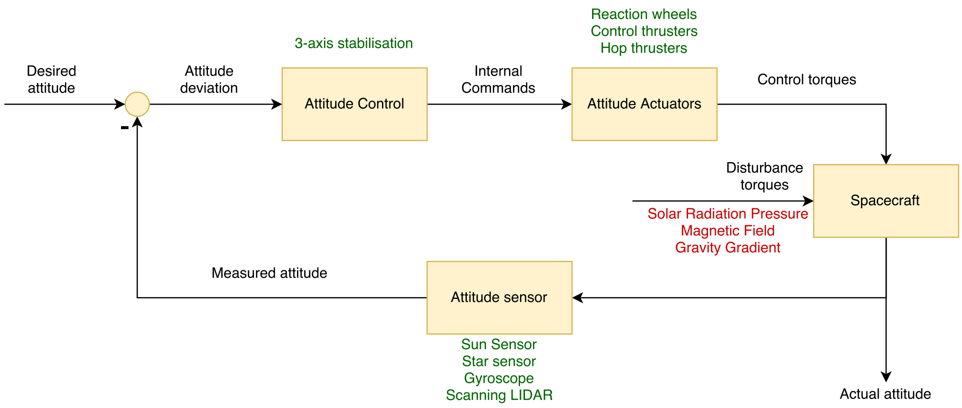

Figure 7.2: Attitude control loop with the units and the disturbances at their appropriate location.

7.1.5.2. SENSOR SELECTION

To detect if the wanted stability of the ADCS method is achieved, sensors are required. The sensors that were chosen are: star sensors, sun sensors, gyroscopes and a Scanning LIDAR.

STAR SENSOR

Star sensors are mostly used on 3-axis stabilised spacecraft. They can track one or more stars to derive 2- or 3-axes of attitude information. Since the spacecraft is not spin stabilised, the star sensor is used as a tracker. The star sensor has a performance rate of 0.0003° to 0.01°[58]. The star sensor that was used for reference has a mass of 5 kg and a power consumption of 5.6 Watt. This star sensor also gives an accuracy range of 0.000916° to 0.00308° in the pitch and yaw axis and 0.0094° to 0.08° in the roll axis[2]. These sensors must be located on the sides of the spacecraft, so that they could point towards the stars to function.

SUN SENSOR

Sun sensors detect visible-light or infrared to measure one or two axes between their mounting base and incident sunlight. These sensor are very reliable but require a clear field of view. The performance rates are 0.005° to 3°[58]. The sun sensor that was used as a reference has a mass of 0.3 kg and a power consumption of 1 Watt. The Sun sensor has an accuracy of 0.02° and the main function of this sensor is to locate the Sun to accurately point the solar arrays[3].

[2] http://www.leonardocompany.com/en/-/aastr, consulted on 19/06/2017.
[3] http://www.leonardocompany.com/documents/63265270/65745274/S3_Smart_Sun_Sensor_LQ_mm07948_.pdf, consulted on 19/06/2017.

It would be better to place the sun sensor on the first stage, in front of the solar array. This then solves the problem of the solar arrays blocking the view of the Sun sensor with the Sun.

Gyroscopes

Gyroscopes measure the speed of angle of rotation for am inertial reference frame. The performance rate is $8.33 \cdot 10^{-7}$ °/s to 0.000278°/s [58]. The gyroscope that was used for the references has a mass of 0.2 kg and a power consumption of 0.1 Watt. These have basis stability of $1.39 \cdot 10^{-7}$ °/s[4]. A gyroscope does not need any external knowledge, thus it can be placed inside the structure of the spacecraft. A location near the centre of mass would be optimal, but if this is not possible, the deviation to the location of mass must be taken into account in the program for the ADCS.

Scanning LIDAR

A scanning LIDAR uses a pulsed laser light to measure the distance to a target. This would be useful on the hovercraft to detect the distance to the ring and ring particles heading towards the hovercraft. The scanning LIDAR that was used for the references has a mass of 16 kg and a power consumption of 6 Watt on average [54]. This LIDAR should have a range of 6 km. The LIDAR would be placed at the bottom of the hovercraft, in the same direction as the payload.

Reaction Wheels

Reaction wheels are active stability control actuators of the spacecraft, compared to a momentum wheel which is passive. Four reaction wheels were found to be sufficient to control every axis of the spacecraft and have one left for redundancy. The configuration that they have also has an influence on how much torque they could provide per axis. The configuration that was chosen would be RW 1 on the x-axis, RW 2 on the y-axis, RW 3 in the z-axis and RW 4 tilted on the (x, y) plane, this can be seen in Figure 7.3. This gives a control torque of 0.22 Nm maximum per axis. The reaction wheels that were used for reference have a mass of 3.6 kg and power consumption of 7 Watt each. Each reaction wheel give a maximum torque of 0.11 Nm [5].

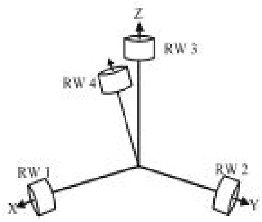

Figure 7.3: Reaction wheel configuration. [59]

Control Thrusters

12 small thrusters were chosen to control the hovercraft and the orbiter. These thrusters have a thrust range of 0.28-0.99 N. For the second stage six control thrusters were chosen of 22 N thrust each. They are further explained in the Section 7.4.

Hop Thruster

For the hopping manoeuvres of the hovercraft four thrusters were chosen to achieve this motion. These thrusters have a thrust of 22 N each. These are further explained in Section 7.4.

7.1.6. Trajectory Navigation & Control

7.1.6.1. Requirements

To satisfy user requirements on science and performance, the spacecraft has to travel to Saturn, insert into its orbit, be able to perform manoeuvres to reach the hover orbit and perform the mission operations. This imposes requirements on trajectory navigation and control. Trajectory navigation and control will have to be performed during the transfer, orbit insertion, pumpdown phase and hover orbit. For navigation, the AOCS shall provide hardware and software capable of autonomous on-board determination of the spacecraft orbital state which includes position, velocity and time [60]. Position, velocity and time will have to be determined within a certain amount of accuracy. The commanded ΔV manoeuvres to control the trajectories will have to be within a certain accuracy. Attitude manoeuvres will have to be performed within a certain amount of time. The control and navigation of the trajectories will have to be performed autonomous for certain phases of the mission.

[4] http://www.northropgrumman.com/capabilities/hrg/documents/hrg.pdf, consulted on 19/06/2017.
[5] http://bluecanyontech.com/wp-content/uploads/2017/03/DataSheet_RW_06.pdf, consulted on 19/06/2017

7.1.6.2. AUTONOMY

Autonomy is required because the signal transmission delay is approximately 90 minutes from Saturn to Earth. This implies that no ground control communication is possible during critical mission phases like fly-bys, orbit insertion and other events. In addition, the environment around Saturn is not fully known which implies that the spacecraft should be able to recognise certain hazards and respond to the situation. Two driving requirements for autonomy on the spacecraft are defined [61]. A Fault Detection, Isolation & Recovery (FDIR) technique is required in the system to have a fail-safe operation mode for when a failure is detected. If the communication link is lost due to disturbances, the spacecraft shall be able to reacquire its communication.

7.1.6.3. NAVIGATION HARDWARE & METHOD

On board computers will use the spacecraft antennas, star trackers and sun sensors to obtain the position and velocity of the spacecraft. Selection of the sensors was based on the driving ADCS requirements, described in Subsection 7.1.3. These sensors will also meet the navigation accuracy requirements on position and velocity estimation. Required position and velocity accuracy requirements are unknown, however, it is known that Cassini met its position and velocity requirements for the transfer, insertion and manoeuvres with similar sensor equipment [62]. Since current sensors perform with higher accuracy, the spacecraft will also be able to meet its requirements on position and velocity. In addition, algorithms on position and velocity estimation have improved over time.

The ground station antennas are used to transmit radio signals to the spacecraft and back to the ground station to measure its position and velocity. An atomic clock is used in this process to measure the frequency changes, also known as the Doppler shift. Star trackers and Sun sensors are used to determine directional data from the spacecraft to the Sun and other stars. This data can be analysed and processed by algorithms such as the Kalman filter to achieve autonomous navigation. The combination of antennas and star sensors for position and velocity data will increase the accuracy and reliability of the data, increasing autonomous capabilities.

To perform calculations on the trajectory an inertial reference frame is used where a grid is placed over the solar system and fixed relative to the star background[6]. With accurate knowledge of planetary ephemerides, it is possible to determine the gravitational forces working on the spacecraft. By combining all the different data, it is possible to create models that have a more accurate position estimation. By taking several measurements over a certain of period of time, it is possible to determine the velocity and the future position of the spacecraft.

7.1.6.4. TRAJECTORY CONTROL HARDWARE & METHOD

Trajectory control consists of Trajectory Correction Manoeuvres (TCM). Velocity changes for the TCMs will be performed by the main rocket engine. If smaller velocity changes are required, the reaction control system is used which consists of 12 control thrusters for the orbiter and 12 control thrusters for the hovercraft. The hovercraft will have 4 additional hop thrusters to maintain distance from the ring plane. TCMs in the transfer are required due to the trajectory error that builds up over time. These manoeuvres are planned and calculated by the ground segment. The hovercraft requires autonomous Orbit Trim Manoeuvres (OTM) in the hovering orbit.

PARTICLE AVOIDANCE STRATEGY

Using the camera instruments required to perform scientific measurements on the rings, described in Section 2.10, it is possible to detect the ring plane. A scanning LIDAR will be implemented in the hovercraft to additionally detect the distance to the ring plane. The LIDAR can detect the ring plane in higher resolution and also provide ranging [54]. Using the LIDAR in combination with the cameras, the reliability of the critical hovering phase increases. Once the algorithm detects the spacecraft is too close to the ring plane, a hop manoeuvre is performed.

To verify if the chosen trajectories are feasible and map hazardous collision possibilities, a WAC was equipped to the side of the spacecraft. This location was chosen such that the spacecraft can make measurements and map out the trajectories without rotating. This WAC will make photos of the rings in a radial direction to Saturn. These photos are sent to the ground control centre and analysed to choose a safe trajectory for transfer in between the rings. The images should be made during start of the first hover orbit and should be sent to the ground station as soon as possible. If hazardous situations are identified, the ground station should make an appropriate plan to approach this. From the side WAC, the distance from the hovercraft to Saturn itself could be estimated with aid of the shadow of the particles on the outer atmosphere of Saturn.

Additionally, stereo imaging can be used for ring collision hazards. However, stereo images of sufficient quality can be made at maximum 60 times the distance between the distance of the cameras [54]. If this option is used, the WAC of the scientific payload and the navigation particle detection WAC would be used. This could be useful to map hazardous smaller particles in the range between 30 and 60 meters.

Transferring between orbits is critical in terms of navigation for the HC. The manoeuvre includes jumping over the inclined ring particles and move the HC inwards. Here is where the relative velocity compared to the ring particles would be the highest. To detect ring particles at the sides and the bottom of the hovercraft, the LIDAR, WAC, NAC which are pointed towards the ring plane are used. Additionally the WAC on the side is used.

[6] `https://www.scientificamerican.com/article/how-do-space-probes-navig/`, consulted on 19/06/2017.

Since particles could also be detected at the side of HC, flip mirrors will be implemented in the cameras to point them into a different direction. The WAC provides context for the LIDAR and narrow angle which are more directional and precise. With the aid of these precise instruments the distance to this particle is estimated. This configuration of instruments would be able to detect a 1.2 m object at 3 km away. Further studies of the potential range of detection should be investigated.

With this information the HC should have to apply the pre-programmed avoidance manoeuvre. When a hazardous object is identified, the HC would thrust towards the ring plane to reach a higher altitude to avoid the object. This manoeuvre would be done by the hop thrusters. These will ignite till the HC is over the the approved distance change. This distance change is calculated by multiplying the diameter of the object by 2 and adding the height of the HC. The multiplier of 2 is a safety factor to avoid the particle. If this manoeuvre is performed while in hopping orbit, the HC would then continue the standard hovering mode. But when manoeuvring in a transfer orbit, the HC must then compensate for this and go back in the appropriate transfer orbit.

The time of this manoeuvre can be estimated by adding the detection time, ignition time and the time for manoeuvring. The detection time was estimated to be 0.5 seconds, using detection methods of self driving cars as reference [63]. The ignition time was estimated to be 0.02 seconds for the hop thrusters. This was estimated by assuming that the plumbing length is around 70 cm, the chamber pressure was assumed to be around 10 bar and the flow velocity was found with Bernoulli's incompressible equation. The manoeuvre time depends on the size of the detected particle. The bigger the particle is the more time the manoeuvre takes. To estimate this, Equation 7.5 was used. This formula gives the relationship between distance, velocity, acceleration and time.

$$V_0 t_m + \left(\frac{F_T}{M_{HC_0} - \dot{m} t_m} - \frac{\mu_{Saturn} h}{r^3} \right) \frac{t_m^2}{2} = \Delta d = 2D + h_{HC} \tag{7.5}$$

Equation 7.5 was derived using Newtons second law to calculate the acceleration due to the thrusters, the axial acceleration towards the ring as calculated in [54], and the distance change that was previously discussed [55].

These were then calculated for every orbit and diameter range of 0 to 10 meters. The maximum manoeuvre time that is estimated was 26.97 seconds for a diameter of 10 meters. By adding the detection time and ignition time to the results, avoidance time was found to range from 6.95 to 27.49 seconds.

7.1.7. AOCS Power consumption

The power consumption of the ADCS could differ and depends on which sensors or actuators are turned on. To get a good overview of this, some modes of the spacecraft were introduced. These are as follows:

- Sun Acquisition Mode (SAM) takes place at the beginning of the interplanetary transfer phase when the solar arrays are functional.
- Safe/Hold Mode (SHM) is applied when the spacecraft detects that there could be a loss of control or damage to the spacecraft.
- Orbit Control Mode (OCM) is applied during Saturn orbit insertion, pump down phase and the operational phase.
- Main Engine Boost Mode (MEBM) is applied when the spacecraft has to manoeuvre to change orbit.
- Thrust Transition Mode (TTM) will be applied between a different mode and TTM.

When analysing the different modes, every mode has its appropriate sensors and actuators that are used. The gyroscope is the only sensor that is functional in all the different modes, since the spin rate of the spacecraft has to be continuously monitored to counteract this movement if necessary.

A clear indication of the units that are used per mode is given in Table 7.5. This table also includes the total power this subsystem consumes per mode. The total power is calculated by summing up the power usage of every unit that is used during the mode.

Table 7.5: An overview of the modes and the power usage per mode.

Modes	Units in use	Power consumption [W]
SAM	Gyroscopes, Sun sensors, Reaction wheels, Control thrusters	29.1
SHM	Gyroscopes, Reaction wheels, Control thrusters	28.1
OCM for HC	Gyroscopes, Star sensors, Reaction wheels, Control thrusters, LIDAR, WAC	45.6
OCM for OC	Gyroscopes, Star sensors, Reaction wheels, Control thrusters	33.7
MEBM	Main engines, Control thrusters, Gyroscopes, Star sensors	5.7
TTM	Gyroscopes, Star sensors, Reaction wheels, Control thrusters	33.7

7.1.8. COST ESTIMATION

For the cost estimation, the parametric cost estimation process that is described in Space Mission Analysis and Design was used [58]. This process uses the weight of the subsystem as an input and then converts this to a cost of the subsystem. This is based on historical data of previous space missions. The formula to get the cost is given by Equation 7.6. The X variable in this equation is the mass of the AOCS subsystem and this has to stay between a range of 20 to 160 kg to give reliable outcomes.

$$FY17\$K = 1.427 \cdot 464 X^{0.867} \tag{7.6}$$

In this equation the inflation factor to year 2000 is also present. Thus the amount that the formula gives is the cost in thousands of dollars in year 2017. The AOCS has a mass of 44.5 kg for the hovercraft and 24.8 kg for the orbiter. With this mass the cost for the AOCS would be around 15.89 million euros for the hovercraft and 10.71 million euros for the orbiter.

7.1.9. RAMS ANALYSIS

For this AOCS design, reliability strongly depends on the chosen sensors and actuators. These have to cope with the harsh environment and reach their designed life span. All of the sensor types that have been chosen, have already been on previous missions to deep space including Cassini [64]. This leads to a higher reliability of these sensors. This is the same case for the actuators, Cassini had almost the same type of actuators [64]. The reaction wheels themselves have the biggest issue with reliability. However, this is mitigated through redundancy.

One of the less reliable points of this design is the collision avoidance manoeuvring. This system is usually not applied in satellites since a collision is very rare for satellites in Earth orbit. If the satellite does have an active payload on-board, as in humans on-board, collision avoidance has to be included. Thus the ISS space station uses a collision avoidance strategy, but this is linked with the ground station that would make a strategy plan and link it up back to the ISS [7]. This is not possible for a spacecraft at Saturn, data from Saturn takes 90 minutes to reach Earth.

The availability of the units described in the design would not be an issue. As already stated most of these units have already been used in previous missions, thus the technology readiness level is very high. These units are built by various companies and institutes with a lot of variations of types and development of the technology. The LIDAR that is considered is used in a concept study from NASA [54]. This technology is operational but further studies have to be done in the design of the interactions between the instruments.

7.1.10. VERIFICATION AND VALIDATION FOR AOCS

7.1.10.1. V&V FOR THE MODELS

To calculate the disturbance torques on this spacecraft, a code was written. This code was verified with a unit test. This was done by applying the white box testing, here inputs have to be chosen and the appropriate outputs must be known. Then unit of the code was then run separately to see if the appropriate output was found. Afterwards the code was pseudo-validated with some examples from SMAD [58]. Examples were given for FIRESAT II and SCS, which are Earth pointing satellites. After applying the input of these satellites the following percentage differences were found between the model and the validation data given in Table 7.6.

Table 7.6: Table with the difference of the model to actual satellites.

Disturbance torques	**FireSat II**	**SCS**
Solar radiation pressure	2.27 %	0.6 %
Magnetic Field	0.52 %	0.87 %
Gravity-Gradient	4.67 %	3 %

7.1.10.2. VERIFICATION PLAN FOR FURTHER DESIGN PHASE

To ensure that the AOCS meets its requirements during operation, a verification procedure will take place. The steps of this procedure can be seen in Figure 7.4. First, the design and performance verification will take place. In this step, the AOCS modes, architecture, equipment and tuning is analysed if it meets the functional requirements. Hardware and software verification follows after design and performance verification. In this phase the AOCS is tested whether it represents real-time performance. Each sensor and actuator shall be verified individually in conditions that represent the conditions of the mission. Since real flight conditions and the space environment can not be replicated accurately, the AOCS will not be fully verified. However, the facilities and simulations shall be representative of the real flight conditions.

After hardware & software verification, the AOCS will be verified at satellite level. In this phase, the AOCS will be tested with an end-to-end test. This ensures that the integrated system components pass on the right information between each other with the corresponding software.

[7] https://orbitaldebris.jsc.nasa.gov/quarterly-news/pdfs/odqnv16i2.pdf, consulted on 19/06/2017

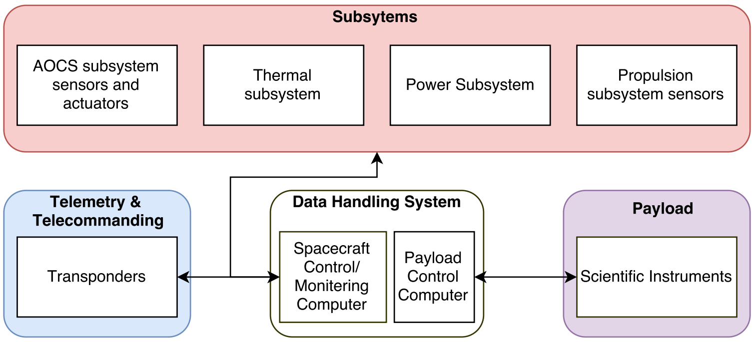

Figure 7.5: A broad overview of the interrelation between the data handling and subsystems, payload and telecommand and telemetry.

When verification at satellite level is completed, the ground interface verification will take place. In this phase, the flight dynamics system and the AOCS interfaces are verified with the complete software. This is the final AOCS verification phase before launch. After launch, the AOCS will continue to be verified with in-flight tests such as health and performance checks. Further elaboration on requirements for the verification plan of the AOCS can be found in European Cooperation for Space Standardization (ECSS) document ECSS-E-ST-60-30C [60].

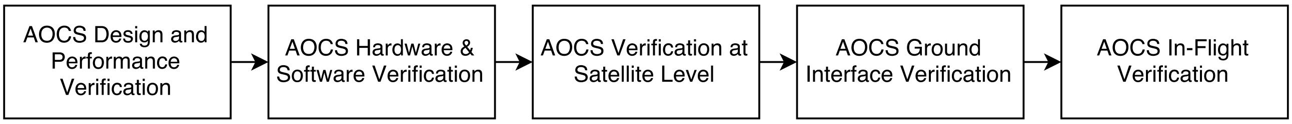

Figure 7.4: Steps for AOCS Verification [60].

7.2. DATA HANDLING

A spacecraft is a data collecting centre, where a variety of experiments are performed and collected. All the data collected needs to be processed and compressed so that it can be transmitted to Earth.

To select an on-board data processing system certain aspects, such as the type of data that has to be transmitted, estimation of peak data rates, requirements regarding inter-relations and the number of nodes, and an approximation of power consumption, noise and circuits were considered. The MIL-STD-1553 (MIL) bus configuration along with the LEON3 - FT processor was considered to be the optimal choice. Why this choice was best for SAURON will be presented in this chapter. Initially, a few aspects are discussed, which is followed by preliminary estimations for processor speed, storage and software requirements.

7.2.1. TOP LEVEL SYSTEM DESCRIPTION

Figure 7.5 depicts the top level relation between the data handling system and other systems of the spacecraft. The data handling system has been split into two main components, one being responsible for the control and performance monitoring of the spacecraft while the other is solely dedicated to management, storage and processing of data gathered from the scientific instruments. There is a feedback loop between the on-board computer and the subsystems group. Inputs from various temperature, pressure sensors and actuators placed in different subsystems are taken at regular time intervals. These inputs are then processed and an appropriate adjustment command is provided to the subsystem. Details regarding each of these processes are explained in Subsection 7.2.2.

7.2.1.1. COMMUNICATION ARCHITECTURE

Different architectural approaches are used to connect the different components on a spacecraft in the industry. These approaches are based on the performance in terms of data transfer and redundancy. The main three are, centralised unit, bus or a star, with each of them having their pros and cons [65]. The main architecture that is considered for SAURON is a hybrid with the bus network (MIL-STD-1553B) being the baseline. The reasoning for this will follow. A centralised system is easy to use for small systems; for big systems it becomes difficult to handle, monitor data and difficult to expand. The networked/star system has a high data rate but the biggest drawback is that a faulty communication could block communication. On the other hand, the bus network has limited data rates (1Mbit/s)[8] but is easy to monitor and is flexible to requirements and easy to integrate and test [66]. Even though the bus concept is old, it is still used in spacecraft such as Cassini, Deep Space 1, New Horizons and the transponder of Juno which proves its reliability [58] [67] [68].

[8] http://www.esa.int/Our_Activities/Space_Engineering_Technology/Onboard_Computer_and_Data_Handling/Mil-STD-1553, consulted on 17/05/2017.

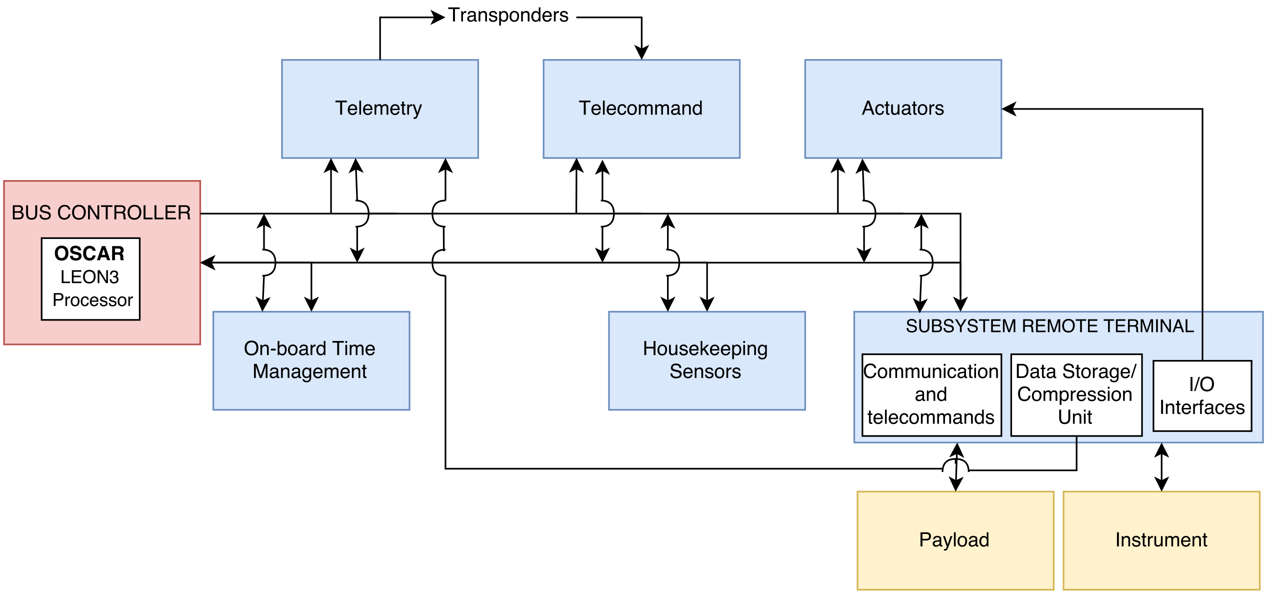

Figure 7.6: Preliminary data handling block diagram with MIL-STD-1553 bus network components and connections. It shows the inter-relation between various components involved in C&DH. The two channels make the system redundant.

The advantage with MIL is its compatibility with other network types. This provides flexibility and easily allows for extension of the network[9]. Thus, if it is later realised that certain terminals might require high speed data transfer a star system could be incorporated. Figure 7.6 represents the top level components that form the bus network. The main bus controller is the master while the remote terminals and other connections, which in this case would be the different instruments and the remote terminal, are the "slaves"[10]. In order to transfer data among the various components two protocol levels are used, namely low level and higher level. The low level protocols are used to convey messages between whereas the higher level is used to control devices and transmit urgent data. The two main wire lines make this data bus redundant. As the data rate of the bus is low (700 μs for conveying 64 bytes of data) engineers have developed strategies to tackle latency [66]. The scope of analysing these is too detailed for the report.

7.2.2. ON-BOARD COMPUTING

7.2.2.1. TELECOMMAND AND TELEMETRY

According to Hult and Parkes [66], a telecommand function delivers command packages to the on-board devices. These command packets are generated, embedded into various protocol layers at ground stations and then uplinked via a radio. Telemetry is defined as housekeeping data and payload data [69]. Just like telecommands, the telemetry data is converted for downlink and sent via radio. The functionality, procedures and standards involved in ground to space, or vice versa, link communication is agreed upon internationally by the Consultative Committee for Space Data Systems (CCSDS) and the European Cooperation for Space Standards (ECSS). Understanding and explaining these protocols and functionalities is beyond the scope of this report though it goes without saying that SAURON will abide by these regulations.

Since telemetry and telecommand is the only way to communicate with the spacecraft, proper functioning of this is ensured by performing constant checks for voltage, current, power and temperature at various points. These points are known as telemetry data points. For normal operations Cassini generated housekeeping data every sixty-four seconds and has 9000 telemetry channels [70] [71]. Table 7.7 represents telemetry points for different spacecraft [72]. Since Cassini is more than two decades old and there is lack of literature and knowledge about the number of telemetry check points for other deep space missions, Earth observation satellites presented in Table 7.7 will be used to make an approximation. Given that the hovercraft would be going close to the ring particles, its relay communication with the orbiter is key for constant checks and survival. Hence, 10000 telemetry points are predicted for the hovercraft and 15000 for the orbiter since it has to cope with uplink and downlink data from ground and the hovercraft.

7.2.2.2. HOUSEKEEPING SENSOR DATA COLLECTION AND ACTUATOR CONTROL

Constant checks are made on all the subsystems by the central computer. The computer sends signals at set intervals and waits for a response [73]. The software that would be on-board of SAURON would have a segment dedicated to gather data from the various sensors placed all over the spacecraft and monitor the overall health of the spacecraft. Hult and Parkes segregate these sensors into two categories and call them the non-intelligent sensors and the intelligent sensors [66]. The non-intelligent or the "*pure sensors*" consist of thermistors, magnetic torquers, voltmeters,

[9] http://www.mil-1553.com/mil-std-1553, consulted on 13/06/2017.
[10] TU Delft Space Technology Lectures: https://www.youtube.com/watch?v=ukX5_ICh-Zg, consulted on 12/06/2017.

Table 7.7: Table representing the number of telemetry points for different spacecraft. The type of spacecraft ranges from a cubesat to the largest civilian Earth observation satellite. [72]

Spacecraft	Number of telemetry points
Delfi C3	114
Delft n3Xt	135
Intelsat 5	520
Eutelsat II	840
SPOT	~500
Midcourse Space Experiment (MSX)	~400
European Remote Sensing Satellite (ERS)	6600
Environmental Satellite (ENVISAT)	13700

etc. Data from these is communicated to a dedicated remote terminal where analogue signals are converted to digital signals. Based on this, data rates for housekeeping sensors can be estimated by using Equation 7.7. The intelligent sensors refer to instruments or other sensors that are capable to process/digitalise data directly.

$$DR_{analogue} = f_c \cdot N_{Nyq} \cdot n_{bits} \tag{7.7}$$

Substituting f_c equal to 10 Hz, N_{Nyq} as 2.2 [72] and n_{bits} as 8 [74] from NASA, the $DR_{analogue}$ is found to be 176 bits per second. Given that 10000 and 15000 points were assumed for the hovercraft and the orbiter respectively, a data rate of 1.7 Mbps and 2.6 Mbps can be expected. However these are preliminary estimations and there are a number of assumptions that have been made which could hamper the design, the consequences and limitations are discussed in detail in recommendations in Section 11.2.

7.2.2.3. TIME KEEPING

Most of the spacecraft make use of the on-board time (OBT) function. This is equivalent to a local clock on the spacecraft. With time the OBT deteriorates with respect to the clock relative to the Coordinated Universal Time (UTC), however this can be readjusted using telemetry techniques. These techniques are more specifically described by the ECSS [75].

7.2.3. PAYLOAD DATA MANAGEMENT AND COMPUTING

The payload computing section of the data handling system is responsible for gathering, routing, storing, compressing and encoding the data for telemetry. Each instrument that is used on SAURON is described in detail in Section 2.10. Not all of the aforementioned topics will be discussed, only storage, data processing and compression will be discussed in the following subsections.

7.2.3.1. STORAGE

Storage determines the amount of data that can be gathered over the mission duration. It plays a key role in determining the processing power but at the same time is limited by the telecommunication capabilities i.e. uplink and downlink. Table 7.9 summarises the data rates of all the instruments aboard SAURON. It can be easily deduced that the cameras have the highest data rates and are the driving factor in determining the storage size.

Ideally, storage should be sized for the period with no downlink; however, there is an added complexity to this mission. To begin with the only means of downlink is via the orbiter, thus there are periods where the orbiter is in eclipse from the ground and the hovercraft. The eclipse periods are 2 hours and 2.04 days, respectively, which reoccurs every 6 days. These are explained in detail in Section 7.6. The steps that were followed to arrive at a preliminary storage estimation for the instruments was as follows:

1. Add the data of all the instruments.
2. Multiply with the eclipse period.

Assuming all the instruments are turned on for the complete eclipse period a total memory of 9 Terabits or 1125 GBytes is required. Further, assuming a compression of ratio would make this 281 GBytes, which would still take 2.4 hours to transmit to the orbiter (given the maximum data rate of 283 Mbits/s remains for this time). However, transmission of this data to Earth would take 1.6 years. Thus, this much amount of data simply cannot be collected. It is known that New Horizons has a storage of 8 GB or 64 Gigabits solid state storage units[11]. Assuming SAURON collects this amount of data (each spacecraft collecting 4 GB), it would take just under 15 days for complete data transmission to Earth. It would imply that during the eclipse between the orbiter and hovercrafts, the cameras on the orbiter can stay on for 14 mins while the others can stay on for 367 mins. These values have been acquired by making a model and playing

[11] http://pluto.jhuapl.edu/Mission/Spacecraft/Systems-and-Components.php

with the ratios of instrument duration. It is important to note that the method described above provides a storage requirement only for the instruments. A separate compartment for storage of telemetry and telecommands is kept aside from this storage value.

Table 7.8: Tables representing mass and cost

Table 7.9: A summary of the data rates of all the on-board instruments along with the transmission data rates between the hovercraft-orbiter and orbiter-Earth.

Instrument	**Data Rate [kbps)]**
Narrow Angle Camera	30000
Wide Angle Camera	10000
Radio Science	100
Dust Analyser	5 (2 Mb/cycle)
Spectrometer	10 (10 Mb/map)
Magnetometer	4
Plasma Spectrometer	1000

Table 7.10: Cost estimation of data handling subsystem.

	Transmission Data Rates
Hovercraft to Orbiter	283 Mbits/s (max)
Orbiter to Earth	48kbits/s

A new technique is proposed to transmit the data for SAURON. Unlike traditional spacecraft that first gather data and then transmit it to Earth data gathered could be stored on-board as backlog data. There are two reasons for doing so. First being the in-ability of orbiter to transmit all the data back to Earth, secondly the life of the hovercraft is lower than that of the orbiter, once the orbiter becomes dysfunctional the backlog can be cleared since no new data would be recorded.

7.2.3.2. Compression of Data

Most of the instruments aboard the spacecraft have a data rate ranging from a few Kbps for instruments such as magnetometers to a few Mbps for the cameras. To maximise the amount of data transmitted to Earth, the data is compressed. There is lossy and lossless types of compression. Certain algorithms defined by CCSDS are used to determine the type and best compression ratio for data collected from cameras and spectrometers [76]. In simple words, it is converting images to JPEG to minimise data storage. Some camera instruments possess the capabilities to do so whereas some are done by the on-board computer.

7.2.3.3. Data Processing

The processor that was selected to process the data is the LEON3-FT. To estimate the processing speed required for all the various types of data that would be gathered by SAURON, typical values from [58] were taken, this has been tabulated in Table 7.11. Since no appropriate source with a breakdown of how much processing power each component uses for any previous space mission was found, a sensitivity analysis for data in Table 7.11 was performed. The typical execution frequency and typical throughput values were incremented by 20, 50 and 100 percent respectively. These increments were taken to assess the impact on the processing speed. On top of this a 20% margin on the total values were taken because the table does not include payload data processing.

To calculate the clock speed, the (Kilo Instructions Per Second) KIPS were multiplied with the 6, 20 and 50 cycles per second. The cycle per second represents the time between two pulses of an oscillator that is used to measure time on electronics[12]. The results are tabulated in Table 7.12. From this, one can conclude that the worst case scenario calls for a 73 MHz computer. Hence, placing two LEON3-FT, should suffice the need for processing data and would also make the system redundant. There are other competitors in the market that possess the same or even better capabilities but the LEON3 is European made, making it easily accessible. Furthermore, the LEON3 is incorporated in OSCAR, an off the shelf computer made by Airbus Defence and Space [77]. The LEON3 has a radiation protection of 300krad, which is sufficient. Upon further research, more companies with better performance capabilities were found; however, due to lack of time an assessment with those processors could not be performed. This will be discussed in depth in Section 11.2.

7.2.4. Software

Information regarding the software used on different spacecraft is limited as each space mission varies in its objectives. So the software used is altered accordingly, though there are a certain features that are known. At the top most level it is known that the programming language that is mostly used is C/C++. From the data provided in the Spacecraft Mission Analysis and Design typical values for the total Lines Of Code (LOC) for complex spacecraft were found to be 38000 [58]. This value seems to be reasonable as Cassini had approximately 32000 LOC [78]. Given that the hovercraft is in a more risk prone environment for an eclipse period of two days, it needs absolute automation which increases the lines of codes. A model to size the software is presented in detail in SMAD, the third edition [79]. Though

[12] https://www.computerhope.com/jargon/c/clockcyc.htm, consulted on 14/06/2017.

Table 7.11: Assessing sensitivity on the KIPS and Execution frequency by a factor of 20,50 and 100 percent. Doing so would help in acquiring the clock speed,hence the processing speed, for the worst case scenario.

Function	**Typical Throughput [KIPS]**	**Typical Execution Frequency [Hz]**	**120% Typical Throughput [KIPS]**	**120% Typical Execution Frequency [Hz]**	**150% Typical Throughput [KIPS]**	**150% Typical Execution Frequency [Hz]**	**200% Typical Throughput [KIPS]**	**200% Typical Execution Frequency [Hz]**
Communications								
Command Processing	7.0	10.0	8.4	12.0	10.5	15.0	14.0	20.0
Telemetry Processing	3.0	10.0	3.6	12.0	4.5	15.0	6.0	20.0
Attitude Sensor Processing								
Rate Gyro	9.0	10.0	10.8	12.0	13.5	15.0	18.0	20.0
Sun Sensor	1.0	1.0	1.2	1.2	1.5	1.5	2.0	2.0
Magnetometer	1.0	2.0	1.2	2.4	1.5	3.0	2.0	4.0
Star Tracker	2.0	0.0	2.4	0.0	3.0	0.0	4.0	0.0
Attitude Determination & Control								
Kinematic Integration	15.0	10.0	18.0	12.0	22.5	15.0	30.0	20.0
Error Determination	12.0	10.0	14.4	12.0	18.0	15.0	24.0	20.0
Precession Control	30.0	10.0	36.0	12.0	45.0	15.0	60.0	20.0
Magnetic Control	1.0	2.0	1.2	2.4	1.5	3.0	2.0	4.0
Thruster Control	1.2	2.0	1.4	2.4	1.8	3.0	2.4	4.0
Reaction Wheel Control	5.0	2.0	6.0	2.4	7.5	3.0	10.0	4.0
Ephemeris Propogation	15.0	10.0	18.0	12.0	22.5	15.0	30.0	20.0
Control Moment Gyroscope	2.0	1.0	2.4	1.2	3.0	1.5	4.0	2.0
Complex Ephemeris	4.0	0.5	4.8	0.6	6.0	0.8	8.0	1.0
Orbit Propogation	20.0	1.0	24.0	1.2	30.0	1.5	40.0	2.0
Autonomy								
Complex Autonomy	20.0	10.0	24.0	12.0	30.0	15.0	40.0	20.0
Fault Detection								
Monitors	15.0	5.0	18.0	6.0	22.5	7.5	30.0	10.0
Fault Correction	5.0	5.0	6.0	6.0	7.5	7.5	10.0	10.0
Other Functions								
Power Management	5.0	1.0	6.0	1.2	7.5	1.5	10.0	2.0
Thermal Control	3.0	0.1	3.6	0.1	4.5	0.2	6.0	0.2
Kalman Filter	80.0	0.0	96.0	0.0	120.0	0.0	160.0	0.0
Total	256.2	102.6	307.4	123.1	384.3	153.9	512.4	205.2
20% Margin	307.4	123.1	368.9	147.8	461.2	184.7	614.9	246.3

Table 7.12: The change in clock speed / processing speed with change in cycles per second while holding the KIPS acquired from Table 7.11 constant. Cps = Cycles/second.

-	**Required Clock Rate** [**MHz**] **for 252.6 KIPS**	**Required Clock Rate** [**MHz**] **for 307.4 KIPS**	**Required Clock Rate** [**MHz**] **for 384.3 KIPS**	**Required Clock Rate** [**MHz**] **for 512.4 KIPS**
Cps (6 cycles)	1.8	2.2	2.8	3.7
Cps (20 cycles)	11.0	7.4	9.2	12.3
Cps (50 cycles)	66.4	44.3	55.3	73.8

there are a number of factors that are required that are not easily available to make these estimations. Performing the software sizing model could have led to a detailed processing measurement and could have assessed the various aspects of the software while being reproducible.

Another aspect that is regular software updates that the system goes through. A period for this could be determined but this is highly dependant on software performance and situations that may arise during the mission.

7.2.5. FAULT DETECTION

The environment in space presents potential harm to electronics. These damages could range from malfunctioning of instruments to data corruption. Hence, the software is embedded with fault detection mechanisms.

7.2.5.1. FAULTS

There are three primary sources of errors. The first is the system not performing what it is intended to or the software is over designed i.e. the hardware is incapable of processing information. Even though, such a situation has only happened once in history, on the Ariane 5 Cluster, but the consequence was instantaneous mission failure [80]. Similarly there were other instances as well where there were software failures, which were fixable. The second error that could happen is due to bit flips. The space environment consists of cosmic radiation. This radiation causes data corruption and causes the electronic components to age faster. Bit flips also known as Single Event Upset (SEU) implies that the binary digits get flipped, so for instance the 1s become 0s and vice versa. Approximately 1 to 10 bit flips could occur in a day, thereby using 16 Mbytes [65]. Lastly, a single-event latchup (SEL) could occur. SELs are defined as sudden spikes in power due to radiation that are fatal to instruments on-board [81]. It causes the chips in instruments or bus controllers to burn. Even though this event is rare the system has to be designed to tolerate such an event. OSCAR has been developed to tackle these single event errors [77].

7.2.5.2. CORRECTION TECHNIQUES

Memory scrubbing is used to tackle SEU. The technique it uses is, that it continuously reads the memory, when an error/fault is found it "scrubs" that section of the memory and continues with recording more data. Another method that is used is known as the reconfiguration module. This contains a watchdog alarm that is an alarm system to detect malfunctioning. This alarm could be regarding power usage, attitude adjustment or thermal levels [65]. All it does is reset the processing function for that unit of the system. A safeguard memory is used to store the system status prior to an error, this way when the system is restarted the software is aware of the data values used previously. These values are sometimes used when the spacecraft might lose its primary power source [66].

According to the Handbook of Space Technology, if three active modules could be used to check the data that is generated by the spacecraft. Two modules would help in identifying where the error is but not in the module in which the error is. Thus, there SAURON would use three modules and make use of Cyclic Redundancy Check (CRC), a technique used to cross check the data acquired.

7.2.6. RAMS ANALYSIS

7.2.6.1. RELIABILITY

OSCAR is SEL immune, SEU tolerant. Furthermore, it is designed to handle up to 20g, which easily complies with the maximum load that the spacecraft will bare throughout its life [77]. The LEON3FT is radiation shielded up to 300krad, which is enough to protect radiation from the environment and the RTGs [82]. As far as the architectural reliability is concerned, the MIL was developed in the 70s and is updated with up gradations in interfaces. Its presence in the market for almost four decades now proves its reliability.

7.2.6.2. AVAILABILITY

The OSCAR is already flight proven and has been utilised on other spacecraft previously. The same is applicable to the processor. LEON series has been in the market, has been used on ESA missions and is acquirable from the

Swedish manufacturer, Cobham Gaisler[13]. The MIL-STD-1553 is military certified and has been used on numerous space missions, including those of ESA[14].

7.2.6.3. MAINTAINABILITY

The on-board data handling system is designed to be redundant, the only errors that could happen are due to software malfunctions. It is due to these reasons that constant software updates and telemetry is required to ensure good performance of the system.

7.2.6.4. SAFETY

The data handling system poses no threats to the system. The production of all the components are safe and sound. Most of the production techniques are expected ti be with the help of automated machines, not a lot of data regarding this is avialable.

7.2.7. MASS AND COST ESTIMATION

7.2.7.1. MASS

The overall estimated mass for the data handling system is 27 kg, where 5 kg is taken from the data of the computer and 6.1 kg for the memory storage unit. The mass estimation for the memory unit is performed via Equation 7.8 [72].

$$m_{rec}[kg] = \frac{C_{rec}[GByte]}{0.041 \cdot C_{rec}[GByte] + 0.3128} m_{rec} = \frac{4}{0.041 \cdot 4 + 0.3128} = 6.2kg \tag{7.8}$$

Added to the total is a margin that would take into account the mass of wires and all the other electrical components. Since there are two spacecraft, each get the same system. The values are tabulated in Table 7.14.

Table 7.13: Tables representing mass and cost

Table 7.14: Mass estimation of data handling subsystem.

Subsystem part	Mass [kg]
OSCAR (Hovercraft)	5
Memory unit (Hovercraft)	6.1
OSCAR (Orbiter)	5
Memory Unit (Orbiter)	6.1
20% Margin	80
Total	27

Table 7.15: Cost estimation of data handling subsystem.

Subsystem part	Cost [€M]
Software Code	70
on-board Computer	10
Total	80

A flaw with this mass estimation is that it does not take into account the various other elements that go into data handling. With the help of tools, such as an estimation for the number of central processing units required in SMAD [79] and requesting data sheets from other spacecraft electronics producers such as DSI Informationstechnic[15] and BAE[16] would have helped assessing processing systems critically.

7.2.7.2. COST

The overall estimated cost of the data handling subsystem is expected to be 100 million euros. The exact breakdown can be found in Table 7.10. Previously, it was mentioned that the spacecraft would have approximately 38000 lines of codes. Since coding is a rare and a crucial element of the data handling subsystem the market cost is per line of code. Using [58] it can be estimated that the coding itself would cost around 70 million euros. Similarly, the cost of OSCAR ranges from 5 to 10 million euros[17]. This range exists due to the adaptability of the computer system. The more complex the system/requirements, the more expensive the computer. Assuming worst case scenario, the the cost can be finalised at 10 million euros. Lastly a margin of 20% should be taken into account for production, development and safety margin costs.

There are certain aspects that undermine the cost of C&DH. An error was made by not taking into account the fact that two spacecraft are being designed and thus the cost for the mission might mean double of what is represented in Table 7.15, though this can be accounted for in the margin for the entire spacecraft. Additionally, it can be assumed that if two similar products are bought from a company there might be a chance of concession. Furthermore, better cost estimates could have been used, such as those provided in [83] and [84].

[13] http://www.gaisler.com/index.php/products/processors, consulted on 17/06/2017.

[14] http://www.esa.int/Our_Activities/Space_Engineering_Technology/Onboard_Computer_and_Data_Handling/Mil-STD-1553, consulted on 17/06/2017.

[15] http://www.dsi-it.de/en/home/, consulted on 25/06/2017.

[16] http://www.baesystems.com/en-us/our-company/inc-businesses/electronic-systems/product-sites/space-products-and-processing/processors, consulted on 25/06/2017.

[17] Private communication, June 20, 2017.

Table 7.16: Power requirements for hovercraft and orbiter for ten operation cases.

Case	System	Orbiter power [W]	Hovercraft power [W]	Reference
Always on	C&DH	15	15	Section 7.2
	Thermal	10	10	Table 7.53
	Communication to other spacecraft	20	20	Section 7.6
	PPU	14	9	Subsubsection 7.3.3.5
	AOCS	39.4	53.3	Section 7.1
1	High payload	88	54	Table 2.4
2	Average payload	44	-	
3	Really high communication to Earth	183	-	Section 7.6
4	High communication to Earth	95	-	Section 7.6
5	Medium communication to Earth	80	-	Section 7.6
6	Low communication to Earth	40	-	Section 7.6
7	Propulsion main thruster	46	46	Table 7.29
8	Propulsion hop thruster	-	82	Table 7.29
9	Orbit control	21.8	21.8	Section 7.4
10	Power from batteries	-13	0	Subsubsection 7.3.3.3

7.2.8. VERIFICATION AND VALIDATION

The models developed to approximate values are from theory. Therefore, the values that are input are already validated values. Since an exactly similar mission has never been performed before, the closest spacecraft to which the derived values could be compared to are deep space missions. So spacecraft such as Cassini, New Horizons, Dawn and Juno were taken for comparison.

7.3. POWER GENERATION AND DISTRIBUTION

This section will present the power subsystem for the two spacecraft and the two transfer stages. The various power generators and the power processing unit (PPU) will be discussed as well. First the requirements generated by the different parts will be discussed, followed by the layout and the characteristics. Different components considered for the subsystem will be assessed and traded-off. Lastly, a brief cost, RAMS and verification and validation of the models generated will be performed.

7.3.1. POWER REQUIREMENTS

This subsection will derive the RTG power requirements from the power requirements of the operations.

7.3.1.1. ORBITER AND HOVERCRAFT

For the orbiter and the hovercraft the power requirements are derived from specific subsystems. There are five 'always on' cases and ten operation specific cases, where one or more can be operational in addition to the 'always on' cases. An overview of the different subsystems, placed in the orbiter and the hovercraft, along with their power requirements can be seen in Table 7.16.

Since not all cases are operational at the same time, it is not necessary to design for such a case. Instead, it is chosen to design for maximum payload power to maximise the science data. For the hovercraft this was also the highest power requirement. Table 7.17 presents the total calculated power of the orbiter and the hovercraft. Then it considers case 1 and 6 for the orbiter and only 1 for the latter. Lastly, a contingency margin of 9% is applied. This results in a power requirement of 173 W for the RTG on board the hovercraft. It is important to note that hopping requires much more energy, however, once the communication link to the orbiter is shut down, the power system is able to provide the power for a few seconds every time. Additionally, the orbiter has to send all data back to Earth, because of the low data rate this takes a lot of time. So the power requirement is increased with case 6. This results in a power requirement including contingency for the RTG of 273 W. When batteries are used and more data rate is required case 6 or case 1 and 6 can be replaced with case 4 or case 3, respectively.

As discussed in Chapter 4, the transfer time increased with 0.44 years, this results in a lower EOL power compared to the design power. This will not have an influence on the mission, only the contingency will reduce a bit. The electronics selected for SAURON can withstand 100,000 RAD [68] in their mission life time. The dose per hour is calculated with Equation 7.9, this results in a dose of 4.7 and 3.8 rem/hr normalised for when the distance between the RTGs and payload is 1.2 and 1.1 meter for the hovercraft and orbiter respectively. The 4 in Equation 7.9 is to transform from rad to rem.

$$D = 4\frac{D_{max}}{t_{mission}} d^2_{RTG-payload} \tag{7.9}$$

Table 7.17: Resulting EOL RTG power requirement.

	Orbiter power [W]	Hovercraft power [W]
Total	226	159
Operation cases	1,6	1
Contingency	21%	9%
Design power value including contingency	273	173
Available EOL power	268	170

Table 7.18: Power requirements for the second stage for three operation cases.

Second stage case	System	Power required [W]
1	Propulsion main thruster	157
2	Propulsion control thrusters (2x)	82
3	Propulsion control thrusters for emergencies (4x)	164

7.3.1.2. SECOND STAGE

The same is done for the second stage. The C&DH subsystem is always on and three power cases are identified (see Table 7.18).The power available from the hovercraft is found to be 153 W: BOM power minus the PPU and C&DH power. The power available from the orbiter is 221 W: BOM power minus the PPU, C&DH and AOCS power. The stage requires 184 W, but the hovercraft cannot provide sufficient power, so the orbiter needs to provide this power. Therefore a cable is needed from the orbiter to the second stage.

7.3.1.3. FIRST STAGE

The input power for the first stage is driven by the amount and the input power of the ion thrusters. There are 5 ion thrusters and these require 7.22 kW each, see Table 7.27 for the characteristics of the NEXT. In Table 7.19 the required power input is listed for when the thrusters are firing. This is used for calculating the maximum BOL power requirement. To calculate the BOL power, the degradation has to be taken into account. This is 1.3% per year[18]. The mass and costs are calculated from the UltraFlex Solar Arrays with a specific power of 150 W/kg and specific costs of 450 €/W [85]. This results in a solar array system of 247 kg providing 37 kW at BOL at a cost of €16.7 million. The overview is listed in Table 7.23. From that table one can observe that the last time the thrusters are firing is after 3.89 year as no manoeuvres are required anymore and therefore the first stage can be separated.

7.3.1.4. REQUIREMENT SUMMARY

From these subsections the following requirements are identified:

- RTGs shall generate 268 W for the orbiter after 15 years.
- RTGs shall generate 170 W for the hovercraft after 14 years.
- RTGs from the orbiter shall generate 269 W for the pump-down phase after 13.94 years.
- Solar arrays shall generate 37 kW for the first stage at BOL.
- The plume of the ion thrusters shall not touch the solar arrays.
- The radiation dose at 1 meter from the RTGs inside the spacecraft shall be less than 4.7 and 3.8 rem/hr for the hovercraft and orbiter respectively.
- RTGs shall provide power for the orbiter and hovercraft.

[18] http://www.lpi.usra.edu/opag/nov_2007_meeting/presentations/solar_power.pdf, consulted on 13-05-2017.

Table 7.19: Required power, distance to Sun, BOL power required and mass over time for the trajectory.

Time [year]	Required powe [kW]	Distance to Sun [AU]	BOL power required [kW]	Mass [kg]
0.11	36.1	1.012	37.0	247
0.23	36.1	0.961	33.5	223
0.34	36.1	0.863	27.0	180
0.46	0.0	0.766	0.0	0.0
0.57	0.0	0.761	0.0	0.0
0.69	30.3	0.855	22.4	149
0.8	36.1	0.954	33.3	222
0.92	36.1	0.987	35.7	238
1.03	36.1	0.932	31.8	212
1.14	0.7	0.78	0.4	3.0
3.89	2.2	3.217	23.8	159

7.3.2. POWER SUBSYSTEM LAYOUT

The Radioisotope Thermoelectric Generators (RTG) are placed on the hovercraft and orbiter next to the main thrusters. This is to maximise the distance between the neutron emitting RTGs and the payload and other radiation sensitive instruments and electronics.

The second stage does not have its own power generation system, so gets its power from the RTGs of the orbiter. This results in a power cable from the orbiter, through the hovercraft to the second stage. The solar arrays are located at upper side of the first stage on a boom of 1.05 meter. This is done so that the solar arrays are not crossing the plume of the ion engine to prevent damage.

7.3.3. CHARACTERISTICS

7.3.3.1. RADIOISOTOPE THERMOELECTRIC GENERATOR AND SHIELDING

RTGs have proven to be a reliable power generation source for deep space missions over the years. RTGs use radioisotopes to generate power. Plutonium-238 and curium-244 have been considered as radioisotope options for SAURON. Plutonium-238 is the most used radioisotope in deep space missions. This is because of its high specific energy and low radiation. Plutonium-238 has a specific power of 560 W/kg and, on average, the flight proven generators have an efficiency of 6.7% and a specific power of 5.3 W/kg [86]. Since plutonium has a half life of 87.7 years, it is suited for a long mission to Saturn. Because it is so popular, the concept is flight proven, but also scarce. NASA does not have enough plutonium left and will probably not share it with a European mission. Russia also stopped selling their plutonium[19]. Thus it is safe to say that plutonium is not available for this mission.

Curium-244 has not been used in any RTG of any space mission yet. However, it can be used to power a GPHS, which in turn could be integrated into an RTG. Since this has never been done before, it does carry some risk. Curium-244 is much easier to obtain than plutonium-238 as it is a side product of nuclear power plants [87]. Curium-244 has a specific power of 2.83 kW/kg and a half life time of 18.1 years [88]. Because of this high specific power, only a fifth of the fuel weight is required to power the generator. The initial power generation should be higher than what is required. Because of its relatively low half life time, after 10 years it only provides 68% of the initial power. Curium-244 produces about 180 times more gamma radiation than plutonium-238 [87] and high neutron flux, because of high change of spontaneous fission [89].

As mentioned previously, the RTGs need to have a power of 173 and 273 W for the hovercraft and orbiter after 13.6 and 14.5 years respectively, see Table 7.17. When using Equation 7.10 the BOL power is 290 and 476 W for the hovercraft and orbiter respectively. To have symmetry an even number of RTGs are needed. If there are four RTGs, the power of one RTG is too low to have a good efficiency [89]. Therefore the hovercraft will carry two RTGs of 150 W usable power each and the orbiter two RTGs of 240 W each. The mass of the RTGs and the shields are calculated with the help of [89]. There are two types of thermoelectric materials that are used to convert thermal heat to electric heat that have been analysed: germanium silicon (GeSi) and lead telluride (PbTe). Germanium silicon has a high specific power, but low efficiency and lead telluride has low specific power but high efficiency. So germanium silicon has a lower RTG mass, but higher shield mass then lead telluride. For the input values for this mission it is found that the germanium silicon is lighter. The differences in output between the two materials are shown in Table 7.20.

$$P_t = P_i \left(\frac{1}{2}\right)^{\frac{t}{\tau}} \tag{7.10}$$

To determine the masses of the RTG and its shielding, the following calculations and determinations are made for GeSi and PbTe, and are tabulated in Table 7.20 [89]. The first column gives the step for easy referencing in the text. The second column gives the step description. Column three and four give the input and output variables of that step. The output values are listed for the hovercraft and the orbiter for both thermoelectric materials in the next four columns. The last column gives the reference for how to get from the input to the output.

For the sake of clarity, steps 3, 7 and 10 are explained in detail. (Step 3) A higher hot junction temperature increases the efficiency, so only the highest temperatures are considered. (Step 7) The distance between the RTG and the payload are taken from the middle of the RTG and the middle of the lower side of the payload bay. (Step 10) It is assumed that the shape of the shields are cuboid. As can be seen in Figure 7.10 some parts of the sides do not seem necessary, however since it is unknown how the neutron radiation behaves at the sides, it is left in. This makes it a bit more heavy.

Table 7.21 presents the input values for Figure 7.10. This along with the goniometric formulae are used to calculate the dimensions of the shield, see Table 7.22. The values of D, p, n and D_p are taken from the layout and (payload) instruments. b is assumed to be 0.5 m and k is such that the distance between the two shields are 0.4 m to have enough space for the engine. g is such that they are as high as possible to prevent heating from the RTGs and engine.

From Table 7.20 it is found that the SiGe based RTG is lighter than the PbTe based RTG. This results in a RTG with SiGe as thermoelectric material with a mass of 91 and 137 kg for the hovercraft and orbiter respectively.

[19] http://www.world-nuclear-news.org/F-can-americium-replace-plutonium-in-space-missions28071401.html, consulted on 16-05-2017.

Table 7.20: Steps to calculate the RTG and shielding mass.

				SiGe		PbTe			
Step	**Description**	**Input**	**Output**	**HC**	**O**	**HC**	**O**	**Unit**	**Reference**
1	Determine required electrical power	Table 7.17	$P_{e_{EOL}}$	173	273	173	273	Watt	Table 7.17
2	Calculate required BOL electrical power	$t_{mission}$, $P_{e_{EOL}}$	$P_{e_{BOL}}$	150	240	160	240	Watt	Table 7.17, Equation 7.10
3	Determine hot junction temperature	[89]	T_H	820	820	600	600	°C	[89]
4	Determine cold junction temperature	T_H, $P_{e_{BOL}}$	T_C	370	370	230	230	°C	[89]
5	Determine generator efficiency	T_H, $P_{e_{BOL}}$, T_C	η	4.8%	4.8%	6.4%	6.4%		Figure 7.7
6	Calculate required BOL thermal power	$P_{e_{BOL}}$, η	P_{th}	3100	5000	2500	3750	Watt	
7	Calculate distance between RTG and payload	p,h,b,g,l	d	1.5	1.5	1.5	1.3	m	Layout
8	Determine allowable dose rate	$t_{mission}$, D_{max}, d	D	4.7	3.8	5.0	4.2	rem/hr	Equation 7.9
9	Determine shield thickness	$P_{e_{BOL}}$, D_{max}	t_{shield}	0.06	0.09	0.06	0.10	m	Figure 7.9
10	Calculate shield dimensions and place	p, h, b, g, l	α, β, γ, s, w, r, u, x					m	Figure 7.10, Table 7.21, Table 7.22
11	Calculate shield mass	s, w, r, u, x, t	m_{shield}	23	37	26	45	kg	Table 7.22
12	Determine RTG mass	T_H, $P_{e_{BOL}}$	m_{RTG}	23	32	30	44	kg	Figure 7.8
13	Total mass for 2 RTGs and shields			91	137	113	178	kg	

Table 7.21: Hovercraft and orbiter input dimensions for Figure 7.10.

Dimensions [m]	**D**	**p**	**h**	**b**	**g**	**k**	$\mathbf{D_p}$
Hovercraft	0.85	1.58	0.627	0.5	0.47	0.27	0.27
Orbiter	0.85	0.6	0.471	0.5	0.46	0.44	0.85

7.3.3.2. RTG AND SHIELDING SENSITIVITY

When increasing the power requirements with 10%, two RTGs of 160 and 260 W BOL are needed for the hovercraft and orbiter each, respectively. This results in a total weight of 98 and 146 kg for RTG and shielding, respectively. This is an increase of 7 and 6% respectively.

7.3.3.3. BATTERIES

Batteries are not necessary, because RTGs constantly provide power. The communication system on the orbiter requires a lot of energy, so when in the eclipse of Saturn, there is no link and no power used. This power is wasted, but with a small battery this power is stored and can be used later. During every orbit there is a 2.1 hours of eclipse time. In such a scenario only case 1 from Table 7.16 is active. This increases the power available with 13 W. Lithium-ion batteries are the most weight, cost and volume efficient [65]. This results in a 2.7 kg mass increase to store 360 Wh at BOL. This effect with the RTG results in 3.4 kg more weight excluding the shielding.

7.3.3.4. SOLAR ARRAYS

From Table 7.19 it was found that the BOL power requirement is 37 kW with a mass of 247 kg. Each of the two arrays are 10 meter in diameter icosagons and have a total cost of €17 million (see Table 7.23 for the characteristics). These arrays are folded like a radial harmonica.

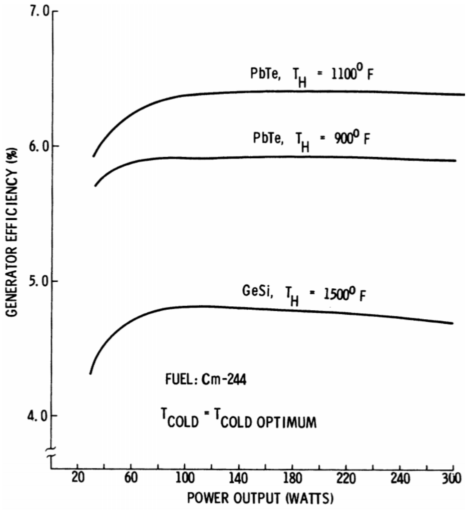

Figure 7.7: Generator efficiency as function of output for curium fuelled RTG for PbTe and GeSi at different hot junction temperatures with the cold junction temperature as optimum temperature[89].

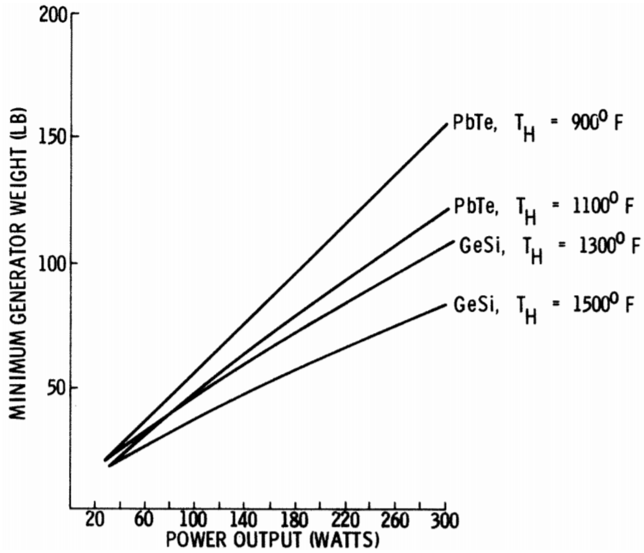

Figure 7.8: Minimum generator mass as function of output power for PbTe and GeSi at different hot junction temperatures[89].

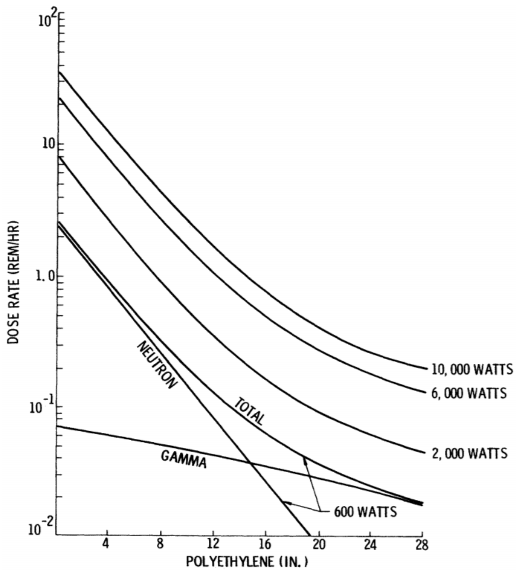

Figure 7.9: Shielding requirement for the radiation dose for different thermal power values[89].

The solar arrays are mounted on a boom. This has two reasons: the ion plume of the NEXT thrusters should not touch with the solar arrays otherwise they will degrade and the second reason is that the arrays are folded upwards and the second stage is wider than the first, so an offset is necessary. This offset is at least 0.95 meter. The offset needed to not intersect with the plume is 1.05 meter. In Figure 7.11 the plume and the solar arrays are visualised.

7.3.3.5. POWER PROCESSING UNIT

From [65] an estimation is made for the mass, power and cost of the MPPT. The RTGs will have access power, decreasing power and voltage over time and a MPPT is used as an PPU. The specific mass is 2.5 kg/W, the specific cost is €90000 per kilogram of MPPT and the power consumption is 5% of the processed power. In Table 7.24 the final values are given per MPPT. For redundancy two MPPTs are included.

The MPPT/PPU connects the RTGs with the parts of the spacecraft that needs power. The orbiter also provides power to the second stage and stores and receives power from the batteries. See Figure 7.12 and Figure 7.13 for the hovercraft and orbiter respectively.

7.3.3.6. CABLES

It is not possible to make a good cable mass estimate. Usually this mass is found when building the spacecraft. Therefore only an approximation is made. Brown (2002) provides an estimation for the cable mass [90]. Equation 7.11 shows the relation between the cable mass and the EOL power an the results are shown in Table 7.25.

$$m_{cable} = 0.071 P_{EOL} + 0.1498 \tag{7.11}$$

Table 7.22: Output values for the dimensions of the shield.

	SiGe Hovercraft	SiGe Orbiter	PbTe Hovercraft	PbTe Orbiter
α	1.21	0.96	1.16	1.05
β	0.79	0.65	0.79	0.85
γ	1.21	1.16	1.21	1.16
t	0.06	0.09	0.06	0.10
r	0.86	0.81	0.99	0.67
s	0.84	0.75	0.96	0.62
u	0.17	0.11	0.16	0.35
w	0.23	0.22	0.23	0.44
x	0.19	0.22	0.19	0.22

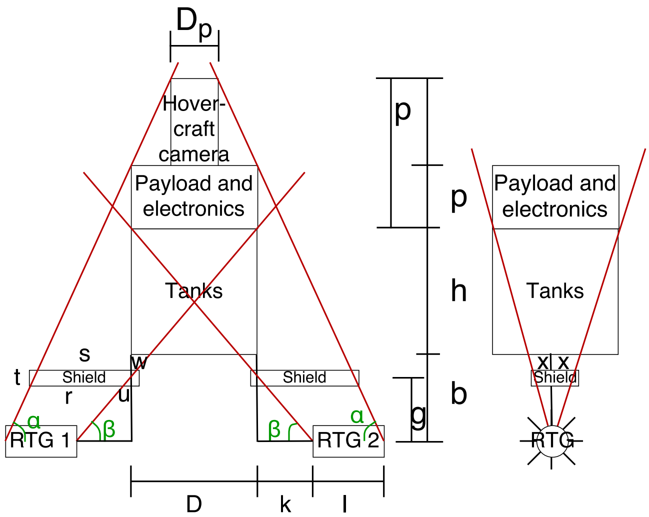

Figure 7.10: Shield dimensions and placement on the hovercraft and the orbiter.

Table 7.23: Solar arrays characteristics.

	Value	Unit
BOL power needed	37	kW
Mass	247	kg
Area total	156	m^2
Number of arrays	2	
Costs total	17	M€
Area per array	78	m^2
Array diameter	10	m
Mass per array	123	kg

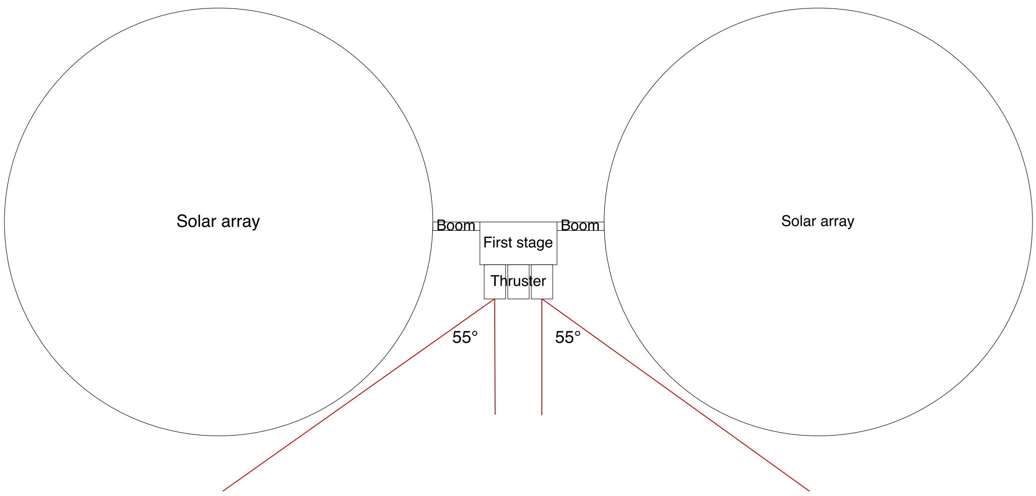

Figure 7.11: Plume of the NEXT on the solar arrays.

Table 7.24: Mass, power and costs for the MPPT/PPU.

MPPT/PPU	Mass [kg]	Power [W] [EOL]	Cost [€]
Hovercraft	0.8	14	72000
Orbiter	1.2	9	108000

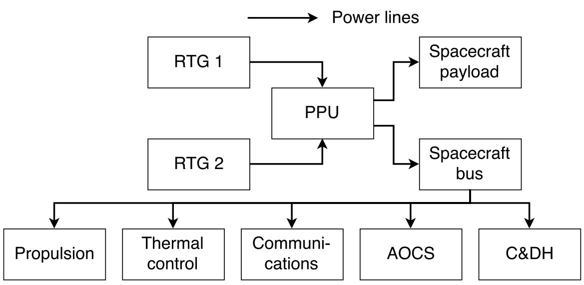

Figure 7.12: Hovercraft power system hardware diagram

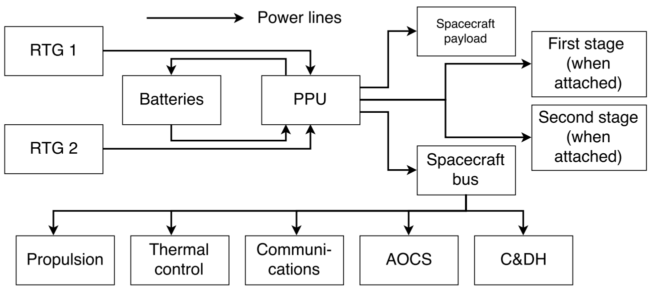

Figure 7.13: Orbiter power system hardware diagram

7.3.4. COST ESTIMATION

The Cu-244 RTG is similar to the Pu-238 RTG, the plutonium fuel pellets can be replaced with the Cu-244 fuel pellets, without mayor changes. Therefore it is assumed that the Cu-244 RTG has the same costs as the Pu-238 RTG. From a mission to Titan [91] the specific costs of the RTG are 23000 \$/Wth FY 2006, 26000 €/Wth FY2017. From [58] the specific costs of the RTG are between the 16000 and 200000 \$/We. The proposed Titan mission from 2007 has a higher specific cost and a more comparable mission, therefore this estimate is chosen. This results in 81 and 129 million euro for the hovercraft and orbiter respectively. The price of the curium is 150 €/g [87, 92, 93], so the total price is €320000 and €525000 hovercraft and orbiter respectively. An overview of the mass and costs of the power system for the hovercraft and orbiter see Table 7.26. The total cost of the power subsystem is €228 million.

7.3.5. RAMS ANALYSIS

The RTGs are flight proven in many planetary missions such as Cassini and Voyager, in none of its missions has an RTG failed. However, RTGs fuelled with Cu-244 are not developed yet. This poses a risk which is mitigated, because the housing and general purpose heat source of the plutonium RTG can be used for the curium RTG too [94], this also reduces the developing time and costs. The reliability is therefore 100% for the RTGs. Solar arrays are flight proven and very reliable. Since solar arrays are placed away from the ion plume, there is no extra degradation. The degradation experienced in flight are taken into account, so this contributes to redundancy. The deployment mechanism is a single redundant system and no failures occurred for the smaller types of solar arrays, so the reliability is 100% as well [85]. The batteries are not crucial for the mission, so parts of it may fail. Therefore they are not checked for reliability.

7.3.6. VERIFICATION AND VALIDATION OF MODEL AND REQUIREMENTS

7.3.6.1. VERIFICATION

The model used for the weight estimation assumes the RTGs of cuboid shape with the hot and cold junction temperatures and the two thermoelectric materials as inputs. The calculations for the efficiency are shown, however the calculations for the mass of the RTG not. No other sources were found to support the calculations of the mass. The input parameters for the efficiency equation are hot and cold junction parameter, the thermal power and a thermal conductance coefficient. The thermal conductance coefficient was not given, so the exact calculation could not be performed. Therefore a qualitative comparison is made with [95]. Mason found for an efficiency of 5% and a hot junction temperature of 1000 °C and a cold junction temperature of 300 °C and specific power of 4.8 W/kg. However the temperature difference is higher in the case of Mason. The source found that when the difference between the hot and the cold junction temperature is smaller, the specific power goes up. This was also indirectly found by [89].

7.3.6.2. VALIDATION

The validation is performed with a handbook on radiation shielding [96]. This source uses rep/hr instead of rem/hr, so the requirement needs to be transformed in the new unit. The conversion factor from rem to rep is 0.02325. This

Table 7.25: Cable masses for the different spacecraft parts.

Cable	Cable mass [kg]
Hovercraft	12
Orbiter	20
Second stage	13

Table 7.26: The mass and cost of the hovercraft and the orbiter.

	Hovercraft Mass [kg]	Hovercraft Costs [k€]	Orbiter Mass [kg]	Orbiter Costs [k€]
RTG excluding Cu-244 fuel	43	80625	60	129000
Cu-244	2.1	320	3.5	525
Shielding	45		73	
Batteries	0	0	2.7	36
Power Processing Unit	1.5	135	2.4	216
Total	92	81000	142	13000

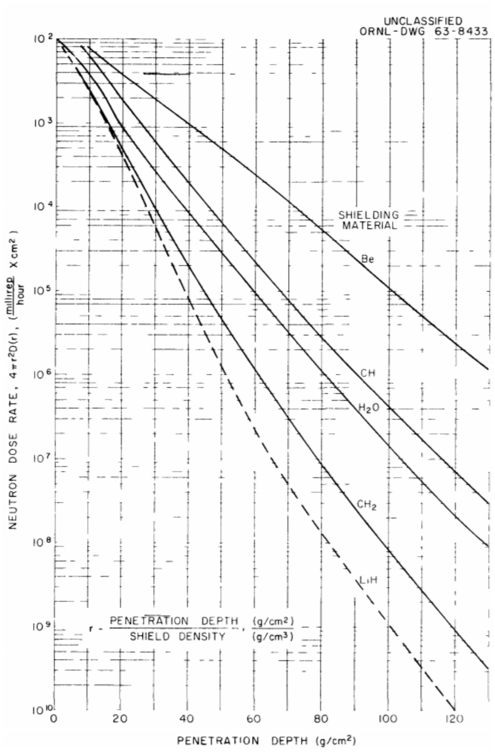

Figure 7.14: Fast neutron dose rate for various materials[96].

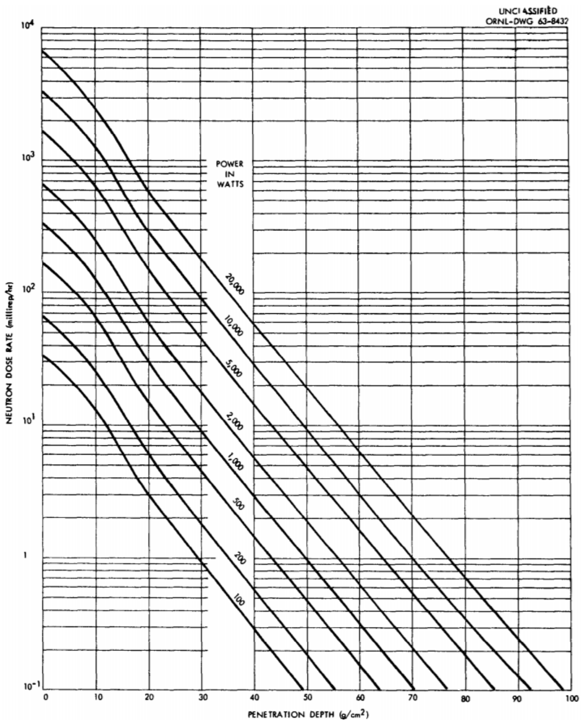

Figure 7.15: Water shielding for various power levels[96].

means a maximum dose of 156 and 173 mrep/hr. From Figure 7.15 this results in area densities of 17 and 20 g/cm^2 of water. With Figure 7.14 this can be transformed to polyethylene: 11 and 16 g/cm^2. Divide this by the density of polyethylene of 0.91 g/cm^3 results in thicknesses of 12 and 17 cm of polyethylene compared to the 6 and 9 cm. An explanation of the higher figures is, because here pure curium is shielded, whereas [89] calculates the shielding required of curium inside a RTG. The RTG casing slows down and absorbs neutrons and thus less external shielding is required.

Typical RTGs have efficiencies of 5%[20]. The efficiency of this RTG is 4.8% so, it is approximately the same. The specific power of 6.6 and 7.5 We/kg is rather high compared to Cassini 5 We/kg [95]. This can be explained that Cassini has plutonium RTGs and these are curium RTGs. Eogers and Ridihalgh (1974) found that curium RTGs will weigh less than plutonium RTGs [97].

7.4. PROPULSION

This section will present the propulsion subsystem for the two spacecraft and the two kick-stages. This subsystem includes the various engines used, the propellant tanks, the feed systems, pipes, valves and attitude control thrusters.

First the requirements of the four different propulsion subsystems will be discussed, followed by the layout and the characteristics of the propulsion subsystems. Next the different components of the propulsion subsystems will be discussed and why these are selected. Later the cost and RAMS characteristics are analysed, followed by the verification and validation of the models used in the design of the subsystem.

[20] http://large.stanford.edu/courses/2013/ph241/jiang1/, consulted on 24-06-2017.

7.4.1. Subsystem Requirements

7.4.1.1. Hovercraft Requirements

The hovercraft will have to perform a lot of small hopping manoeuvres and large transfer manoeuvres. The following requirements were made to help in the manoeuvres involving hopping and transfers.

1. The thrusters, that will perform the transfer, shall have an I_{sp} of at least 320 s.
2. The thrusters, that will perform the transfer, shall shall be able to perform the hopping manoeuvres in an effective burn time.
3. Placing the thruster that performs hopping manoeuvres opposite of the payload pointing direction shall be avoided.
4. The thrusters that perform hopping manoeuvres are required to be ignited very often.
5. The thrusters that perform hopping manoeuvres shall have redundant thrusters.
6. The hovercraft shall have attitude control thrusters that can be used for dumping momentum stored in the reaction wheels.
7. The main thruster shall have a gimbal to correct for any shift in centre of gravity.
8. The tanks shall be configured in such a way that a shift in centre of gravity due to the use of propellant is as low as possible.

7.4.1.2. Orbiter Requirements

The orbiter does not need to perform any hopping manoeuvres, but does need a transfer into its final orbit and attitude control. Therefore, all the requirements that apply to the hovercraft apply to the orbiter except the requirements concerning hopping manoeuvres.

7.4.1.3. Second Stage Requirements

The second stage is required to perform a few large burns during Saturn orbit insertion and orbit circularisation and a lot of small burns during pump down phase. Therefore, the following requirements were made to make this possible.

1. The spacecraft shall be able to perform Saturn orbit insertion within approximately two hours.
2. The main thrusters of the second stage shall have an I_{sp} of at least 330 s.
3. At least one of the main thrusters shall have increased redundancy.
4. This main thruster shall include a gimbal.
5. The tanks in this stage shall be arranged in such a way that changes in the location of the centre of gravity are as low as possible.
6. The second stage shall have attitude control thrusters that are active during the transfer phase.

7.4.1.4. First Stage Requirements

The following requirements relate to the first stage of SAURON.

1. The first stage shall have a solar electric propulsion system.
2. The electric thrusters shall be able to perform low thrust gravity assists.
3. All thrusters used on this stage shall have a gimbal to account for any changes in centre of gravity location.

7.4.2. Propulsion Subsystem Layout

In this subsection a layout will be given for the different propulsion subsystems. First the layout of the hovercraft and orbiter will be given, followed by the second and first kick-stage.

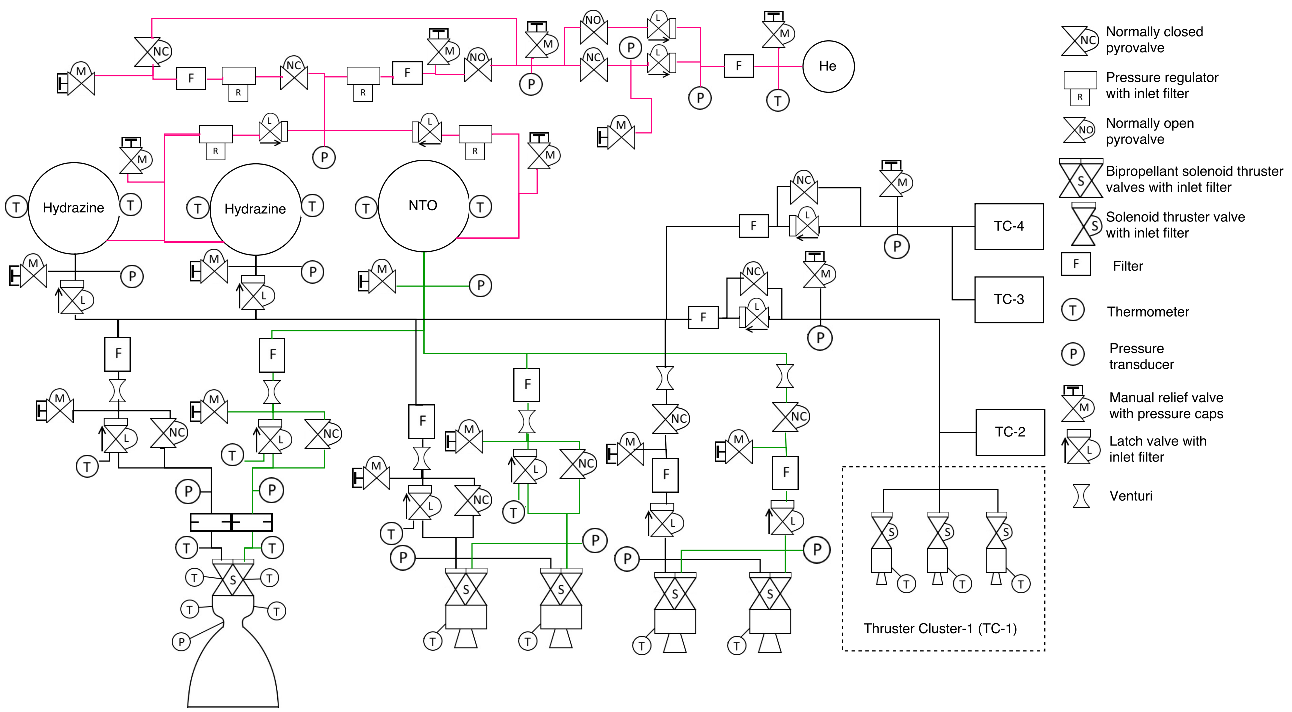

Figure 7.16: The layout of the propulsion subsystem on the hovercraft.

7.4.2.1. HOVERCRAFT PROPULSION LAYOUT

The layout of the subsystem can be seen in Figure 7.16. It uses a hydrazine/NTO main thruster to preform its high ΔV manoeuvres in which efficiency is important. Not pure NTO is used as oxidiser, but a mixture with nitric oxide called MON-3. To perform the small hopping manoeuvres two pairs of smaller bipropellant thrusters are used. These thrusters are located on the same locations as the control thruster clusters. The hovering thrusters are oriented in the same direction as the payload, such that limited rotation is required to perform the hopping manoeuvres. The hovering thrusters can also be used as redundant control thrusters. Since the payload is pointing down while it is connected to the second stage, these thrusters are oriented towards the second stage too and can be used to push push the hovercraft and orbiter away from the second stage during separation. The control thrusters are located in clusters and use hydrazine as monopropellant. Because of this no additional tank is required for the control thrusters. This saves space and tank mass, but does require more redundancy on the pressure feed system. The hovercraft has 3 different tanks for fuel and oxidiser. The fuel tanks are placed next to the oxidiser tanks since placing them on top would make the spacecraft too tall and unable to fit inside the launcher. To make sure the centre of gravity does not shift too much during the burning of fuel, the hydrazine tank is split up in two tanks and placed opposite of each other. The propulsion subsystem of the hovercraft is divided into 4 parts: The pressure feed system, the main thruster, the hovering thrusters and the control thrusters.

The pressure feed system uses one tank of pressurised helium. Two valves are used to lead the helium to the pressure regulators for redundancy. One pressure regulator and a redundant one are used to reduce the high pressure of the helium tank. Multiple relief valves are installed to reduce the pressure in case of an over-pressure on the system. Finally the helium is pressured into the different tanks each using their own pressure regulator to provide the right amount of pressure on each tank.

The main engine is supplied with fuel and oxidiser through two valves including redundancy. The engine itself contains two solenoid valves to regulate the fuel and oxidiser input.

The hovering thrusters are used in a pair to provide the spacecraft with the required ΔV. The primary pair have redundant valves to decrease the risk of failure. If the primary pair does fail, the secondary pair is activated. This pair does not have redundant valves since it is already redundant itself.

The control thrusters are grouped in 4 clusters of 3. There are two different lines including filters and valves that go to 2 clusters each. The valves have a redundancy to decrease the impact of valve failure. Also, when one of the two fuel lines that connect to the control thruster clusters fail, still two clusters are operational. The clusters that are connected to the same line are placed directly on the other side of the spacecraft, as can be seen in Figure 7.18. By using the clusters opposite of each other, the spacecraft would still be able to rotate in all of its three axis using only 2 of the thruster clusters.

7.4.2.2. ORBITER PROPULSION LAYOUT

The layout of the orbiter propulsion subsystem can be seen in Figure 7.17. It uses the same main thruster and the same control thrusters as the hovercraft. It only needs one main engine to perform its orbit transfers and some

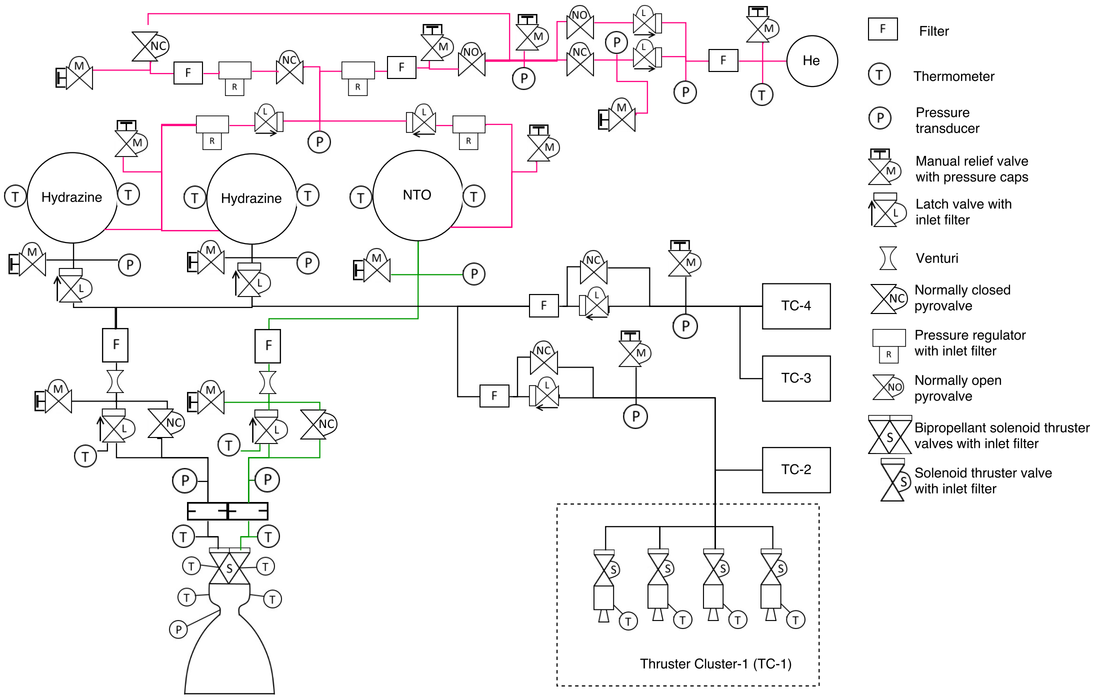

Figure 7.17: The layout of the propulsion subsystem on the orbiter.

control thrusters to dump any momentum and perfrom orbit corrections. The subsystem can be divided into 3 parts: The pressure feed system, the main thruster and the control thrusters.

The layout of the pressure feed system is the same as the one used in the orbiter. The only difference is the size of the tanks in the spacecraft and thus the size of the helium tank. The layout of the main engine and its fuel supply is also the same as the one on the hovercraft as can be seen in Figure 7.16 and Figure 7.17.

Since the orbiter does not have any thrusters used for hovering, it can't use these thrusters as redundant control thrusters. Resulting in 4 control thrusters per thruster cluster. Similar to the hovercraft, the control thrusters have two fuel feed lines with redundant valves. If one of the feed lines fail, the two remaining thruster clusters could still rotate the spacecraft in three different axis. The location of the thruster clusters with respect to the spacecraft can be seen in Figure 7.18.

7.4.2.3. Second Stage Propulsion Layout

The layout of the subsystem can be seen in Figure 7.20 and Figure 7.21. It uses 4 helium tanks, 2 fuel tanks and 2 oxidiser tanks. The tanks can be placed next to each other rather than on top of each other without shifting the centre of gravity too much when fuel is used. This reduces the total height of the spacecraft while staying within the width constraints of the launcher, making it easier to fit the other stages. The layout of the tanks in the second stage can be seen in Figure 7.19. In this figure, two of the 4 helium tanks are stacked in the centre.

The stage uses three main thrusters and four clusters of bipropellant control thrusters. The main thrusters are all ignited for Saturn orbit insertion. Since the second stage is very heavy all of the thrusters are needed to insert before flying by Saturn. During pump down phase a lot of small manoeuvres will need to be performed. For these smaller manoeuvres only the middle engine is ignited. Finally for the orbit circularisation all three main engines are ignited. The control thrusters on the second stage are already activated during the transfer to Saturn since the thrusters on the first stage are not powerful enough to be able to counteract high disturbance torques and for momentum dumping. The subsystem can be divided into 3 parts: The pressure feed system, the main thrusters and the control thrusters.

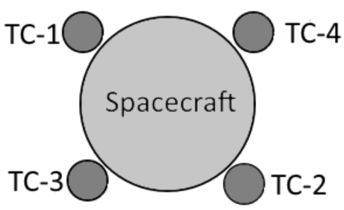

Figure 7.18: The locations of the different thruster clusters with respect to the spacecraft.

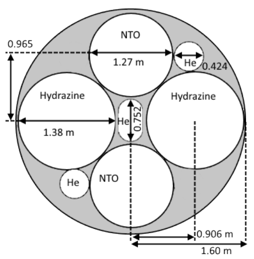

Figure 7.19: The layout of the tanks inside the second stage.

The pressure feed system can be seen in Figure 7.20. The helium tanks are designed to contain more helium than required to completely fill the fuel and oxidiser tanks with the required pressure. In the case of a tank leak, the leaking tank can be closed off and the rest of the mission can be performed. Because a lot of small manoeuvres are required from both the control thrusters and the main thrusters, additional valves are added to deal with this high strain on the pressure feed system compared to the hovercraft and orbiter.

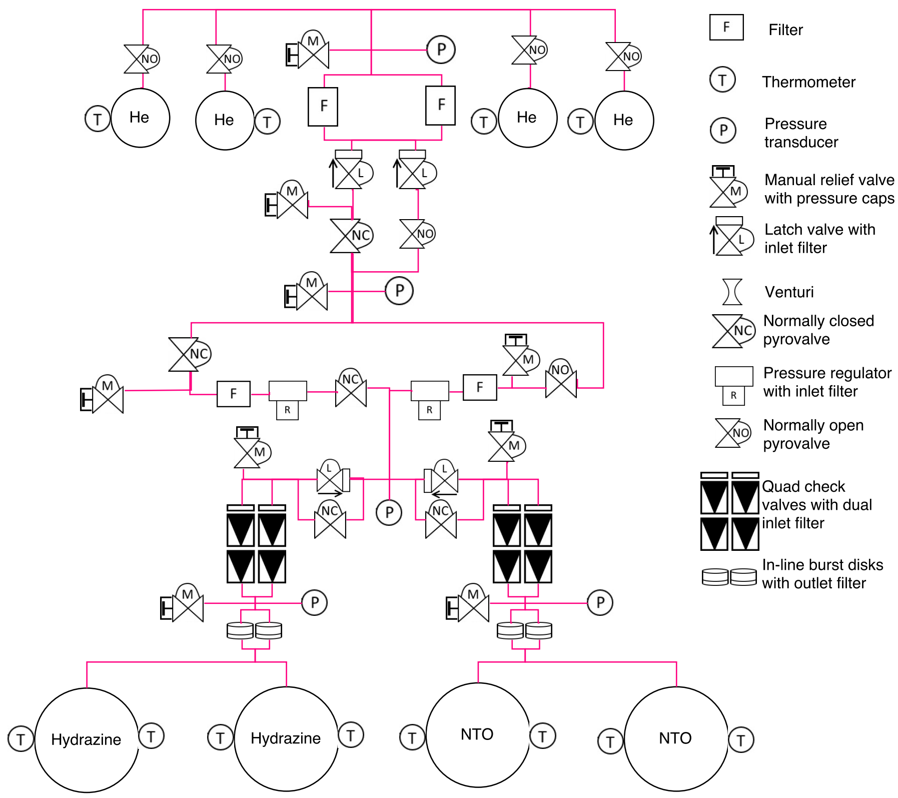

Figure 7.20: The layout of the helium feed system on board the second stage.

During Saturn orbit insertion all three engines are needed to perform the manoeuvre in the required burn time. Therefore, fuel and oxidiser lines feeding the main engines include a redundant line and redundant valves, as can be seen in Figure 7.21. The middle engine has to perform multiple small burns during the pump down phase and has additional redundant fuel lines connecting to the engine, decreasing the chance of engine failure. If the middle engine does fail, the two other engines could take over in order to still perform the mission. The same counts for the circularisation of the orbit. If only one of the engines operates, the circularisation is still possible, but it takes multiple orbits to perform.

The second stage also carries its own control thrusters. These thrusters operate from separation from the launcher until the moment the hovercraft and orbiter separate from the second stage. They are mainly used for momentum dumping, but will counter worst case disturbance torque when needed. Each thruster cluster contains 4 thrusters and has its own valves and filters. In each fuel and oxidiser line there is a redundant valve and in each control cluster there is a redundant thruster. Also, if two of the clusters that are diagonally opposite to each other fail, the stage can still rotate itself in three different axis.

7.4.2.4. FIRST STAGE PROPULSION LAYOUT

The layout of the first stage propulsion subsystem can be seen in Figure 7.22. It uses five NEXT thrusters which propel xenon gas from two xenon tanks and gather power through solar panels. The subsystem consists of 2 parts: The high pressure assembly and the low pressure assembly.

The high pressure assembly consists of two different lines that are connected at the top. They each have redundant proportional flow control valves and a xenon regulator feed system, which also has redundant outputs.

The low pressure assembly consists of three paths each. The NEXT thruster requires xenon flow to its main discharge, discharge and neutraliser cathodes. Latch valves are place in between the three flows which open when one of the proportional flow control valves fail. A power processing unit (PPU) is included in this assembly which supplies the NEXT thruster with the required power.

7.4.3. PROPULSION SUBSYSTEM CHARACTERISTICS

This subsection contains the important characteristics for each of the propulsion subsystems described in Subsection 7.4.2. The characteristics of the different thrusters can be seen in Table 7.27, the characteristics of the tanks can

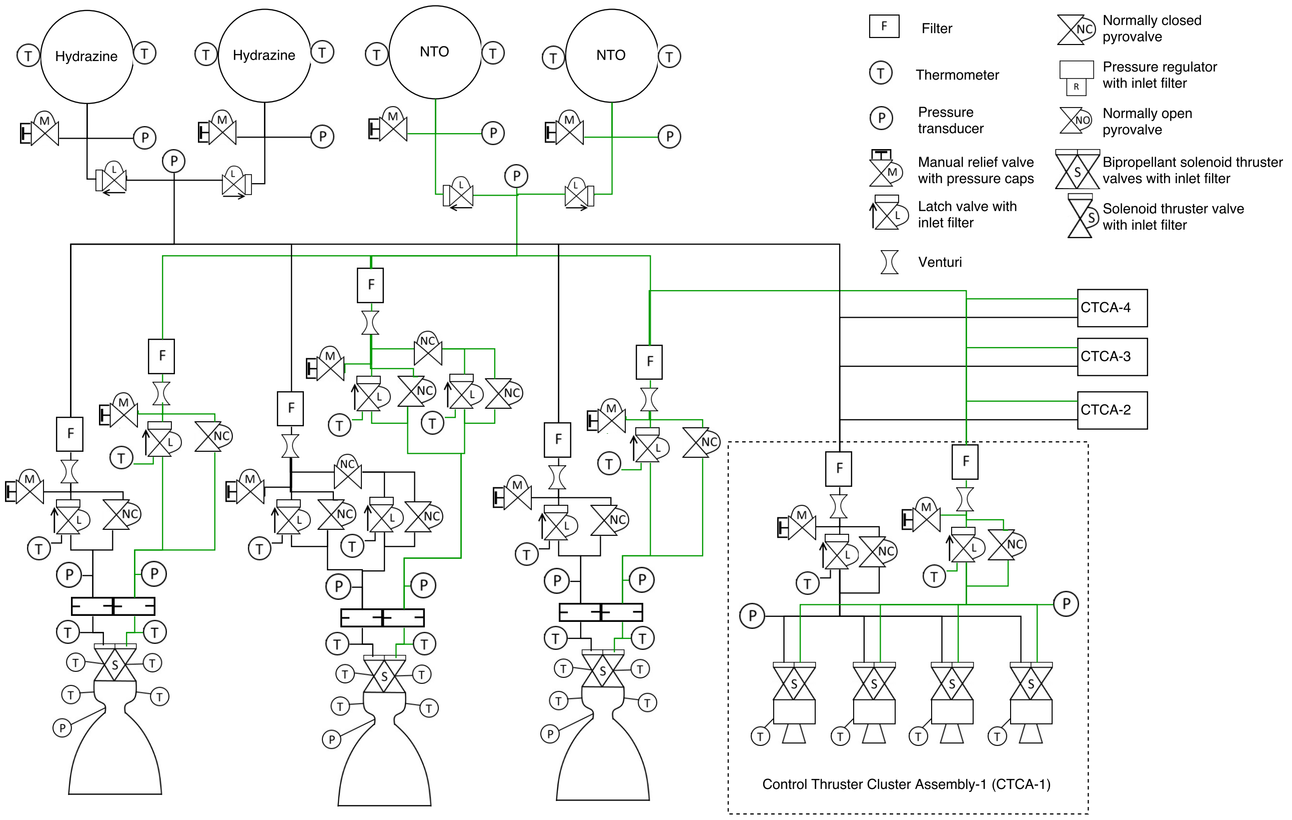

Figure 7.21: The layout of the fuel system on board the second stage.

Table 7.27: Characteristics for the spacecraft thrusters.

Component	**Usage**	**Mass [kg]**	I_{sp} **[s]**	**Thrust [N]**	**Chamber pressure [bar]**
AMBR 623N Dual mode HP rocket engine	Main thruster on second stage.	5.40	333	623	13.8
Hi-pat 445 Dual mode HP liquid apogee thruster	Main thruster on orbiter and hovercraft.	5.44	329	445	9.4
Moog DST-11H	Hovering thruster on hovercraft and control thruster on second stage.	0.77	310	22	5.5
MR-103M 1N	Control thruster on orbiter and hovercraft.	0.16	221-206	0.99-0.28	20.7 - 5.9
NEXT ion thruster	Main thruster on first stage.	12.7	max 4190	max 0.236	2.65 - 0.2

be seen in Table 7.28 and the total mass of the propulsion subsystems and its different parts can be found Table 7.29. How these values are found and calculated is described in Subsection 7.4.4.

7.4.4. PROPULSION SUBSYSTEM COMPONENTS

This subsection will look further into the different components that are selected and why they are selected. Also the mass of each component is determined in this subsection.

7.4.4.1. PROPELLANT SELECTION

The main priority of the propellant selection is to make sure that the propellants can be stored as efficiently as possible for the entire transfer to Saturn. Cryogenic propellants require low temperatures to be stored. Liquid oxygen requires -183 °C and liquid hydrogen -253 °C[21]. During the transfer phase the spacecraft orbits close to the sun, putting a large strain on the thermal control of the second stage and making cryogenic propellants ill-favoured.

For the hovercraft hypergolic propellants are preferred since the thrusters have to fire during every hop, requiring a reliable ignition system. Since the spacecraft dimensions constrain the design, it is chosen to use hydrazine/NTO as propellant. Hydrazine can be used as a bipropellant but also as a monopropellant including a catalyst. The control

[21] https://www.nasa.gov/mission_pages/shuttle/launch/LOX-LH2-storage.html, consulted on 18/06/2017.

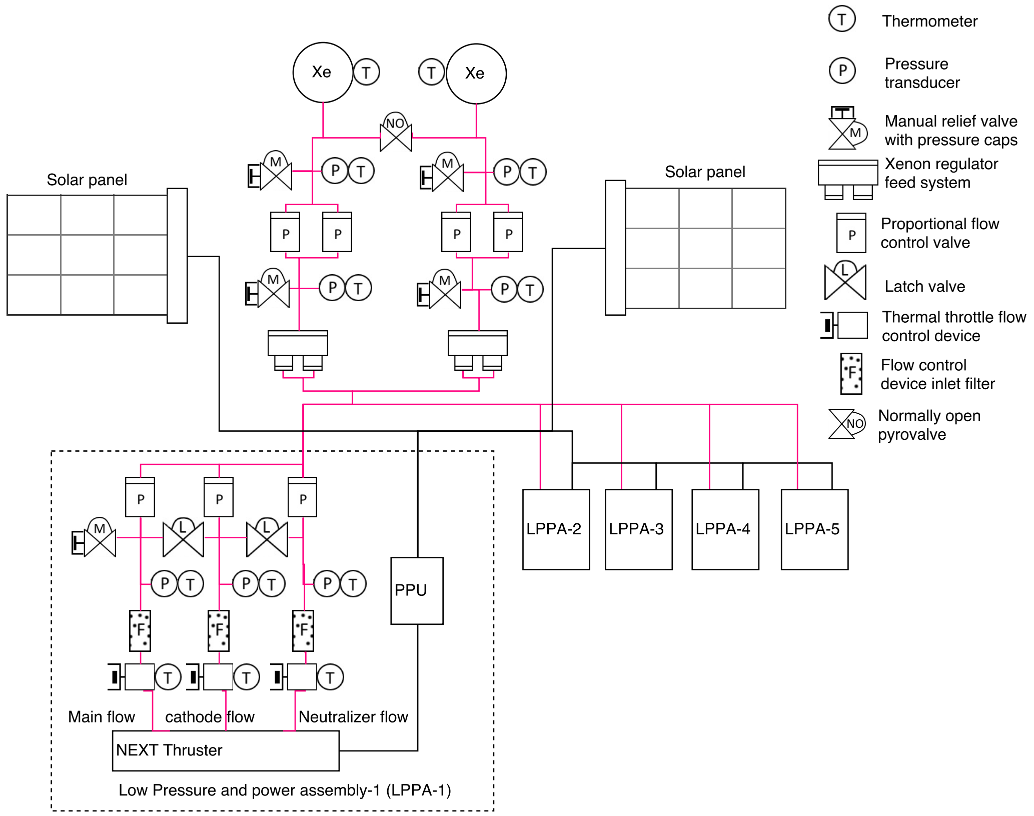

Figure 7.22: The layout of the propulsion subsystem on board the first stage.

thrusters on board the spacecraft do not require a separate tank, but use the same tank as the main thruster, making the tanks more space efficient.

The orbiter uses hydrazine/NTO as bipropellant for its main thruster and hydrazine for its control thrusters. The reasons for this selection are the same as for the hovercraft.

The second stage is required to perform a very large manoeuvre and the propulsion subsystem should be optimised for efficiency to reduce the weight. Electric is not possible for this stage since it is required to perform Saturn orbit insertion which has a low burn time requirement. Thermal nuclear propulsion was researched for this stage, but discarded for a few reasons. First, enriched uranium is required to sustain a fission reaction in a relatively small generator, which is very expensive. The NERVA-1 developed by the United States used enriched uranium of 50% purity and already required a reactor of 5476 kg which is excluding 6 tonnes of shielding around the reactor. The reaction could be sustained without modulation using 90% enriched uranium, but this fuel is very expensive and difficult to control [98]. Excluding cryogenic and exotic propellants, a trade-off was performed between hydrazine, MMH and UDMH in combination with NTO. Eventually hydrazine was selected due to the slightly higher I_{sp} of both the main engines and the control thrusters.

The first stage is a solar electric stage that uses ion thrusters to perform low thrust manoeuvres. Ion thrusters

Table 7.28: Characteristics of the tanks.

Spacecraft	**Tank type**	**Number of tanks**	**Content**	**Volume [L]**	**Dimensions [m]**	**Tank mass [kg]**	**Propellant mass per tank [kg]**
Hovercraft	Fuel	2	Hydrazine	187	0.685⌀ x 0.598 long	9.8	191
	Oxidiser.	1	NTO	201	0.702⌀ x 0.614 long	10.4	290
	Pressurant	1	Helium	18.8	0.331⌀	7.7	0.95
Orbiter	Fuel	2	Hydrazine	90	0.537⌀ x 0.469 long	5.89	91.7
	Oxidiser	1	NTO	82	0.521⌀ x 0.455 long	5.58	119
	Pressurant	1	Helium	9.4	0.262⌀	5.40	0.404
Second stage	Fuel	2	Hydrazine	1520	1.380⌀ x 1.20 long	63.7	1550
	Oxidiser	2	NTO	1190	1.270⌀ x 1.11 long	50.8	1710
	Pressurant	4	Helium	81.4	0.424⌀ x 0.752 long	12.7	3.06
First stage	Fuel	2	Xenon	268	0.907⌀ x 0.673 long	22.2	364.5

Table 7.29: Propulsion subsystem characteristics.

Spacecraft	Tank mass [kg]	Thruster mass [kg]	Pipes and mechanics [kg]	Max operating power [W]	Total mass [kg] (incl. He)
Hovercraft	39.2	10.4	10.9	82 (hover thrusters)	64.1
Orbiter	23.0	8.0	8.59	46 (main thruster)	45.2
Second stage	299	28.6	76.8	135 (main thrusters)	416
First stage	44.5	63.5	243 (including PPU)	36100 (NEXT thrusters)	351

typically use Xenon gas for multiple reasons. Xenon is the heaviest non-radioactive inert gas. Because xenon particles have the more mass more momentum can be exerted on them, reducing the number of particles (n) required to propel the spacecraft. This decreases either the pressure or the volume of the tanks according to the ideal gas law, which can be seen in Equation 7.12.

$$pV = nRT \tag{7.12}$$

7.4.4.2. THRUSTER SELECTION

In the selection of the thruster a few aspects are taken into account. The most important one is the engine I_{sp}. The mission requires a lot of manoeuvres and an efficient engine would decrease the wet mass by a lot. Burn time and minimum impulse are the other main criteria. The thrusters must be able to perform the manoeuvres within the required amount of time. Also the thruster should not be too powerful for the smaller manoeuvres it is required to do.

The hovercraft needs to be able to perform a wide range of manoeuvres. It's transfers from one hovering location to the next requires almost 2 km/s ΔV and should be performed with a high thrust and high efficiency engine. These manoeuvres are performed by the Aerojet Hi-pat 445N Dual mode HP liquid apogee engine. The characteristics of this thruster can be seen in Table 7.27 [99]. While hopping the thruster needs to perform a small manoeuvre, in the order of 0.2 m/s, every few hours. It is therefore desired if the thruster that performs the manoeuvre is facing towards the ring. This way no large attitude correction has to be performed in order to point the engine in the right direction, increasing operating time. This requires the thruster to be on the same side of the spacecraft as the payload. However, the thruster is one of the few components that is resistant to the radiation of the RTG and is therefore preferred to be located on the opposite side of the payload, next to the RTG. To solve this 4 small bipropellant thrusters called the moog DST-11H are added to perform the hopping manoeuvres. The characteristics of this thruster can also be seen in Table 7.27[22]. These thrusters use the same fuel as the main thruster, but have a slightly lower I_{sp}, which is 310s compared to the 329s of the main engine. Only two of these thrusters will be used at a time and they are able to perform the hopping manoeuvres within 3 - 3.6 seconds. Since the hopping manoeuvres only requires a total of 130 m/s ΔV compared to the 2 km/s performed by the main engine, this decrease in engine efficiency does not impact the design much. Additional attitude control thrusters are added to the spacecraft for dumping momentum stored in the reaction wheels. The MR-103M 1N was selected based on it's dimensions, which are 133mm x 53mm, it's compliance with the requirements from the AOCS as can be seen in Section 7.1, and the fact that it uses hydrazine as a monopropellant.

The orbiter only needs to perform a view transfers to enter its final orbit. After that it only requires some orbit maintenance from its attitude control thrusters. The same main thruster is selected for the orbiter as for the hovercraft since the requirements for transfer are still the same. The requirements for the attitude control thrusters are the same as the ones for the hovercraft and therefore the same thrusters are selected.

The second stage is required to perform Saturn orbit insertion within x amount of time. After this, it will have to perform many small manoeuvres during the pump down phase. Since this stage has to provide over 4 km/s ΔV, a high efficiency engine is selected to perform the manoeuvres. The Aerojet AMBR 623N Dual mode HP rocket engine is selected and its characteristics can be seen in Table 7.27 [100]. The main engine by itself is not powerful enough to perform the Saturn orbit insertion in the required amount of time. However, a larger thruster will not be able to efficiently perform the small manoeuvres during the pump down phase. To perform the small manoeuvres and Saturn orbit insertion in the required time, three engines are placed on the second stage. All three combined have enough power to perform Saturn orbit insertion and a single engine perform the manoeuvres during the pump down phase. The same thrusters that are used for hovering on the hovercraft are used as attitude control thrusters on the second stage. High efficiency is required for the attitude control since it is not only used for momentum dumping but also to counter high disturbance torques as explained in Section 7.1. Since the Moog DST-11H is one of the highest performing currently available attitude control thruster they are selected[23].

[22] http://www.moog.com/literature/Space_Defense/Spacecraft/Propulsion/bipropellant_thrusters_rev_0914.pdf, consulted on 18/06/2017.

[23] http://www.moog.com/literature/Space_Defense/Spacecraft/Propulsion/bipropellant_thrusters_rev_0914.pdf, consulted on 18/06/2017.

Table 7.30: Performance characteristics of the NEXT compared to the NSTAR SOA.

Characteristic	NEXT	NSTAR SOA
Thruster Power Range, kW	0.5-6.9	0.5-2.3
Max. Specific Impulse, sec	>4100	>3100
Max. Thrust, mN	236	96
Max. Thruster Efficiency	>70%	>61%
Max. PPU Efficiency	95%	92%
PPU Specific Mass, kg/kW	4.8	6.0
PMS Single-String Mass, kg	5.0	11.4
PMS Unusable Propellant Residual	1.00%	2.40%

The first stage is required to be an electrical stage that performs low thrust gravity assists. Since the spacecraft is very high, a powerful thruster is required to perform the low thrust manoeuvres. The NEXT ion propulsion system is selected for this stage and its characteristics can be seen in Table 7.27. Its maximum power is higher than that of the NSTAR, but provides higher efficiency, lower mass and higher thrust. The differences between the two can be seen in Table 7.30 [101].

7.4.4.3. Propellant Tank Sizing

Due to time constraints in the design of the propulsion subsystem, the tanks are not designed optimally, but their characteristics are taken from exiting tanks or approximated using existing tanks.

The size of the helium tanks is determined by the required pressure in the main tanks. The feed pressure of the engine and the volume of the tanks are used to determine the amount of helium particles using Equation 7.12. The temperature assumed in this case is 294.15 K, which is within the operational limits of the fuel tanks as stated in Section 7.7. A value of approximately 310 bar is assumed to calculate the required volume of the helium tank and a tank is selected from an existing catalogue of pressurant tanks[24]. If the tanks states a different operating pressure than the 310 bar, it will be iterated.

Using existing hydrazine tanks an estimation can be made for the tank mass[25]. Plotting the data of the various tanks results in a function of the tank mass based on the tank volume. This graph and the function resulting from it can be seen in Figure 7.23. To account for an increase in tank mass due to tank shape, a 10% contingency margin is added to the tank mass estimation. The tank mass and dimensions can be seen in Table 7.28.

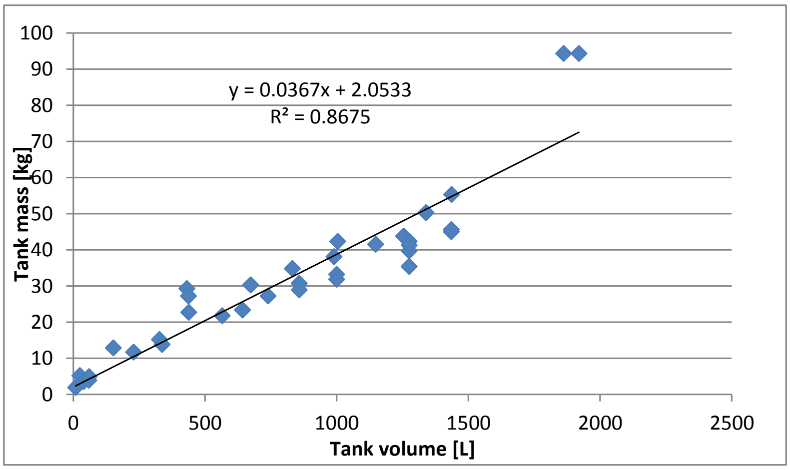

Figure 7.23: The approximation of tank mass with respect to the tank volume.

7.4.4.4. Valves, Pipes and Mechanisms

The valves and pipes were selected only based on weight and if they complied with the requirements. The mass of the different propellant management assemblies can be seen in Table 7.31 [101–103][26]. The mass of the individual components of these assemblies will not be shown in this report. Also note that certain assemblies are used multiple times in the spacecraft and there masses are added in the calculation of the final mass of the propulsion subsystem in Table 7.29.

[24] http://www.psi-pci.com/Data_Sheet_Index_Pressurant-VOL.htm, consulted on 18/06/2017.
[25] http://www.psi-pci.com/Data_Sheet_Index_Diaphragm-VOL.htm, consulted on 18/06/2017.
[26] http://www.space-propulsion.com/brochures/valves/space-propulsion-valves.pdf, consulted on 14/06/2017.

Table 7.31: Masses of the different propellant control assemblies on for each spacecraft stage.

Stage	Component / Assembly	Mass [kg]
Fist stage	High pressure assembly	1.9
	Xenon regulator	5.9
	Power processing unit	34.5
	Low pressure assembly	3.1
	Gimbal	6.0
Second stage	Helium control assembly	33.1
	Fuel/Oxidiser control assembly	36.6
	Gimbal	5.2
Orbiter	Helium control assembly	2.11
	Main fuel control assembly	2.34
	Attitude fuel control assembly	0.90
	Additional pipes	3.24
	Gimbal	5.2
Hovercraft	Helium control assembly	2.11
	Fuel control assembly	5.53
	Additional pipes	3.20
	Gimbal	5.2

Table 7.32: Cost estimation of the propellants and propulsion subsystem.

Subsystem part	Cost [€M]
Hovercraft	1.8
Orbiter	1.3
Second stage	12
First stage	50
Hydrazine	0.10
NTO	0.05
Xenon	0.55
Total	65

7.4.5. Cost Breakdown

The estimated cost of the propulsion subsystems are shown in Table 7.32. The mass of the electrical propulsion subsystem is based on a cost model using the number of thrusters used and the required power of the system [104]. A power of 30kW was assumed using 3 thrusters to calculate this value. The cost of the chemical components are based on the costs of previous missions per kg of propulsion subsystem mass [105]. A value of €29,000 per kg was found for integral propulsion subsystems. Finally the costs of the propellants are added [106] [107], resulting in a total cost for the propulsion subsystem of €65 Million. The source with the price of the propellant is outdated, therefore an inflation factor was added.

7.4.6. RAMS Analysis

This section will analyse the reliability, availability, maintainability, safety and the risk of the propulsion subsystem.

The thrusters used in the different propulsion subsystems are all either flight proven or qualified for flight after testing. Additionally relief valves are placed in the control assemblies to reduce the chance of failure in the pipes due to over-pressure. Also, high reliability valves were selected to increase control assembly reliability. Finally filters are added in the control assemblies to prevent any clogging of the valves or pipes.

The propulsion subsystem on board the hovercraft has a large influence on the availability of the spacecraft. Since the hovercraft has to perform a hopping manoeuvre in between its operating time, the availability of the spacecraft decreases. By attaching hopping thrusters that point in the same direction as the payload the time required to perform this manoeuvre is diminished a lot. The spacecraft does not need to slew anymore and only requires a 3 second burn to perform the entire manoeuvre.

7.4.7. Verification and Validation

In the design of the propulsion subsystem three different tools and models were created. The tank mass model was used to calculate tank mass based on tank volume. The tank dimension calculator is a program used to calculate the dimensions of the tanks which requires the least surface area based on a given volume. The pipe mass calculator is a function that determines the mass of the pipes based on required mass flow, pressure and pipe length.

The tank mass estimation is validated by calculating the tank mass of existing missions. These calculations can be seen in Table 7.33 [102] [108] [109]. The tanks of the Cassini spacecraft are heavier than calculated. This difference can be accounted for by the fact that no data was found on the mass of just the tanks, but only on the entire tank assembly. This includes the tanks thermal control and part of the structure. Another factor might be that the tanks of Cassini are outdated. Cassini was launched in 1997, 7 years earlier than the MESSENGER mission, which was launched in 2004. New developments in tank design could reduce the required tank mass of the spacecraft.

The tank dimension calculator is verified by changing the end-cap constraint in such a way that it becomes a semi-sphere. If the program runs correctly, it should turn the tank into a complete sphere, since that is the shape with the least amount of surface area for a given volume. The area of a sphere is calculated using Equation 7.13.

$$A = 4\pi r^2 \tag{7.13}$$

Table 7.33: Comparison of the tank mass model to actual tanks.

Spacecraft	Tank	Propellant volume [m^3]	Calculated tank mass [kg]	Actual tank mass [kg]	Difference [%]
Cassini	MMH	1.29	54.2	Not available	-
	NTO	1.30	54.6	Not available	-
	Total tank assembly	2.58	109	147	35.1
MESSENGER	Hydrazine (2)	0.17	9.30	8.00	14.01
	NTO	0.16	8.73	8.00	8.41
	All tanks	0.51	27.34	24.00	12.22

In the approach to calculating the surface area of an ellipsoid divides by the sine of the arccosine of the aspect ratio between the axis of the ellipsoid. When this is exactly 1, meaning that the end caps are spherical, a division by 0 is made and the program does not run. However, the dimensions of the tank do approach that of a sphere as the aspect ratio approaches 1, as is expected of the program.

In order to validate the pipe mass calculator the pipe mass of the hovercraft is compared to a commonly used pipe in spacecraft propulsion. The total pipe length is held constant and compared to the standard pipes made of Ti3Al2.5V with a thickness of 0.5 mm and a diameter of 6.4 mm [110]. The standard pipes had a total mass of 2.88 kg, which was 11% lower compared to the 3.24 kg calculated by the program. The higher mass of the calculated pipes is most likely caused by the fact that the program accounts for high pressure lines which require to withstand higher loads and are heavier.

7.5. STRUCTURES

7.5.1. REQUIREMENTS

To perform an analysis of the structure of the whole spacecraft, requirements need to be defined first. The basic requirement is that the structure shall support the payload and spacecraft subsystems with enough strength and stiffness to preclude any failure (rupture, collapse, or detrimental deformation) that may keep them from working successfully [111]. Below a list of requirements regarding the structure subsystem are presented:

- **Structure-01:** The spacecraft mass shall not be more than 3,419 kg.
- **Structure-02:**The spacecraft shall not have a total height of more than 11.5 meters.
- **Structure-03:**The structure shall withstand the worst design loads without failing or exhibiting permanent deformations.
- **Structure-03:**The natural frequency of the spacecraft shall not be less than 8 Hz in lateral direction and 30 Hz in axial direction.
- **Structure-04:**The spacecraft shall withstand the maximum quasi-static load factors of 6 g in axial direction and 2 g in lateral direction

7.5.2. LAUNCH VEHICLE SELECTION

To size the structure of SAURON, first a launch vehicle that will launch the S/C should be chosen based on which the launch loads can be retrieved from its user manual. Based on the analysis that has been performed so far on Astrodynamics and the whole spacecraft weight only heavy lift launch vehicles can be chosen. The launchers that were considered for the mission include the Delta-IV Heavy, Falcon Heavy and Space Launch System Block 1. Below a comparison is presented based on maximum payload, payload fairing dimensions, cost and technology readiness level. In Table 7.34 the values for each criterion is presented for each launcher, which are explained below.

- **Maximum payload:** It is one of the most important criterion since the launcher should be capable of launching into space the required weight of the spacecraft and only a few number of existing launch vehicles can achieve that.
- **Payload fairing dimension:** This criterion imposes the dimensional constraints on the spacecraft and the design of the configuration, which determines the maximum dimensions of subsystems and their relative position.
- **Cost:** The cost of the launch is important for the whole mission, since the total cost of the mission should not be exceeded and launching could costs contribute considerably to the total cost.
- **Technology readiness level:** This criterion also imposes large restrictions to the selection of available launchers since the top level requirement of existing launchers should be satisfied.

Based on Table 7.34 it is clear the only feasible option for launch vehicle is the Falcon Heavy since it is capable of lifting the required weight of SAURON, the launch cost contributes less than the others to the total cost of the mission and has the highest TRL level.

Table 7.34: Specifications of Falcon Heavy, Delta-IV Heavy and SLS Block 1.

	Falcon Heavy[27], [28]	**Delta-IV Heavy** [112]	**Space Launch System** [113]
Maximum payload mass to Mars	16,800 kg	8,500 kg	19,000 kg
Payload fairing dimensions	4.6 m x 11 m	4.5 m x 15 m	4.6 m x 19.1 m
Cost per launch	100,000,000 $	435,000,000 $	500,000,000 $
TRL level	7	9	6

Table 7.35: Quasi-static loads during launch.[112]

Quasi-static loads			
Minimum axial frequency (Hz)	Minimum lateral frequency (Hz)	Maximum axial load (g)	Maximum lateral load (g)
30	8	6	2

7.5.3. SPACECRAFT DESIGN LOADS

7.5.3.1. LOADS

During the lifetime of the spacecraft, different loads are applied on it. The maximum loads are used to design and give dimensions to the primary and secondary structure and other parts of the spacecraft [114]. The dynamic mechanical loads that act on the spacecraft consist of:

- Handling loads
- Transportation loads
- Vibration tests for the qualification of the structure
- Dynamic loads during loads
- Loads on the spacecraft in orbit

The most critical loads which also drive the design of the structure are the launch loads.These loads depend on the launch vehicle selected to launch the spacecraft and are provided by the user manual of the launcher. More specifically, the loads that the structure will experience include the following [114]:

- **Quasic-static loads:** as a result of the propulsion of the launcher's engine, crosswind loads and manoeuvres performed during launch.
- **Sinusoidal vibrations:** during lift-off and the combustion of the engines.
- **Random vibrations**
- **Acoustic loads:** as a result of exhaust noises and the turbulent flows along the launch vehicle.
- **Shock loads:** as a result of the separation of the stages and the separation of the spacecraft from the launcher, the ignition and the stopping of the engines.
- **Pressure variations:** due to the absolute pressure decrease during launch.

The analysis of the structure will be performed based on the quasi-static loads since they drive the design to a great extent and produce the highest loads on the spacecraft during launch. The structure of the spacecraft will also need to comply with the frequency requirements imposed by the launcher.

In Subsection 7.5.2 it was determined that Falcon Heavy would be used to launch SAURON. Because it has not been tested yet and no information is available regarding the loads the spacecraft will experience during launch it was decided that the analysis will be based on data retrieved from similar heavy lift launch vehicles. Data was gathered from the Delta-IV Heavy user manual. In Table 7.35 information regarding the minimum axial and lateral frequencies the S/C needs to satisfy are given together with the maximum axial and lateral quasi-static load factors which occur during launch [112]. The maximum axial load factor corresponds to the maximum compressive load the spacecraft will experience.

Apart from the quasi-static load factors the structure needs to withstand the transportation loads. In Table 7.36 typical load factors for air and ground transportation are shown, from which it is clear that by designing the S/C based on the quasi-static load factors we assure that it will not get damaged during transportation [114].

Table 7.36: Transportation loads.[114]

Medium/Mode	**Lateral load factor**	**Vertical load factor**
Air	± 1.5	± 3
Ground (truck)	± 2	± 6

Table 7.37: Inertia measurements of all stages

Stage	Centre of mass (x,y,z) [mm]	Ix [kg m^2]	Iy [kg m^2]	Iz [kg m^2]
SEP	(0,0,1122)	3616	29260	29458
SOI	(0,0,1457)	4798	4170	7804
Hovercraft	(-1.1,-1.5,1079)	189	507	404
Orbiter	(-2.3,-2.7,966)	435	208	361
Total	(0.3,-3,3015)	31164	57981	38029

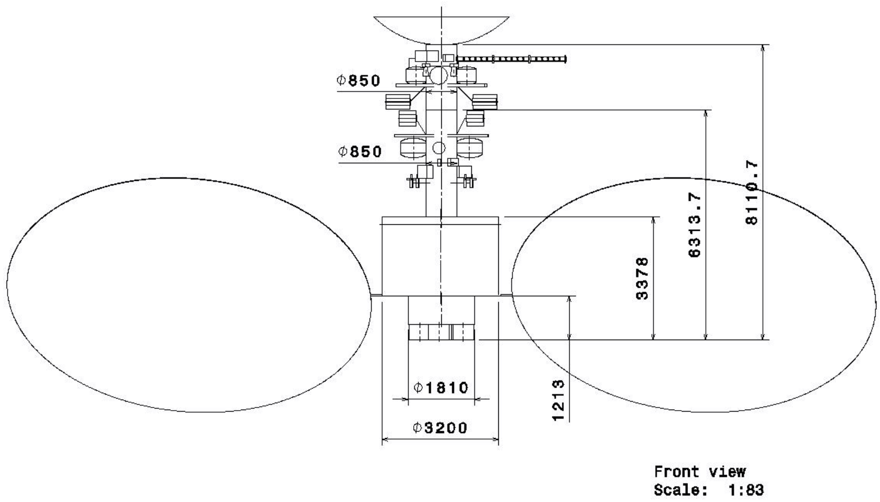

Figure 7.24: Spacecraft layout.

7.5.4. SPACECRAFT CONFIGURATION AND LAYOUT

The structure of the spacecraft was decided to be a cylindrical shape. This way there is an easy integration of the spacecraft to the adapter connecting it to the launch vehicle [115]. The cylinder is hollow with a required thickness determined for the solar electric stage and and Saturn insertion stage to be 4.2 mm and for the hovercraft and orbiter 2.6 mm. Each stage is divided into two modules, the propulsion module and the electronics module on top of it. Inside the cylinder the tanks of the propulsion system of each stage will be attached, except for the helium tanks which will be attached in the outer surface. For the hover orbiter and the main orbiter though the fuel tanks will also be attached on the outside. Inside the structure the thermal subsystem will be running from top to bottom to ensure all parts are functioning under their allowable temperature range. Regarding the main orbiter, the structure will be used to attach the payload and the antenna on top of the spacecraft. The overall dimensions of all the stages were determined based on the propulsion tank, engine, payload and RTG dimensions. In Figure 7.24 the layout of the whole spacecraft with the corresponding dimensions is presented. The overall structure height of the spacecraft was calculated to be 8.1 meters. These dimensions comply with the allowable ones for the Falcon Heavy payload fairing. In Figure 7.25-7.26 the dimensions of the orbiter and hovercraft are provided together with the position of the electronics bus module. Each spacecraft has a cylinder diameter of 0.85 meter. The centre of mass of each stage and of the whole spacecraft is given in Table 7.37 in addition with the moment of inertia for each axis around the centre of mass. The result were obtained by placing all components on each stage and at their desired location and using CATIA to determine the centre of mass and moment of inertia.

In Figure 7.27-7.28 the internal layout of the orbiter and hovercraft is shown with the corresponding components of each spacecraft.

7.5.5. MATERIAL SELECTION

Material selection is an important aspect of the design process of the structure of the spacecraft and has significant effects for mass, production costs, etc. The selection is based on the most important material properties which include [114]:

- Strength and Stiffness
- Density

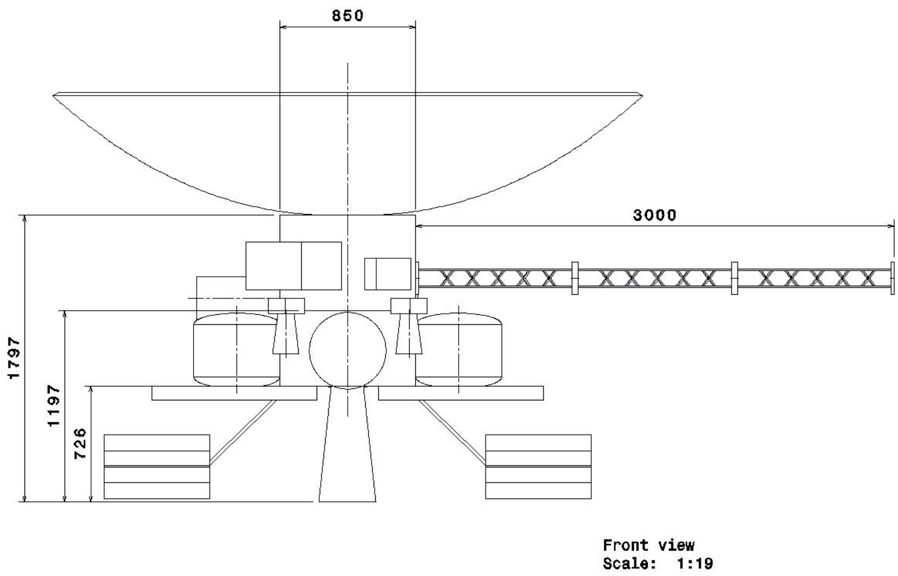

Figure 7.25: Main orbiter

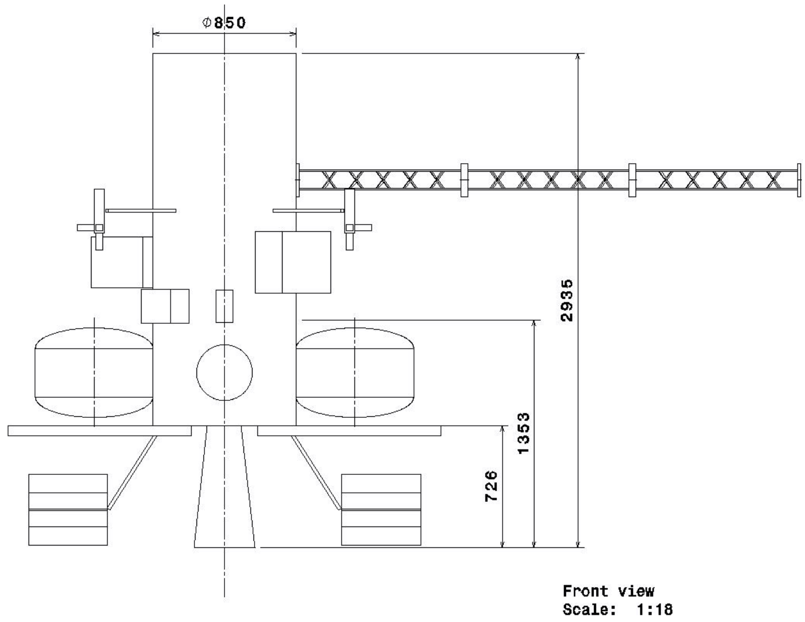

Figure 7.26: Hovercraft

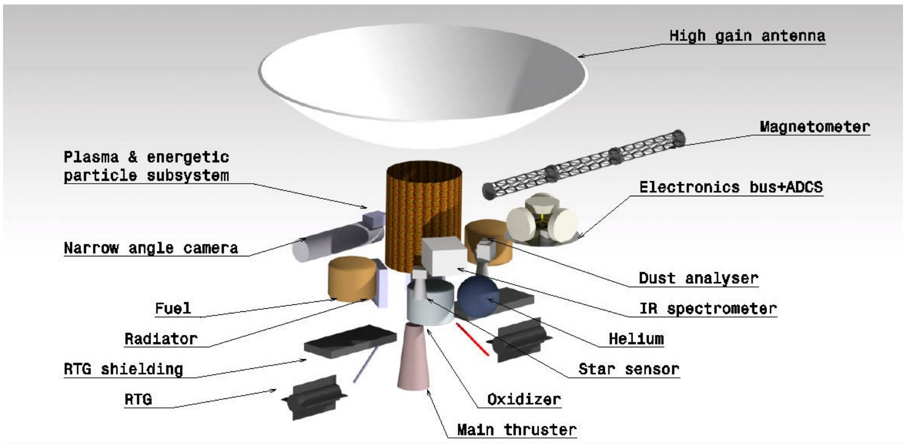

Figure 7.27: Hovercraft

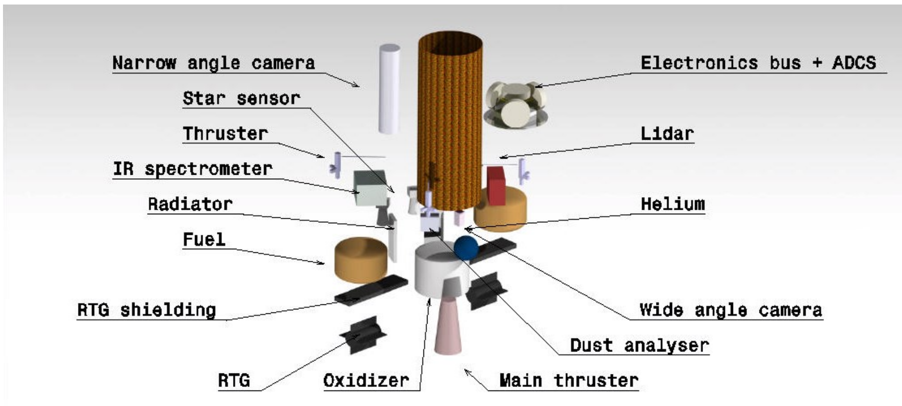

Figure 7.28: Hovercraft

Table 7.38: Material properties of Aluminium 8090, Aluminium 7075-T7 and Titanium Ti-6Al-4V.

Material	**Density ρ kg/m^3**	**Yield strength MPa**	**E modulus GPa**	**elongation %**	**Coefficient of thermal expansion μm/m°C**
Aluminium-Lithium 8090	2.54	370	77	7	21.4
Aluminium 7075-T7	2.81	503	71.7	11	23.6
Titanium Ti-6Al-4V	4.43	880	113.8	14	9.7

- Yield strength
- Thermal conductivity
- Availability
- Cost

The materials that were considered for the structure of the SAURON include Aluminium 8090, Aluminium 7075-T7 and Titanium Ti-6Al-4V. In Table 7.38 the corresponding material properties for each material are presented[29], [30], [31]

For each material the structural analysis method performed in Subsection 7.5.6 was performed and a new total mass was found. Out of the three option the best came out to be Aluminium 8090 giving the lowest mass of the structure. For this reason it was chosen as the final material for the design. Comparing the coefficient of thermal expansion, it can be said that even though titanium scores the best out of the three, it has high density which results in a heavy structure mass. The value of 21.4 for Aluminium 8090 is considered high, however, with the correct design of the thermal subsystem no major problem can be caused to result to structure failure.

7.5.6. STRUCTURAL ANALYSIS

The analysis of the structure of the spacecraft was done based on the approach retrieved from [79]. The sizing of the structure was done based on a monocoque design by firstly analysing the whole structure as one design and later dividing it to the corresponding sections. The first section includes the SEP and SOI stages and the second section the hovercraft and the orbiter. An approach to add detail on the analysis and optimise the structure with the use of a skin and stringers was also considered. The two main aspects that were used for the design of the structure were the stiffness requirements and the quasi-static load factors. The structure was designed to comply with the minimum axial and lateral frequency requirements and the maximum axial and lateral loads imposed from the launcher. In order to analyse the complicated structure and to simplify the analysis some assumptions needed to be made. The degree in which the analysis is simplified indicates the accuracy of the solution. The assumptions that were made are presented below:

- The structure of the spacecraft can be modelled as a beam.
- The spacecraft will be idealised in launch configuration as a cantilevered cylinder.
- All the mass of the spacecraft is uniformly distributed.
- The structure can be idealised as a single-degree-of freedom spring-mass system.
- The loads on the spacecraft during launch are applied on its centre of mass.

The first aspect that was taken into account was the stiffness of the spacecraft. To avoid resonance, the S/C should be sufficiently stiff and its fundamental natural frequencies in all directions must be larger than the minimum frequencies generated from the launcher that excite the S/C [72]. By assuming the structure to be a beam with uniform distribution of mass and thickness Equation 7.14 and Equation 7.15 were used to determine the minimum required thickness.

$$f_{nat,axial} = 0.56\sqrt{\frac{EI}{ML^3}} \tag{7.14}$$

$$f_{nat,lateral} = 0.25\sqrt{\frac{A_{cyl}E}{ML}} \tag{7.15}$$

Moreover, the structure needs to withstand the maximum quasi-static loads, including a safety factor. The quasi-static loads are a combination of the steady-state static loads and the low frequency sinusoidal loads. By considering these loads, gravity is taken into account and it is assumed that they act on the centre of gravity of the spacecraft. Axial load is directed along the vehicle axis and lateral load perpendicular to this axis. Since these loads could occur simultaneously during launch the design of the structure will be based on that. For the structure's design two failure modes will be investigated namely failure due to buckling and yielding.

With the given load factors listed in Table 7.39 the corresponding loads on each stage of the spacecraft can be calculated by multiplying the load factors with the weights of each stage.

[29] http://www.azom.com/article.aspx?ArticleID=8789, consulted on 20/06/2017.
[30] http://asm.matweb.com/search/SpecificMaterial.asp?bassnum=mtp641, consulted on 20/06/2017.
[31] http://asm.matweb.com/search/SpecificMaterial.asp?bassnum=MA7075T6, consulted on 20/06/2017.

The equivalent axial load applied on the hollow cylindrical structure of each section could be found using Equation 7.16. An ultimate safety factor of 1.5 was used for the design of the structure.

$$P_{eq} = P_{axial} + \frac{2M}{R_{cyl}} \tag{7.16}$$

A yield strength of 370 MPa for the Aluminium-Lithium 8090 was used for Equation 7.17.

$$\sigma_{yield} = \frac{P_{ult}}{A} \tag{7.17}$$

Next step to the design process is to size for compressive strength. Firstly, based on the thicknesses that were found so far for stiffness and yielding, the maximum should be used not only to assure that all aforementioned failure modes are satisfied but also to check whether the structure will buckle with this thickness or not. Equation 7.18-7.20 were used to calculate the critical buckling stress for the cylinder. In case the critical buckling load is less than the ultimate load applied iteration needs to be made. Comparing these values with the ultimate load applied on the structure it is clear that the cylinder is not adequate and it will buckle before the ultimate load is reached. Through a number of iterations an increased thickness was found to allow the structure to buckle when the ultimate load is applied. The maximum thickness for the structure that satisfies all the requirements is for the first section 4.2 mm and for the second section 2.6 mm.

$$\phi = \frac{1}{16}\sqrt{\frac{R}{t}} \tag{7.18}$$

$$\gamma = 1 - 0.901(1 - e^{-\phi}) \tag{7.19}$$

$$\sigma_{cr} = 0.6\gamma\frac{Et}{R} \tag{7.20}$$

With the final thickness obtained, by applying Equation 7.21 the total mass of the spacecraft was found to be 394 kg. In Table 7.40 the dimension properties and the mass of each section can be seen.

$$m_{structure} = 2\pi R t L \rho \tag{7.21}$$

By idealising the structure of each stage to be represented by a single cylinder and assuming that all of the mass of SAURON is uniformly distributed, the structure is over designed. Especially for the hovercraft and orbiter which are found on top of the fist and second stage and do not have to experience all of the loads. It is clear that the first stage has to be stronger that the other since it will have to carry all of the weight of the SAURON.

With the above approaches there were some limitations that were noticed in the model which lead to over design. Strategies to improve this are discussed on the recommendations.

7.5.7. SHIELDING

To assure the integrity of the hover orbiter when it approaches the rings, hovers over them and changes location shielding should be required. Shielding of the spacecraft will assure that all critical subsystem do not get damaged during any encounter with ring particles. In order to size for the shielding of the S/C several parameters should be taken into account. These include the dimensions of possible encounters, their respectful velocities to the S/C and the number of encounters during the lifetime of the S/C.

The first step to the design process is to check whether the skin of the structure of the S/C is adequate enough to withstand any impacts from ring particles and do not fail during the mission. In order to evaluate the performance of the skin Equation 7.22 was used [116]. A value of 3 for the damage parameter was chosen, to prevent incipient spall. In Figure 7.29 the ballistic limit diameter of a ring particle is given for a range of velocities. For a particle moving at a velocity of 2 km/s the S/C can only survive when the particle has a diameter of 0.45 cm or lower. Taken into account that Saturn's ring particles range from 1 cm to a few meters, the skin of the structure might not be sufficient and extra shielding should be added. Though due to the lack of information regarding the exact velocities the hovercraft will face against the particles and their corresponding diameters. little can be said about the required shielding. Further research should be done to quantify the velocities and diameters of ring particles the hovercraft might encounter.

Table 7.39: Cylinder applied loads.

Type of load	Load factor	Limit load
Axial	6	1098975 (N)
Lateral	2	366325 (N)
Bending moment	2	1034420 (Nm)

Table 7.40: Mass of each stage.

	Height [m]	Radius [m]	mass [kg]
Stage 1	1.213	0.91	74
Stage 2	2.1657	1.6	236
Hovercraft	2.935	0.425	52
Main orbiter	1.797	0.425	32
Total	8.1	-	394

Apart from single wall shielding, Whipple shield was considered throughout the design. Though due to lack of time further calculations on the required thickness of each shielding plate was not performed and it is left for future work.

$$d_{cr} = \left(\frac{tBHN^{0.25}(\rho_{shield}/\rho_{particle})^{0.5}}{k0.54(V\cos\theta/c)^{2/3}} \right)^{18/19} \tag{7.22}$$

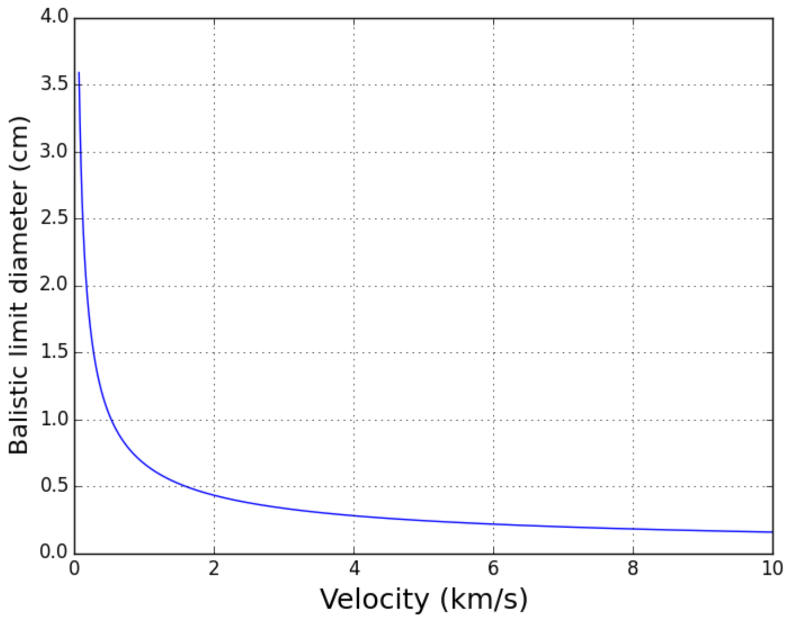

Figure 7.29: Single wall- ballistic limit diameter of particle as a function of its velocity.

7.5.8. RAMS Analysis

The structures of the spacecraft is directly linked to the success of the mission. The spacecraft needs to withstand the loads that it experiences during its lifetime. The choice of aluminium in space applications especially for the primary structure of spacecraft gives a high reliability to the mission [114].

Availability of materials is an important aspect to the structure of the spacecraft. Therefore rare materials should be avoided in the construction of large components. The availability of production methods should also be taken into account when designing certain components. However, since the structure design is not performed in detail this is not taken into account in this report but should be included in the detailed design.

In order to make sure the structure is maintainable after assembly some parts of the structure will have to remain open or be able to open after assembly. This has as an advantage that the subsystems inside the spacecraft are still accessible before launch. In case of a delay, certain components may have to be replaced before the new launch date and must be accessible from the outside.

Safety for the structure subsystem concerns the procedures for manufacturing and assembling the spacecraft. Concerning Aluminium, since it is non-reactive and if it is handled correctly human or safety issues can be limited [32]. Safety procedures for aluminium have widely been used to minimise any risks that might arise.

7.5.9. Verification and Validation

The design of the structure subsystem of the spacecraft was based on two models. One model was used to calculate the centroid of each stage and for the whole spacecraft based on the masses and dimensions of all subsystems and the

[32] http://www.aalco.co.uk/datasheets/Aluminium-Alloy-Material-Safety-Aluminium_251.ashx

second one to calculate the thicknesses for each failure mode. The model for the calculation of centroid was verified with software CATIA. By placing all subsystem with their corresponding masses and dimensions for each stage the centroid was provided from Catia and compared to the one found with the model. The second model was verified by performing the calculations done for the example provided in [79] and comparing with the results, which ended up matching to each other.

Validation procedures would translate to comparing the thicknesses found with ones from existing spacecraft structures. Thicknesses for space missions vary in the range of 0.1 to 10 mm thus validating the final outcome of 4.2 and 2.6 mm.[33]

7.5.10. RECOMMENDATIONS

From the design done so far it can be said that the structure of the spacecraft is over designed and has a high weight. Further analysis can be made that optimises the structure by reducing the thickness and including stiffeners to the design. This can be achieved by splitting the stages into each separate stage and analysing them separately. More accurate analysis can also be performed that use computerised techniques with Finite element method to arrive at the required optimum weight and configuration of the spacecraft.

7.5.11. COST

The estimated cost for the structure of the spacecraft was found to be 69 million euros. The parametric cost estimation process described in Space Mission Analysis and Design was used, which is based on historical data of previous space missions. The cost was found with Equation 7.23, where X represents the mass of each of the structure based on Table 3. The factor 1.0757 correspond to inflation factor to 2017.

$$FY17\$K = (646X^{0.684} + 22.6X)(1.0757) \tag{7.23}$$

7.6. TELECOMMUNICATIONS

This section presents the design of the telecommunications subsystem. It includes the antennas, transceiver units, wave guides and the selection of frequencies and modulation techniques.

The structure of this section follows the general steps that were taken during the design process, which were adapted from SMAD [58].

7.6.1. SYSTEM DESCRIPTION

This subsection presents an overview of the telecommunications subsystem design, in terms of layout and performance. First, the orbiter and hovercraft are addressed, after which the link budgets are discussed. For more details on the individual components, refer to Subsection 7.6.2.

The hardware block diagram for the orbiter is shown in Figure 7.31, presenting the general structure of the telecommunication system.

The performance characteristics of the orbiter telecommunications system can be found in Table 7.43. Estimations were made for cost, power consumption, data rates and communication specifics. The actual link performance is shown in tables Table 7.41 and Table 7.42, for the orbiter-Earth and hovercraft links, respectively. Where applicable, the used assumptions are stated in the 'Remarks' column.

The hardware block diagram of the hovercraft is comparable to that of the orbiter (Figure 7.31). For that reason, no separate diagram is included.

For the inter-satellite link, a Python model was made to estimate the fluctuation in data rate during one synodical period (P_S), enabling assessment of the transmittable data during this period. At the beginning of this time frame, the orbiter and hovercraft are in different orbits but are in opposition; i.e., both are on the same line on the same side of Saturn. During the P_S, the relative angle between the two spacecraft grows and with it also the distance. A sketch of the geometry is given in Figure 7.30. From this image, Subsubsection 7.4.2.4 is derived using the cosine rule:

$$D^2 = R_O^2 + R_H^2 - 2R_O R_H \cos\theta \tag{7.24}$$

Where θ is the relative angle and the other variables as depicted in the image. As data rate is inversely proportional to distance through the link budget, the Python script iterates over θ and calculates the distance and data rate at that point. Additionally, the program calculates the perpendicular distance between the line-of-sight and Saturn's centre of gravity, to check whether the planets eclipses the hovercraft, breaking the link.

7.6.1.1. LINK BUDGETS

The link budget summarises the performance of the telecommunications subsystem design, as it provides estimates for required transmitter power and antenna gain. The required inputs are derived from the requirements on data rates,

[33] https://www.ruag.com/en/products-services/space/satellite-structures-mechanisms-and-mechanical-equipment/satellite-structures/satellite-central-structures

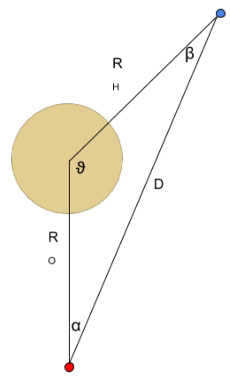

Figure 7.30: Geometry of the planar position of both spacecraft. R_O and R_H are the orbit radii of the orbiter and hovercraft, respectively. The Greek letters indicate the angles as used in the formulae.

ground station compatibility, bit error rate and the mission itself. It allows for quick assessment of the impact on link margin when an input variable is changed.

Since the top-level system design employs two probes at Saturn, link budgets have been made for the inter-satellite link and the orbiter-Earth link, as relaying of data and commands from and to the hovercraft is required for mission completion. Both spacecraft are downlinking science data, receiving commands and sending telemetry data. Additionally, both shall support emergency links in case of tumbling or a large pointing error that prohibits normal linking.

Each of the links poses its own challenges on the communications subsystem design. The inter-probe link is constrained to quasi-omnidirectional antennas to ensure higher availability of the hovercraft and ease requirements on its AOCS subsystem. This comes with a price: its gain is lower - in the order of 5 to 10 dBi [79] - as compared to directional antennas. Together with tighter power requirements, the link data rate is limited although the worst-case distance between the two terminals is approximately 6000 times smaller than the maximum distance between the orbiter and Earth. This leads to the demands on the orbiter-Earth link: a 10 AU distance at conjunction of the planets, high bit rate requirements for science data, and limited spacecraft power all drive the link budget.

Various solutions to these challenges were found in different parts of the link. Optimised encoding techniques like Turbocode allow for coding rates of up to 1/6, thereby reaching a threshold Eb/No ratio of -0.1 dB (see Subsection 7.6.3). This reduced ratio in turn allows for a lower received signal power, thus increasing the space for more bandwidth or reducing transmitter power and antenna dish dimensions. Another way of allowing more data throughput is the use of simple digital modulation techniques, such as binary phase shift keying (BPSK). Although less favourable in terms of signal bandwidth, it provides a lower required Eb/No ratio. At the receiver end during downlinking, the use of NASA's 70-m DSN antennas can provide a gain of up to 74.6 dBi in the X-band and 78.9 dBi when using the 34-m dishes in the K_a-band[34].

7.6.2. Description of Components

This section describes the characteristics of the components that together form the TT&C subsystem. First, the core of the system is addressed. It consists of the transponders, responsible for signal generation, (de)modulation, and de-/encoding. It is followed by a discussion of the transducer (i.e., antenna) unit and the associated RF signal distributor. Lastly, the amplifiers and the C&DH interface are treated.

The system provides two transponders (Xpdr), of which one includes a wide band transmitter to provide high data rates for science downlinking in the Ka-band; the other operates in the X-band. The transponders incorporate transmitting, receiving, ranging, and Doppler tracking. The uplink signal is phase-locked to the downlink to ensure high accuracy ranging and tracking [117].

The antenna unit features a high gain antenna (HGA) for up-/downlinking with Earth, a medium gain antenna for communication with the hovercraft, and a low gain antenna for emergency operations. For calculating the antenna beamwidth of the HGA, which provides the pointing requirement for the AOCS subsystem, Equation 7.25 from Minoli

[34] https://deepspace.jpl.nasa.gov/dsndocs/810-005/, consulted on 19/06/2017.

Table 7.41: Orbiter to Earth downlink budget.

Link element	Value	Unit	Remarks
Tx power	19	dBW	
System loss	-0.9	dB	
Antenna gain	59	dBi	3.7 m parabolic reflector
Pointing loss	-1.0	dB	
EIRP	76.4	dBW	
Space loss	-306	dB	f = 32 GHz, 10 AU
Atmospheric loss	-1.0	dB	
Power Rx Earth	-230	dBW	
Antenna gain	78	dBi	DSN 34-m X-band antenna
Pointing loss	-1.0	dB	
System loss	-3.0	dB	
Rx power	-157	dB	
Noise temperature	28	K	
Noise density	-214	dBW/Hz	
Symbol rate	288	dBKbps	Including FEC
Eb/No	2.90	dB	
Threshold Eb/No	-0.10	dB	BPSK + Turbocode 1/6
Link margin	3.0	dB	

Table 7.42: Hovercraft to orbiter downlink budget.

Link element	Value	Unit	Remarks
Tx power	16.0	dBW	
System loss	-0.9	dB	
Antenna gain	7.0	dBi	LGA
Pointing loss	-1.0	dB	
EIRP	21.1	dBW	
Space loss	-217	dB	0.0016 AU (worst case)
Atmospheric loss	-0.0	dB	Path outside atmosphere
Power Rx Orbiter	-196	dBW	
Antenna gain	25	dBi	MGA
Pointing loss	-1.0	dB	
System loss	-3.0	dB	
Rx power	-175	dB	
Noise temperature	50	K	
Noise density	-212	dBW/Hz	
Symbol rate	33.6	dBKbps	Including FEC
Eb/No	2.90	dB	
Threshold Eb/No	-0.1	dB	BPSK & Turbocode 1/6
Link margin	3.0	dB	

Table 7.43: Top-level performance of the telecommunications subsystem on the orbiter. Note: cost, mass, power, and data rates are estimations.

Parameter	Value	Unit	Remarks
Cost	120	M€	
Mass	120	kg	80 kg orbiter; 40 kg hovercraft
Telemetry rate Orbiter-Earth	48	kbit/s	At Saturn and during conjunction
Telemetry rate Hovercraft-Orbiter	2.27 to 283×10^3	kbit/s	Min and max values, depending on range
DL carrier frequency	32	GHz	Ka band
UL carrier frequency	7.2	GHz	X band
HGA diameter	3.7	m	
Modulation	BPSK	-	
Code rate	1/6	-	Turbocode

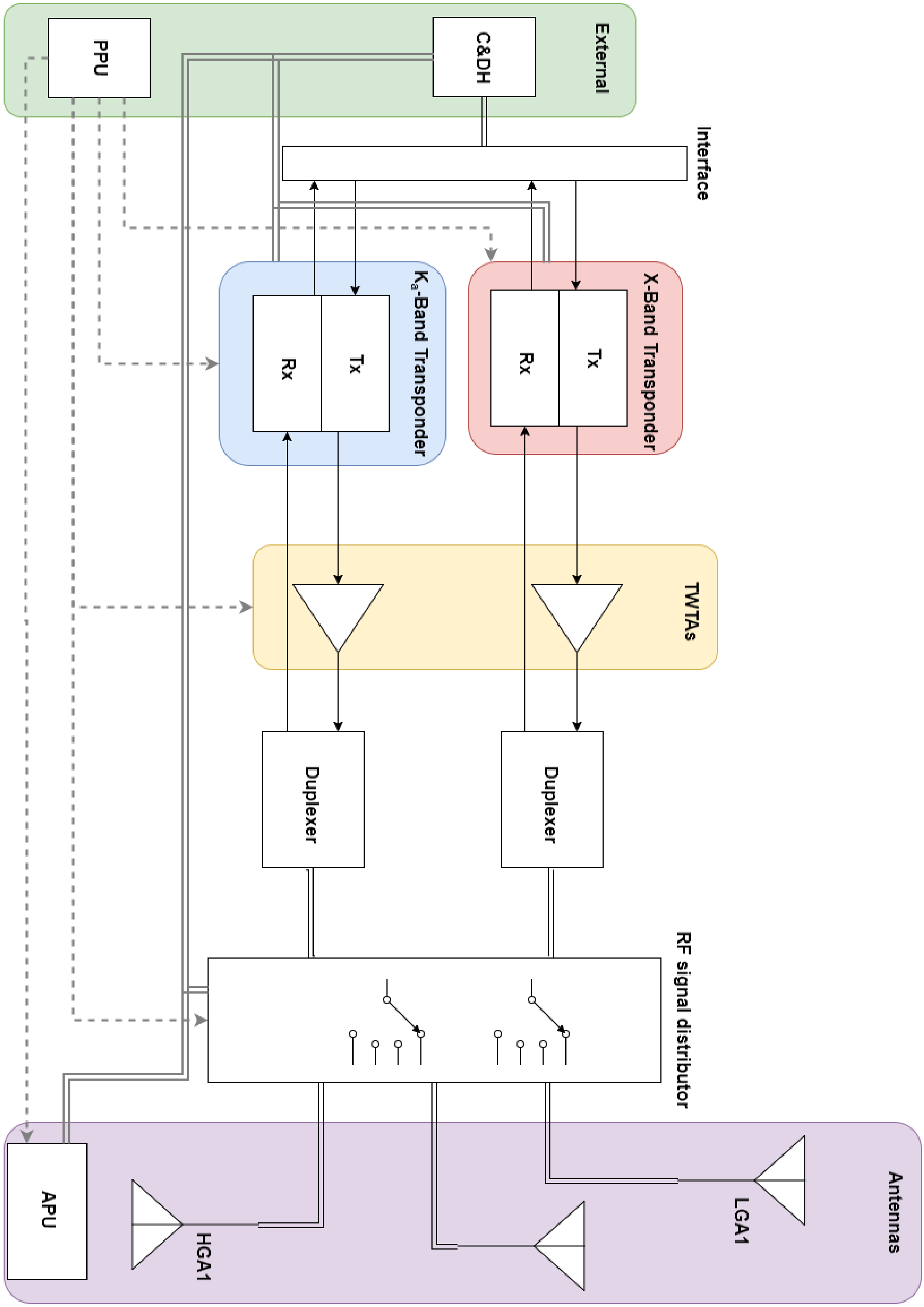

Figure 7.31: Block diagram for the telecommunications system on the orbiter. Single solid lines represent signal flow, double black solid lines represent data buses, double grey solid lines represent status and mode buses, and dashed lines represent power flow.

Table 7.44: Mass breakdown of the telecommunications subsystem on the orbiter.

Element	Units	Input power [W]	Mass [kg]	Remarks/sources
Transponder	2	17 (per unit)	6	[119]
TWTA	2	130 (per unit at maximum output)	5	[120]
Diplexer	2	-	4	[120]
RF distributor	1	-		
Cables	-	-	13	Cassini
HGA	1	-	50	Interpolated from Cassini and Juno missions
MGA	1	-		
LGA	1	-		
Total	**10**	**147**		

Table 7.45: Mass breakdown of the telecommunications subsystem on the hovercraft.

Element	Units	Input power [W]	Mass [kg]	Remarks/sources
Transponder	2	17 (per unit)	6	[119]
TWTA	2	67 (per unit at maximum output)	5	
Diplexer	2	-	4	
RF distributor	1	-		
Cables	-	-	13	Cassini
HGA	0	-	0	No HGA included on hovercraft
MGA	1	-		
LGA	2	-		
Total	**10**	**84**		

[118] was used, valid for circular parabolic reflector dishes:

$$\mathrm{HPBW} = 70\frac{\lambda}{D} \tag{7.25}$$

The gain of a parabolic antenna in the boresight, i.e., at the tip of main lobe, can be described using Equation 7.26 [118]:

$$G = \eta\frac{4\pi}{\lambda^2}A_{dish} = \eta\frac{4\pi}{\lambda^2}\frac{1}{4}\pi D_{dish}^2 = \eta\left(\frac{\pi D_{dish}}{\lambda}\right)^2 \tag{7.26}$$

Equation 7.27 provides the gain in dB:

$$G_{dB} = 10\log_{10}\eta\left(\frac{\pi D}{\lambda}\right)^2 \tag{7.27}$$

In the formulae above, HPBW is the half-power beamwidth in degrees, λ the signal wavelength in meters, D the antenna diameter in meters, G the boresight antenna gain, η the antenna efficiency, and A the antenna area in meters squared.

The HGA is connected to the Antenna Pointing Unit, which provides high-accuracy pointing and stability for the dish during science downlinking. This way, antenna pointing is made partially independent of orbiter attitude, allowing simultaneously transmitting data to Earth and communication with the hovercraft.

The antennas are linked to the rest of the system through the RF signal distributor. It is a network of cables and switches that connect the diplexers to the antennas. There are redundant routes in the distributor to overcome system failures in the case one link in the chain fails (see Subsection 7.6.4).

7.6.2.1. Mass and Power Breakdown

In Table 7.44, the mass and input power of each of the components in the orbiter subsystem are shown. The details for the hovercraft can be found in Table 7.45.

7.6.3. Component Trade-Offs

7.6.3.1. Transponders

The selection of transponders for a satellite is largely determined by the selection of the modulation/coding scheme and the frequency band. The first determines the required Eb/No ratio and bandwidth occupation, whereas the latter

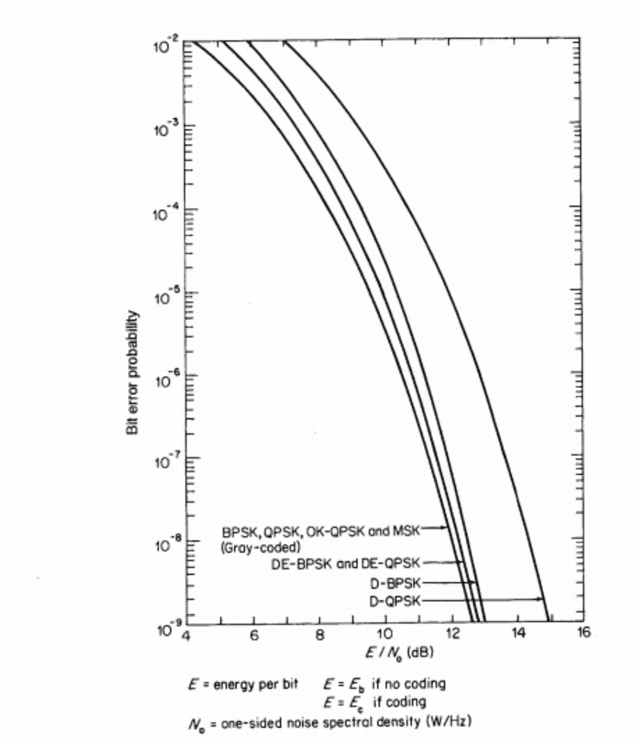

Figure 7.32: Diagram showing the relationship between bit error probability and required Eb/No ratio for BPSK, QPSK, and other digital modulation types.

affects available bandwidth, space loss and atmospheric loss [121].

The combination of modulation and coding technique affects the detectability of the signal at the receiver end. The relationship between these two factors is depicted in Figure 7.32. It can be seen that Binary Phase Shift Keying (BPSK), with an M of $2^1 = 2$, requires a lower Eb/No for the same Bit Error Ratio (BER) compared to Quadrature Phase Shift Keying (QPSK). The latter has 2 bits per symbol, so that $2^2 = 4$ different symbols are obtained. Another gain in the detectability threshold is obtained by using Forward Error Coding (FEC). Efficient coding schemes approach the Shannon limit, which defines the minimum Eb/No for a given BER [117]. In Subsection 7.6.2, it was stated that the transponders will use Turbocode with a coding rate of 1/6, reducing Eb/No threshold to about -0.1 dB, as demonstrated by the Juno spacecraft [120]. This threshold value assumes a BER of 10^{-7} as stipulated by the ITU [122]. The downside of coding rate of 1/6 is that for every bit of information, five extra bits are added to aid in signal detection. This effectively enlarges the data rate by a factor of $\frac{1}{1/6} = 6$, so that less information can be transmitted for a given bandwidth. However, from the link budget calculations it appeared that strong error coding is necessary to overcome the 10 AU distance.

As link data rate is not only restricted by received bit energy, but also by channel bandwidth restrictions, using the Ka-band can improve link throughput by enabling a bandwidth of about 500 MHz as opposed to 50 MHz in the X-band. Edwards and DePaula also mention the high occupation of the X-band, which limits the theoretical bandwidth to an effective 8 MHz [123]. Data rate is linked to bandwidth occupation by Equation 7.28 [124]:

$$B = \frac{R_c}{\Gamma} = \frac{R_c}{\log_2\left(\frac{M}{1+\alpha}\right)} \tag{7.28}$$

Where B is bandwidth in Hz, R_c is the encoded stream data rate in bit/s, M is the number of symbols after encoding, and Γ is the spectral efficiency in bit/s per Hz. From the equation, one can see that bandwidth decreases as more symbols are used during transmission. As BPSK modulation (M = 2) was chosen, a 50 MHz bandwidth would be equivalent to a maximum theoretical data rate of 28.3 Mbit/s using a roll-off factor of 0.35. Using the same values for a 500 MHz bandwidth, one would obtain ten times (283 MBit/s) the data rate.

7.6.3.2. AMPLIFIERS

For the amplification of the transmitter output, the two options that are most commonly applied in spacecraft, were considered: a Solid State Power Amplifier (SSPA) and a Travelling Wave Tube Amplifier (TWTA) [125]. Given the system requirement on mission success, one of the main selection criteria is the reliability of the device. Together with power efficiency and mass, it formed the basis for the amplifier trade-off.

7.6.3.3. SIGNAL TRANSDUCERS

A transducer is used to convert the amplified signal to an electromagnetic wave, for spacecraft usually in the form of an antenna. However, another option has arisen: the use of optical communication links can provide higher data rates compared to radio-frequency (RF) links, as the narrower beam can achieve a higher concentration of radiated beam power [126]. On the other end of the balance, there are the microrad pointing requirements due to the low beam divergence, high losses in the atmosphere due to rain, turbulence and other effects and detection difficulties when pointing to a receiver at a small angle from the Sun [127]. The latter is the case for Saturn-to-Earth pointing, as Earth's orbit is 9 times smaller than Saturn's.

7.6.4. RAMS ANALYSIS

This section addresses the reliability, availability, maintainability and safety of the telecommunications subsystem.

As the telecommunication subsystem is directly responsible for mission success, high reliability of the components is important. The choice of TWT amplifiers over their solid-state variants improves reliability considerably. Another way of ensuring small failure rates is the implementation of space-tested products into the spacecraft.

Availability is another factor highly related to telecommunications. If a communication link cannot be established, no contact is possible between the spacecraft and Earth. For that reason, a high degree of redundancy is added to the system. Multiple transponders, cross-connections and several antennas are included to ensure maximum availability. The low and medium gain antennas provide low data rate access in case of HGA off-pointing or adverse spacecraft attitude during operations like hovering.

In the case of prolonged storage of the spacecraft before launch, the subsystem design allows for quick replacement or maintenance due to its modular design. All components, e.g., amplifiers, transponders and diplexers, can be replaced without the need for replacement of the other components.

Safety of the subsystem is guaranteed as it does not require hazardous liquids, gasses or solids.

7.6.5. VERIFICATION & VALIDATION

The model as described in Subsection 7.6.1 requires verification and validation to be able to use it. This section presents the procedures and results in the V&V process as applied to the model.

7.6.5.1. VERIFICATION

To verify the inter-satellite eclipse model, an extreme case of the problem was examined. It assumes one of the two spacecraft to be at a very large distance from the central body, such that its period is much larger than that of the inner body. This situation is comparable with calculating the solar eclipse by Saturn on the inner spacecraft, and can be quickly calculated by hand to compare with the Python model. A sketch of the case is given in Figure 7.33 and shows that the calculation requires straightforward geometry, as indicated in Equation 7.29:

$$\epsilon = \arcsin \frac{R_{\text{Saturn}}}{R_{\text{S/C}}} \tag{7.29}$$

Where ϵ is the eclipse half-angle in degrees, R_{Saturn} the radius of Saturn in km, and $R_{\text{S/C}}$ the radius of the inner spacecraft's orbit in km. The eclipse time can then be computed by Equation 7.30:

$$T_{\text{Eclipse}} = T_{\text{Orbit}} \frac{2\epsilon}{360} \tag{7.30}$$

In which T_{Eclipse} is the eclipse time in seconds, T_{Orbit} the orbital period of the spacecraft in seconds, and ϵ the eclipse half-angle as computed above. If one computes the eclipse time from this method for a spacecraft orbiting at 130,000 km from the centre of Saturn, an eclipse time of 2.04 hours is found. The program finds a time of 2.03 hours. The discrepancy between the results is likely due to the discretisation used (i.e., the angular step size) and slightly different values for μ_{Saturn} and Saturn's radius. However, the difference is very small and it can be said that the program works as expected.

7.6.5.2. VALIDATION

The next step is to validate the program, i.e., whether it calculates the right times. As it is impossible to get real-life data on eclipse times, a comparable program called Satellite ToolKit (STK) from AGI was used. It uses J4-propagation models to calculate epheremides and is able to calculate access times between two satellites. Using an inner satellite radius of 130,000 km and an outer radius of 140,000 km, the program gave an eclipse time (i.e., time between to successive accesses) of 36 hours and 25 minutes; the Python script returned 37 hours and 15 minutes.

The two values differ with 2.2%. Several reasons can be pointed out that could explain this discrepancy:

- The Python script is based on the assumption that there are no perturbing effects due to the moons, Saturn's oblateness, and third body dynamics. STK does account for those factors as it uses an advanced J4-propagator. Therefore, it is expected that STK's output values are closer to their real-life counterparts.

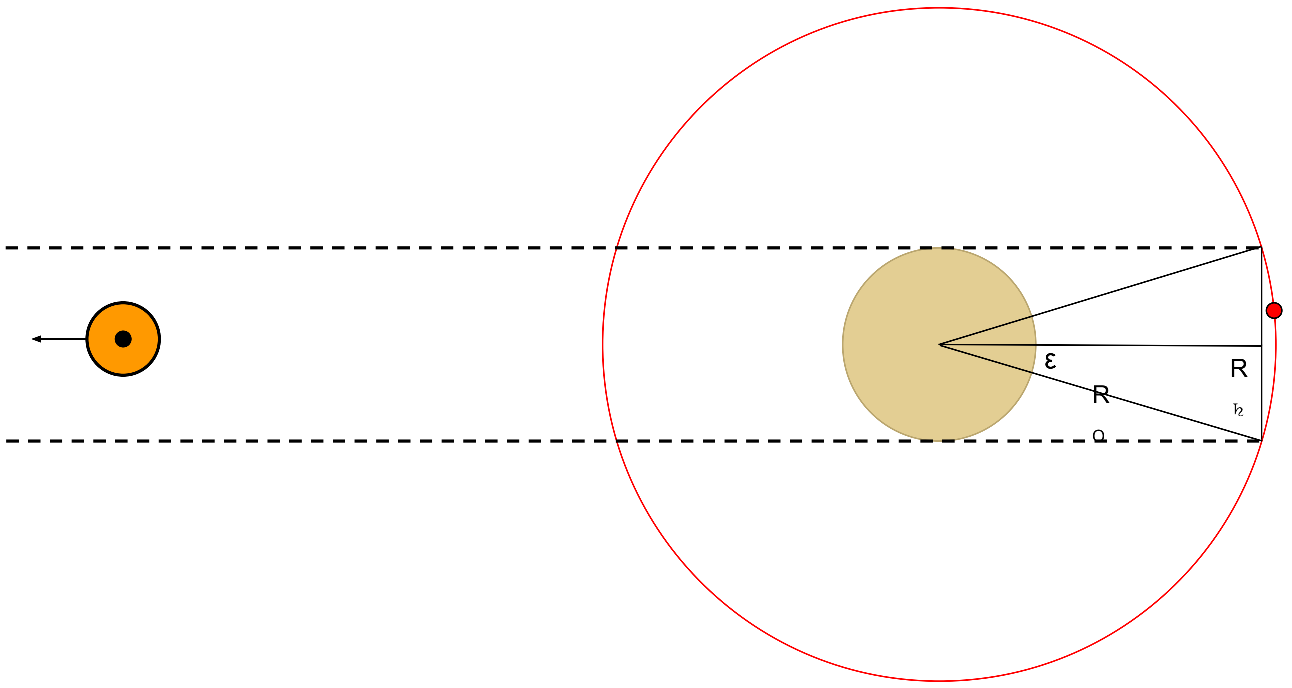

Figure 7.33: Sketch of the situation taken for verification of the eclipse model earlier in this chapter. The outer spacecraft is placed at a very large distance (comparable to that of the Sun) and the eclipse time for the inner spacecraft is then calculated by hand.

- The Python program does not model atmospheric effects which could cause premature link breakage when the line-of-sight is close to tangent to the planet. However, STK uses a model to compute the atmospheric attenuation of the link by examining the received Eb/No ratio and comparing it to the threshold value to see whether the link is possible or not.
- A minor factor is the possible differences in constants used for the computations, such as the gravitational constant, mass of the central body (i.e., Saturn), and the planet's radius.

7.7. Thermal Control

This section will present the thermal control subsystem for the spacecraft. Passive and active techniques will be considered for the thermal control subsystem, but this depends on the thermal environment and temperature distributions.

This chapter will begin with stating the subsystem requirements and operational temperature ranges for the spacecraft. The thermal environment will be determined for the spacecraft. Afterwards, a thermal node model will be presented and explained, including verification and validation. Appropriate thermal control techniques and radiator/heater requirements will be developed based on the results from the thermal node model and the subsystem requirements. A mass, power and cost estimate will be given. Lastly, a RAMS analysis will be done.

7.7.1. Thermal Requirements and Constraints

Determining the thermal requirements is important, because it shows which thermal control techniques can be used to ensure that no components from the spacecraft fail. Table 7.46 and Table 7.47 show the operating and survivability temperature ranges for the spacecraft components and scientific instruments, respectively. The thermal node results in Subsection 7.7.3 need to satisfy these temperature ranges.

7.7.2. Thermal Environment

The thermal environment provides a heat flux input for the spacecraft. This is needed in determining the steady state temperatures in Subsubsection 7.7.3.1 and Figure 7.7.3.1. The thermal environment includes the following:

- Direct solar flux
- Planetary solar reflection due to albedo
- Planetary infrared radiation (IR)
- Heat flux input from spacecraft components

Table 7.46: Operational and survivability temperature ranges for the spacecraft components [79].

Spacecraft Component	Typical Temperature Ranges [° C]	
	Operational	Survival
Bipropellant Mix (Monomethylhydrazine + Nitrogen Tetroxide)	-5-15	-10-20
Lithium Ion Batteries [65]	-10-35	-20-40
Central Computers [77]	20-40	N.A
Hydrazine Fuel Lines and Tanks	15-40	5-50
Star Trackers	0-30	-10-40
Gyroscopes	0-40	-10-50
Reaction Wheels	-10-40	-20-50
Power Box Baseplates	-10-50	-20-60
Command and Data Handling Box Baseplates	-20-60	-40-75
Solar Panels	-150-150	-200-160

Table 7.47: Operational temperature ranges for the scientific instruments.

Scientific Instrument	Operational Temperature Ranges [°C]
Plasma and Energetic Particle Analyser [46]	0-20
Wide Angle Camera [37]	0-20
Narrow Angle Camera [38]	-25-10
Dust Analyser [39]	-15-40

- Solar panel reflection and infrared radiation
- Nearby spacecraft solar reflection and infrared radiation

The effect of nearby spacecraft and solar panels will be minimal, unless they are within a few metres of each other[35]. The orbiting and hovering spacecraft will not induce more reflected or radiated heat unto each other, including the first and second stages.

The input heat fluxes were calculated by adding the contribution of direct solar radiation (Q_{Sun}), reflected solar radiation from the planet (Q_a), emitted planetary IR radiation (Q_{IR}) and heat flux input from the spacecraft components (P_i), taking into account the area of each face (A_i). This can be seen in Equation 7.31 [128].

$$Q_i = Q_s A_i + Q_a i A_i + Q_{IR} A_i + P_i \tag{7.31}$$

The Q_s can be calculated, using Equation 7.32, knowing the solar flux at Saturn (S), the absorptivity (α) of the material, the area of the surface (A_i) and the angle of incidence between that area and the sun (θ) [79].

$$Q_s = S\alpha A_i \cos(\theta) \tag{7.32}$$

The Q_a from each planet can be calculated, using Equation 7.33, knowing the albedo of each planet (a), the area seen from the planet to the surface (A_{p-i}), S and α [79].

$$Q_a = SaF_{p-i}\alpha A_{p-i} \tag{7.33}$$

The Q_{IR} from each planet can be calculated, using Equation 7.34, knowing S, a, F_{p-i}, A_{p-i} and ϵ [79].

$$Q_{IR} = S\frac{1-a}{4}F_{p-i}A_{p-i}\epsilon \tag{7.34}$$

The thermal heat fluxes need to be calculated when the spacecraft is in its hottest and coldest state, because these will give the critical values for checking that all the subsystem requirements are met.

7.7.3. THERMAL NODE ANALYSIS

A thermal node analysis determined the hottest and coldest temperatures, each surface and component would attain. This method involved assigning different faces and components node numbers. Then, measuring the thermal equilibrium of the structure, which provided steady state temperatures.

Steady state analysis involved solving the final equilibrium temperature, assuming the change of temperature over time was negligible. Transient analysis was the opposite. The nodal analysis was done only for the steady state temperatures and not for transient state temperatures, because a small time constant would mean it would take less time

[35] Lemmen, M., private communication, June 22, 2017.

for the temperature to reach its equilibrium temperature. Considering that the transfer time to Venus and Saturn were larger than the time constants, steady state analysis was used [35]. The steady state nodal analysis equation can be found in Equation 7.35 [128].

$$Q_i + \sum_i R_{ij}\sigma(T_i^4 - T_j^4) + \sum_k C_{ij}(T_i - T_j) = 0 \tag{7.35}$$

Equation 7.35 depended on the input heat flux (Q_i), the conductive heat transfer from one node to another node (C_{ij}) and the radiative heat transfer from one node to another node (R_{ij}). Please note that $R_{ij} = R_{ji}$ and $C_{ij} = C_{ji}$. The value for C_{ij} depended on the shape of the node. For example, a flat plate is represented by Equation 7.36 where it depended on the thermal conductivity of the node (k), the base (b), the length (l) and height (d) of the node[35].

$$C_{plate} = k\frac{bd}{l} \tag{7.36}$$

The conductive factor for a circle will also be used. The conductive factor for a circular plate can be seen in Equation 7.37, where the thickness (t) and k are needed[35].

$$C_{circularplate} = \frac{1}{4\pi tk} \tag{7.37}$$

The equation for R_{ij} can be seen in Equation 7.38[36].

$$R_{ij} = \epsilon_i A_i B_{ij} \tag{7.38}$$

The Gebhart factor (B_{ij}) gave a first estimation to the radiative exchange between two surfaces[37].

$$B_{ij} = F_{ij}\epsilon_j + \sum_k (1-\epsilon_k)F_{ik}B_{kj} \tag{7.39}$$

7.7.3.1. COLDEST CASE: APPROACHING SATURN

The assigned nodes for the orbiter and hovercraft can be seen in the legend of Figure 7.34 and Figure 7.35. Node five and six represent a set of components, inside the both satellites, held by two separate aluminium discs.

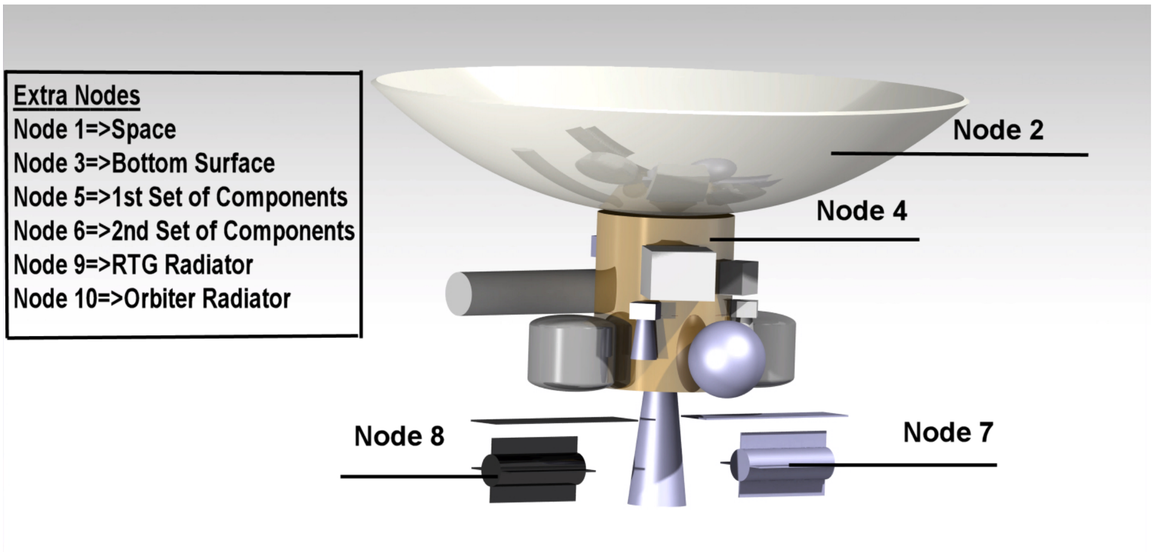

Figure 7.34: Assigned nodes for the orbiter in the cold case

The thermal and material properties for these nodes can be seen in Table 7.48, except for node one.

These will be used as inputs for Equation 7.31 to Equation 7.34 to give the heat fluxes, which can be found in Table 7.49. These will also be used to make the conductive and radiating matrices for both the orbiter and hovering satellite. These matrices were calculated using Equation 7.36 to Equation 7.39 and using the connections based from Figure 7.36. Figure 7.36 shows which nodes have conduction and radiative connections to each other. Figure 7.36 applies to both satellites. This will give the connections to construct the radiative and conduction matrices.

[36] http://www.dspe.nl/knowledge-base/thermomechanics/, consulted on 21/06/2017.
[37] http://www.dspe.nl/knowledge-base/thermomechanics/, consulted on 21/06/2017.

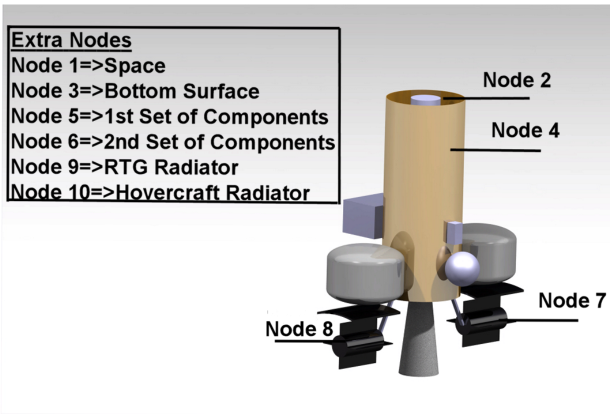

Figure 7.35: Assigned nodes for the hovercraft in the cold case

Table 7.48: Material and thermal properties for each node [129].

Node #	Orbiter					Hovering Satellite				
	Material	ϵ	α	A_i [m^2]	k [$\frac{W}{mK}$]	Material	ϵ	α	A_i [m^2]	k [$\frac{W}{mK}$]
2	Aluminium with white paint	0.85	0.2	0.6	167	Aluminised Kapton	0.8	0.4	0.6	167
3	Aluminised Kapton	0.8	0.4	0.6	167	Aluminised Kapton	0.8	0.4	0.6	167
4	Aluminised Kapton	0.8	0.4	2.9	167	Aluminised Kapton	0.8	0.4	5.9	167
5 & 6	Aluminium	0.6	0.2	0.6	167	Aluminium	0.6	0.2	0.6	167
7 & 8	Curium RTG with Aluminium Kapton covering/shielding	0.8	0.4	0.9	167	Curium RTG with Aluminium Kapton covering/shielding	0.8	0.4	0.8	167
9	Aluminium RTG radiator black	0.9	0.9	0.6	167	Aluminium RTG radiator black	0.9	0.9	0.6	167
10	Aluminium Radiator black	0.9	0.9	0.6	167	Aluminium Radiator black	0.9	0.9	0.6	167

Figure 7.36 shows that all the nodes have a radiative coupling to space. Node four has conduction couplings to every node except node ten. Additionally, node seven and eight have a radiative coupling to node ten. Node two and five have a radiative coupling to each other just like node three to six.

The coldest case will only include an environmental heat input from Q_s. On approach to Saturn, it will be assumed that the effect of Q_a and Q_{IR} will be negligible. This will give the coldest case for the orbiter and the hovering satellite. These values, using Equation 7.32 to Equation 7.34, can be seen in Table 7.49 for each of the nodes except node one, because node one is space. In addition, the P_i can be seen in Table 7.49.

Table 7.49: Heat inputs for each node of the hovering satellite and orbiter at their coldest cases.

Node #	Orbiter					Hovering Satellite				
	Q_s [W]	Q_a [W]	Q_{IR} [W]	P_i [W]	Q_i [W]	Q_s [W]	Q_a [W]	Q_{IR} [W]	P_i [W]	Q_i [W]
2 & 4 & 9 & 10	0	0	0	0	0	0	0	0	0	0
3	3	0	0	0	3	3	0	0	0	3
5	0	0	0	55	55	0	0	0	50	50
6	0	0	0	45	45	0	0	0	50	50
7	0	0	0	4665	2765	0	0	0	100	100
8	0	0	0	5000	5000	0	0	0	3100	3100

Figure 7.37 and Figure 7.38 show the steady state temperatures of each node for the orbiter and hovering satellite, including the nodal heat fluxes. It is imperative that node five and six from each satellite stay around room temperature, because this is where the devices and components will be placed. This is satisfied according to Figure 7.37 and Figure 7.38.

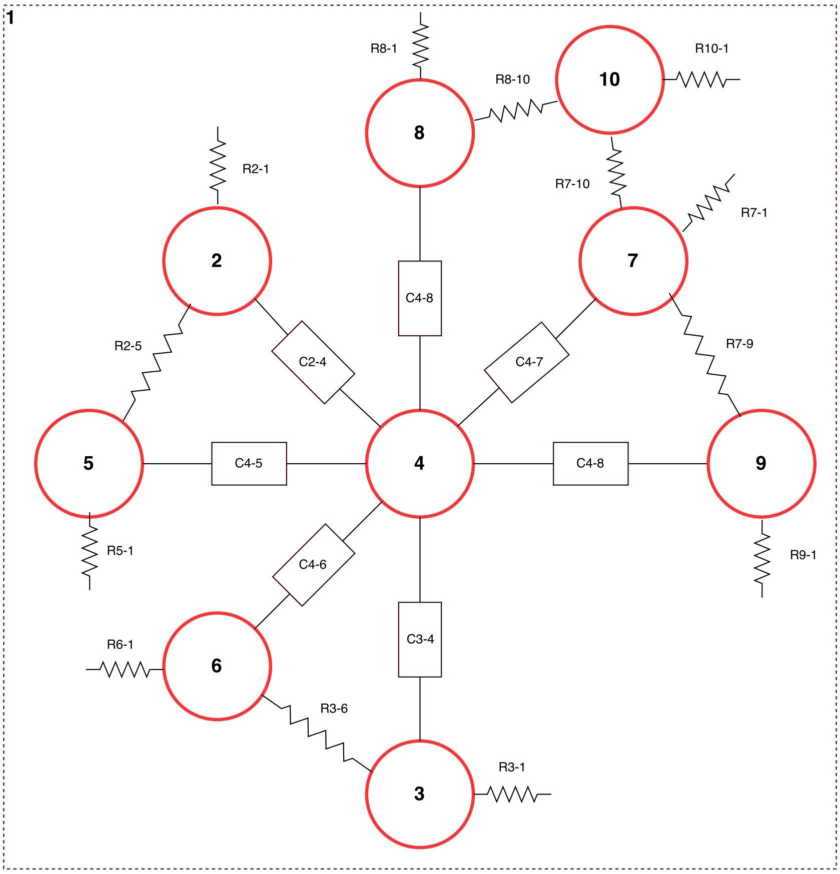

Figure 7.36: Conduction and radiative nodal network of the cold case for the orbiter and hovering satellite.

HOTTEST CASE: AT VENUS

Nodes are assigned to different faces, radiators and the RTGs on the spacecraft. The assigned nodes can be seen in Figure 7.39.

The method for the hot case was the same as was explained for the cold case. However, the input data for these methods differed. The nodal network can be seen in Figure 7.40. The material and thermal properties of the nodes are given in Table 7.50.

Table 7.50: Material and thermal properties for the nodes in the hot case [129].

Node #	Material	ϵ	α	A_i [m^2]	k [W/mK]
2	Aluminium painted white	0.85	0.2	0.6	167
3	Aluminised Kapton	0.8	0.4	2.9	167
4	Aluminised Kapton	0.8	0.4	5.9	167
5	Aluminised Kapton	0.8	0.4	14.9	167
6	Aluminised Kapton	0.8	0.4	4.4	167
7	Solar Panels	0.75	0.75	156	1000
8 & 9	Curium RTG with Aluminised Kapton Covering	0.8	0.4	1.0	167
10 & 11 & 14 & 15	Aluminium Radiator painted black	0.9	0.9	0.6	167
12 & 13	Curium RTG with Aluminised Kapton Covering	0.8	0.4	0.8	167
16 & 17	Aluminium Radiator painted black	0.9	0.9	0.25	167

The different heat flux inputs can be seen in Table 7.51. Due to Venus' albedo of 0.8, the spacecraft receives a noticeable input from Q_a, along with Q_s. This can be seen in Table 7.51.

The steady state temperatures for each node can be seen in Figure 7.41. The figure shows how the orbiter and hovercraft still remain around room temperature, 25°C-35°C. This shows that the electrical components and devices will be able to handle the high heat inputs, when SAURON reaches Saturn.

THERMAL CONTROL TECHNIQUES

From the temperatures derived from the hot and cold case of SAURON, suitable thermal control techniques were identified to suitably handle the thermal environment at Venus, Saturn and throughout the transfer. The surfaces of

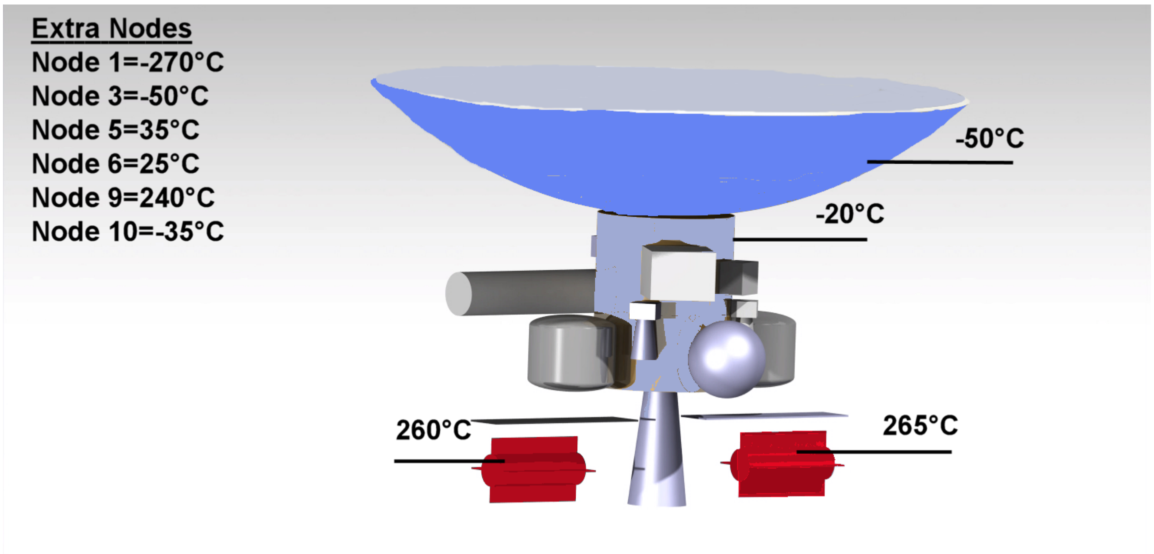

Figure 7.37: Steady state temperatures for the orbiter approaching Saturn

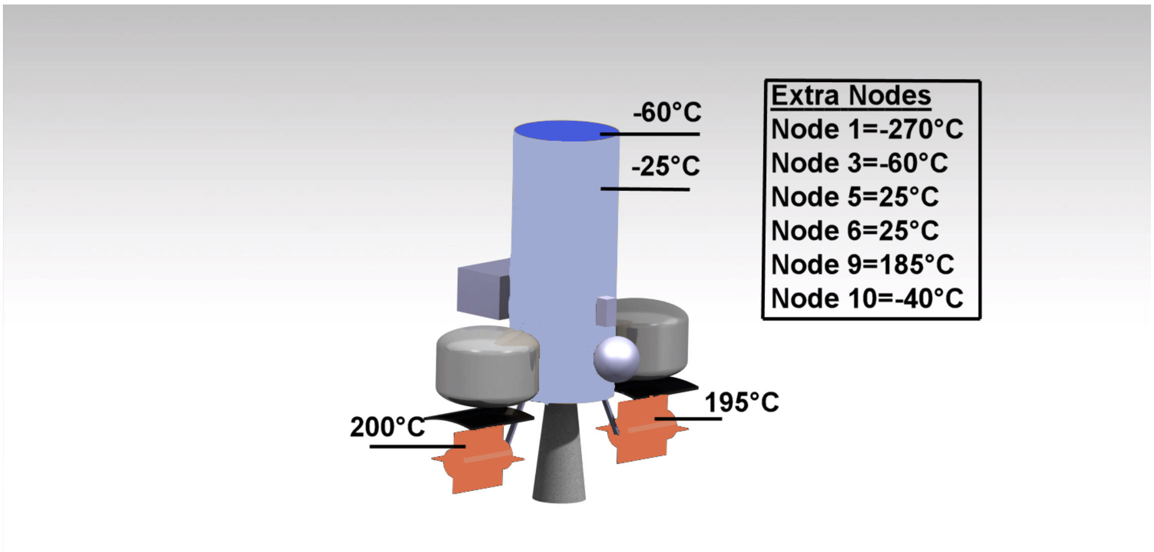

Figure 7.38: Steady state temperatures for the hovercraft approaching Saturn

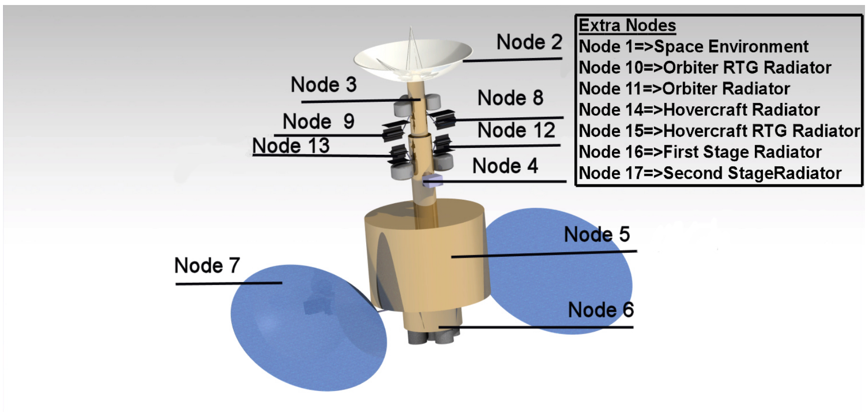

Figure 7.39: Node assignments of the spacecraft for the hot case

the orbiter and hovercraft were covered with 1mm thick aluminised kapton to give ample thermal protection. The antenna of the orbiter was painted white to ensure the satellite and its electronics would not overheat in the event it faced the sun. The surfaces of the first and second stage required 1mm of aluminised kapton.

At the hot case, radiators were needed to help cool the surfaces of the satellite. four 0.75m x 0.75m, one for each stage, were needed to reduce the temperatures of SAURON. Each RTG was also given a 0.75x0.75 m radiator, because

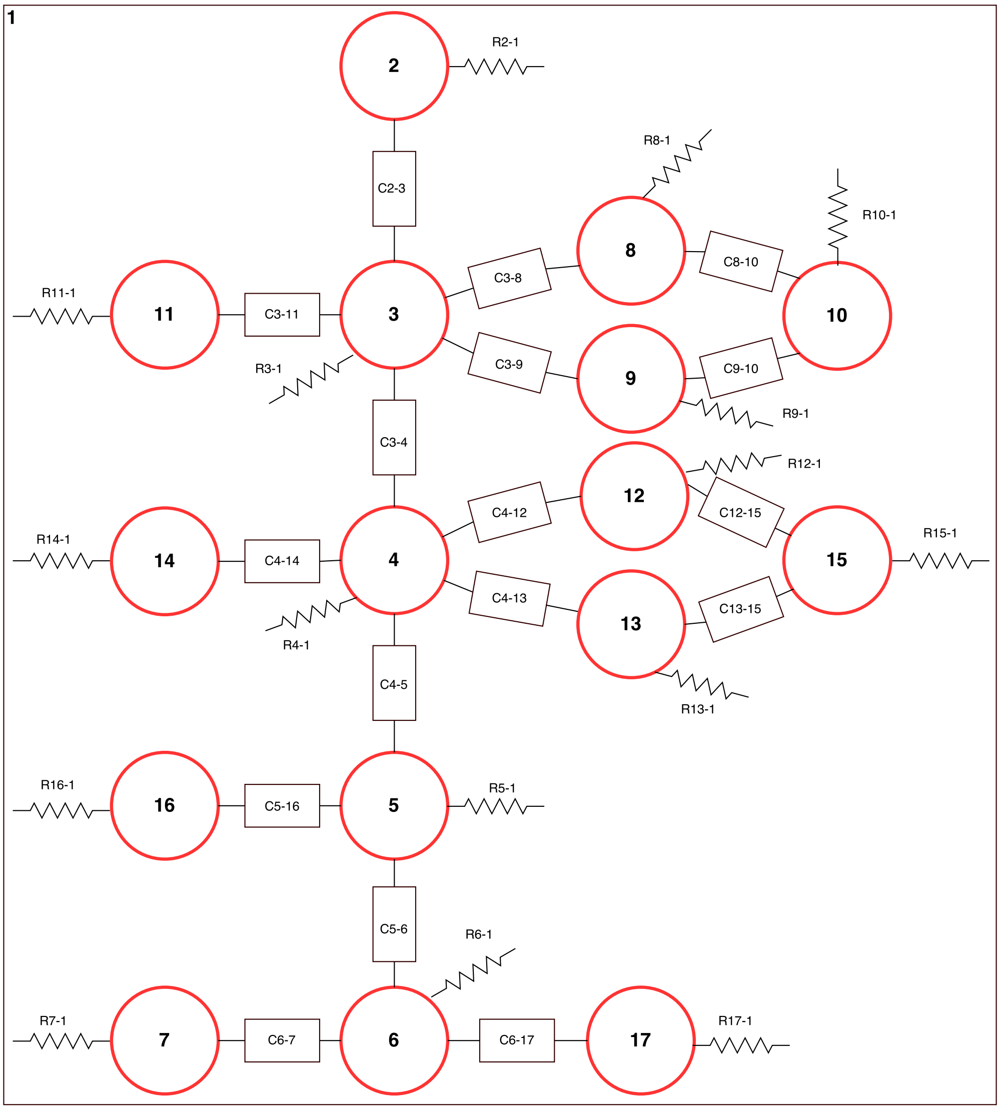

Figure 7.40: The nodal network of the hot case.

Table 7.51: The heat flux inputs of each node from the hot case.

Node #	Q_s [W]	Q_a [W]	Q_{IR} [W]	P_i [W]	Q_i [W]
2	0	175	80	0	255
3	950	180	40	0	1170
4	1965	375	80	0	2420
5	4970	200	945	0	6115
6	1465	60	280	0	1805
7	305838	182658	19571	0	508067
8	0	0	0	5000	5000
9	0	0	0	5000	5000
12	0	0	0	3100	3100
13	0	0	0	3100	3100
10 & 11 & 14 & 15 & 16 % 17	0	0	0	0	0

the Curium RTGs expel a lot of heat radiation, which can heat up the satellite. Therefore, radiators are needed for the RTGs to reduce this.

At the cold case, the radiated RTG heat was used to keep the temperatures of node five and six of the orbiter and hovercraft around room temperature. This will be done by using variance conductance heat pipes that will run along the surfaces of the hovercraft and orbiter. The heat pipes will have grooves and use ammonia as the cooling liquid for the spacecraft. 3.4 m of pipe will be needed to ensure the components in the hovercraft and orbiter remain at room temperature. Most heat pipes have an efficiency of 30% [35] and this was taken into account in determining the heat input for node five and six, as seen in Table 7.49.

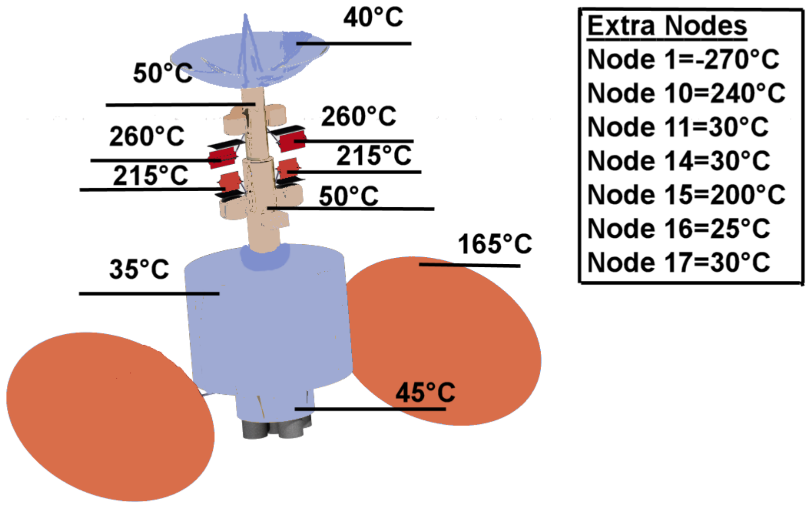

Figure 7.41: Steady state temperatures of the satellite at Venus

7.7.4. VERIFICATION

This section will discuss the verification of the program, results and requirements. To verify the code and the results, the situation where a thin plate was placed between Saturn and the Sun, with the same dimensions and properties as node four from the cold case orbiter, was analysed. This situation will only have a solar power input, 15 W/m^2, and will have a radiative factor of 1.44 W/K. Since, this is a double node thermal model, it can be calculated by hand. If it gives the same result as the code, then the code is verified. In addition, if the steady state temperature is within 5% of the value from node four of the orbiter cold case, then the results can be assumed to be verified and correct. The value was calculated by hand by using Equation 7.40 [79].

$$Q_s + P_i = R\sigma(T_i^4 - T_{space}^4) \tag{7.40}$$

P_i for the case above was equal to the radiative and conduction heat inputs from node four of the orbiter cold case. This value was approximated from the code and was equal to 738 W. Calculating by hand gave a temperature of -20°C, which was identical to T_4 from the orbiter cold case. Therefore, it was verified that the results are correct. The value was also similar to the value calculated by hand, which means that the code was also verified.

It is important to ensure that the thermal requirements stated in Subsection 7.7.2 are met.All the components were verified to be kept in their operational temperature ranges. Nodes 5-6 for the orbiter and hovering satellite in the cold case were given the lowest temperature the components will experience in Figure 7.37 and Figure 7.38. For the cold case, the components were verified to be able to work, because the temperature of node 5-6 for the hovering satellite and the orbiter are around 25°C. All the components can work at this temperature. The only exception are the solar panels, which the orbiter and hovercraft do not have with them.

Figure 7.41 gave larger temperature values that the components needed to endure in nodes 3-6 in the hot case. Knowing that the orbiter was the only stage with lithium ion batteries, node three had a steady state temperature of 50°C, which is out of the battery temperature range. Therefore, extra insulation needs to be wrapped around the batteries to ensure they function properly and do not overheat. The solar panels are within the temperature range.

7.7.5. VALIDATION

To validate the method, the use of an Earth orbit satellite example, provided by Martin Lemmen, will be used. This involves a double node analysis where the first node is space and the second node is the spacecraft. The nodal temperature of the satellite is 30 °C. If the model can emulate this answer to within a 5% margin then, the method can physically represent reality. The inputs for this case are in Table 7.52.

With the input values from Table 7.52, the steady state temperature recorded was 31.2 °C. This is 4% off the real value. Therefore, this model can be concluded to be pseudo-validated.

7.7.6. MASS, POWER AND COST

This section will present the mass, power and costs of the thermal subsystem, for SAURON. These values for SAURON and its separate stages are summarised in Table 7.53. The power used by the thermal subsystem only applies to the cold case near Saturn, because this is the point when the heat pipes are activated to increase the temperature of the components to their operating temperature ranges. The methods to calculating the mass, power and cost will be explained in the next few paragraphs.

Table 7.52: Input values for the validation model.

Input	Value
$S_{Earth_{average}}$ [W/m^2]	890
Power from Earth [W/m^2]	237
$\epsilon_{effective}$	0.098
$\alpha_{effective}$	0.033
A_{i} [m^2]	0.5
Q_{i} [W]	26.3

Table 7.53: Mass, power and cost of the thermal subsystem of SAURON.

Spacecraft Stage	Mass [kg]	Power [W]	Cost [€M]	Comments/Remarks
Orbiter	10	10	9	At hot case the power is 0 W.
Hovering Satellite	20	10	18	At hot case the power is 0 W.
First stage	21	0	19	-
Second stage	6	0	6	-
Total	57	20	52	-

The mass of the thermal subsystem consisted of aluminised kapton for covering the satellite and the addition of heat pipes. The heat pipes have an approximate mass of 0.15 kg/m [79]. The total length of the heat pipes shall be 3.4 m. In addition, the aluminised kapton is also considered part of the thermal subsystem. The total mass of aluminised kapton that will cover the entire spacecraft will make up 99% of the total spacecraft.

For power, the heating pipes will make use of the thermal power radiated from the RTGs. The two RTGs from the orbiter radiate 5000 W of power each, while the hovering satellite's two RTGs radiate 3100 W of power each. The heat pipes will only be needed for the coldest case, therefore no power will be used by the thermal subsystem at the hottest case. To keep the components within their operating ranges at node five and six, for the cold case, 55 W of power needs to be added to node five and 45 W to node six of the orbiter. The hovering satellite requires 50 W of power at these nodes. The radiating heat of two RTGs will be used for heating the spacecraft, therefore the total power needed by the subsystem is 20 W.

The total cost for the thermal control subsystem was calculated using a parametric cost estimation method. The inputs required for this method, were the total mass and power of the thermal subsystem. The method involves the use of Equation 7.41 to estimate the cost [79].

$$\begin{aligned} C_{thermal} &= 63 + 4.2m^2 + 181P^{0.22} \\ C_{thermal} &= €52M \end{aligned} \tag{7.41}$$

7.7.7. RAMS ANALYSIS

The thermal subsystem reliability is key in ensuring all components and work and that the structure of the satellite does not fail. The use of radiators and heat pipes to control the temperatures of the satellite make the thermal subsystem reliable, compared to the use of cryogenic systems and multiple heaters. However, the radiators will remain active when the satellite is in its cold environment. This is undesirable, but will be done, because adjustable radiators which can close themselves are less reliable. This is due to the fact that it has more moving parts and is more prone to damage by space particles.

The availability of the thermal subsystem depends on whether the satellite is in its hot or cold environment. In the hot environment near Venus the radiators will take most effect. In the cold environment the heat pipes will be activated, but the radiators will still be active. The maintainability and safety of the thermal subsystem is good, since it does not use any hazardous material and is straightforward to keep maintained.

8

Performance Analysis

8.1. Sensitivity Analysis

In the detailed design phase, the links between the subsystem and changes in design are very clear. The subsystem that are most dependent on other subsystems are power, propulsion, thermal control and structures. There are some subsystems that have a direct link with each other, i.e. the AOCS with propulsion and payload with data handling.

The goal of this mission is to gather as much scientific data as possible, so that the scientific yield could be as high as possible. Thus, it would be favourable to take as many science instruments as possible. This would have a big influence on the rest of the subsystem as stated previously. To illustrate these changes better a sensitivity analysis is performed on the the most influential changes in design parameters. These are changes in the payload weight, ΔV and power requirements. The changes in ΔV could originate when another interplanetary transfer trajectory would be chosen. This could reduce or increase the total ΔV cost of the mission.

The power requirement is determined on the number of instruments that have to operate at the same time. This requirement is thus sensitive to a change in this number of instruments or to individual increases in power.

The mass contingencies of the subsystems, except the payload, are between 18 and 23% see Table 6.1. So every subsystem can grow with around 20% without increasing the total mass. When giving the payload also a 20% contingency, the total mass will increase from 10846 kg to 11014 kg and 11208 kg for the hovercraft and orbiter, respectively. This is an increase of 1.6% and 3.3%, respectively for the hovercraft and orbiter.

8.2. Sustainability

During the development and production of SAURON certain steps were considered to make the mission sustainable. The three indicators that are considered to measure sustainability were defined in the Project Plan [130], namely environmental, economical and socio-political. Even though quantifying sustainability is difficult, this section will take into account these indicators along with the different phases and steps involved in the design and manufacturing process.

8.2.1. Development phase

The whole idea of launching two spacecraft in one launch for a deep space mission is a new concept that has never been tried before. At the same time, deploying two satellites at the same time is not something new. Spacecraft are piled on top of each other to deploy multiple satellites at once. SAURON will make use of the same mechanism at Saturn.

After deployment the hovercraft will come in close proximity of the rings. Given the time gap between a command to travel from ground to the orbiter and finally to the hovercraft, the hovercraft has to be made autonomous. Use of particle detection and active avoidance has to be incorporated as well. This calls for complex software and hardware development. From a socio-political perspective, various companies across Europe could be employed to perform research, development and conduct testing. This spreads out employment opportunities, this way the tax payers are satisfied as the money they put into ESA goes to widening and expanding their economy[1], but at the same time spreading out resources prolongs the use of electricity, increase in burning of fossil fuels since more people use different means of transport, since the job would be spread across parts would have to be transported from one part to another for production, testing and assembly. Furthermore, SAURON will make use of the Falcon Heavy launcher to lift off, a launcher which its is going to be tested in the summer of 2017. This would be discussed more in Subsection 8.2.4.

[1] http://www.esa.int/Our_Activities/Space_Engineering_Technology/A_solid_investment, consulted on 23.06.2017.

Table D-1 Summary of Accident Source Terms (Page 1 of 2)

Mission Segment	Mission Phase	Source Term Contribution	Initiating Accident Probability[a]	Conditional Probability[b]	Total Probability[c]	Mean Source Term, Ci
Pre-Launch	0	GPHS-RTG	6.7×10^{-5}	7.8×10^{-1}	5.2×10^{-5}	4.68×10^{1}
		LWRHU[(d)]	6.7×10^{-5}	1.6×10^{-1}	1.1×10^{-5}	9.6×10^{-1}
		Combined	6.7×10^{-5}	7.6×10^{-1}	5.1×10^{-5}	4.7010^{1}
Early Launch	1	GPHS-RTG	6.2×10^{-3}	1.1×10^{-1}	6.7×10^{-4}	1.76×10^{2}
		LWRHU	6.2×10^{-3}	2.9×10^{-2}	1.8×10^{-4}	2.12×10^{-1}
		Combined	6.2×10^{-3}	1.1×10^{-1}	6.7×10^{-4}	1.76×10^{2}
Late Launch	3-8	GPHS-RTG	2.1×10^{-2}	1.0×10^{-1}	2.1×10^{-3}	2.61×10^{0}
		LWRHU	2.1×10^{-2}	1.9×10^{-7}	3.9×10^{-9}	1.54×10^{-4}
		Combined	2.1×10^{-2}	1.0×10^{-1}	2.1×10^{-3}	2.61×10^{0}
VVEJGA	-	GPHS-RTG	8.0×10^{-7}	7.9×10^{-1}	6.3×10^{-7}	3.20×10^{4}
		LWRHU	8.0×10^{-7}	1.0×10^{0}	8.0×10^{-7}	6.22×10^{2}
		Combined	8.0×10^{-7}	1.0×10^{0}	8.0×10^{-7}	2.58×10^{4}

a. Initiating accident probability associated with launch-vehicle or space-vehicle related failures.
b. Conditional probability associated with accident environment sequence and fuel release conditions.
c. Product of initiating accident probability and conditional probability.
d. The LWRHU analysis used an earlier estimate of the initiating probability of Phase 0 accidents.

Figure 8.1: A decrease in the probability of accidents of different phases of the mission can be noted [131].

8.2.2. MATERIALS AND MANUFACTURING

As far as the spacecraft are concerned, they are going to be made of aluminium 8090. This is an alloy which mostly consists of Aluminium and Lithium with traces of other elements. It has existed since the 70s and has been used on spacecraft tanks. It makes use of a special technique known as friction stir welding which involves heating the alloy due to friction and then welding it. Quantifying the amount of pollutants that would be produced from production and manufacturing processes is difficult. Furthermore, not much research has been conducted in terms of sustainability in the space industry.

8.2.3. POWER SUBSYSTEM

Even though there was a requirement to limit the use of radioactive elements, it is important for the reader to realise that in a deep space mission such as this one, radioactive elements are unavoidable. There is barely any sunlight available to make use of solar panels to generate power. Added to this is the actual question of solar panels being sustainable or not[2]. Quantifiable data regarding the production of solar panels was difficult to find, however the amount of carbon emissions spent on extraction of ores, to transportation and production of these panels compared to its utility is incomparable. Though usage of the solar electric thrust has allowed the decrease in usage of propellants. Still extra precaution has been taken while using radioactive elements. The spacecraft survives on solar electric propulsion that also contributes to the batteries on board to a certain extent. Furthermore, instead of using Plutonium , Curium is easy to accesses as it is only a product of nuclear reactions at a thermal power plant. Though due to curium's short half life, a larger quantity of it is required aboard the spacecraft.

Radioactive elements do pose a number of threats to humans and thus, all regulations posed by the European Commission on handling of radioactive elements would be followed. The environmental assessment of the Cassini mission report estimated the probability of contamination for various stages. It was found that the probability of an accident occurring within the first few minutes was 1 in 1400, as represented in Figure 8.1. The likelihood of impact only reduced post launch phases [131]. Something similar can be predicted for SAURON.

8.2.4. PROPULSION AND PROPELLANTS

8.2.4.1. LAUNCHER

The advantage of using the Falcon Heavy is that it is being designed to be sustainable. Given the fact that most of the launchers used till date are expendable, SpaceX launchers are designed to recover the first stage. The Falcon Heavy makes use of the liquid oxygen (LOX) and kerosene (RP-1) combination for propulsion, which upon combustion produces carbon-dioxide and carbon-monoxide. Both the oxidiser and the propellant are less toxic compared to other mixtures. Exposure to LOX might cause severe frostbite and that to RP-1 may cause irritation to eyes and skin. Though the consequences are severe if exposure to RP-1 is prolonged [132].

[2] http://news.nationalgeographic.com/news/energy/2014/11/141111-solar-panel-manufacturing-sustainability-ranking/, consulted on 17/06/2017.

8.2.4.2. Spacecraft

On the other hand the spacecraft make use of hydrazine and NTO which are hypergolic propellants and thus need to be stored with extra precaution. The products of these two chemicals upon combustion is carbon-dioxide, carbon-monoxide and nitrogen. NTO is toxic when inhaled and may cause frostbites and burns, however, hydrazine is hazardous to skin, eyes and toxic to kidneys, lungs and nervous system. All steps that are defined by ESA regarding storage, handling and safety of hydrazine will be followed. Employees with experience shall be deployed to supervise all procedures that involve hydrazine. It is due to this reason that a launcher with hydrazine was not taken into consideration. The propellant would only be used in space to perform manoeuvres[132].

8.2.5. Planetary Protection

The spacecraft Cassini found possibilities of prebiotic life on the moons, Titan and Enceladus[3]. SAURON will ensure that it prevents contamination of celestial bodies orbiting Saturn. Both the hovercraft and the orbiter would be disinfected. Landing the hovercraft on a celestial body was considered but was found to be infeasible due to planetary protection laws, given by NASA, which states that the parties involved "shall pursue studies of outer space, including the Moon and other celestial bodies, and conduct exploration of them so as to avoid their harmful contamination and also adverse changes in the environment of the Earth resulting from the introduction of extraterrestrial matter and, where necessary, shall adopt appropriate measures for this purpose" [133].

8.2.6. End-of-life Strategy

One important aspect of the spacecraft's sustainability is its end-of-life strategy. A good, sustainable end-of-life strategy should be carried out in a such a way, that the risk and its effects on the environment, in space, and on the celestial bodies is minimised as much as possible. After assessing the numerous possibilities for end of life, it was decided that the hovercraft would either be left in the rings or in the Cassini division, whereas the orbiter would slowly deorbit into Saturn, like Cassini. To remove the hovercraft out of the rings, extra propellant would be required to provide it the ΔV. Doing so might help in keeping Saturn clean but would directly impact the Earth environment; more propellant would increase the mass which would increase the need for more propellant and perhaps a larger launcher. Lastly, the hovercraft is enabled with low gain antennas, thus if an unforeseen event causes the orbiter to get damaged or once the power production of the hovercraft decreases significantly, the hovercraft could still transmit some data.

The purpose of two spacecraft was to observe Saturn in both close and distant proximity. The orbiter performs observations on the entire body, as a whole. Therefore, even after the hovercraft is dis-functional, the orbiter would still perform and would slowly deorbit into Saturn's dense atmosphere, where it will burn up during entry. This guarantees that no microbes from Earth that may have survived the journey will not contaminate the previously stated moons in the event that the spacecraft somehow collides with them. Furthermore, this end-of-life procedure is already being performed by the spacecraft Cassini. Therefore, reference to how the Cassini spacecraft performs this manoeuvre can be used to speed up the design of this strategy in the future. The end-of-life manoeuvre will involve a series of short period orbits around Saturn until it comes into contact with Saturn's atmosphere.

8.3. Return on Investment

Quantifying the financial return of space exploration is not straightforward. Instead of having a financial figure, the return on space exploration is better expressed in terms of how it has benefited humanity. This effect could also be seen in various sectors. ESA estimates that investing in space industry is boosted by a multiplier: every €1 invested in space returns an average of €6 to the wider economy. Thus space contributes to growth, employment and competitiveness across many economic sectors. ESA also estimates that the revenues are divided in these three types of revenues. 17% of the revenues are direct revenues, these direct revenues represent only the tip of the iceberg of the total financial impact of space on the economy. 47% of the revenues are indirect revenues, the indirect revenues of the space sector include the purchases made by and labour supplied by companies providing input to the space manufacturing and satellite services industry. 36% of the revenues are induced revenues, the induced revenues account for the increased spending that results from the industry's existence; for example, a space engineer's increased spending on goods and services[4]. For the Cassini mission, the investment gave 5000 people employment in the mission development and support employment.

The most important contribution (albeit the hardest to quantify) was to excite and encourage a new generation of young people to pursue careers in science and technology[5].

Determining the return on investment for interplanetary space missions is difficult to express in terms of revenue. Scientific measurements are often made public after a specified amount of time and thus selling them would not be possible. One way to determine the return on the investment is to put a measure to the scientific yield of the mission.

[3] https://saturn.jpl.nasa.gov/mission/grand-finale/overview/, consulted on 13/06/2017.
[4] http://www.esa.int/Our_Activities/Space_Engineering_Technology/A_solid_investment, consulted on 24/06/2017.
[5] http://om-blog.orbitalmaneuvers.com/2014/08/31/the-cost-of-cassini-at-saturn/, consulted on 24/06/2017.

This could be done by seeing if the scientific data could fulfil the following criteria. The more criteria are fulfilled with the scientific data, the higher the scientific return on investment. The criteria are the following [134]:

- Answers fundamental questions in a scientific field. This could further help the understanding of scientific phenomena.
- Leads to discoveries or other advances in knowledge that were not foreseen in the initial project proposal.
- Guidance or insights for design of following missions are provided.
- Demonstrates the applicability and longevity of the data products. These could be measured by, for example, the number of papers authored by scientists outside the missions team and the amount and history of file transfers from the data archives.
- Leads to a number of PhD. thesis or has other substantial training impacts from the results of the mission.
- Stimulates articles in the popular press.
- Shows long-lasting product, e.g., textbook and encyclopedia entries
- Influences social and economic issues that lead to better-informed policies.

9

PRODUCTION, OPERATIONS AND LOGISTICS

Chapter 9 presents production, operation and logistic activities concerned with the SAURON mission. First, the production plan is presented that shows the Manufacturing, Assembly, Integration & Test (MAIT) process. Section 9.2 presents the logistic overview of the mission after which Section 9.3 describes mission operations tasks. The control centre and ground station are described in Section 9.4 and Section 9.5, respectively. Section 9.6 shows the estimated cost for the operations. Finally, Section 9.7, Section 9.8 and Section 9.9 describe the post-DSE activities.

9.1. PRODUCTION PLAN

The production plan presents the outline of activities required to construct the spacecraft system. Figure 9.1 shows the MAIT process organisation. Component manufacturing starts when the detailed design is completed. Once the components are verified, the assembly process initiates. Assembly links components into elements and combines elements for verification and validation purposes. Once the elements or subsystems are established and verified, they get integrated into the system. If possible, validation takes place to validate the user requirements of the system. Figure 9.2 elaborates on the flow of MAIT.

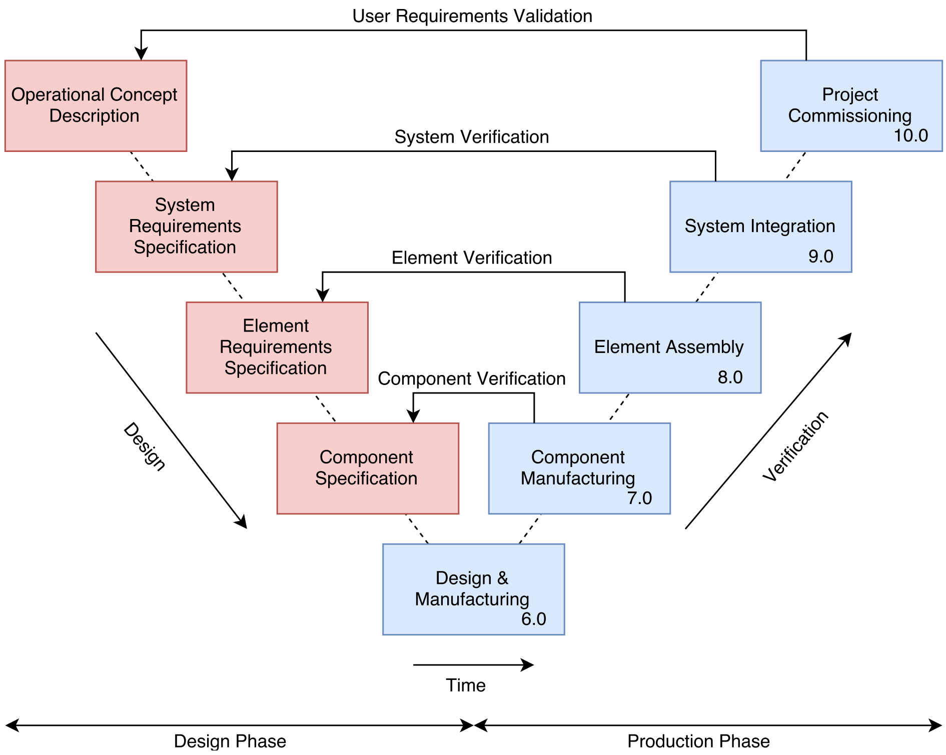

Figure 9.1: MAIT Process Organisation[1].

[1] http://skatelescope.org/aiv/, consulted on 19/06/2017

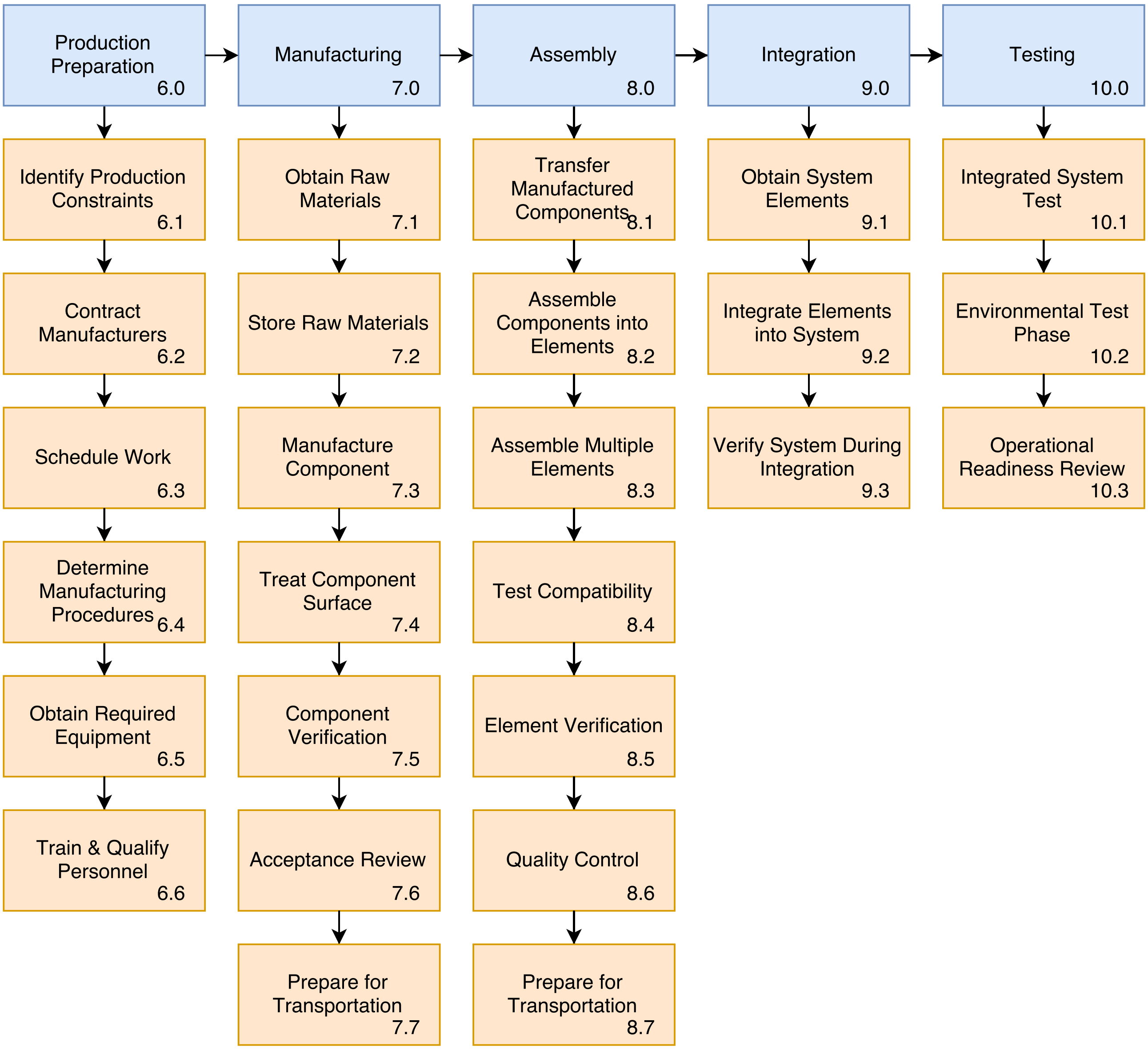

Figure 9.2: MAIT Flow Diagram.

9.1.1. Production Preparation

Before MAIT, the production will have to be prepared. One of the first steps for could be identification of production constraints. Product constraints could be the handling of the RTGs and should be identified in time. If the constraints are not identified, problems could arise later in the MAIT process. The manufacturers of the component hardware and software have to be contracted and the scheduling and procedures have to be established. The production preparation and planning will be performed by the production manager with support from the systems engineers and product assurance engineers. When the procedures and the schedule are established, the required equipment has to be obtained. Finally, the personnel is acquired and trained.

9.1.2. Manufacturing

Manufacturing will construct the small scale parts. The obtaining of raw materials, storage and manufacturing will be performed in an efficient and sustainable way to eliminate waste. Each component will have to be verified. The acceptance review is part of the verification process and insures that the part does not contain errors, is authorised for use and is certificated. Components and elements will be manufactured by companies, universities and research labs. As this is done in different countries, the components have to be transported to a base location for assembly. The base location will probably be an ESA facility.

9.1.3. Assembly

During assembly, the components get linked and connected to create elements. This is done to test compliance of the elements on smaller scale before integration. Compatibility between the elements is tested and the element is verified. The RTGs will be assembled and stored in a facility that is able to handle the hazards of Curium-244.

9.1.4. Integration

During the integration phase, the elements get combined into aggregates until the complete system is built up. Integrating the different elements and aggregates requires verification through analysis and simulations. Using analysis can be practical if simulations are not feasible for the particular aggregate. The RTGs will not be integrated until testing is performed.

9.1.5. Testing

During testing, exact definitions of the number of tests and required data has to be determined. Using the planned facilities, the complete spacecraft will be tested through an Integrated System Test (IST). The IST tests the spacecraft at each operational mode. Redundancy and transitioning between operational states is included. The IST is performed in such a way that it resembles the spacecraft mission as accurately as possible. Therefore, the mission sequence will also be followed from launch till hover orbit. After the IST, an Environmental Test Phase (ETP) will take place where system performance is demonstrated during flight conditions. This is the final validation of the system which will use models based on tests and analyses. During ETP, material defects are identified through tests and the data is collected. The data can be used by the ground segment as reference data during the mission [135]. The RTGs are separately transported to a facility where it is integrated and tested. Once tested, it is disassembled and brought back to the storage facility.

9.1.6. MAIT Cost

The MAIT cost is based on the cost of the subsystems and payload. SMAD estimates 13.9 % of the subsystems and payload cost for production cost of small satellites [58]. As the spacecraft to be built will not be small, the estimate of 13.9 % could deviate from actual production costs. It is expected that the production costs will be higher since both an orbiter and hovercraft have to be constructed. Therefore a margin of 50 % was taken into account, estimating the production cost to be 20.9 % of the subsystems and payload. This equals to approximately €123 million.

9.2. Logistic Overview of Mission

This section describes the logistic overview of the mission. The pre-launch, launch and post-launch logistic phases are described.

9.2.1. Pre-Launch

The spacecraft is planned for launch on 12 June 2024 at Cape Canaveral due to requiring the Falcon Heavy launch vehicle. Completion of spacecraft assembly is planned for 12 June 2023, one year before the launch date. The SAURON spacecraft assembly and integration is approximated to take less than 9 months, since Cassini assembly took 9 months. Assembly and integration of the subsystem hardware and software onto the spacecraft framework is planned to start on 1 September 2022 in an ESA facility. Before this date, the separate subsystems and other components will have to be manufactured and assembled by the contracted companies. Components such as sensors and actuators, required to build the subsystem, will be acquired from a single company and transported to a company that will be responsible for the complete subsystem. Most of the suppliers will be be situated in Europe to maximise sustainability. Components unavailable in Europe will be transported to Europe.

Assembly starts with wires and connectors to create a framework for testing procedures. First, subsystems are integrated into the framework, after which the payload instruments are installed. The power subsystem will require the RTGs to be transported from the storage facility to the assembly facility. This will be done in a later stage when most of the subsystems are implemented. Once RTG integration and testing is completed, they are transported back to the storage facility and will be integrated prior to launch at the launch complex. When the complete spacecraft is assembled and integrated, ISTs on, for example, acoustics, vibrations and thermal performance are performed. After testing validates the system, a plane will transport the spacecraft to the Cape Canaveral launch complex. Prior to launch, the launch vehicle has to be transported to the launch pad. The RTGs will be integrated in the spacecraft and the payload will be integrated to the launch vehicle. At the launch site, checkouts and processing take place to ensure validation of the complete system. System testing to ensure requirement validation, interface validation, cable connecting, instrument validation and propellant loading are some examples of the performed activities. Regular checkouts are planned to assure that everything follows the procedure. In case of a launch delay, the propellant of the SRO will be removed after which the SRO is put into storage. Instrument maintenance and software upgrades are performed when the SRO is kept into storage.

9.2.2. Launch & Early Orbit Phase

The launch and early orbit phase starts with launch support 8 hours before the launch [65]. A final readiness test, data flow tests and data confidence tests are performed to verify the ground system and its network. Approximately an hour after launch, the spacecraft will detach from the launch vehicle. The spacecraft will point to the Sun and deploy its solar arrays. The radio-frequency contact with the ground station is configured for the control centre to take control of the spacecraft. Additionally, the AOCS and data handling system is configured. The operations for the early orbit phase will be conducted by ESTRACK Control Centre. The team controls the ground network and communication network. The flight dynamics team will have to analyse the dynamic behaviour of the spacecraft, respond if anomalies cause problems and generate commands for the AOCS. Regarding the anomalies, a project support team is situated in the control centre in which experts on the subsystems of the spacecraft can communicate with the flight dynamics team.

9.2.3. In-Orbit Test Phase

The main focus of this phase is activating and checking the payload, calibrating the instruments and verifying if the system performs as expected. Additional AOCS operations will be performed in case trajectory corrections are required. All the subsystems will be tested for their performance. Moreover, it is checked if the payload interferes with the subsystems. The payload instruments are tested in their operational modes to collect their performance data. The scientists verify if the data is correct and advise if calibrations events are required. Power-up sequences will only be performed when ground coverage is available to control and monitor the spacecraft in case a power-up sequence fails.

9.3. Mission Operations Tasks

There are several tasks associated with mission operations. This section describes the main tasks.

9.3.1. Spacecraft Monitoring

The spacecraft monitoring team receives the telemetry data. The team is responsible for processing the data, displaying it for the flight controllers and encoding telecommands to send out. Analysis of the data allows for trend determination to monitor the health of the spacecraft. The processed data is passed on to the navigation and flight dynamics team.

9.3.2. Anomaly Handling

Anomaly handling is performed by the control team. The team presents an anomaly report that describes the errors of the ground segment, the spacecraft and the payload [65]. If the anomaly poses a threat to the system, a detailed investigation is required. The investigation will be presented in a report where proposals are discussed on how to deal with the anomaly. The operations manager stores the reports in the database to make it accessible for the project teams.

9.3.3. Data Acquisition & Distribution

Telemetry data, auxiliary data and catalogues are stored at the control centre in a data disposition system. Auxiliary data contains information about the science data, mission planning and command requests. The catalogues contain all the data sets with the corresponding time period. To deliver the data to the disposition system, the details, status, identification status and data have to be supplied. The data can be accessed at the control centre where it is available for at least the complete duration of the mission. If access from other locations is required, the data will have to be transferred where network functions and protocols are required [65]. If the data is required at the user centre, the data has to be requested from the control centre. The requests have to be approved, authenticated and authorised to give data accessibility to the user centre. An area within the control centre will be available where requests for payload commands take place. The gathered scientific data will be analysed by scientists at the European Space Astronomy Centre (ESAC).

9.3.4. Navigation & Flight Dynamics

Monitoring the spacecraft attitude requires analysis of the data from the sensors described in the ADCS design, Subsection 7.1.5. The attitude data allows to monitor and control the ADCS. Orbit determination is done by analysing the radio signals transmitted between spacecraft and ESTRACK antennae. The Doppler shift data will aid in calculating the current and expected trajectory. Star sensors aid in performing manoeuvres at Saturn as comparing taken images can yield accurate position and velocity estimates. If the current trajectory deviates too much from the required trajectory, TCMs will be planned and executed to correct the trajectory. The flight dynamics team will perform calculations on contact periods, eclipses, positions, velocities and fuel consumption to determine spacecraft operations.

9.4. Control Centre

The European Space Operations Centre (ESOC), located in Darmstadt, Germany, will conduct the operations to control and monitor the spacecraft during its mission. ESOC contains workstations with screens to display relevant information. Besides the room that monitors and control the spacecraft, other rooms are required for the flight dynamics team and ground network control team. Additionally, a separate room exists for configuration and handling of the computer systems.

9.4.1. ESOC CONTROL TEAM STRUCTURE

Figure 9.3 shows the structure of the mission control team of ESOC. The flight operations director is the team leader. The operations support team, ground operations manager, flight dynamics coordinator and spacecraft operations manager all report to the flight operations director. ESOC personnel works in a certain team on a certain task, such as orbit determination & prediction. The orbit determination & prediction team reports to the flight dynamics coordinator as seen in the figure. There is communication between the managers to exchange information between the departments. The spacecraft operations manager is additionally in contact with the spacecraft support team which is not ESOC personnel. This personnel is from the industry and could contain additional information about the subsystem required for the ESOC personnel.

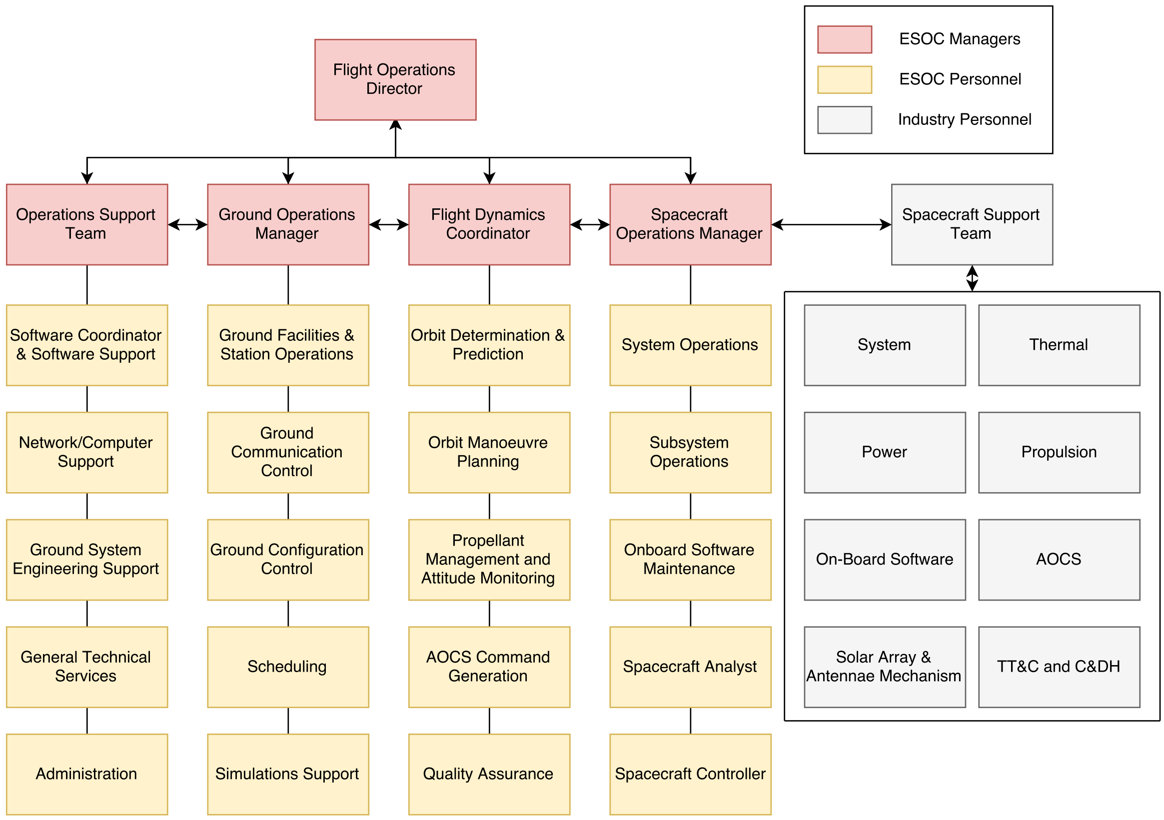

Figure 9.3: ESOC Control Team Structure [65] (Source: ESA).

9.4.2. HARDWARE COMPONENTS

ESOC makes use of a computer backbone to which individual computers are connected. These individual computers are each tailored specifically to the need of their user, to optimise computing power. The experts involved in the mission communicate using a voice conferencing system, which can include both internal and external experts. Human spaceflight missions also often include video systems and an older version is used for unmanned missions. Each of these facilities is powered from a set of batteries, which enables the system to bridge short power outages. If an interruption does occur a diesel-powered generator will take over the power supply. ESOC is guarded by fingerprint scanners and guard personnel, as well as firewalls and proxy systems to protect the operations and systems from people trying to harm it.

9.4.3. SOFTWARE COMPONENTS

The control centre uses specialised software to support its operations. The telemetry and command system is used for satellite monitoring and control. It alarms users when telemetry requirements are violated and manages, displays and sends commands to the spacecraft. The Data Display System ensures that an intuitive user interface is present to manage the telemetry and command data.

Mission planning also has its own dedicated software, allowing for both manual and automatic planning through graphical editors.

The last set of software are the operations support tools. These include time displays, maps showing the current orbital position and the project documentation.

9.5. GROUND STATION NETWORK

The ground station is responsible for the communications between the spacecraft and the operations control centre. ESA has erected three deep-space antennas (DSA) at locations separated 120° in longitude, providing all-day coverage to deep-space probes[2]. Thus, at least one of the three antennas is always visible. DSA-1 (New Norcia, Australia) supports communication in the S and X bands, DSA-2 (Cebreros, Spain) supports X and Ka bands, and DSA-3 also supports X and Ka bands [136]. According to ESA, "there are plans to upgrade the station for data reception in the Ka-band (32 GHz)[3], enabling SAURON to transmit science data to this station as it will exploit the Ka band for this link.

Several operations are followed during a ground station flyover. The ground station receives a scheduled entry from the control centre indicating the mission, the required antenna, and the time the antenna is required for. Before the flyover, the systems are configured with the current orbit data. A data flow test is conducted where simulated telemetry data is used to test the receive function of the station [65]. A command test follows to verify the uplink. If verification is completed, the antenna is pointed to the required direction to start the communication process. During the flyover, the link with the spacecraft is established. The received data about payload and navigation is stored in the ground station and distributed to the control centre. After the flyover, the data is further processed. A 'post-pass' report will describe flyover and address anomalies [65].

9.6. OPERATIONS COST ESTIMATION

For cost estimation of the operations, equations from the Mission Operations Cost Estimation Tool (MOCET) were used. The model is developed by The Aerospace Corporation in cooperation with NASA its science office for mission assessment. The model is based on regression analysis. It was validated by comparing model operations cost to actual operations cost for 44 planetary & near-Earth missions. The standard deviation for planetary missions was found to be 25 %.

Table 9.1 contains the relevant parameters of the cost estimation model for mission operations. Y gives the average monthly cost for the phase in million dollars of the fiscal year 2013. The transfer takes 125 months, total insertion and pumpdown will take 42 months approximately and the orbital operations, during which the main measurements at Saturn are taken, will take 12 months for the orbiter and 1 month for the hovercraft. Additionally, a one year mission extension was analysed for the operational costs. The dollars of the fiscal year 2013 were converted to the euro of 2013 with a ratio of 1.33, after which inflation was accounted for with a ratio of 1.0227 for the euro between April 2013 and April 2017[4]. The results of the equations was multiplied by the number of months to get the total cost for each phase. Table 9.2 shows the costs for the phases and the total cost of the mission operations.

The definition and selection of the parameters is seen in Table 9.3. NASA describes a flagship mission class as having an assigned budget of more then 800 million dollars[5]. During the transfer, checkouts will be performed on the spacecraft, which increase the cost for the transfer. Quiescent operations are going to take place, which implies that during the transfer the operations will not be intensive for the complete duration of the phase. During quiescent operations it still is possible to access spacecraft health. Months of insertion & approach is described as months of approach, orbit insertion and orbit reduction in the MOCET. This equation will be used to estimate pumpdown aswell, since pumpdown is similar to insertion in terms of operations. The pumpdown phase takes approximately 3 to 3.5 years. Using 42 as selected number for months yields an invalid result for the insertion & pumpdown phase as 'Mo' is an exponent in the equation. This is due to the lack of a specific equation for pumpdown in MOCET. Approach and SOI would take less than a month. In context of the equation, the assumption was made that selecting 1 for months of insertion and approach would give the most reliable cost estimate, for the operational cost during insertion and pumpdown. The result of the equation is then multiplied by 42 months, the approximate duration of the pumpdown, to yield an accurate estimate. An other assumption that was made is the number for the orbiting body. The Aerospace Corporation cost model symposium sheets provided the options seen in Table 9.3. Saturn orbit operations are expected to be similar as Mars orbit operations. However, as hovering has to performed and communication has to occur between the spacecraft, orbital operations will be more complex. An exponent of 6 was assumed to be the best choice for orbiting body. Selecting 4 or 8 for this exponent would change the cost at maximum €10 million. The hovercraft will carry eight instruments and the orbiter four instruments. The mission of the orbiter could be extended. For prime mission average monthly cost in the mission extension phase, the equation result of the orbital operations for the orbiter was used. A single mission extension was used as input.

[2] http://www.esa.int/Our_Activities/Operations/Estrack/Estrack_ground_stations, consulted on 21/06/2017.
[3] http://www.esa.int/Our_Activities/Operations/Estrack/New_Norcia_-_DSA_1, consulted on 21/06/2017.
[4] https://www.statbureau.org/en/eurozone/inflation-calculators?dateBack=2013-4-1&dateTo=2017-4-1&amount=1000, consulted on 20/06/2017.
[5] https://www.nasa.gov/sites/default/files/files/20_MOCET_NASA_Cost_Symposium_Briefing_2015-08-21.pdf, consulted on 21/06/2017.

Table 9.1: Relevant Parameters for Cost Estimation of the Mission Operations.

Phase	Equation	Months	Inputs	SEE	Y
Transfer	$Y = 1.2869^{MC}2.7334^{CO}0.6501^{Q}$	125	MC, CO, Q	31.9 %	3.787
Insertion & Approach	$Y = 1.3111^{MC}1.0914^{Mo}$	42	MC, Mo	16.2 %	2.460
Orbital Operations Hovercraft	$Y = 1.1072^{MC}1.1420^{OB}1.0455^{NI}$	1	MC, OB, NI	26.4 %	4.297
Orbital Operations Orbiter	$Y = 1.1072^{MC}1.1420^{OB}1.0455^{NI}$	12	MC, OB, NI	26.4 %	3.760
Mission Extension	$Y = P(-0.236 \cdot ln(N) + 0.8443)$	12	P, N	7.2 %	3.174

Table 9.2: Total Operations Cost For Each Phase.

Phase	Cost [Million €]
Transfer	364
SOI/Pumpdown	79
Orbital Operations Hovercraft	3
Orbital Operations	35
Mission Extension for 1 Year	38
Total Cost Without Mission Extension	481
Total Cost with Mission Extension	519

Table 9.3: Operations Cost Model Input Selection.

Input	Definition	Options	Selected
MC	Mission Class	1 Medium, 2 Large, 3 Flagship	3
CO	Checkout Operations	0 No, 1 Yes	1
Q	Quiescent Operations	0 No, 1 Yes	1
Mo	Months of Insertion/Approach	1 to N	1
OB	Orbiting Body	1 Moon, 2 Asteroid, 3 Mercury, 4 Mars	6
NI	Number of Instruments	1 to N	8, 5
P	Prime Mission Average Monthly Cost	-	3.760
N	Number of Mission Extensions	1 to N	1

9.7. PROJECT DESIGN & DEVELOPMENT LOGIC

Figure 9.4 shows the logical order of activities that will be performed for the project after DSE completion. More information on the general activities during the phases can be accessed in ECSS-M-ST-10C [137]. An explanation of the phases is presented in Section 9.8.

9.8. PROJECT WORK BREAKDOWN STRUCTURE

To determine all the tasks that are required for the post-DSE design phase a work breakdown structure is created. The workpackages are grouped into 7 different phases. The work breakdown structure can be seen in Figure 9.5

Phase 0 is the first phase and only consists of analysis of the concepts like the one made during the DSE.

Phase A is the feasibility phase. During this phase the mission and the spacecraft requirements are analysed. Also a functional analysis on the total mission is performed and critical technologies, which require development, are identified.

In phase B the preliminary definition of the design is made. Each concept will be investigated based on their functions, interfaces and architecture, and finally a trade off will be made.

Phase C is the phase in which the complete detailed design is made. The design is verified and validated and the final design is prepared for manufacturing, testing and assembly.

In phase D the final design is made. Selected instruments and interfaces are tested, components are manufactured and the complete spacecraft is assembled and prepared for launch.

In phases E and F the mission and the end of life of the spacecraft are described. Each mission phase is also described in the functional flow and functional breakdown in Chapter 4 and will therefore not be elaborated further.

9.9. PROJECT GANTT CHART

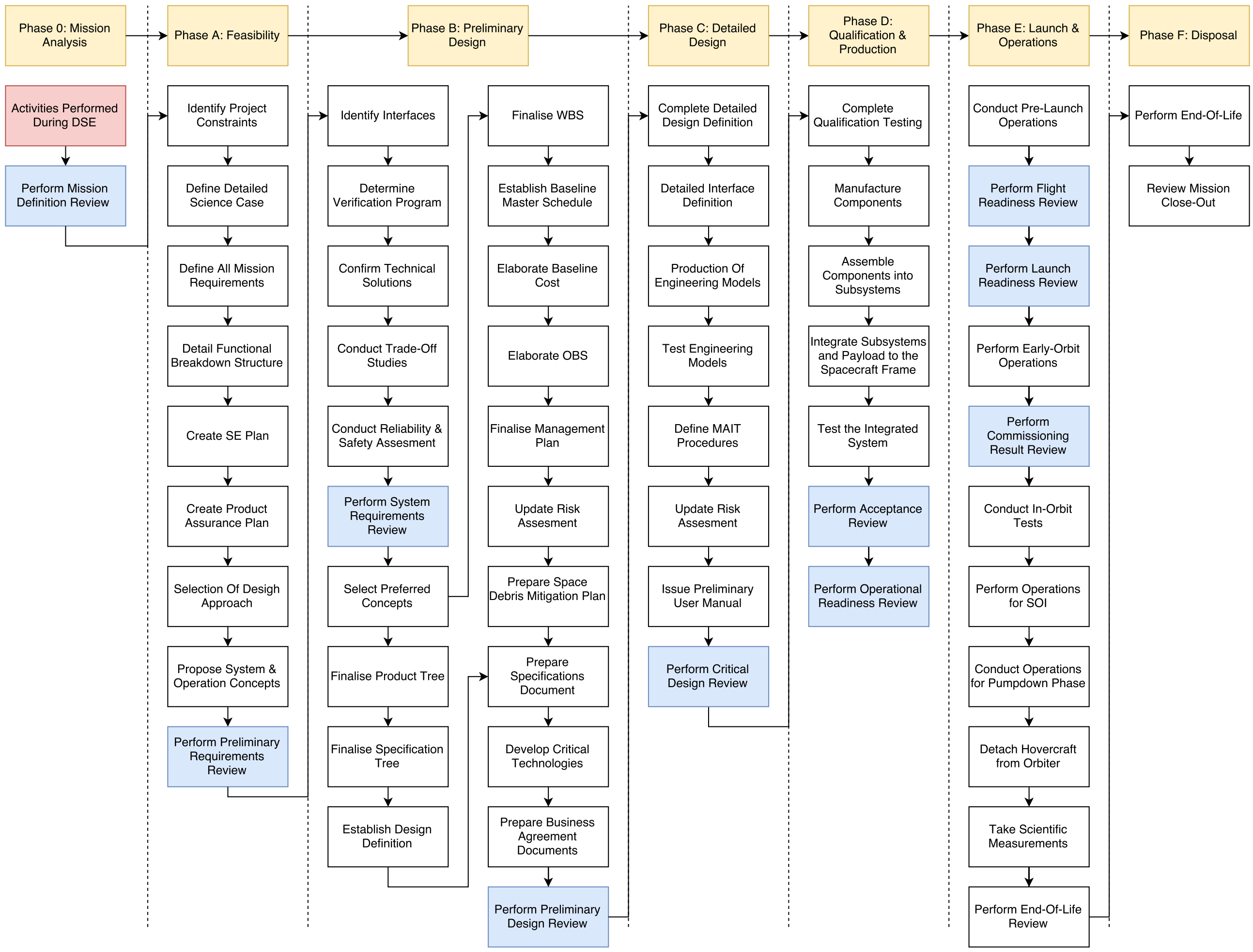

Figure 9.4: Post-DSE PDD.

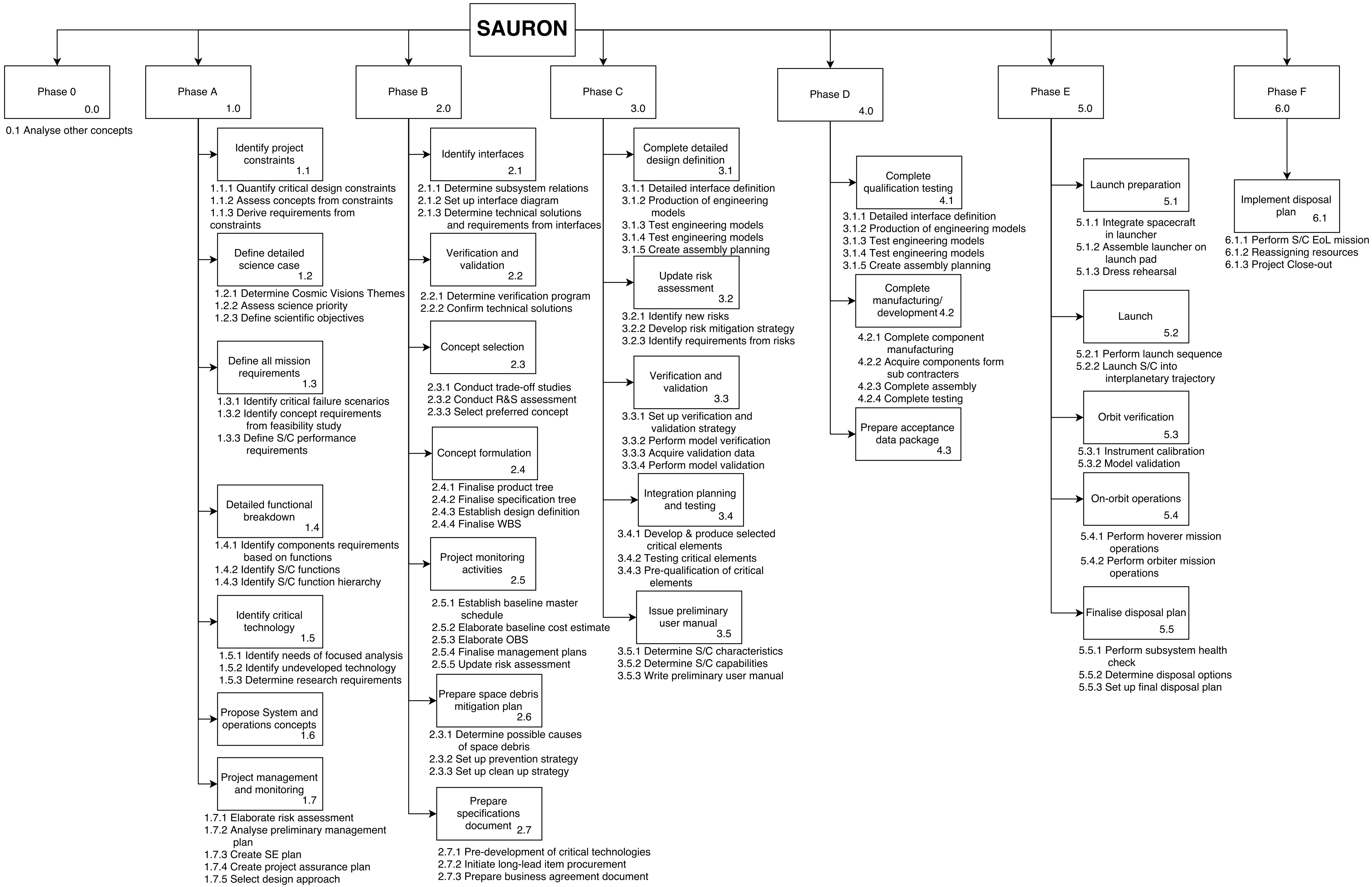

Figure 9.5: Post-DSE work breakdown structure.

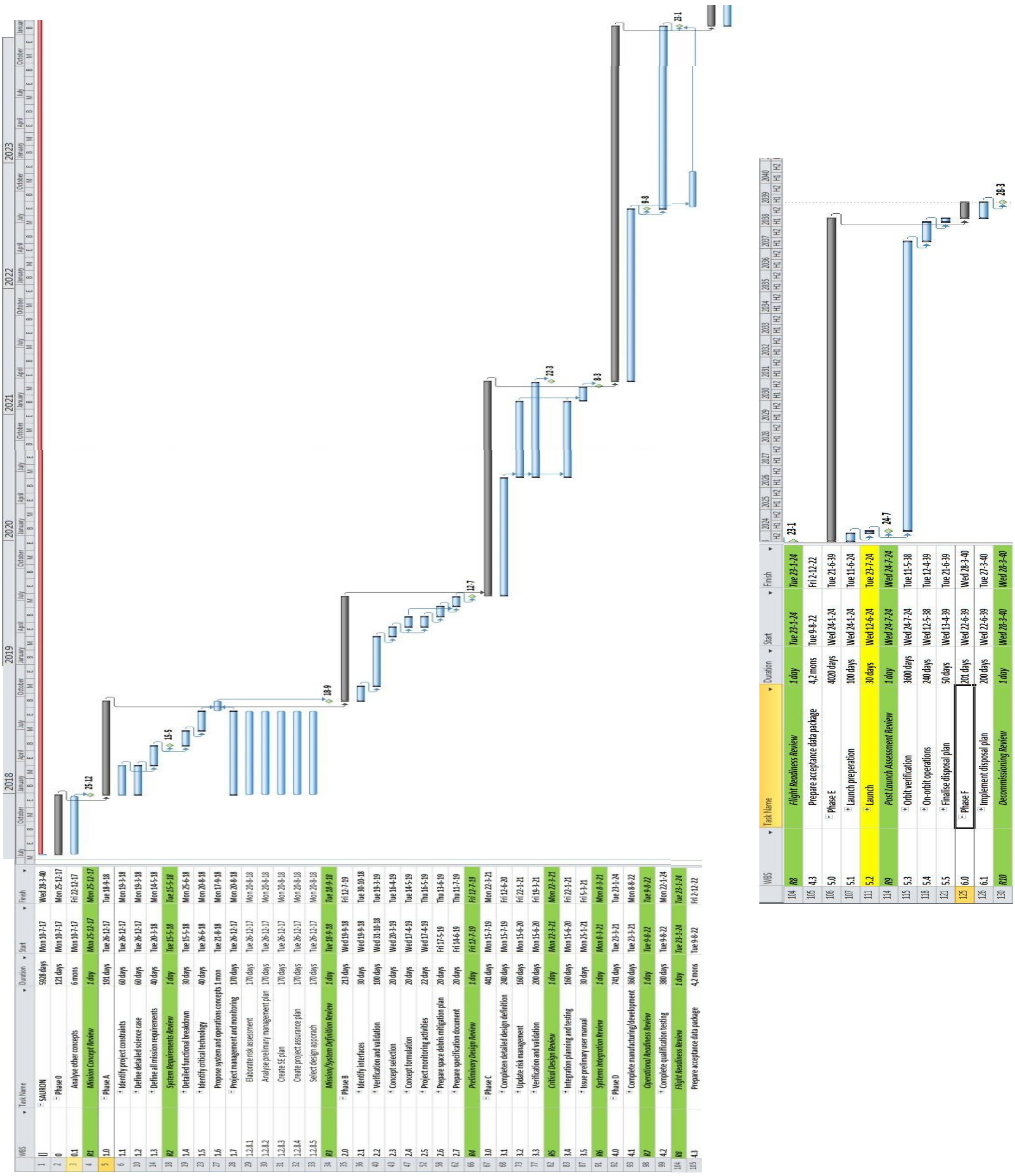

10

Verification and Validation

The following chapter discusses the verification and validation required for the mission. First, a summary of the verification of the currently used models will be given. Afterwards, the verification and validation for the following stages will be discussed.

10.1. Verification and Validation of Current Design

The verification and validation procedures for the models are presented in their respective subsystem chapters. The requirements compliance matrix can be found in Table 10.1 and Table 10.2.

10.2. Verification for Next Stages

For the stages following this report, verification and validation procedures have to be set up to prove that the design meets the requirements. These procedures follow the ECSS requirements as described in ECSS-E-ST-10-02C [138]. The activities relating to verification are shown in Figure 10.1.

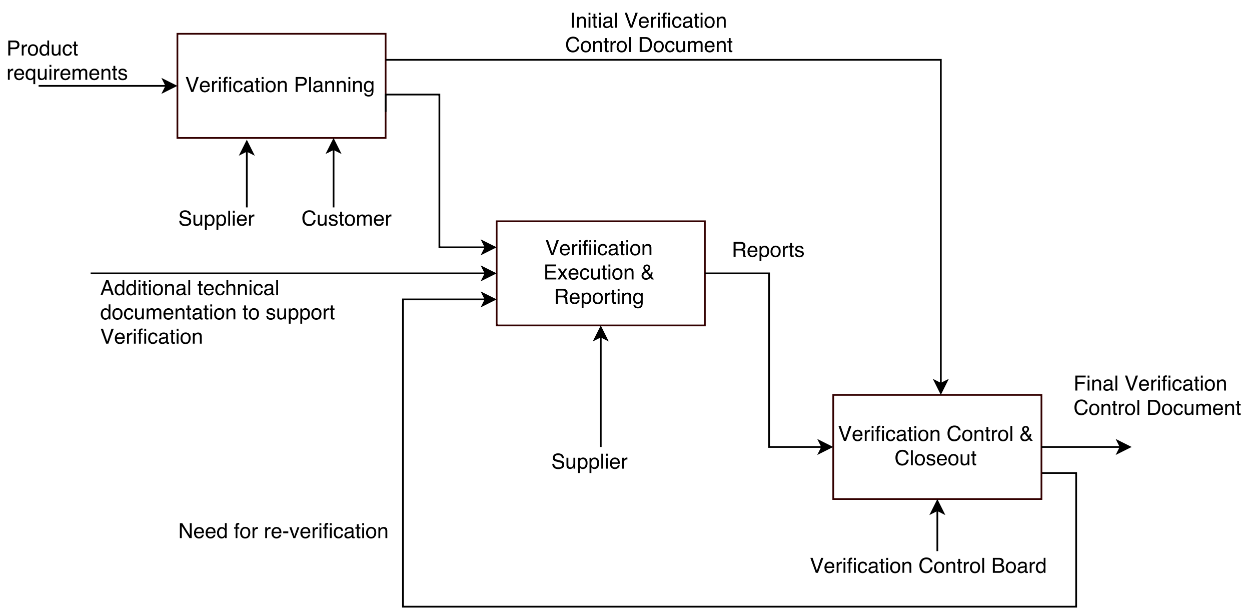

Figure 10.1: Verification process and activities [138].

10.2.1. Verification Planning

The first step in the verification process is to create a verification planning, together with the customers and suppliers. This planning is largely based on the requirements, but also on the available resources, facilities, cost and schedule. It is made for all levels of the system, i.e., from component level up to the overall system. A selection has to be made from the possible verification methods; test, analysis, demonstration and inspection. The method is determined from the verification level (equipment, subsystem, element, segment and overall system) and the nature of the requirement with which the element is verified. Lastly the stage (qualification, acceptance, pre-launch and in-orbit),

Table 10.1: Requirements compliance matrix.

ID	Description	Value	Compliant
SRO-Sys-01	The hovering spacecraft shall be observable for 60% per synodic period.	Communications chapter	Yes
SRO-Sys-02	The total wet mass shall not be more than 16,000 kg in Falcon Heavy	11,900 kg	Yes
SRO-Sys-03	The system shall comply with the dimensions of the launcher payload bay	Defined in general layout	Yes
SRO-Sys-04	The system shall be compatible with the selected launcher		Yes
SRO-Sys-05	The system shall be able to withstand a quasi static load of at least 4.4g axial	Safety factor of 1.5	Yes
SRO-Sys-06	The system shall be able to withstand a dynamic load of at least 6g	Safety factor of 1.5	Yes
SRO-Sys-08	The system shall be able to cope with particle impacts of 167693.97 impulse	......	Yes
SRO-Sys-09	The system shall be able to operate at the environmental heat input fluxes of 15W/m^2 to 4342 W/m^2	Discussed in Thermal Control	Yes
SRO-Sys-10	The system shall be able to withstand the environmental conditions at Saturn.	Defined in environment	Perhaps
SRO-Sys-11	The system shall not hover closer than 2 km above the rings	Defined in mission analysis	Yes
SRO-Sys-12	The mission shall have a 95% or bigger succes rate, this is excluding launch failure.		Yes
SRO-Sys-13	After performing measurements, the spacecraft shall send the gathered data back to Earth	Communication system designed for this	Yes
SRO-Sys-14	The mission design shall include an end-of-life manoeuvre which complies with ESCC regulations.	EOL chapter	Yes
SRO-Sys-15	Mission cost shall not exceed €1.5 billion including launch and operations.	System performance	Yes
SRO-Sys-16	Titan and Enceladus shall not come into direct contact with the spacecraft.	Traj. not meeting moons	Yes
SRO-Sys-17	The mission concepts shall include at least one design that does not use radio isotopes	Found unviable	Yes
SRO-Sys-18	Exposure to and handling of potentially hazardous materials shall be compliant with present-day regulations, such as IAEA Safety Standards. [further regulations TBD]	Considered in PP	Yes
SRO-Sys-19	The entire system shall comply with all regulations regarding deep space missions.	COSPAR met	Yes
SRO-Sys-20	The maximum number of space debris that shall be expelled into Earth orbit when exiting Earth's atmosphere is 1 for single, 2 for multiple spacecraft launch.	Stages landed, second stages left	Yes
SRO-Sys-21	Solid rocket motors shall avoid releasing solid combustion particles greater than 1mm into the GEO protected region.	Discussed in Propulsion	Yes
SRO-Sys-22	The launch date shall be no later than December 31, 2025.	June, 2025	Yes
SRO-Sys-23	Only launchers that have a readiness level of 6 shall be selected.	Falcon Heavy	Yes
SRO-Sys-24	The use of technology shall be restricted to technology available to ESA.	Curium RTG needs dev	Perhaps
SRO-Sys-30	The total measurement duration at a distance of at least 150,000 km from Saturn shall be 1 year.	Main orbiter outlives this	Yes
SRO-Sys-31	The spacecraft for close proximity observations shall have a maximum hover distance of 3 km.	Possibly extended by landing	Yes
SRO-Sys-32	The minimum close proximity hover duration shall be 1 month.	Budgets based on this	Yes
SRO-Sys-33	The measurements shall be made on at least the B- and A-ring.	Both rings covered	Yes

Table 10.2: Requirements compliance matrix (continued).

ID	Description	Value	Compliant
SRO-Sys-34	The ring particles' properties shall be observed at multiple key locations that are defined in the mission analysis.	propeller belts, gaps, edges	Yes
SRO-Sys-35	One measurement point shall be 180deg apart from the others.	multiple locations selected	Yes
SRO-Sys-43	The satellite shall remain fully functional under the influence of the magnetic field of $4.6 \cdot 10^{18}$ T·m3 for the duration of its primary mission	Defined in Environment	Perhaps
SRO-Sys-45	The satellite shall be able to observe the object under study from 2 different angles that are at least TBD degrees apart.	Two spacecraft measure at different angles	Yes
SRO-Sys-46	The satellite shall be able to transmit signal to Earth detectable at -0.1 dB Eb/No.	2.9	Yes
SRO-Sys-47	The satellite shall provide images at visual wavelengths with a resolution of at least 0.1 m/pixel.	0.05m/pixel for hover	Yes
SRO-Sys-48	The satellite shall observe the composition of the individual ring particles and structures with minimum sizes of 1cm	0.05m/pixel for hover	Yes
SRO-Sys-49	The satellite shall be able to determine the dimensional properties of ring particles and structures with minimum sizes of 1cm.	0.05m/pixel for hover	Yes
SRO-Sys-50	The satellite shall be able to observe the interactions between ring particles with minimum sizes of 1cm.	0.05m/pixel for hover	Yes
SRO-Sys-51	The satellite shall observe the ring dynamics with a resolution of 0.1 m/pixel.	0.05m/pixel for hover	Yes
SRO-Sys-54	Observations of the magnetic field shall be provided with a resolution of 25pT m/pixel.	10 pT resolution	Yes
SRO-Sys-56	Additional measurements shall be performed at objects of interest that are visited during the transfer trajectory.	Venus and Earth for calibration	Yes
SRO-Sys-57	Additional measurements shall be investigated by market analysis and consultation of scientists within the first 2 weeks of the conceptual design phase.	Multiple interviews	Yes
SRO-Sys-58	The satellite shall be able to perform an orbit insertion manoeuver.	SOI stage designed	Yes
SRO-Sys-59	The satellite shall be compliant with ESTRACK	Designed for	Yes
SRO-Sys-63	The system shall have a natural frequency of at least 30Hz lateral and 8 Hz axial	Values are met	Yes

where the verification will be implemented, is determined. The results from these investigations are concluded in the verification plan, which is to be delivered to ESA.

In addition to the above mentioned elements, this verification plan includes a full description of the system that is to be verified, any applicable reference documents and the exact procedures for the verification and validation of the system.

The most preferred verification method is testing. However, testing is not always possible. Then verification by analysis is preferred. When this is not possible or applicable, verification by review-of-design or inspection is applied.

10.2.1.1. Model Philosophy

Several models are developed to perform verification. Prototypes will be built to test any new instruments for survivability under the mission conditions. The engineering model will be created to verify all the interfaces.

10.2.2. Verification Preparation

After the verification planning, the preparation step is started. In this phase, the specified requirements to be verified, the product and the necessary equipment, are collected. Also, this step includes the preparation of the verification environment.

10.2.3. Verification Execution

During the execution phase, any specified verification steps are undertaken and all the data is collected and recorded.

10.2.4. VERIFICATION REPORTING

During the reporting phase, the obtained data is analysed for its quality, integrity, correctness, consistency and validity. Any variations from the expected values are reviewed and reported. Based on these findings, either the verified object is delivered to the next phase, or it returns for re-engineering if it does not meet the requirements.

10.2.5. VERIFICATION CONTROL AND CLOSEOUT

The Verification Control Board (VCB) monitors the verification process. Additionally, it decides when the verification is finished based on the requirements and verification objectives. To finish, the customer confirms the end of the verification.

A Verification Control Document (VCD) is made which includes the process description, verification summary status and verification control data. This is provided to the VCB and ESA.

10.3. PRODUCT VALIDATION FOR NEXT STAGES

To ensure that the final product, i.e., the resulting spacecraft, will perform the mission under the expectations of the stakeholders, validation is performed in later project phases, especially during integration. Although validation requires a verified product, both processes can be performed concurrently to speed up the design. It is conducted by the entity performing the product integration, but also by third parties to ensure independent qualification [139].

10.3.1. VALIDATION PROCESS OVERVIEW

Similarly to the verification process, validation requires several inputs and steps to output a validated end product. A global schematic of the process is given in Figure 10.2, based on the description in the NASA Systems Engineering Handbook [140]. The process consists of the planning, preparation, execution, reporting, analysis, and final reporting phases. The execution and reporting are done in parallel. Key to the process is its iterative nature, e.g., if analysis shows that the product does not meet the expectations of the stakeholders, the validation procedure is repeated (in case of procedural deficiencies), or a negotiation process with the stakeholders is initiated.

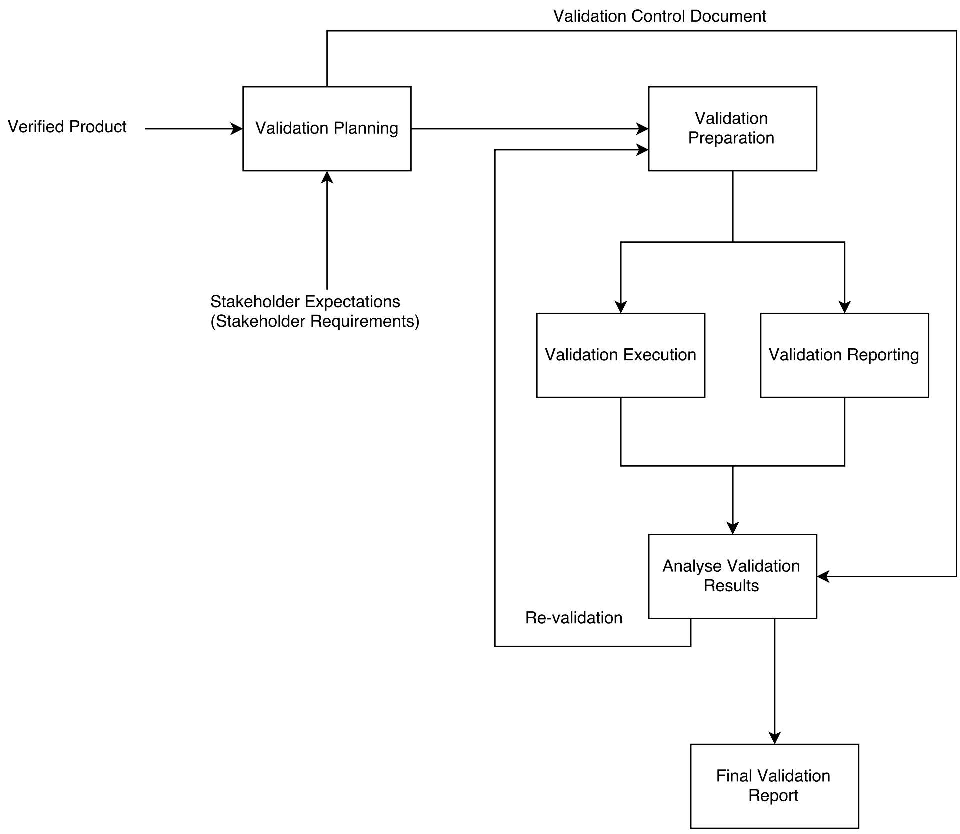

Figure 10.2: The post-DSE Validation Process.

10.3.1.1. VALIDATION PLANNING

In the same fashion that applies to verification planning, the first step in the validation process is planning. All aspects of the system that require validation are established, together with the method applicable to that particular aspect. Validation methods are comparable to those used in verification. Testing, simulation, demonstration, inspection, and analysis can all be used. Again, these methods differ in required labour and cost effectiveness.

The output of the planning phase is a validation plan that describes the expectations of the customer and stakeholders, how those are to be confirmed during validation, the aspects of the system that need validation, the resources, locations, and methods. The plan is used during the analysis of the process results to assess whether validation has succeeded or not.

10.3.1.2. Validation Preparation

After planning, the preparation phase is started. It consists of building/collecting the elements to validate, gathering the necessary resources, transporting the system to the validation location, and preparing the validation equipment. However, not all of these steps are necessary for each validation method. Proper preparation is key to efficiently perform the actual validation procedures.

10.3.1.3. Validation Execution

During this phase of the process, the actual activities are performed which are necessary to prove that the product fulfils the stakeholders' expectations. These can be either testing, inspection, analysis, or demonstration [140]. These methods differ in cost effectiveness, nature of the product, required labour, and accuracy. For example, testing is done to ensure that a product still functions in its target environment. However, the creation of this environment in testing facilities on Earth can be expensive and therefore reduce the cost effectiveness of the method. If a product can be validated by mere inspection, this method is preferred as it is labour-extensive and cheaper as compared to the other methods.

10.3.1.4. Validation Reporting

A crucial part of the validation process is documenting the process. By comparing the contents of the validation reports to the stakeholder expectations report, one can assess whether the system or subsystem meets the expectations of the customer.

10.3.2. Specific Validation Procedures for the SAURON Mission

This section presents the methodology of system validation as applied to SAURON. The following functionalities and derived expectations were considered unique to the mission design at hand:

- **The spacecraft shall hover within 3 kilometres from the rings during at least one month:** Being the key challenge of the mission, proving that the spacecraft will be able to hover within the specified distance during one month is not trivial. Risks as imminent particle impacts, propulsion subsystem malfunction and others (see Chapter 5) make validation crucial. Testing of the spacecraft and its constituent parts will be necessary to show that the system can still operate after particle impacts within the specified limits. For instance, stress testing the spacecraft could entail firing light particles (but similar in dimensions to real ring particles) to assess whether the correct mitigation function is activated and executed.

- **All gathered science data shall be sent back to Earth for analysis:** Because of the large (10 AU) distance at opposition of Earth and Saturn, validation of the communication link should be conducted. This could be done by setting the effective isotopic radiated power (EIRP) to a value comparative to the power received at Earth during the real mission, to check whether the signal can still be detected and can provide the required data rate. This requires modelling of atmospheric effects, link disturbances by ring particles, and pointing losses. Another aspect that is to be accounted for, is the potential blocking of the antenna field of view due to other spacecraft components such as engines, beams, etc.

11
Conclusions and Recommendations

11.1. Conclusions

The presented mission analysis of a dual spacecraft design that is able to investigate the composition and particle dynamics of Saturn's rings, shows compliance with the user requirements on science, performance, reliability and cost. The hovercraft will perform the science measurements at an altitude 2-3 km above the A- and B-ring and send it to the orbiter, which transmits the data back to Earth. The hovering measurements last for at least month and the orbiter measurements for at least a year. Mission success, which implies full completion of the primary science objectives, shall be larger than 95 %. Besides the primary science objectives, additional scientific measurements will be taken on ring-moon interactions, spokes, material clumping and the physical interaction between the rings and atmosphere while not exceeding the mission cost of €1.5 billion, which includes production, operations and launch. The presented design describes an orbiter, hovercraft and two kick stages that will satisfy the user requirements and additional science goals with a cost of €1.46 billion.

The scientific payload of the spacecraft consists of all the instruments that are brought to Saturn to perform the measurements. The orbiter carries a wide and a narrow angle camera, a dust analyser, a magnetometer, a radio science instrument, an IR spectrometer, a UV imaging instrument and finally a plasma and energetic particle package. The hovercraft carries a wide and narrow angle camera, a dust analyser and a magnetometer. Using these instruments all of the scientific objectives can be permormed.

A PyKEP/PyGMO framework provided the foundation of the developed model to optimise a low thrust multiple gravity assist trajectory. The problem was solved using the Sims-Flanagan method in parallel with the Monotonic Basin Hopping meta-algorithm and the Sparse Non Linear Optimiser (SNOPT). The solution was found to be an Earth-Venus-Earth-Earth-Saturn trajectory, powered by a SEP stage, with a duration of 10.4 years. The trajectory requires a total of 729 kg of propellant mass. The Falcon Heavy was selected to insert SAURON into a trajectory with a launch energy of 2.25 $km^2\,s^{-2}$. A SOI, including periapsis raise manoeuvre (PRM) of 460 m/s will initiate the pumpdown tour, which requires a total of 350 m/s. After the tour, SAURON will stage into a orbiter and a hovercraft. The hovercraft will hover for 1 month performing measurements at 6 locations. A total ΔV of 1790.9 m/s is required for the hovercraft. While the hovercraft is performing the primary mission, the orbiter is in a 142000 km circular orbit relaying the data, received from the hovercraft, back to Earth. It will also perform secondary scientific objectives.

To control the attitude and navigation of the spacecraft, a 3-axis stabilisation method was chosen which is the only method that could provide the pointing accuracy needed. Design driving requirements were established by considering the accuracy of every subsystem. To comply with these requirements, star sensors and gyroscope were chosen. There is a Sun sensor on the first stage of the spacecraft. On the hovercraft a LIDAR and a Wide Angle Camera (WAC) were added. The LIDAR is used for estimating the distance to the ring plane. The LIDAR with WAC and the Narrow Angle Camera (NAC) are used to detect hazardous ring particles. To estimate the actuators, the disturbance torques had to be quantified. For this purposed reaction wheels and control thrusters were chosen.

The processing speed that was required to manage the worst case scenario was 78 MHz and a storage of 64 Gbits was determined. To cater to these needs the LEON3-FT processor on the OSCAR computer was selected. To connect all the various components together a military standard, MIL-STD-1553, was selected. Certain correction methods, such as memory scrubbing and the usage of watchdog timers, would be embedded in the software. These techniques would constantly correct and check for the data corruption.

The power of the hovercraft and orbiter is generated with each two RTGs with a total power of 300 and 440 W respectively. The second stage is powered with the excess power of the orbiter. The first stage is powered with two 10 m diameter solar arrays. These provide power for the five NEX thrusters.

The propulsion system uses five different engines and three different propellants. The hovercraft and the orbiter use a Hi-pat 445 Dual mode HP engine for orbit changes using hydrazine/NTO and MR-103M 1N hydrazine thrusters for attitude control. The Moog DST-11H hydrazine/NTO thrusters are used as attitude control thrusters on the second stage and as small manoeuvre thrusters on the hovercraft. Three AMBR 623N Dual mode HP thrusters are used as main engines using hydrazine/NTO. Finally the 5 NEXT engines are used in the first stage which expel xenon using solar electrical power.

The configuration of the spacecraft includes four stages. The first stage incorporates the solar electric propulsion unit and is found at the bottom, on top of it the second stage is found, referred to as the Saturn orbit insertion stage. On the top the hovercraft and main orbiter are found. The structure of each stage is divided into two modules, namely the propulsion module, where the propulsion and the power generation units are mounted, and the electronics bus module, where all required electronics, payload and attitude determination system are found. It is designed to be a cylinder with a uniform thickness of 5.47 mm which results in a total mass of 531 kg.

Thermal control involves covering the spacecraft with aluminised kapton and painting the top of the orbiter with white paint. In addition, radiators were used for the RTGs and the cylindrical surfaces of the spacecraft. These passive techniques are sufficient in keeping the spacecraft cool at Venus. However, the use of active heat pipes is needed for the spacecraft near Saturn.

After link budget analysis of the orbiter-Earth and the inter-satellite links, the configuration of the telecommunications subsystem was established. Both systems incorporate two transponders (one Ka, one X band), two travelling wave tube amplifiers, two diplexers, and a redundant signal distribution network. The orbiter further includes one high gain antenna (HGA) with a Ka band gain of 59 dBi, one medium gain antenna (MGA) and one low gain antenna (LGA). The hovercraft includes one MGA and two LGAs. The resulting effective data rates are 48 kbit/s for the orbiter-Earth downlink, 2.3 kbit/s for the inter-satellite worst case downlink, and 283 Mbit/s for the inter-satellite closest-range downlink. The masses of the subsystem are approximately 80 kg for the orbiter and 40 kg for the hovercraft, with respective costs of 76.6 and 43.3 million euros.

11.2. RECOMMENDATIONS

To help in designing the final concept, for the final report, the following measures are recommended to improve the design:

- **Use a unified cost estimation method.** The current estimation method depends on the individual subsystems and is taken from multiple sources. For this reason, it is logical to assume that the cost estimate could be fine tuned by using the same estimation model for each of the subsystems. NASA's Project Cost Estimating Capability (PCEC) has been selected for this purpose, but time constraints have prevented its integration in the current design.
- **Investigate the increase in distance between RTGs and payload.** Investigating this distance could reveal more information on the hazardous influence of the RTGs on the payload.
- **Investigate other thermoelectric materials with higher efficiency.**
- **Investigate other types of energy conversion methods with higher efficiency.**
- **Investigate the use of concentrated solar arrays.** Using concentrated solar arrays could lower the mass of the spacecraft.
- **Increase the search space of trajectories.** A lot more runs need to be done with the model to find the best trajectory. This is mostly a question of time. Eventually the model should find a feasible trajectory. Also, incorporating different trajectory sequences might give light to "hidden gems", i.e. most favourable trajectories.
- **Add more nodes to the thermal analysis, so that each component can be represented by a single node.** This way verifying the operational temperature ranges can be more accurate.
- **Use more accurate method for finding the heat transferred by heat pipes.** It was just assumed that the RTG provided energy with a 30% efficiency.
- **Perform a transient thermal analysis to ensure the difference in temperatures between steady and transient are similar.**
- **Further analyse tank mass.** The mass of the tanks are not calculated using any of the actual mission loads, but estimated using literature with an additional safety factor. As a result the tank masses are not optimised for this mission yet.
- **Investigate actual thruster efficiency.** The efficiency of the thrusters given by the manufacturers is the efficiency of steady state firing. During start up and shut down of the engine the efficiency might be lower, resulting lower average I_{sp}.
- **Investigate the use of optical communications.** Due to the high distance, radio frequency (RF) communications with Earth from Saturn have relatively low data rates. The use of laser communications could improve the data rates considerably but requires more research to establish pointing requirements and the feasibility for SAURON.

- **Optimise the structure of the spacecraft**. Optimisation could be performed by adding more detail to the analysis, by adding stringers and frames to the design or by performing a finite element analysis on the structure.
- **Analyse the vibroacoustic environment during launch for the spacecraft.** The acoustic environment during launch imposes several constraints to the design of the spacecraft. It gives requirements for the design of the secondary structures as well.
- **Analyse the sinusoidal and random loads during launch**. The sinusoidal and random loads imposed by the launch vehicle drive the design of the secondary structures to a large extent, thus a thorough investigation should take place.
- **Do an iteration that will make all contingencies 18% again, as what it used to be.**
- **The characteristics of the instruments to detect ring collision must be further analysed.** In this report an estimate of the range and diameter that the instruments could detect was taken form concept study[54]. Quantifying this could give a deeper understanding in the system.
- **Having a better correlation with the AOCS design and the control thrusters would make the design much more efficient.**
- **Having more information and number of sensors for housekeeping.** Currently, there was lack of knowledge about the highest analogue frequency provided by any on-board house keeping sensing. Once these values are determined for sure, they could be considered into the data processing calculations to arrive at a better approximation.
- **Limitations with the data processing calculations.** Currently the sensitivity on data provided in SMAD has been used to arrive at processing speeds. The table used is based on a 12 bit processor, therefore it is not accurately representative of current day technology computers that naturally may have a higher performance. To present a proper processing table all the other parameters need to be research properly.
- **Selection of processor.** It was realised only later that there were other processors and companies in Europe that produce better performing processors. Due to lack of this knowledge the processor selection criteria was not critical. Next time a trade-off regarding this is crucial.
- **Perform a detailed trade-off for the science payload.** Currently, the number of science payload instruments has been maximised and includes redundancy for all of the science objectives. A more detailed study can be performed, which investigates the advantages and disadvantages of including and excluding certain instruments. This would require a way to quantify scientific yield and asks for a calculation of the cost, mass and power for each of the considered instruments sets.
- **Investigate the use of principal investigators and dedicated science team.** In the current stage of design, only the instruments themselves have been selected. Each of the instruments is likely to have a principal investigator and a supporting science team dedicated specifically to them. Setting up this structure would help understand the underlying organisation and resources required for the instruments and could refine the cost estimate.
- **Include Science Traceability Matrix.** The use of a Science Traceability Matrix would help in the visualisation of the scientific mission. It presents the main science themes along with their respective objectives. From here, requirements flow down and based on these instruments are appointed to each objective. This matrix has been created for this mission and filled out entirely, but the page limit has prevented it from being present in the report.
- **Investigate mission extension to study Saturn's moons.**

Bibliography

[1] Arridge, C., Khurana, K., Russell, C., Southwood, D., Achilleos, N., Dougherty, M., Coates, A., and Leinweber, H., "Warping of Saturn's magnetospheric and magnetotail current sheets," *Journal of Geophysical Research: Space Physics*, vol. 113, 2008.

[2] Fischer, G., Gurnett, D., Kurth, W., Ye, S.-Y., and Groene, J., "Saturn kilometric radiation periodicity after equinox," *Icarus*, vol. 254, 2015, pp. 72–91.

[3] Meltzer, M., *The Cassini-Huygens Visit to Saturn: An Historic Mission to the Ringed Planet*. Springer, Oakland, CA, 2015.

[4] Badman, S., Jackman, C., Nichols, J., Clarke, J., and Gérard, J., "Open flux in Saturn's magnetosphere," *Icarus*, vol. 231, 2014, pp. 137–145.

[5] Farmer, A. and Goldreich, P., "Spoke formation under moving plasma clouds," *Icarus*, vol. 179, 2005.

[6] Crary, F., "Saturn's Other Ring Current," in *European Planetary Science Congress, EPSC Abstracts, Vol. 9*, 2014.

[7] Colwell, J., Nicholson, P., Tiscareno, M., Murray, C., French, R., and Marouf, E., "The Structure of Saturn's Rings," in *Saturn from Cassini-Huygens*, Dougherty, M., Ed. Springer Netherlands, Dordrecht, The Netherlands, 2009.

[8] Tiscareno, M., "Planetary Rings," Center for Radiophysics and Space Research, Cornell University, Tech. Rep., 2012.

[9] Cuzzi, J., Clark, R., Filacchione, G., French, R., Johnson, R., Marouf, E., , and Spilker, L., "Ring Particle Composition and Size Distribution," in *Saturn from Cassini-Huygens*, Dougherty, M., Ed. Springer Netherlands, Dordrecht, The Netherlands, 2009, pp. 459–509.

[10] Porco, C., Baker, E., Barbara, J., Beurle, K., Brahic, A., Burns, J., and Charnoz, S., "Cassini Imaging Science: Initial results on Saturn's Rings and Small Satellites," *Science*, vol. 307, 2005, pp. 1226–1236.

[11] Tiscareno, M. *et al.*, "The Population of Propellers in Saturn's A Ring," *The Astronomical Journal*, vol. 135, no. 3, 2008, p. 1083.

[12] Porco, C., Thomas, P., Weiss, J., and Richardson, D., "Saturn's Small Inner Satellites: Clues to Their Origins," *Science*, vol. 318, no. 5856, 2007, pp. 1602–1607.

[13] Jacobson, R., Spitale, J., Porco, C., Beurle, K., Cooper, N., Evans, M., and Murray, C., "Revised Orbits of Saturn's Small Inner Satellites," *The Astronomical Journal*, vol. 135, no. 1, 2007, p. 261.

[14] Goldreich, P. and Tremaine, S., "The formation of the Cassini division in Saturn's rings," *Icarus*, vol. 34, 1978, pp. 240–253.

[15] Bosh, A., Olkin, C., French, R., and Nicholson, P., "Saturn's F Ring: Kinematics and Particle Sizes from Stellar Occultation Studies," *Icarus*, vol. 157, no. 1, 2002, pp. 57–75.

[16] Kminek, G. and Rummel, J., "COSPAR's Planetary Protection Policy," *Space Research Today*, no. 193, 2015.

[17] Farrell, W., Kurth, W., Gurnett, D., Persoon, A., and MacDowall, R., "Saturn's rings and associated ring plasma cavity: evidence for slow ring erosion," *Icarus*, vol. 292, 2017, pp. 48–53.

[18] O'Donoghue, J., Stallard, T., Melin, H., Jones, G., Cowley, S., Miller, S., Baines, K., and Blake, J., "The domination of Saturn's low-latitude ionosphere by ring 'rain'," *Nature*, vol. 496, 2013, pp. 193–195.

[19] Hedman, M. and Nicholson, P., "How massive is Saturn's B ring? Clues from cryptic density waves," in *AAS/Division of Dynamical Astronomy Meeting*, ser. AAS/Division of Dynamical Astronomy Meeting, vol. 46, May 2015, p. 200.05.

[20] Nicholson, P. D., Hedman, M., and Buckingham, R., "The puzzling structure in Saturn's outer B ring," in *AAS/Division of Dynamical Astronomy Meeting*, ser. AAS/Division of Dynamical Astronomy Meeting, vol. 48, Jun. 2017, p. #401.04.

[21] Morishima, R., Spilker, L., Ballouz, R.-L., and Richardson, D. C., "N-body ray-tracing modeling of Saturn's rings for analysis of UVIS/VIMS optical depths and CIRS temperatures," in *AAS/Division for Planetary Sciences Meeting Abstracts*, ser. AAS/Division for Planetary Sciences Meeting Abstracts, vol. 48, Oct. 2016, p. 121.10.

[22] Altobelli, N., Lopez-Paz, D., Pilorz, S., Spilker, L., Morishima, R., Brooks, S., Leyrat, C., Deau, E., Edgington, S., and Flandes, A., "Two numerical models designed to reproduce Saturn ring temperatures as measured by Cassini-CIRS," *Icarus*, vol. 238, 2014, pp. 205–220.

[23] Salmon, J. and Canup, R., "Accretion of Saturn's Inner Mid-sized Moons from a Massive Primordial Ice Ring," *The Astrophysical Journal*, vol. 836, no. 1, 2017.

[24] Postberg, F., Khawaja, N., Reviol, R., Nölle, L., Klenner, F., and Srama, R., "Organic compounds from Enceladus in E ring ice grains," in *EGU General Assembly Conference Abstracts*, ser. EGU General Assembly Conference Abstracts, vol. 19, Apr. 2017, p. 13686.

[25] El Moutamid, M., Nicholson, P., French, R., Tiscareno, M., Murray, C., Evans, M., French, C., Hedman, M., and Burns, J., "How Janus' orbital swap affects the edge of Saturn's A ring?" *Icarus*, vol. 279, 2016, pp. 125–140.

[26] Hoffmann, H., Chen, C., Seiß, M., Albers, N., and Spahn, F., "Analyzing Bleriot's propeller gaps in Cassini NAC images," in *AAS/Division for Planetary Sciences Meeting Abstracts*, ser. AAS/Division for Planetary Sciences Meeting Abstracts, vol. 48, Oct. 2016, p. 107.03.

[27] Chen, C., Hoffmann, H., Spahn, F., and Seiß, M., "Images Analysis of the Propeller Bleriot orbiting in Saturn's outer A Ring," in *American Astronomical Society Meeting Abstracts*, ser. American Astronomical Society Meeting Abstracts, vol. 227, Jan. 2016, p. 141.18.

[28] Tiscareno, M., Burns, J., Sremcevic, M., Beurle, K., Hedman, M., Cooper, N., Milano, A., Evans, M., Porco, C., and Spitale, J., "Physical Characteristics and Non-Keplerian Orbital Motion of 'Propeller' Moons Embedded in Saturn's Rings," *The Astrophysical Journal*, vol. 718, no. 2, 2010, p. L2.

[29] Esposito, L., Albers, N., Meinke, B., Sremcevic, M., Madhusudhanan, P., and Colwell, J., "A predator-prey model for moon-triggered clumping in Saturn's rings," *Icarus*, vol. 217, 2012, pp. 103–114.

[30] Porco, C., Weiss, J., Richardson, D., Dones, L., Quinn, T., and Throop, H., "Simulations of the dynamical and light-scattering behavior of Saturn's rings and the derivation of ring particle and disk properties," *The Astronomical Journal*, vol. 136, no. 5, 2008.

[31] Colwell, J., Esposito, L., and Sremcevic, M., "Self-gravity wakes in Saturn's A ring measured by steller occultation from Cassini," *Geophysical Research Letters*, vol. 33, 2006.

[32] Colwell, J., Esposito, L., Sremcevic, M., Stewart, G., and McClintock, W., "Self-gravity wakes and radial structure in Saturn's B ring," *Icarus*, vol. 190, 2007, pp. 127–144.

[33] Tiscareno, M., Mitchell, C., Murray, C., Di Nino, D., Hedman, M., Schmidt, J., Burns, J., Cuzzi, J., Porco, C., Beurle, K., and Evans, M., "Observations of Ejecta Clouds Produced by Impacts onto Saturn's Rings," *Science*, vol. 340, 2013, pp. 460–464.

[34] D'Aversa, E., Bellucci, G., Filacchione, G., Cerroni, P., Nicholson, P. D., Carrozzo, F. G., Altieri, F., Oliva, F., Geminale, A., Sindoni, G., and Hedman, M. M., "IR spectra of Saturn's ring spokes and multiple shines in the Saturn-rings system," in *EGU General Assembly Conference Abstracts*, ser. EGU General Assembly Conference Abstracts, vol. 19, Apr. 2017, p. 9140.

[35] Hamilton, D., "Charged Dust Dynamics at Saturn," in *40th COSPAR Scientific Assembly*, ser. COSPAR Meeting, vol. 40, 2014.

[36] Bell III, J., Wolff, M., Malin, M., Calvin, W., Cantor, B., Caplinger, M., Clancy, R., Edgett, K., Edwards, L., Fahle, J., Ghaemi, F., Haberle, R., Hale, A., James, R., Lee, S., McConnochie, T., Noe Dobrea, E., Ravine, M., Schaeffer, D., Supulver, K., and Thomas, P., "Mars Reconnaissance Orbit Mars Color Imager (MARCI): Instrument description, calibration, and performance," *Journal of Geophysical Research*, vol. 114, 2009.

[37] Hansen, C., Caplinger, M., Ingersoll, A., Ravine, M., Jensen, E., Bolton, S., and Orton, G., "Juno's Outreach Camera," *Space Science Reviews*, 2014, pp. 1–32.

[38] Robinson, M., Brylow, S., and Tschimmel, M. e. a., "Lunar Reconaissance Orbiter Camera (LROC) Instrument Overview," *Space Science Reviews*, vol. 150, 2010, pp. 88–124.

[39] Riedler, W., Torkar, K., Rüdenauer, F., Fehringer, M., Schmidt, R., Arends, H., Grard, R., Jessberger, E., Kassing, R., Alleyne, H., Ehrenfreund, P., Levasseur-Regourd, A., Koeberl, C., Havnes, O., Klöck, W., Zinner, E., and Rott, M., "The MIDAS Experiment for the Rosetta Mission," *Advanced Space Research*, vol. 21, no. 11, 1998, pp. 1547–1556.

[40] Magnes, W., Pierce, D., Valavanoglou, A., Means, J., Baumjohann, W., Russell, C., Schwingenschuh, K., and Graber, G., "A sigma-detla fluxgate magnetometer for space applications," *Measurement Science Technology*, vol. 14, no. 7, 2003.

[41] The JUICE Science Study Team, "JUICE - Assessment Study Report," European Space Agency, Tech. Rep., 2011.

[42] *Optical design of the composite infrared spectrometer for the Cassini mission*, 1993.

[43] Christensen, P., Bandfield, J., Hamilton, V., Ruff, S., Kieffer, H., Titus, M. M., T.N., Morris, R., Lane, M., Clark, R., Jakosky, B., Mellon, M., Pearl, J., Conrath, B., Smith, M., Clancy, R., Kuzmin, R., Roush, T., Mehall, N., G.L. Gorelick, Bender, K., Murray, K., Dason, S., Greene, E., Silverman, S., and Greenfield, M., "Mars Global Surveyor Thermal Emission Spectrometer experiment: Investigation description and surface science results," *Journal of Geophysical Research*, vol. 106, 2001, pp. 23 823–23 871.

[44] Gladstone, G., Stern, S., Retherford, K., Black, R., Scherrer, D., J.R. Slater, Stone, J., Feldman, P., and Crider, D., "LAMP: The Lyman Alpha Mapping Project aboard the NASA Lunar Reconnaissance Orbiter Mission," *Astrobiology and Planetary Missions*, vol. 150, 2005, pp. 161–181.

[45] Stern, S., Slater, D., Scherrer, J., Stone, J., Dirks, G., Versteeg, M., Davis, M., Gladstone, G., Parker, J., Young, L., and Siegmund, O., "ALICE: The Ultraviolet Imaging Spectrograph Aboard the New Horizons Pluto-Kuiper Belt Mission," *Space Science Reviews*, vol. 140, no. 1-4, 2008, pp. 155–187.

[46] Mauk, B., Haggerty, D., and Jaskulek, D. e. a., "The Jupiter Energetic Particle Detector Instrument (JEDI) Investigation for the Juno Mission," *Space Science Reviews*, 2013, pp. 1–58.

[47] Hansen, C. J. and Orton, G. S., "JunoCam: Science and Outreach Opportunities with Juno," *AGU Fall Meeting*

Abstracts, Dec. 2015.

[48] Habib-Agahi, H., Mrozinski, J., and Fox, G., "NASA instrument cost/schedule model," in *2011 IEEE Aerospace Conference*, 2011.

[49] Garrett, H., Ratliff, J., and Evans, R., "Saturn Radiation (SATRAD) Model," Jet Propulsion Laboratory, Tech. Rep., 2005.

[50] Izzo, D., "PyGMO and PyKEP: Open Source Tools for Massively Parallel Optimization in Astrodynamics (The Case of Interplanetary Trajectory Optimization)," European Space Research and Technology Centre, Noordwijk, the Netherlands, Tech. Rep. GSFC-E-DAA-TN14154, May 2012.

[51] Gill, P. E., Murray, W., and Saunders, M. A., "SNOPT: An SQP Algorithm for Large-Scale Constrained Optimization," *SIAM Journal on Optimization*, vol. 12, 2002, pp. 979–1006.

[52] Englander, J. A. and Englander, A. C., "Tuning Monotonic Basin Hopping: Improving the Efficiency of Stochastic Search as Applied to Low-Thrust Trajectory Optimization," NASA Goddard Space Flight Center, 8800 Greenbelt Road, Greenbelt, Tech. Rep. ACT-RPR-MAD, May 2014.

[53] Sims, J. A. and Flanagan, S. N., "Preliminary Design of Low-Thrust Interplanetary Mission," NASA, Washington, D.C., Tech. Rep. 20000057422, Januari 1997.

[54] P. Nicholson, L. S. and Tiscareno, M., "Planetary Science Decadal Survey Saturn Ring Observer," National Aeronautics and Space Administration, Jet Propulsion Laboratory, California Institute of Technology, Pasadena, CA, Tech. Rep. -, Jun 2010.

[55] Spilker, T. R., "Saturn Ring Observer," *Acta Astronautica*, vol. 52, no. 2–6, 2003, pp. 259 – 265.

[56] Harland, D. M. and Lorenz, R. D., *Space Systems Failures-Disasters and Rescues of Satellites, Rocket and Space Probes*. Praxis, 2005.

[57] Rioux, N., "ANSI/AIAA guide for estimating spacecraft systems contingencies applied to the NASA GLAST mission," in *Aerospace Conference, 2006 IEEE*. 2006, p. 17.

[58] Wertz, J. R., Everett, D. F., and Puschell, J. J., *Space Mission Engineering: The New SMAD*, 1st ed. Microcosm Press, 2011.

[59] Ismail, Z. and Varatharajoo, R., "A study of reaction wheel configurations for a 3-axis satellite attitude control," *Advances in Space Research*, vol. 45, no. 6, 2010, p. 750–759.

[60] *Satellite attitude and orbit control system (AOCS) requirements*, ESA Requirements and Standards Divison, ESTEC, 2200 AG Noordwijk, The Netherlands, Jul 2013.

[61] Schilling, K., "Control Lessons Learned during the Cassini/Huygens Mission to Explore the Saturnian Moon Titan," *Design Considerations & Integrated Optimization Factors for Distributed Nano UAV Applications*, vol. 1, no. 4, 2007, pp. 4.1 – 4.20.

[62] *Cassini Spacecraft Attitude Control System Flight Performance*, ser. AIAA Guidance, Navigation, and Control Conference and Exhibit, aug. 15-18 2005.

[63] Fremont, V., Bui, M., Boukerroui, D., and Letort, P., "Vision-Based People Detection System for Heavy Machine Applications," *Sensors*, vol. 16, no. 1, 2016, p. 128.

[64] Lee, A. and Hanover, G., "Cassini Spacecraft Attitude Control System Flight Performance," *AIAA Guidance, Navigation, and Control Conference and Exhibit*, 2005.

[65] Ley, W., Wittmann, K., and Hallmann, W., *Handbook of Space Technology*. WILEY, 2009.

[66] Hult, T. and Parkes, S., *The International Handbook of Space Technology*, 1st ed. Springer-Verlag Berlin Heidelberg, 2014.

[67] Fountain, G. H., Kusnierkiewicz, D. Y. *et al.*, "The New Horizons Spacecraft," Southwest Research Institute Planetary Science Directorate, Southwest Research Institute 1050 Walnut St, Suite 300 Boulder, CO 80302, Tech. Rep., 2016.

[68] Ciarcia, S., Simone, L., Gelfusa, D., Colucci, P., Angelis, G. D., Argentieri, F., Iess, L., and Formaro, R., "More and Juno Ka-Band Transponder Design, Performance, Qualification and In-Flight Validation," Laboratorio di Radio Scienza, Via Eudossiana 18, 00186 Roma, Italy, Tech. Rep., 2013.

[69] ECSS Secretariat, "Space Engineering Communications," European Cooperation for Space Standardisation, ESA-ESTEC Requirements & Standards Division, Noordwijk, The Netherlands, Tech. Rep. ECSS-E-ST-50C, jul 2008.

[70] Dougherty, M. K. *et al.*, *The Cassini-Huygens Mission: Orbiter In Situ Investigations*. Springer, 2004, vol. 2, ch. The Cassini Magnetic Field Investigation.

[71] Henry, C. A., "An Introduction to the Design of the Cassini Spacecraft," Jet Propulsion Laboratory, JPL, California Institute of Technology, Pasadena, California, Tech. Rep., Oct 2001.

[72] Zandbergen, B., "Spacecraft (bus) Designing and Sizing," Delft University of Technology, Faculty of Aerospace Engineering, Delft University of Technology, Delft, Netherlands, Nov 2015.

[73] Doody, D., *Deep Space Craft: An Overview of Interplanetary Flight*. Springer, NASA Jet Propulsion Laboratory, (Caltech), Pasadena, California, USA, 2009.

[74] NASA, *Goes N Data Book*. NASA, 2005, ch. Telemetry and Command System.

[75] Secretariat, E., "Ground systems and operations — Telemetry and telecommand packet utilization," European Cooperation for Space Standardisation, ESA-ESTEC Requirements & Standards Division Noordwijk, The Netherlands, Tech. Rep. ECSS-E-70-41A, Jan 2003.

[76] M. Cabral, R. V. C. M., R. Trautner, "Efficient Data Compression for Spacecraft Including Planetary Probes," European Space Research and Technology Centre (ESTEC), TEC-EDP, ESA/ESTEC, Noordwijk, The Netherlands, Tech. Rep., 2010.

[77] Airbus Defence and Space, *OSCAR*, Airbus Defence and Space.

[78] Siewiorek, D. P. and Narasimhan, P., "Fault-Tolerance Architectures for Space and Avionics Applications," Carnegie Mellon University, Electrical and Computer Engineering Department Carnegie Mellon University, Pittsburgh, PA, Tech. Rep., 2014.

[79] Larson, W. J. and Wertz, J. R., *Space Mission Analysis and Design.*, 3rd ed. Space Technology Library, 1999.

[80] Nuseibah, B., "Ariane 5: Who dunnit?" *IEEE Software*, May 1997, pp. 15–16.

[81] NASA, "Single Event Effect Criticality Analysis," National Aeronautics and Space Agency, Goddard Space Flight Center Greenbelt, Maryland, Tech. Rep. 431-REF-000273, Feb 1996.

[82] Sturesson, F., Gaisler, J., Ginosar, R., IEEE, S. M., and Liran, T., Eds., *Radiation Characterization of a Dual Core LEON3-FT Processor*, ser. 21378. 2011.

[83] Touesnard, B., "Software Cost Estimation: SLOC-based Models and the Function Points Model," UNB, Tech. Rep. 1, 2004.

[84] Malcom, H. and Utterback, H. K., "Flight Software in the Space Department: A Look at the Past and a View Toward the Future," *John Hopkins APL Technical Digest*, vol. 20, 1999, pp. 522–532, http://www.jhuapl.edu/techdigest/TD/td2004/malcom.pdf.

[85] Murphy, D., "MegaFlex-the scaling potential of UltraFlex technology," in *53rd AIAA/ASME/ASCE/AHS/ASC Structures, Structural Dynamics and Materials Conference 20th AIAA/ASME/AHS Adaptive Structures Conference 14th AIAA*, 2012, p. 1581.

[86] Bennett, G., Lombardo, J., and etal., "Mission of Daring: The General-Purpose Heat Source Radioisotope Thermoelectric Generator," The American Institute of Aeronautics and Astronautics, 4th International Energy Conversion Engineering Conference and Exhibit, San Diego, California, Tech. Rep. 2006-4096, Jun 2006.

[87] Johansson, R., "Curium in Space," Master's thesis, KTH Royal Institute of Technology, Jun 2013.

[88] Ragheb, M., "Radioisotopes Power Production," mragheb.com, University of Illinois at Urbana-Champaign, Tech. Rep., 2013.

[89] Stivers, G., "Radioisotope thermoelectric space power supplies," *IEEE Transactions on Aerospace*, vol. 2, no. 2, 1964, pp. 652–660.

[90] Brown, C. D., *Elements of spacecraft design*. Aiaa, 2002.

[91] Reh, K., Elliot, J., Spilker, T., Jorgensen, E., Spencer, J., and Lorenz, R., "Titan and Enceladus $1 B mission feasibility study report," *JPL D-37401B*, 2007.

[92] Langham, R. C., "Feasibility study and system architecture of radioisotope thermoelectric generation power systems for usmc forward operating bases," 2013.

[93] Kulcinski, G., "Basic elements of static RTGs," *University of Wisconsin-Madison*, 2003.

[94] Aller, P. F. and Miskuff, R. J., "A modular heat source for Curium-244 and Plutonium-238," in *9th Intersociety Energy Conversion Engineering Conference*, 1974, pp. 147–151.

[95] Mason, L. S., "Realistic specific power expectations for advanced radioisotope power systems," *Journal of propulsion and power*, vol. 23, no. 5, 2007, pp. 1075–1079.

[96] Arnold, E., "Handbook of shielding requirements and radiation characteristics of isotopic power sources for terrestrial, marine, and space applications," Oak Ridge National Lab., Tenn., Tech. Rep., 1964.

[97] Eogers, P. E. and Ridihalg, J. l., "Cost-Effective Radioisotope Thermoelectric Generator Designs involving Cm-244 and Pu-238 Heat Sources," *Journal of Spacecraft and Rockets*, vol. 11, no. 10, 1974, pp. 704–709.

[98] Turner, M. J., *Rocket and spacecraft propulsion: principles, practice and new developments*. Springer Science & Business Media, 2008.

[99] Krismer, D., Dorantes, A., Miller, S., Stechman, C., and Lu, F., "Qualification testing of a high performance bipropellant rocket engine using MON-3 and hydrazine," in *39th AIAA/ASME/SAE/ASEE Joint Propulsion Conference and Exhibit*, 2003, p. 4775.

[100] Anderson, D., Pencil, E., Liou, L., Dankanich, J., and Munk, M., "Status and Mission Applicability of NASA's In-Space Propulsion Technology Project," in *45th AIAA/ASME/SAE/ASEE Joint Propulsion Conference & Exhibit*, 2009, p. 5125.

[101] Patterson, M. and Benson, S., "NEXT ion propulsion system development status and performance," in *43rd AIAA/ASME/SAE/ASEE Joint Propulsion Conference & Exhibit*, 2007, p. 5199.

[102] Leeds, M., Eberhardt, R., and Berry, R., "Development of the Cassini spacecraft propulsion subsystem," in *32nd*

Joint Propulsion Conference and Exhibit, 1996, p. 2864.

[103] Johnson, K. S., Cockfield, R. D., El-Genk, M. S., and Bragg, M. J., "Power and propulsion for the Cassini mission," in *AIP Conference Proceedings*, vol. 746, no. 1. 2005, pp. 232–239.

[104] Hofer, R. R. and Randolph, T. M., "Mass and cost model for selecting thruster size in electric propulsion systems," *Journal of Propulsion and Power*, vol. 29, no. 1, 2012, pp. 166–177.

[105] Fox, B., Brancato, K., and Alkire, B., "Guidelines and metrics for assessing space system cost estimates," DTIC Document, Tech. Rep., 2008.

[106] Kieckhafer, A. and King, L. B., "Energetics of propellant options for high-power Hall thrusters," *Journal of propulsion and power*, vol. 23, no. 1, 2007, pp. 21–26.

[107] Wright, A. C., "USAF Propellant Handbooks. Nitric Acid/Nitrogen Tetroxide Oxidizers. Volume II." DTIC Document, Tech. Rep., 1977.

[108] Santo, A. G., Gold, R. E., McNutt, R. L., Solomon, S. C., Ercol, C. J., Farquhar, R. W., Hartka, T. J., Jenkins, J. E., McAdams, J. V., Mosher, L. E. *et al.*, "The MESSENGER mission to Mercury: Spacecraft and mission design," *Planetary and Space Science*, vol. 49, no. 14, 2001, pp. 1481–1500.

[109] Wiley, S., Dommer, K., Engelbrecht, C., and Vaughan, R., "MESSENGER Propulsion System Flight Performance," in *42nd AIAA/ASME/SAE/ASEE Joint Propulsion Conference & Exhibit*, 2006, p. 4689.

[110] Putzar, R. *et al.*, "Vulnerability of shielded fuel pipes and heat pipes to hypervelocity impacts," in *4th European Conference on Space Debris*, vol. 587, 2005, p. 459.

[111] Calvi, A., "Spacecraft Loads Analysis An Overview," Powerpoint, Nov 2011.

[112] Alliance, U. L., *Delta IV Launch Services User's Guide*, LLC/United Launch Services, LLC, Centennial, CO 80155, jun 2013.

[113] *SPACE LAUNCH SYSTEM (SLS) PROGRAM MISSION PLANNER'S GUIDE (MPG) EXECUTIVE OVERVIEW*, 2014.

[114] Wijker, J. J., *Spacecraft Structures*, 1st ed. Springer-Verlag, Berlin Heidelberg, 2008.

[115] Sarafin, T. P. and Larson, W. J., *Spacecraft Structures and Mechanisms: From Concept to Launch*, 1st ed. Microcosm, Inc, 1995.

[116] *Handbook for Designing MMOD Protection*, 2009.

[117] Liu, J., *Spacecraft TT&C and Information Transmission Theory and Technologies*, 1st ed. Springer-Verlag, Berlin Heidelberg, 2015.

[118] Minoli, D., *Satellite Systems Engineering in an IPv6 Environment*, 1st ed. CRC Press, Boca Raton, FL, USA, 2009.

[119] DeTiberis, F., Simone, L., Gelfusa, D., Simone, P., Viola, R. *et al.*, "The X/X/KA-band deep space transponder for the BepiColombo mission to Mercury," *Acta Astronautica*, vol. 68, no. 1, 2011, pp. 591–598.

[120] Mukai, R., Hansen, D., Mittskus, A., Taylor, J., and Danos, M., "Juno Telecommunications," Jet Propulsion Laboratory, CIT, Pasadena, California, Tech. Rep., 2012.

[121] Ippolito, L., *Satellite Communications Systems Engineering*, 2nd ed. John Wiley & Sons, Somerset, NJ, USA, 2017.

[122] ITU, "Allowable error performance for a satellite hypothetical reference digital path," International Telecommunication Union, Standard ITU-R S.614-4, 2005.

[123] Edwards, C. and DePaula, R., "Key telecommunications technologies for increasing data return for future Mars exploration," *Acta Astronautica*, vol. 61, no. 1, 2007, pp. 131 – 138.

[124] Maral, G. and Bousquet, M., *Satellite Communications Systems: Systems, Techniques and Technology*, 4th ed. John Wiley & Sons, Chichester, England, 2002.

[125] Lohmeyer, W., Aniceto, R., and Cahoy, K., "Communication satellite power amplifiers: current and future SSPA and TWTA technologies," *International Journal of Satellite Communications and Networking*, vol. 34, no. 2, 2016, pp. 95–113.

[126] Hemmati, H., "Laser communications: From terrestrial broadband to deep-space," in *2014 16th International Conference on Transparent Optical Networks (ICTON)*, July 2014, pp. 1–3.

[127] Hemmati, H. and Caplan, D., "Optical Satellite Communications," in *Optical Fiber Telecommunications VIB: Systems and Networks: Sixth Edition*, Kaminow, I., Li, T., and Willner, E., Eds. Oxford Academic Press Inc., Oxford, England, 2013, pp. 121–162.

[128] Gaite, J. and Fernandez-Rico, G., "Linear approach to the orbiting spacecraft problem," Universidad Politecnia Madrid, Tech. Rep. 3, 2012.

[129] Martinez, I., "Thermo-optical properties," Tech. Rep., 1995-2017.

[130] Flannigan, O., Johri, K., Van der Leer, R., Van Lierop, C., Meeuwissen, B., Mekic, A., Pappadimitriou, A., Puts, E., Sfikas, K., and Vis, S., "Saturn Ring Observer-Project Plan," Delft University of Technology, Delft, The Netherlands, Tech. Rep., May 2017.

[131] Office of Space Science, "Supplemental Environmental Impact Statement for the Cassini Mission," NASA, jun 1997.

[132] SSP10, "ecoSpace : Final Report," International Space University, Parc d'Innovation 1 rue Jean-Dominique Cassini 67400 Illkirch-Graffenstaden France, Tech. Rep., 2010.

[133] United Nations, "United Nations Treaties and Principles on Outer Space," United Nations, New York, NY, Tech. Rep., 2008.

[134] National Research Council & Division on Engineering & Physical Sciences & Space Studies Board & Commission on Physical Sciences, Mathematics & Applications & Space Studies Board Ad Hoc Committee on the Assessment of Mission Size Trade-Offs for Earth & Space Science Missions, *Assessment of Mission Size Trade-offs for NASA's Earth and Space Science Missions*, 2000.

[135] P. Fortescue, G. S. and Stark, J., *Spacecraft Systems Engineering*, 4th ed. Wiley, The Atrium, Southern Gate, Chichester, West Sussex, PO19 8SQ, United Kingdom, 2011.

[136] Besso, P., Bozzi, M., Formaggi, M., Pasian, M., and Perregrini, L., "Feasibility study of the upgrade to K band of ESA Deep Space Antennas," in *2008 IEEE Antennas and Propagation Society International Symposium*, July 2008, pp. 1–4.

[137] "Project Planning and Implementation," European Cooperation for Space Standardisation, ESA-ESTEC Requirements & Standards Division Noordwijk, The Netherlands, Tech. Rep. ECSS-M-ST-10C, 2008.

[138] "Space Engineering Verification," European Cooperation for Space Standardisation, ESA-ESTEC Requirements & Standards Division Noordwijk, The Netherlands, Tech. Rep. ECSS-E-70-41A, 2009.

[139] NASA, *Systems Engineering Handbook*, 1st ed. National Aeronautics and Space Administration, Washington, D.C., 2007.

[140] Kapurch, S. and Rainwater, N., *NASA Systems Engineering Handbook*. NASA, Washington, D.C., 2007.